Stem Cells International

Targeting Adult Mesenchymal Stem Cells Plasticity for Tissue Regeneration

Lead Guest Editor: Giorgio Mori
Guest Editors: Giacomina Brunetti, Filiberto Mastrangelo, and Elisabetta A. Cavalcanti-Adam

Targeting Adult Mesenchymal Stem Cells Plasticity for Tissue Regeneration

Stem Cells International

Targeting Adult Mesenchymal Stem Cells Plasticity for Tissue Regeneration

Lead Guest Editor: Giorgio Mori
Guest Editors: Giacomina Brunetti, Filiberto Mastrangelo, and Elisabetta A. Cavalcanti-Adam

Copyright © 2017 Hindawi. All rights reserved.

This is a special issue published in "Stem Cells International." All articles are open access articles distributed under the Creative Commons Attribution License, which permits unrestricted use, distribution, and reproduction in any medium, provided the original work is properly cited.

Editorial Board

James Adjaye, Germany
Dominique Bonnet, UK
Silvia Brunelli, Italy
Bruce A. Bunnell, USA
Kevin D. Bunting, USA
Benedetta Bussolati, Italy
Yilin Cao, China
Kyunghee Choi, USA
Pier Paolo Claudio, USA
Gerald A. Colvin, USA
Varda Deutsch, Israel
Leonard M. Eisenberg, USA
Marina Emborg, USA
Tong-Chuan He, USA
Boon C. Heng, Hong Kong
Toru Hosoda, Japan
Xiao J. Huang, China
Thomas Ichim, USA
J. Itskovitz-Eldor, Israel
P. Jendelova, Czech Republic
Arne Jensen, Germany
Atsuhiko Kawamoto, Japan
Mark D. Kirk, USA
Valerie Kouskoff, UK
Andrzej Lange, Poland
Laura Lasagni, Italy
Renke Li, Canada
Tao-Sheng Li, Japan
Susan Liao, Singapore
Shinn-Zong Lin, Taiwan
Yupo Ma, USA
Athanasios Mantalaris, UK
Eva Mezey, USA
C. Montero-Menei, France
Karim Nayernia, UK
Sue O'Shea, USA
Stefan Przyborski, UK
Bruno Pèault, USA
Peter J. Quesenberry, USA
Pranela Rameshwar, USA
B. A. J. Roelen, Netherlands
Peter Rubin, USA
Hannele T. Ruohola-Baker, USA
Donald S. Sakaguchi, USA
Ghasem Hosseini Salekdeh, Iran
Heinrich Sauer, Germany
Coralie Sengenes, France
Shimon Slavin, Israel
Shay Soker, USA
Giorgio Stassi, Italy
Ann Steele, USA
Alexander Storch, Germany
Corrado Tarella, Italy
Hung-Fat Tse, Hong Kong
Marc L. Turner, UK
Jay L. Vivian, USA
Dominik Wolf, Austria
Qingzhong Xiao, UK
Zhaohui Ye, USA
Wen-Jie Zhang, China

Contents

Hindawi
Stem Cells International
Volume 2017, Article ID 4532179, 2 pages
https://doi.org/10.1155/2017/4532179

Editorial

Targeting Adult Mesenchymal Stem Cells Plasticity for Tissue Regeneration

Giorgio Mori,[1] Giacomina Brunetti,[2] Filiberto Mastrangelo,[1] and Elisabetta A. Cavalcanti-Adam[3]

[1]*Department of Clinical and Experimental Medicine, University of Foggia Medical School, Via L. Pinto, 71122 Foggia, Italy*
[2]*Department of Basic Medical Sciences, Neuroscience and Sense Organs, Section of Human Anatomy and Histology, University of Bari "A. Moro", Piazza Giulio Cesare 11, 70124 Bari, Italy*
[3]*Institute of Physical Chemistry, Department of Biophysical Chemistry, University of Heidelberg and Max Planck Institute for Intelligent Systems, Stuttgart, Germany*

Correspondence should be addressed to Giorgio Mori; giorgio.mori@unifg.it

Received 27 February 2017; Accepted 27 February 2017; Published 21 June 2017

Copyright © 2017 Giorgio Mori et al. This is an open access article distributed under the Creative Commons Attribution License, which permits unrestricted use, distribution, and reproduction in any medium, provided the original work is properly cited.

Tissue damage derived from tumors, traumatic events, inflammatory diseases, or just aging causes life quality impairment. Thus, tissue regeneration not only represents the main goal of regenerative therapy but also is certainly one of the greatest challenges of modern medicine.

Mesenchymal stem cells (MSCs) can be isolated from different source tissues in the adult organism. MSCs can differentiate in mature cells of different lineages; thus, if opportunely targeted, they have the potential to regenerate and heal the injured tissue. The scientific contributions which are part of this special issue present and analyzed these items both in the form of research articles and reviews.

The bone marrow is still the gold standard tissue for harvesting MSCs: different clonal cells were analyzed showing heterogeneity; alkaline phosphatase assay could indicate the precursor's lineage (M. Elsafadi et al.). Dental tissues also contain MSCs: in particular, the dental follicle [1] and dental bud [2] are striking sources of cells which readily differentiate into the osteoblastic lineage. Dental pulp stem cells successfully undergo osteogenic differentiation [3] and their reparative behavior could be increased by platelet lysate supplementation (P. Marrazzo et al.). For bone tissue regeneration and vascularized bone grafts, both adipose tissue and periodontal ligament stem cells could be differentiated into bone cells, and in particular, adipose cells can be successfully cryopreserved for tissue banking (I. Roato et al.).

A great challenge in regenerative therapy is the guidance of wound healing. MSCs promote wound healing, and human umbilical cord MSCs accelerate wound repair and hair follicle regeneration via Wnt overexpression (L. Dong et al.). Interestingly, as shown by X. Liu et al., overexpression of semaphorin 3A in adipose-derived stem cells leads to a phenotype switch toward the osteoblastic lineage by upregulating the Wnt pathway as well. These studies on alternative sources of MSCs highlight the importance of molecular signals that might direct MSC fate and more specifically guide them to form mineralized tissue [4].

To increase healing at bone fracture sites, several approaches that stimulate physically the differentiation of MSC have been developed. Pulsed electromagnetic fields promote bone marrow MSCs osteogenic differentiation by activating TGF-β signaling pathway and stimulating the expression of microRNA21 (N. Selvamurugan et al.). Given that natural composition and structure of the extracellular environment has a profound impact on MSC osteogenic differentiation [5], a variety of scaffolds and matrix-based materials are used in dentistry and craniofacial surgery. Combining both the priming MSC with stem cell chemical modulators and the use of 3D printing-based materials represents a successful strategy not only for the treatment

of cardiovascular disease but also for fostering revascularization of grafts in a variety of tissues.

Giorgio Mori
Giacomina Brunetti
Filiberto Mastrangelo
Elisabetta A. Cavalcanti-Adam

References

[1] G. Mori, A. Ballini, C. Carbone et al., "Osteogenic differentiation of dental follicle stem cells," *International Journal of Medical Sciences*, vol. 9, no. 6, pp. 480–487, 2012.

[2] A. Di Benedetto, G. Brunetti, F. Posa et al., "Osteogenic differentiation of mesenchymal stem cells from dental bud: role of integrins and cadherins," *Stem Cell Research*, vol. 15, no. 3, pp. 618–628, 2015.

[3] G. Mori, G. Brunetti, A. Oranger et al., "Dental pulp stem cells: osteogenic differentiation and gene expression," *Annals of the New York Academy of Sciences*, vol. 1237, no. 1, pp. 47–52, 2011.

[4] E. Giorgini, C. Conti, P. Ferraris et al., "FT-IR microscopic analysis on human dental pulp stem cells," *Vibrational Spectroscopy*, vol. 57, no. 1, pp. 30–34, 2011.

[5] E. H. Schwab, M. Halbig, K. Glenske, A. S. Wagner, S. Wenisch, and Cavalcanti-Adam EA, "Distinct effects of RGD-glycoproteins on integrin-mediated adhesion and osteogenic differentiation of human mesenchymal stem cells," *International Journal of Medical Sciences*, vol. 10, no. 13, pp. 1846–1859, 2013.

Hindawi
Stem Cells International
Volume 2017, Article ID 2450327, 17 pages
https://doi.org/10.1155/2017/2450327

Research Article

Pulsed Electromagnetic Field Regulates MicroRNA 21 Expression to Activate TGF-β Signaling in Human Bone Marrow Stromal Cells to Enhance Osteoblast Differentiation

Nagarajan Selvamurugan,[1] Zhiming He,[2] Daniel Rifkin,[3] Branka Dabovic,[3] and Nicola C. Partridge[2]

[1]*Department of Biotechnology, School of Bioengineering, SRM University, Kattankulathur, Tamil Nadu, India*
[2]*Department of Basic Science and Craniofacial Biology, New York University College of Dentistry, New York, NY, USA*
[3]*Department of Cell Biology, New York University School of Medicine, New York, NY, USA*

Correspondence should be addressed to Nicola C. Partridge; ncp234@nyu.edu

Received 23 September 2016; Revised 5 January 2017; Accepted 12 February 2017; Published 23 April 2017

Academic Editor: Elisabetta A. Cavalcanti-Adam

Copyright © 2017 Nagarajan Selvamurugan et al. This is an open access article distributed under the Creative Commons Attribution License, which permits unrestricted use, distribution, and reproduction in any medium, provided the original work is properly cited.

Pulsed electromagnetic fields (PEMFs) have been documented to promote bone fracture healing in nonunions and increase lumbar spinal fusion rates. However, the molecular mechanisms by which PEMF stimulates differentiation of human bone marrow stromal cells (hBMSCs) into osteoblasts are not well understood. In this study the PEMF effects on hBMSCs were studied by microarray analysis. PEMF stimulation of hBMSCs' cell numbers mainly affected genes of cell cycle regulation, cell structure, and growth receptors or kinase pathways. In the differentiation and mineralization stages, PEMF regulated preosteoblast gene expression and notably, the transforming growth factor-beta (TGF-β) signaling pathway and microRNA 21 (miR21) were most highly regulated. PEMF stimulated activation of Smad2 and miR21-5p expression in differentiated osteoblasts, and TGF-β signaling was essential for PEMF stimulation of alkaline phosphatase mRNA expression. Smad7, an antagonist of the TGF-β signaling pathway, was found to be miR21-5p's putative target gene and PEMF caused a decrease in Smad7 expression. Expression of Runx2 was increased by PEMF treatment and the miR21-5p inhibitor prevented the PEMF stimulation of Runx2 expression in differentiating cells. Thus, PEMF could mediate its effects on bone metabolism by activation of the TGF-β signaling pathway and stimulation of expression of miR21-5p in hBMSCs.

1. Introduction

Abundant reports describe the effects of electricity on bone growth and fracture repair, and a variety of pulsed electromagnetic field (PEMF) devices have been developed to produce electromagnetic fields at the fracture site. These widespread PEMF devices utilize noninvasive inductive coupling and can be used along with every method of fracture fixation [1, 2]. The stimulation of bone at the fracture site by the introduction of electromagnetic fields may be similar to the resulting stimulation from mechanical loading [1]. The beneficial therapeutic effects of such selected low energy, time varying PEMF promote fracture healing in nonunions [3], increase lumbar spinal fusion rates [4, 5], and have been found to affect bone metabolism by decreasing bone resorption and increasing bone formation [6–8]. PEMFs have also been reported to stimulate the synthesis of extracellular matrix (ECM) proteins [9] and may also affect several membrane receptors including those for parathyroid hormone, low density lipoprotein, insulin-like growth factor-2, insulin, and calcitonin [10]. Several growth factors such as bone morphogenetic proteins 2 and 4 (BMP-2, BMP-4) and transforming growth factor-beta (TGF-β) have been reported to be secreted from osteoblasts upon PEMF treatment [11]. It has been shown that electromagnetic stimulation could raise net Ca^{2+} flux in human osteoblast-like cells, and the increase in the cytosolic Ca^{2+} concentration could initiate activation of signaling pathways resulting in regulation of expression

of bone matrix genes [12, 13]. Accelerated osteogenesis has been found in bone marrow-derived mesenchymal stem cells by PEMF treatment [14] and this promotion of ECM deposition was more efficient compared with adipose-tissue mesenchymal stem cells [15].

Previously we have reported that both BMP-2 and PEMF (Spinal-Stim® by Orthofix, Inc., Lewisville, TX) separately stimulated proliferation of rat primary calvarial osteoblastic cells and stimulated expression of early osteoblast differentiation genes in culture [7]. In this study, we investigated the effects of PEMF (Cervical-Stim® by Orthofix, Inc., Lewisville, TX) on human bone marrow stromal cells (hBMSCs) proliferating and differentiated to osteoblastic cells. In addition, the underlying molecular mechanisms by which PEMF stimulates differentiation of hBMSCs into osteoblasts are not well understood. Thus, we also aimed to investigate the PEMF effects on proliferation, differentiation, and mineralization of hBMSCs by Affymetrix microarray analysis. The TGF-β signaling pathway and microRNA 21 (miR21) were most highly regulated by PEMF. Thus, in this study we systematically investigated the mechanism of action of PEMF effects on osteogenesis via TGF-β and miR21 using hBMSCs.

2. Materials and Methods

2.1. Cell Culture. Fresh human bone marrows from 21–68-year-old women were used. These were either purchased from Lonza (Walkersville, MD) or left over tissue from surgical procedures at New York University Hospital for Joint Diseases. Since these were deidentified, this is not considered Human Subjects Research by the New York University School of Medicine Institutional Review Board. In both cases, the bone marrows were freshly collected, never frozen, and immediately diluted 1 : 1 in Hank's Balanced Salt Solution (HBSS; GIBCO Laboratories, Grand Island, NY) containing 20 IU/mL of sodium heparin (Sigma Chemical Co., St. Louis, MO). The diluted bone marrow was layered over an equal volume of Ficoll-Paque Plus (GE Healthcare, Piscataway, NJ) and centrifuged at 400g for 40 min at 18°C. The mononuclear cells at the interface layer were collected, washed three times with HBSS, resuspended and seeded into a tissue culture flask, and incubated at 37°C in the presence of 5% CO_2 overnight. The next day, nonadherent cells were removed from the culture flask. Adherent cells (BMSCs) were grown to confluence then placed in 6-well plates at 6.4×10^4 cells/well for exposure to PEMF or control. All cells were incubated at 37°C in the presence of 5% CO_2. The medium used for culturing these cells was α-MEM (Corning, Tewksbury, MA) containing 15% fetal bovine serum (FBS; GIBCO, Grand Island, NY) and Penicillin-Streptomycin (GIBCO, Grand Island, NY).

2.2. PEMF Exposure. The PEMF was generated as previously described [7] but was set to have similar waveform characteristics to a commercial, clinically approved proprietary device (Cervical-Stim by Orthofix Inc., Lewisville, TX). Cervical-Stim is the only device approved by the FDA for cervical fusion use and has been reported to be safe and effective [16]. The specific differences from our previous publication [7] were a burst frequency of 15 Hz and a burst period of 67 ms. The induced magnetic field was vertical relative to the surface of the plates. The PEMF waveform was routinely checked for its consistency using a field probe and oscilloscope. The first PEMF exposure was initiated 24 h after seeding cells in wells (day 1) and continued through the entire experiment. Control plates were placed in an identical incubator on Plexiglas shelves. The CO_2 concentration, humidity, and temperature of the control and treatment incubators (upper and lower chambers of the same double incubator) were identical and were not affected by the PEMF.

2.3. Cell Number. Cells were grown in normal growth medium and were trypsinized, resuspended, and counted using a hemocytometer when they reached 70–80% confluence on day 10 or 20 of culture, respectively, for the BMSCs from the younger (21–30) women versus those from the 31–65-year-old women.

2.4. Osteoblast Differentiation. Human BMSCs were seeded at 6.4×10^4 cells/well in 6-well cell culture plates and cultured for 10 days or 20 days in normal cell culture medium (αMEM + 15% FBS + 1% Penn/Strep) before they reached confluence. They were then cultured for an additional 13 (differentiation) or 23 (mineralization) days in osteogenic medium [normal growth medium supplemented with 10^{-4} M L-ascorbic acid, 10^{-8} M dexamethasone, and 1.80 mM potassium phosphate monobasic (Sigma, St. Louis, MO)]. The medium was changed three times/week.

2.5. Von Kossa Staining. For Von Kossa staining, 6 replicates of BMSCs were treated with PEMF or control daily from day 1 of culture. On day 23, 33, or 43, the cells were fixed with 95% ethanol for 15 min at 37°C, then rinsed and rehydrated through 80%, 50%, and 20% ethanol and then water, and incubated with 5% silver nitrate solution for 1 h at 37°C. The cells were rinsed with water, exposed to UV light for 10 min, and photographed. Von Kossa staining was analyzed by computer based morphometry (ImageJ: NIH, Bethesda, Maryland).

2.6. Extracellular Regulated Kinases Activation and Western Blot Analyses. Human BMSCs treated with control or PEMF for 5 and 10 days in the proliferation phase were washed with cold phosphate buffered saline (PBS) and lysed in Cell Lysis Buffer (Invitrogen, Grand Island, NY) containing protease and phosphatase inhibitor cocktails (Sigma). Cell lysates were centrifuged at 10,000 rpm for 10 minutes at 4°C and supernatants were saved and used for Western blot analysis. Twenty μg of total cell protein was loaded per well and separated on 4–15% Mini-Protean TGX precast gels (Bio-Rad, Hercules, CA), followed by transferring to nitrocellulose membranes (Bio-Rad, Hercules, CA). The membranes were blocked and incubated with primary rabbit antibodies (Phospho-p44/42 MAPK (Erk1/2) (Thr202/Tyr204), p44/42 MAPK (Erk1/2) (137F5), or Cdk2 (sc-163; Cyclin dependent kinase 2, loading control)) overnight at 4°C. The membranes were then probed with secondary antibody conjugated with

Table 1: Primers used in this study.

Gene name	Forward primer (5′ > 3′)	Reverse primer (5′ > 3′)
ALP	TGGACGGCCTGGACCTCGTT	AGGGTCAGGAGTTCCGTGCG
COL1A1	GGAGGCACGCGGAGTGTGAG	CCTCTTGGCCGTGCGTCAGG
Osteocalcin	GAGCCCCAGTCCCCTACCCG	GACACCCTAGACCGGGCCGT
FOSB	GCGCCGGGAACGAAATAAAC	TTCGTAGGGGATCTTGCAGC
LEPR	GTGGGGCTATTGGACTGACT	CTTTGAGAGTCCAGCAGGCA
TBRG1	GCTAGATTCCTAGAGGCCCG	GGCATCGGATCCTAAGTCGG
FBN2	CTTTAGGCCGGTTATGCAACG	AATAAGCCCTTCGTCGGCTC
SOX11	TTGGAAGCGGAGAGCAACCT	TGCGTTCGATCTTGGACCAT
CTNNA1	GGCAGCCAAAAGACAACAGG	GGCCTTATAGGCTGCGACAT
AKT3	CTCTATTATTTGGGCTGAGTCATCA	CCCCTCTTCTGAACCCAACC
CXCL12	GACAAGTGTGCATTGACCCG	TGTAAGGGTTCCTCAGGCGT
THBS1	CCTCTACTCCGGACGCAC	GCCCCGGTGAGTTCAAAGAT
COL5A1	CGGGGACTATGACTACGTGC	CTCCAAGTCATCCGCACCTT
GPC4	CAGAGGTCCAGGTTGACACC	TCGGCTTTCTCATTGGCACT
MMP16	TGCGGAACGGAGCAGTATTT	TGTGCTTGTGCTGCCATTTC
TGFB2	CCCCGGAGGTGATTTCCATC	AACTGGGCAGACAGTTTCGG
CDH11	CCCAGTACACGTTGATGGCT	ACGTTCCCACATTGGACCTC
SPP1	GCCTCCTAGGCATCACCTG	CTTACTTGGAAGGGTCTGTGGG
IL8	GGTGCAGTTTTGCCAAGGAG	TTCCTTGGGGTCCAGACAGA
RPL13A	AAGTACCAGGCAGTGACAG	CCTGTTTCCGTAGCCTCATG
hsa-miR-21-5p	UAGCUUAUCAGACUGAUGUUGA	

horseradish peroxidase. Finally, the bands were visualized by adding Super Signal West Dura Extended Duration Substrate (Thermo Scientific, Pittsburgh, PA) according to the manufacturer's instructions. The primary antibodies to total ERKs and phosphorylated ERKs were obtained from Cell Signaling Technology (Danvers, MA), while the antibody to Cdk2 was obtained from Santa Cruz Biotechnology, Inc. (Dallas, TX). The secondary antibody (goat-anti-rabbit) conjugated with horseradish peroxidase (HRP) was obtained from Santa Cruz Biotechnology. Results were captured and quantitated by ChemiDoc XRS+ software (Bio-Rad, Hercules, CA). Both the Phospho-ERK1/2 and total ERK 1/2 were normalized to Cdk2 and then expressed as a percent of the values obtained in untreated control cells.

2.7. Microarray Assays. Human BMSCs of a 27-year-old healthy female donor were used for microarray experiments. Only hBMSCs expanded from the second to sixth passages were used for the experiments. PEMF treatment (Cervical-Stim) was initiated 24 h after hBMSCs were seeded, with 4 h daily exposure every day throughout the experimental period. Quadruplicate cell samples from both PEMF-treated and control groups were collected simultaneously at time points of hBMSC proliferation, osteoblast differentiation, and mineralization phases. Total RNA was isolated from cells by using TRIzol reagent (Thermo Scientific, Pittsburgh, PA) and then purified with RNeasy mini kit from Qiagen (Valencia, CA). Prior to microarray analysis, the RNA integrity was assessed by Agilent 2100 Bioanalyzer (Santa Clara, CA) and the best quality triplicate samples were chosen for the subsequent analyses. Microarrays and data analyses with Affymetrix Human U133 plus 2.0 Gene Chips (Santa Clara, CA) were performed at University of Medicine and Dentistry of New Jersey Genome Center according to the manufacturer's instructions. In the case of gene expression where it was significantly found to be above 1.5-fold after PEMF treatment, gene ontology analysis was carried out by DAVID Bioinformatics Resources 6.7 software (NIAID, NIH).

2.8. Real-Time RT-PCR. Total RNA was isolated from cells using the total RNA isolation kit from Qiagen (Valencia, CA). For determination of expression of genes other than miR21-5p, 100 ng of total RNA from each sample was used for cDNA synthesis using TaqMan Reverse Transcription Reagents (Roche, Indianapolis, IN). Quantitative (q)PCR reactions were performed according to the real-time thermocycler machine (Realplex) manufacturer's instructions (Eppendorf, Hauppauge, NY), which allowed real-time quantitative detection of the PCR products by measuring the increase in SYBR green fluorescence caused by binding of SYBR green to double-stranded DNA. The Power SYBR green master mix kit for PCR reactions was purchased from Invitrogen. The qPCR was performed in triplicate with reaction conditions of 95°C, 10 min, 1 cycle; 95°C, 15 sec; and 58.5°C, 1 min, for 40 cycles. Gene expression was analyzed with threshold cycle (CT) values averaged from triplicate samples and normalized to their CT values of housekeeping gene RPL13A. Primers were designed by NCBI primer Blast software. Table 1 lists the human-specific primers used for PCR amplification.

For miR21-5p and snoR10-1, the reagents and primer sets for RT-qPCR were purchased from Qiagen. One ug of total RNA was reverse-transcribed into cDNA using the

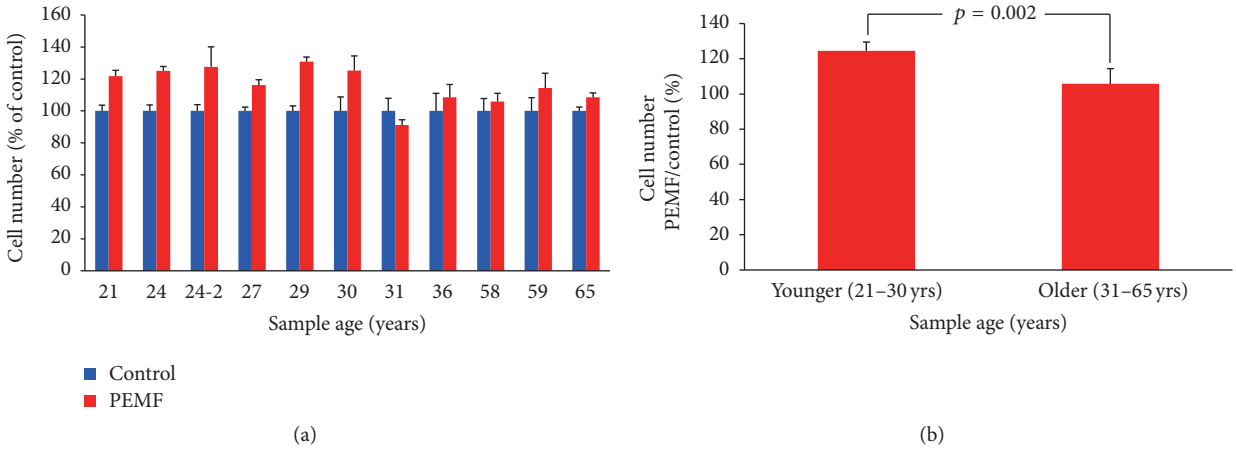

Figure 1: Effect of PEMF on hBMSC preosteoblastic cell number. (a) Human preosteoblasts derived from bone marrow stromal cells of 21–36-year-old women were treated with PEMF for 10 days; cells from 58-, 59-, and 65-year-old women were treated with PEMF for 20 days. Cell number/well was calculated using a hemocytometer (n = 3–6 wells). (b) Aggregation of the data into the two age groups, n = 5-6. The statistical p value for the younger versus older samples is shown using Student's t-test analysis.

miScript II kit with miScript HiSpec Buffer according to the manufacturer's instructions. The cDNA was then diluted 10 times and utilized as a template to amplify miR21-5p and snoR10-1 with the miScript SYBR Green PCR kit using the appropriate primers. snoR10-1 was used as normalizing gene control. The qPCR was performed in triplicate with reaction conditions of 95°C 15 min for Taq DNA polymerase activation, 94°C 15 sec denaturation, 55°C 30 sec annealing, and 70°C 30 sec extension for 40 cycles. Gene expression results of miR21-5p from either control or PEMF-treated groups were normalized to their relative snoR10-1 results.

2.9. TGF-β Signaling. Human BMSCs were cultured and treated with control or PEMF as described above. For TGF-β and BMP signaling assays, osteoblasts were treated with PEMF at days 23 and 33 and were also treated with TGF-β2 (R&D System, Minneapolis, MN) as a positive control for the TGF-β pathway. The day before assay, the cells were starved overnight (0.1% FBS medium) to reduce endogenous signaling activity. At day 23 at the same time as PEMF exposure started, 5 ng/mL TGF-β2 was added to the medium of positive control wells. Cell lysates from different groups were collected at 0, 2, and 4 h time points after treatment to examine Smad2, Smad3, and Smad1/5/8 protein phosphorylation by Western blot analysis as described above. Phospho-Smad2 (Ser465/467, 138D4)/Smad2 (D43B4), phospho-Smad3 (Ser423/425, C25A9)/Smad3 (C67H9), and phospho-Smad1/5/8/Smad1/5 antibodies were obtained from Cell Signaling Technology (Danvers, MA). In TGF-β neutralization experiments, 30 ug/mL normal rabbit IgG or TGF-β pan antibody (R&D System, Minneapolis, MN) was added to osteogenic medium during the entire differentiation period. At day 23, two non-PEMF-treated cell groups were also included with 5 ng/mL of TGF-β2 as positive controls. After 2 h of PEMF exposure, all sample groups were collected for Western blots and RT-qPCR assays.

2.10. Transient Transfection. Cells were seeded in growth medium in 6-well plates at a density of 10^5 cells/well on the day before the transfection. miR-21 is now referred as miR-21-5p, based on the latest miRBase release (V.21). miR21-5p inhibitor (Applied Biosystems: 4464084) designed to bind with endogenous miR21, when introduced into cells, inhibits its activities. miR21-5p mimic (Applied Biosystems: 4464066) was designed to be similar to that of endogenous miR21. A negative control miRNA (Applied Biosystems: 4464076) was included in the study. The X-treme Gene transfection reagent obtained from Roche, USA, was mixed with 50 nM of negative control miRNA, miR21 mimic, or miR21 inhibitor, and transient transfection was carried out [17] for 3 or 6 days along with PEMF treatment every day for 4 h.

2.11. Statistical Analysis. Statistical analysis was done by one-way ANOVA, Student's t-test, or Wilcoxon Ranking. Significant difference is $p < 0.05$. All data are shown as mean ± standard deviation with n as indicated.

3. Results

3.1. PEMF Effects on Proliferation and Differentiation of Human BMSCs from Subjects of Different Ages. We previously reported that PEMF generated by Spinal-Stim stimulated cell proliferation and expression of early differentiation marker genes in rat primary calvarial osteoblastic cultures [7]. In the present study we used PEMF (Cervical-Stim) to determine its effect on osteoblasts using human bone marrow cells. PEMF significantly stimulated the cell number of preosteoblasts from BMSCs of young women (21–30 years old) while not stimulating those of BMSCs from 31–65-year-old women (Figures 1(a) and 1(b)). It should also be noted that the hBMSCs from aged individuals (58, 59, and 65 years old) also required much longer time (20 days) to approach a similar cell culture density to those from the younger women. Since PEMF had an effect on preosteoblastic cell number from

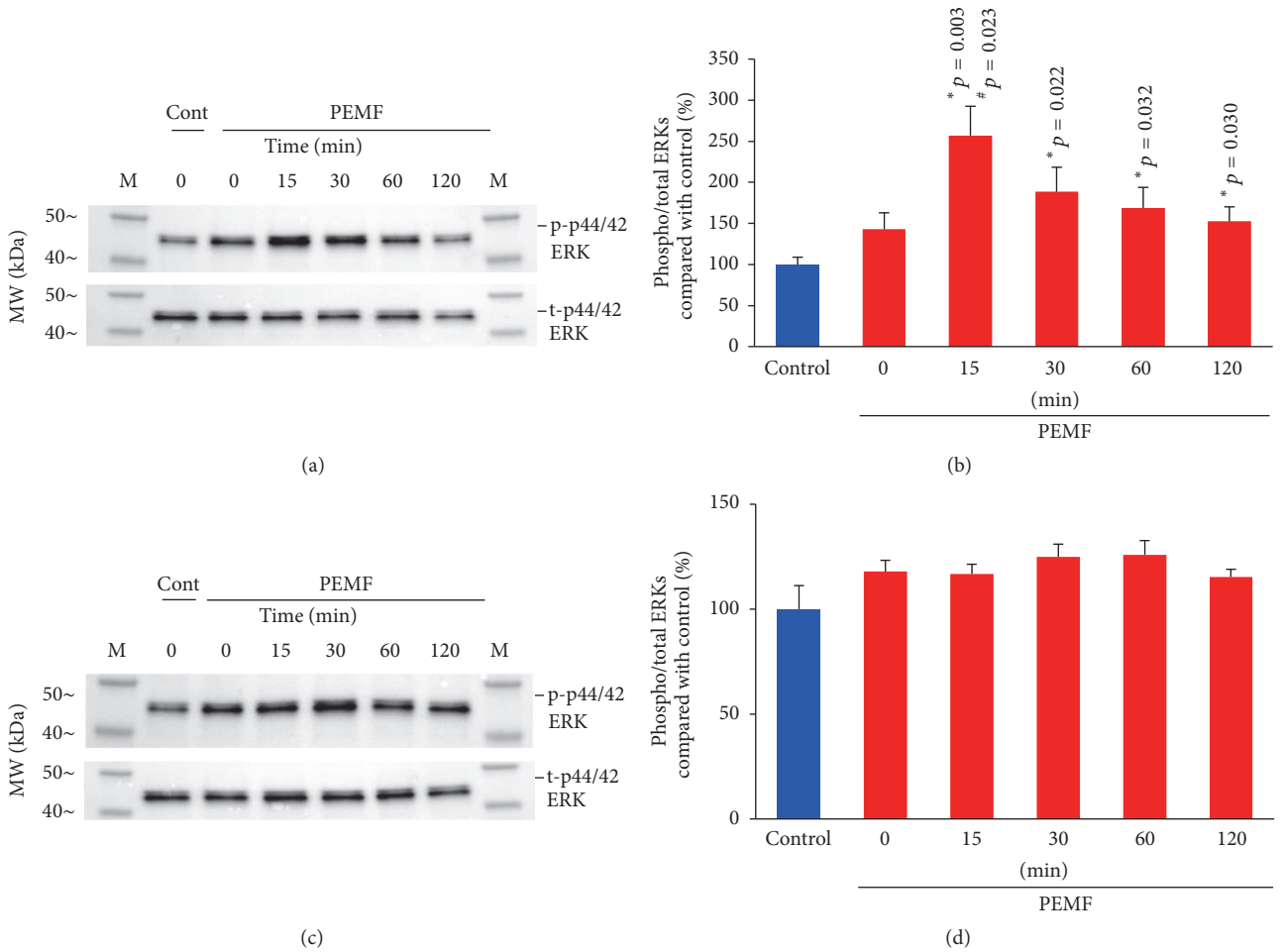

Figure 2: Effect of PEMF on ERK activation. Human BMSCs from two different 24-year-old women and a 27-year-old woman were subjected to 4 h daily PEMF treatment for either 4 days or 9 days. On the 5th (a) or 10th day (c), their cells were treated with PEMF for different time periods as indicated and whole cell lysates were obtained and subjected to Western blot analyses; cells from a 24-year-old woman are shown as an example. ((b) day 5, (d) day 10) The quantitation of activated or phosphorylated ERKs for cells from 2 separate 24-year-old women and a 27-year-old woman was determined by normalization of phosphorylated ERKs to total ERKs after normalization to Cdk2 as a loading control and expressed as a percent of untreated control cells. The results are shown for the cells of the 3 individuals. ∗ indicates significant increase compared to control. # indicates significant increase compared to 0 times of PEMF on the 5th day. The p value ≤ 0.05 is considered as significant using one-way ANOVA.

the younger women and cell proliferation involves activation of intracellular signaling pathways, especially extracellular regulated kinases (ERKs), we determined activation of these enzymes by PEMF. As shown in Figure 2(a), PEMF increased ERK activation (phosphorylation) after 15 min on day 5 in BMSCs from a 24-year-old woman. A similar effect was also found in hBMSCs from other younger female subjects (24- and 27-year-old women's cells) and the quantitative analysis of ERK activation (phosphorylated ERKs) from the three individuals after normalization to total ERKs confirmed the above result (Figure 2(b)). There was no significant activation of ERKs from any of these cells on the 10th day of PEMF treatment (Figures 2(c) and 2(d)).

To determine the role played by PEMF in osteoblast differentiation and mineralization of hBMSCs, experiments were carried out at molecular and cellular levels. At the molecular level, the mRNA expression of alkaline phosphatase (ALP), type I collagen (COL1A1), and osteocalcin (OC), which are known osteoblast differentiation and mineralization marker genes, was determined using qRT-PCR analysis. PEMF significantly increased mRNA expression of ALP and Col1 but not OC in BMSCs that had been allowed to proliferate, differentiate, and mineralize (Figure 3(a)). We next determined the effect of PEMF on mineralization in BMSCs by Von Kossa staining (Figures 3(b) and 3(c)). PEMF significantly stimulated mineralization of BMSCs in the mineralization phase and did not in the differentiation phase.

3.2. PEMF Regulation of Genes during hBMSC Proliferation by Microarray Analysis. A sample from a young individual was used for microarray analyses because PEMF significantly enhanced cell growth for young individuals compared to old individuals as shown in Figure 1. For assessment of the effect

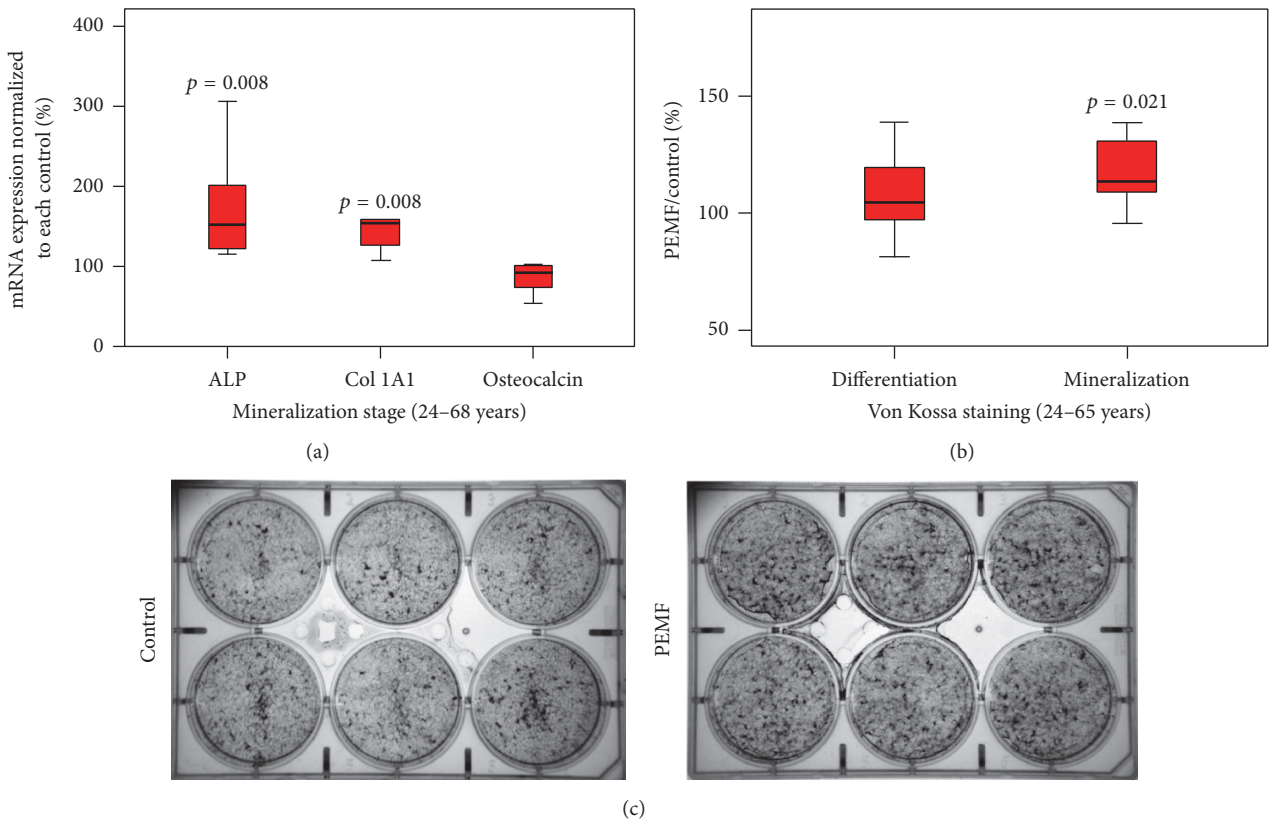

Figure 3: Effect of PEMF on expression of osteoblastic marker genes and mineralization in hBMSCs. Differentiating preosteoblasts from 24–68-year-old women were grown in the presence of osteoblast differentiation medium after confluence was reached and were treated with PEMF for 33 days or 43 days (59–68-year-old samples) of culture. (a) Total RNA was isolated and subjected to qRT-PCR using specific primers for human ALP, type I collagen, OC, and RPL13A. $n = 9$. (b) Cells were then subjected to Von Kossa staining and the mineralized calcium deposits were quantified. $n = 9$. Statistical analyses were conducted using Wilcoxon signed rank test. The p value ≤ 0.05 is considered as significant compared with the controls. (c) An example of Von Kossa staining and mineralized calcium deposits for hBMSCs of a 24-year-old female after 33 days of osteogenic culture in the presence or absence of daily Cervical-Stim PEMF.

of PEMF on gene expression during hBMSC proliferation, on the 5th day of PEMF treatment 2 h after initiating the PEMF signal (pilot studies had shown significant PEMF stimulation of Cyclin gene expression at this time and day, data not shown), total RNA was isolated and used for the subsequent test with Affymetrix Human U133 plus 2.0 Gene Chips. After identifying significantly regulated genes, gene ontology analyses were performed by DAVID Bioinformatics Resources 6.7 software. The results indicated that PEMF stimulation of proliferating hBMSCs mainly affected genes of cell cycle regulation, cell structure, extracellular matrix (ECM), and some growth receptors or kinase pathways. There were a total of 114 known genes upregulated and 17 known genes downregulated at this time point (partially listed in Table 2). We have also included the decrease in fibrillin 2, even though it was not −1.5-fold, since this sequesters members of the TGF-β family and is the subject of our later research in this report.

3.3. PEMF Regulation of Genes in Differentiated and Mineralized hBMSCs by Microarray Analysis. In the differentiation (day 23) and mineralization stages (day 33) after daily 4 h PEMF treatment, a total of 37 (partially listed in Table 3) and 173 (partially listed in Table 4) known genes, respectively, were identified as significantly regulated. In these two stages, PEMF regulated preosteoblast gene expression and most genes were downregulated including transcriptional regulators, metabolism, proteases, and regulators and also cell adhesion and binding proteins and cytoskeletal and structural proteins. Changes in gene transcription of candidate genes chosen from microarray analyses were verified and confirmed by RT-qPCR on RNA from differentiated hBMSCs from 3 females, aged 24, 27, and 31 years (Table 5). Notably, the TGF-β signaling pathway seems to be most highly regulated by PEMF. In particular, RT-qPCR showed that fibrillin 2 (FBN2) was significantly decreased in expression by 65 ± 14%, while TGF-β2 mRNA significantly increased to 155 ± 44% and TGF-β regulator 1 (TBRG1) mRNA significantly increased to 143 ± 23%, relative to controls. In contrast, in mineralizing cells (Table 6), there was no decrease in FBN2 expression and a lesser significant increase in TGF-β2. It appears that PEMF stimulated a number of components of the TGF-β pathway in differentiating and mineralizing osteoblasts. It is notable that no components of the BMP pathway were seen to be regulated.

Table 2: Genes regulated by PEMF during hBMSCs proliferation by microarray analysis. Cells were from a normal 27-year-old female. Total RNA was isolated at day 5 after 2 h of PEMF treatment and used for microarray assays as described in Materials and Methods. Analysis by Student's t-test.

Gene symbol	Gene title	Fold-change (Avg PEMF versus avg controls)	p
	Cell adhesion and binding and cytoskeletal and structural proteins		
MMP1	Matrix metallopeptidase 1 (interstitial collagenase)	4.57	$2.16E-03$
PRC1	Protein regulator of cytokinesis 1	3.22	$4.34E-04$
CCBE1	Collagen and calcium binding EGF domains 1	2.97	$1.32E-04$
CLDN1	Claudin 1	2.71	$2.26E-04$
CENPK	Centromere protein K	2.40	$5.36E-03$
GAS2L3	Growth arrest-specific 2 like 3	2.39	$4.74E-03$
CLDN11	Claudin 11	2.31	$5.59E-04$
NUSAP1	Nucleolar and spindle associated protein 1	2.16	$5.04E-03$
COL15A1	Collagen, type XV, alpha 1	2.12	$1.64E-04$
HAPLN1	Hyaluronan and proteoglycan link protein 1	2.03	$1.37E-04$
IBSP	Integrin-binding sialoprotein	1.97	$2.17E-03$
FBN2	Fibrillin 2	−1.12	$1.98E-02$
COL14A1	Collagen, type XIV, alpha 1	−2.30	$1.56E-02$
MMP12	Matrix metallopeptidase 12 (macrophage elastase)	−3.27	$1.19E-04$
MGP	Matrix Gla protein	−3.98	$2.80E-06$
	p53 signaling pathway, apoptosis, and survival antiapoptotic TNFs/NF-kB/IAP pathway		
BIRC5	Baculoviral IAP repeat containing 5	3.30	$3.60E-06$
GTSE1	G-2 and S-phase expressed 1	2.48	$1.02E-03$
SESN3	sestrin 3	−2.47	$3.72E-07$
	Cell cycle role of APC (anaphase-promoting complex) in cell cycle regulation, cell cycle/checkpoint control		
CDK1	Cyclin-dependent kinase 1	5.07	$1.01E-03$
CDC20	Cell division cycle 20 homolog (*S. cerevisiae*)	3.00	$3.32E-04$
CCNB2	Cyclin B2	2.41	$1.83E-03$
NDC80	NDC80 kinetochore complex component homolog (*S. cerevisiae*)	2.38	$7.59E-04$
TYMS	Thymidylate synthetase	2.36	$9.43E-05$
CCNB1	Cyclin B1	2.35	$2.17E-03$
NEK2	NIMA- (never in mitosis gene a-) related kinase 2	2.12	$2.19E-02$
CCNA2	Cyclin A2	1.95	$6.42E-03$
TTK	TTK protein kinase	1.95	$1.77E-02$
	Akt signaling		
CCL2	Chemokine (C-C motif) ligand 2	2.83	$6.76E-05$
CSF2RB	Colony stimulating factor 2 receptor, beta, low-affinity	2.31	$2.04E-03$
	Other receptor, kinase, and regulator		
CDKN3	Cyclin-dependent kinase inhibitor 3	2.45	$2.32E-04$
PDGFRA	Platelet-derived growth factor receptor, alpha polypeptide	2.26	$2.52E-05$
CTSC	Cathepsin C	2.14	$5.32E-04$
LEPR	Leptin receptor	−2.19	$1.46E-04$
FGFR2	Fibroblast growth factor receptor 2	−2.04	$8.83E-05$

3.4. PEMF Activation of TGF-β Signaling via Smad2 in Differentiated and Mineralizing Osteoblasts. To validate the PEMF effect on activation of the TGF-β signaling pathway, hBMSCs were subjected to differentiation (day 23) and mineralization (day 33) as described. During differentiation and mineralization, the cells were continuously treated with PEMF for 4 h each day. At days 23 and 33, cells were subjected to control, TGF-β2, or PEMF treatments for 0, 2, and 4 h. TGF-β2 was used as a positive control for activation of TGF-β signaling. Whole cell lysates were prepared and subjected

Table 3: Genes regulated by PEMF in differentiating hBMSCs. Cells were from a normal 27-year-old female. Total RNA was isolated at day 23 of PEMF treatment. Analysis by Student's *t*-test.

Gene symbol	Gene title	Fold-change (Avg PEMF versus avg controls)	*p*
	Transcriptional regulator, RNA metabolism, and RNA transport		
SPEN	Spen homolog, transcriptional regulator (*Drosophila*)	−1.74	2.68*E* − 02
FOXO3, FOXO3B	Forkhead box O3; forkhead box O3B pseudogene	−1.87	3.04*E* − 02
MIR21	MicroRNA 21	1.61	2.92*E* − 02
	Metabolic process		
AKT3	v-akt murine thymoma viral oncogene homolog 3	−1.58	2.39*E* − 02
	Growth factor and regulator		
TBRG1	Transforming growth factor beta regulator 1	1.72	9.85*E* − 03
	Receptor		
LEPR	Leptin receptor	1.55	5.20*E* − 03
	Cell adhesion, motility, and cytoskeletal		
ARPC5	Actin related protein 2/3 complex, subunit 5, 16 kDa	1.50	1.93*E* − 02
FBN2	Fibrillin 2	−1.45	1.47*E* − 02
	Signaling transduction, pathway		
THBS1	Thrombospondin 1	−1.24	1.33*E* − 02

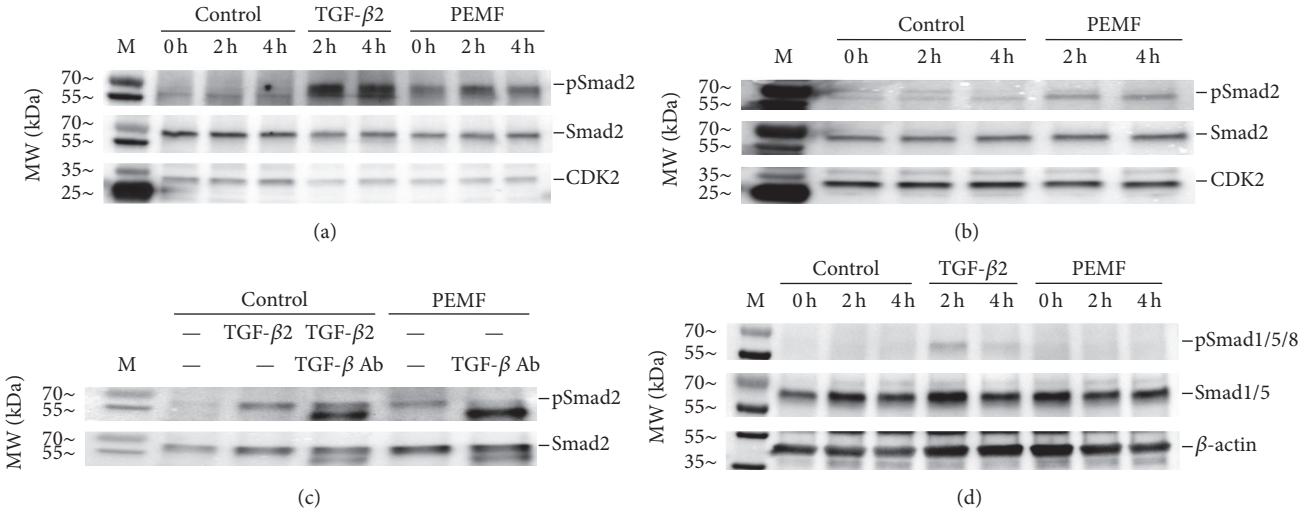

Figure 4: PEMF resulted in activation of the TGF-β signaling pathway in human osteoblastic cells during differentiation and mineralization. (a) Whole cell lysates after PEMF treatment of hBMSCs of a 24-year-old female at day 23 (differentiation) and (b) at day 33 (mineralization) were subjected to Western blot analysis using the antibodies as indicated for Smad2 and Cdk2. TGF-β2 (5 ng/mL) was added to control (non-PEMF-treated) cells on days 23 and 33 as positive controls. (c) The pan-TGF-β neutralizing antibody (30 ug/mL) was added to the osteogenic medium of hBMSCs from a 24-year-old female during the entire differentiation period and lysates were prepared on day 23 of PEMF treatment, 2 h after PEMF was started or TGF-β2 was added and subjected to Western blot analysis. TGF-β2 (5 ng/mL) was added to control (non-PEMF-treated) cells on day 23 as a positive control. Cdk2 was used as loading control. (d) The same lysates were subjected to Western blot analysis for phosphorylation of Smad1/5/8 as indicated.

to Western blot analyses using the antibodies for phosphorylated and total Smad2. The results show that PEMF stimulated activation of Smad2 by increased phosphorylation at day 23 in differentiated osteoblasts (Figure 4(a)) and less at day 33 in mineralizing osteoblasts (Figure 4(b)). To determine the specificity of activation of the TGF-β signaling by PEMF, osteoblasts were pretreated with pan-TGF-β antibody before PEMF treatment. The results show that the PEMF-stimulated Smad2 activation in differentiated osteoblasts (day 23) was blocked when cells were pretreated with pan-TGF-β antibody (Figure 4(c)). Since a recent paper has described a different PEMF signal as acting through the BMP pathway on rat calvarial osteoblasts [18], we examined whether Smad1/5/8 was phosphorylated in response to the Cervical-Stim signal

Table 4: Genes regulated by PEMF in mineralizing hBMSCs. Cells were from a normal 27-year-old female. Total RNA was isolated at day 33 of PEMF treatment. Analysis by Student's *t*-test.

Gene symbol	Gene title	Fold-change (Avg PEMF versus avg controls)	*p*
	Cell adhesion, motility, and cytoskeletal		
COL1A2	Collagen, type I, alpha 2	−1.60	$1.81E-02$
COL3A1	Collagen, type III, alpha 1	−1.61	$9.49E-03$
FN1	Fibronectin 1	−1.93	$2.31E-04$
FBN2	Fibrillin 2	1.38	$2.49E-02$
VIM	Vimentin	−1.67	$1.39E-02$
	Transcriptional regulator, RNA metabolism, and RNA transport		
MIR21	MicroRNA 21	−2.16	$1.28E-02$
HNRNPA1 LOC728844	Heterogeneous nuclear ribonucleoprotein	−1.91	$1.41E-02$
	Cell cycle, cell growth, and apoptosis		
CCNL1	Cyclin L1	−1.79	$1.65E-03$
CCNL2	Cyclin L2	−2.07	$3.18E-03$
	Hormone, growth factor, and cytokine		
CXCL12	Chemokine (CXC motif) ligand 12 stromal cell-derived factor 1	1.60	$3.83E-03$
IL15	Interleukin 15	−1.55	$4.70E-03$
IL8	Interleukin 8	−2.00	$3.71E-02$
TBRG1	Transforming growth factor beta regulator 1	−2.35	$8.96E-03$
TGFB2	Transforming growth factor, beta 2	1.39	$2.75E-02$
	Metabolic process		
INSIG1	Insulin induced gene 1	1.52	$2.36E-02$
	Signaling transduction, pathway		
DAB2	Disabled homolog 2, mitogen-responsive phosphoprotein (*Drosophila*)	−1.62	$3.65E-02$
THBS1	thrombospondin 1	1.52	$3.67E-03$
TIFA	TRAF-interacting protein with forkhead-associated domain	−1.51	$3.02E-03$
	Protease and regulator		
SERPINE1	Serpin peptidase inhibitor, clade E member 1	−2.04	$2.81E-03$
BAG2	BCL2-associated athanogene 2	−1.61	$1.14E-03$

Table 5: Real-time RT-PCR of three different female donor samples' hBMSCs, aged 24, 27, and 31 years in the differentiation stage. Analysis by Student's *t*-test.

Gene symbol	Gene title	Average PEMF/control %	*p*
COL1A1	Collagen, type I, alpha 1	133 ± 24%	$3.90E-02$
COL5A1	Collagen, type V, alpha 1	136 ± 25%	$3.44E-02$
CTNNA1	Catenin (cadherin-associated protein), alpha 1, 102 kDa	124 ± 3%	$8.27E-05$
FOSB	FBJ murine osteosarcoma viral oncogene homolog B	127 ± 33%	$1.11E-01$
SOX11	SRY- (sex determining region Y-) box 11	138 ± 24%	$2.59E-02$
SPP1	Secreted phosphoprotein 1	131 ± 41%	$1.31E-01$
TGFB2	Transforming growth factor, beta 2	155 ± 44%	$4.87E-02$
TBRG1	Transforming growth factor beta regulator 1	143 ± 23%	$1.65E-02$
AKT3	v-akt murine thymoma viral oncogene homolog 3 (protein kinase B, gamma)	74 ± 15%	$2.06E-02$
FBN2	Fibrillin 2	35 ± 14%	$7.38E-04$
IL8	Interleukin 8	56 ± 35%	$4.87E-02$

Table 6: Real-time RT-PCR analysis of three different female donor samples' hBMSCs, aged 24, 27, and 31 years in the mineralization stage. Analysis by Student's t-test.

Gene symbol	Gene title	Average PEMF/control %	p
CDH11	Cadherin 11, type 2, OB-cadherin (osteoblast)	130 ± 36%	$1.10E-01$
COL1A1	Collagen, type I, alpha 1	144 ± 47%	$9.20E-02$
CXCL12	Chemokine (C-X-C motif) ligand 12	146 ± 20%	$8.48E-03$
FBN2	Fibrillin 2	149 ± 54%	$9.82E-02$
FOSB	FBJ murine osteosarcoma viral oncogene homolog B	165 ± 27%	$6.97E-03$
GPC4	Glypican 4	128 ± 25%	$6.23E-02$
IL8	Interleukin 8	162 ± 68%	$9.49E-02$
LEPR	Leptin receptor	130 ± 19%	$2.53E-02$
MMP16	Matrix metallopeptidase 16 (membrane-inserted)	135 ± 68%	$2.07E-01$
SOX11	SRY- (sex determining region Y-) box 11	137 ± 37%	$7.60E-02$
SPP1	Secreted phosphoprotein 1	132 ± 52%	$1.74E-01$
TGFB2	Transforming growth factor, beta 2	128 ± 21%	$3.99E-02$
TBRG1	Transforming growth factor beta regulator 1	113 ± 14%	$9.71E-02$
THBS1	Thrombospondin 1	142 ± 58%	$1.37E-01$

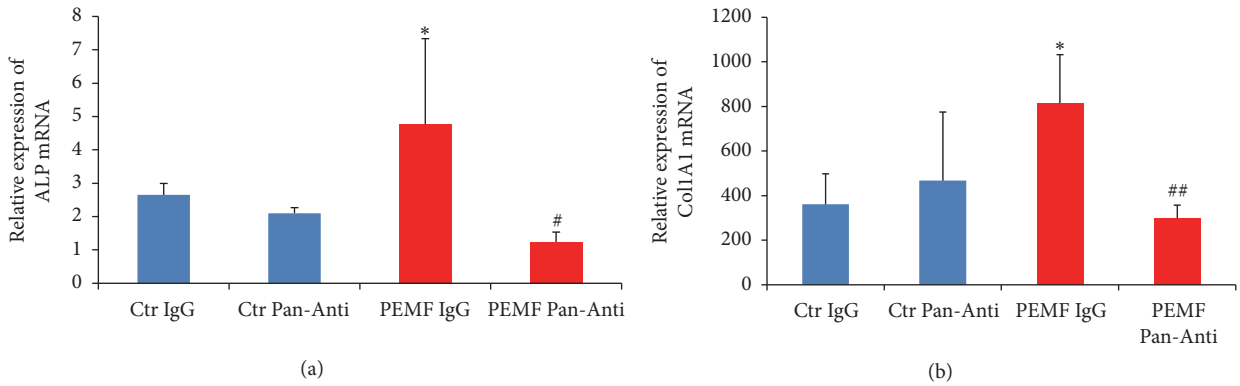

Figure 5: PEMF resulted in stimulation of expression of osteoblast differentiation marker genes via the TGF-β signaling pathway. Differentiated human osteoblasts derived from hBMSCs from a 30-year-old female were used. Total RNA was isolated after incubation with IgG or pan-TGF-β antibody (Pan-Anti) and treatment with control (Ctr) or PEMF and subjected to RT-qPCR using the primers for (a) ALP and (b) collagen 1A1 genes. RPL13 was used to normalize gene expression. $n = 3$. $*$ indicates significant increase compared with control IgG. # indicates significant decrease compared to all groups with ALP mRNA expression; ## indicates significant decrease compared to control or PEMF treatment with IgG incubation with collagen 1A1 mRNA expression; analysis by one-way ANOVA.

in hBMSCs (Figure 4(d)). We were unable to observe any stimulation of this pathway, in contrast to the activation of the Smad2 pathway, even though the strong positive control, TGF-β2, slightly stimulated Smad1/5/8 phosphorylation, as has been observed by others [19, 20].

3.5. PEMF Stimulates Osteoblast Marker Gene Expression by Activation of the TGF-β Signaling Pathway. To determine if TGF-β signaling is responsible for the PEMF effect on expression of osteoblast differentiation marker genes such as ALP and type I collagen, this pathway was inhibited and RNA collected from differentiated osteoblasts at day 23 and subjected to RT-qPCR analysis. We found that PEMF significantly stimulated mRNA expression of ALP (Figure 5(a)) and type I collagen (Figure 5(b)) in differentiated osteoblasts. When cells were pretreated with pan-TGF-β antibody, PEMF stimulation of expression of these genes was significantly decreased (Figures 5(a) and 5(b)). Thus, this result indicates that the osteogenic effect of Cervical-Stim PEMF on hBMSCs is mediated via the TGF-β signaling pathway.

3.6. PEMF Stimulation of miR21-5p Expression in Differentiating Osteoblasts. MicroRNAs are considered to be regulators of osteogenesis and bone formation. The microarray analysis of hBMSCs subjected to differentiation at day 23 identified the stimulation of expression of miR21 (Table 3). To verify this, total RNA was obtained with differentiated hBMSCs from females aged 24 × 2, 27, 29, and 30 (young individuals) and 31, 36, 58, and 68 (older individuals) years and subjected to RT-qPCR. The result shows that the expression of miR21-5p was 155% increased in cells from the younger women but not significantly increased in cells from the older individuals after PEMF treatment (Figure 6).

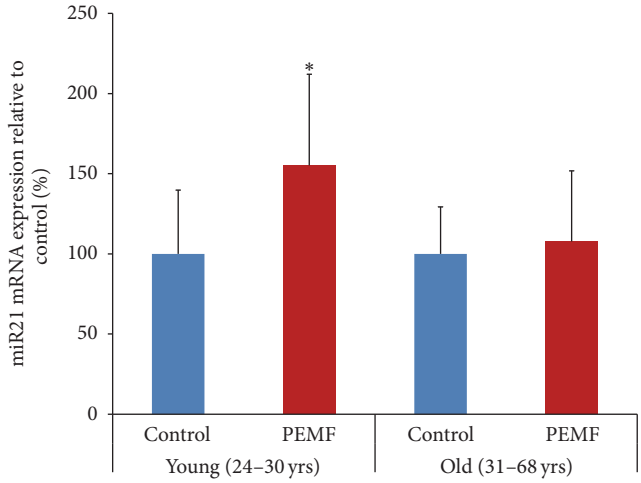

Figure 6: PEMF stimulated expression of miR21-5p in differentiated human osteoblasts. Total RNAs from control or PEMF-treated hBMSCs of females (24 × 2, 27, 29, and 30 years old, $n = 5$) at day 23 of differentiation or (31, 36, 58, and 68 years old) at day 23 or 33 of differentiation were isolated and subjected to RT-qPCR using the miScript II kit with miScript HiSpec Buffer and miScript SYBR Green PCR Kit. snoR10-1 was used to normalize miR21-5p expression and the expression is shown as a percentage of the relevant control samples. ∗ indicates significant increase compared to control using one-way ANOVA.

3.7. PEMF and miR21-5p Stimulation of Osteoblast Differentiation Marker Gene Expression. It is evident that PEMF stimulated miR21-5p expression in differentiated osteoblasts from younger individuals (Figure 6) which strongly suggested a role for miR21-5p in promotion of osteoblast differentiation. To determine this role, hBMSCs were transiently transfected with negative control miRNA or miR21-5p mimic for 3 days and concurrently subjected to 4 h PEMF treatment every day for 6 days. Total RNA was isolated and subjected to RT-qPCR analysis. When cells were treated with PEMF, there was significantly increased ALP mRNA expression. The miR21-5p mimic alone had no effect but together with PEMF treatment caused a significant increase in ALP mRNA expression compared with PEMF treatment alone (Figure 7(a)). With type I collagen mRNA expression, no significant effect was seen with respect to PEMF, miR21-5p mimic, or both treatments under these conditions (Figure 7(b)).

3.8. PEMF Regulation of Smad7 via miR21-5p in Differentiating Osteoblasts. In silico analysis (http://www.microrna.org/microrna/home.do) was used to identify the putative target genes of miR21-5p for its functional importance towards osteogenic commitment. Among them some antagonistic effectors of osteogenesis such as Smad7, Smurf1, and Crim1 were found. The 3′UTR regions of Smad7, Smurf1, and Crim1 held at least 6-nt perfect complementarities to the miR21-5p seed region (Figure 8(a)). To validate these putative target genes of miR21-5p, hBMSCs were transiently transfected with either negative control miRNA or miR21-5p inhibitor and concurrently treated with PEMF for 4 h each day for 3 days. To determine the expression level of these target genes, total RNA was isolated, followed by RT-qPCR analysis. There was no significant change in mRNA expression of Smurf2 (Figure 8(b)) and Crim1 (Figure 8(c)) in the cells in the presence of PEMF treatment, miR21-5p inhibitor, or both. In the case of Smad7, there was a significant decrease in its mRNA expression after PEMF treatment, and inclusion of miR21-5p inhibitor reversed the PEMF effect resulting in increased Smad7 mRNA expression (Figure 8(d)). From these results we suggest that Smad7, an antagonist of TGF-β signaling, is likely to be miR21-5p's target gene and PEMF downregulates its mRNA expression via miR21-5p in differentiating osteoblasts. In fact, at least two groups have shown that the 3′-UTR of Smad7 is, indeed, a target for miR21-5p, resulting in a decrease in Smad7 protein levels [21, 22].

3.9. PEMF Regulation of Runx2 Expression via miR21-5p and Smad7 in Differentiating Osteoblasts. Since Runx2 is required for osteoblast differentiation and PEMF stimulated expression of osteoblast differentiation marker genes (Figure 3), we next examined the PEMF stimulation of expression of Runx2 in differentiating hBMSCs and the role played by miR21-5p. Human BMSCs were transiently transfected with either negative control miRNA or miR-21-5p inhibitor, followed by PEMF treatment. Total RNA was isolated and subjected to RT-qPCR analysis. The result showed that there was a significant increase in expression of Runx2 mRNA in response to PEMF treatment and this effect was blocked by miR21-5p inhibitor in differentiating osteoblasts (Figure 9). From these results, we suggest that PEMF promotes its osteogenic effect via stimulation of miR21-5p expression and activation of TGF-β signaling in hBMSCs. A figure summarizing that the mechanisms we conclude are involved in PEMF stimulation of BMSCs and osteoblast differentiation is shown in Figure 10.

4. Discussion

Numerous studies have shown that mechanical stimulation of bone progenitors including ultrasound [23], mechanical strain [24, 25], and compression as well as shear forces has a stimulatory effect on bone progenitors involved in bone healing of critical size defects and nonunions in vivo. A broad set of investigations has aimed to unravel potential underlying molecular mechanisms and growth factor pathways involved with sophisticated in vitro methods [26]. A number of mechanisms have been proposed by which mechanical cues on different physical scales and identities can incorporate into growth factor signaling [27]. In particular, the major TGF-β growth factor superfamily of ligands (including TGF-β 1 and 2 as well as BMPs) and their downstream signaling via Smad2/3 and Smad1/5/8 transcription factors, respectively [28, 29], appears to be affected by mechanical stimulation in a diverse set of cells, with the majority of research focussing on bone progenitors, for example, BMSCs, osteoblasts, osteocytes, and chondrocytes. This is a large and ongoing field of study.

The molecular mechanisms responsible for the effect of PEMF on bone formation [14, 30] have not been completely elucidated. We found that PEMF promoted preosteoblast proliferation from hBMSCs from individuals up to age 30, but

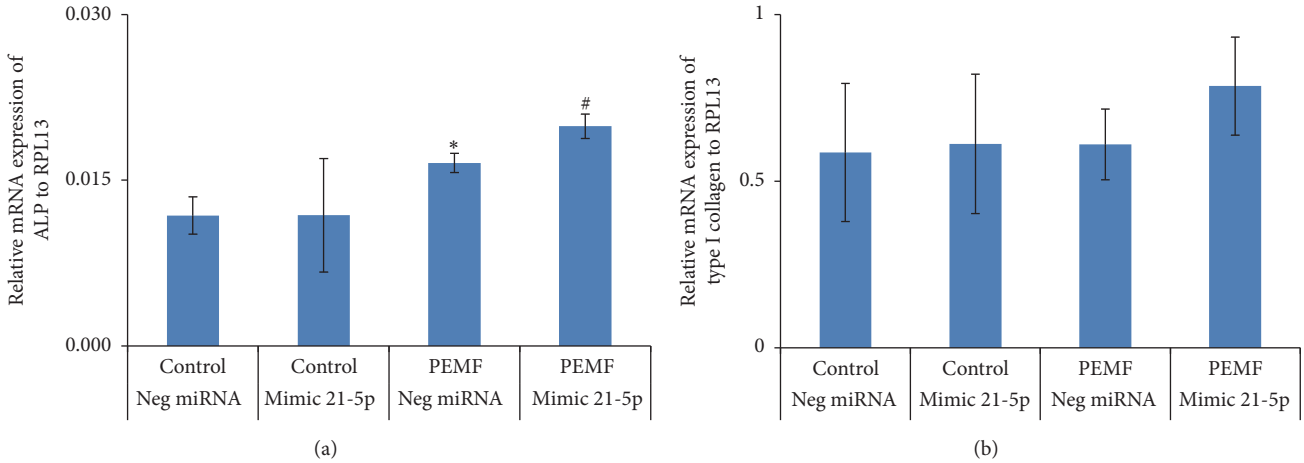

Figure 7: PEMF resulted in stimulation of expression of ALP mRNA and its effect was further enhanced by miR21-5p. Human BMSCs from a 31-year-old female were transiently transfected with 50 nM of negative control miRNA or miR-21-5p mimic for 72 h in osteogenic medium and PEMF treatment was carried out for 4 h each day for a total of 6 days. Total RNA was isolated and RT-qPCR was carried out using the primers for ALP (a) and collagen 1A1 (b) genes. Expression of the mRNAs is shown relative to the RPL13 gene. $n = 3$. $*$ indicates significant increase compared to negative control miRNA transfection. # indicates significant increase compared to all treatments. Analysis by one-way ANOVA.

not older individuals, and stimulated differentiation marker gene expression of mineralizing hBMSCs of all ages. To dissect the mechanisms, PEMF effects on proliferation, differentiation, and mineralization of hBMSCs were examined by Affymetrix microarray analyses. We found that PEMF stimulation of hBMSC proliferation mainly affected genes of cell cycle regulation, cell structure, ECM, and some growth receptors or kinase pathways (Table 2). At the cellular and molecular levels, PEMF has been reported to promote the synthesis of ECM proteins and exert a direct effect on the production of proteins that regulate gene transcription. PEMF may affect several membrane receptors and stimulate osteoblasts to secrete several growth factors such as BMP-2 and BMP-4 and TGF-β. PEMF has been reported to affect osteoblast cellular proliferation and differentiation of bone cells in vitro by enhancing DNA synthesis [14, 31], increasing the expression of bone marker genes during differentiation and mineralization [7], and enhancing calcified matrix production. Several experimental studies also demonstrated that PEMF stimulation could potently promote osteogenesis and enhance bone mineralization both in vivo and in vitro [32–34].

The microarray data for PEMF regulation of differentiation and mineralization of hBMSCs showed regulation of transcriptional regulators, metabolism, proteases, cytokines and growth factors, and also cell adhesion and binding proteins and cytoskeletal and structural proteins (Tables 3 and 4). Identifying the signaling pathways and their associated regulatory mechanisms of PEMF action on osteogenesis might further promote its use in clinical applications. Thus, PEMF regulated preosteoblast gene expression during the differentiation and mineralization stages, and candidate genes chosen from microarray analyses were confirmed by RT-qPCR (Tables 5 and 6). Notably, the TGF-β signaling pathway and miR21 seem to be most highly regulated by PEMF. Thus, in the present study, we systematically investigated the mechanism of action of PEMF effects on osteogenesis via activation of TGF-β signaling and miR21-5p expression using hBMSCs.

The TGF-β/BMP signaling pathway plays a fundamental role in the regulation of bone organogenesis through the activation of receptor serine/threonine kinases. Perturbations of TGF-β/BMP activity are almost invariably linked to a wide variety of clinical outcomes including skeletal anomalies [28]. Phosphorylation of TGF-β (I/II) or BMP receptors activates intracellular downstream Smads, the transducer of TGF-β/BMP signals. In our studies, PEMF (Cervical-Stim) treatment activated only the Smad2 signaling component in differentiated hBMSCs (Figure 4) and activation of this signaling pathway appeared to be essential for PEMF stimulation of early osteoblast differentiation marker genes such as ALP and type I collagen (Figure 5). It is notable that it did not appear to activate the BMP pathway through Smad1/5/8 phosphorylation. The TGF-β/BMP signaling effect may be complex and highly time- and space-specific during skeletal development and bone formation. Very recently, Xie et al. [18] have described a different PEMF signal as operating through the BMP receptor on the primary cilium of rat calvarial osteoblasts in culture. Our accumulated data do not indicate that the BMP pathway is involved in the signaling mechanism of either Spinal-Stim or Cervical-Stim but we cannot rule out that it may have a role if investigated further. This signaling cascade can be modulated by various factors and other pathways [35, 36]. Activation of Wnt/Lrp5/β-catenin or calcium-related mechanisms by PEMF treatment for osteogenic activity have also been reported [37, 38].

Osteoblast differentiation is tightly controlled by several regulators including miRNAs [17, 39, 40] that can regulate expression of genes during differentiation of MSCs towards osteoblasts, resulting in the osteogenic lineage. Differential expression of miRNAs could be responsible for activation

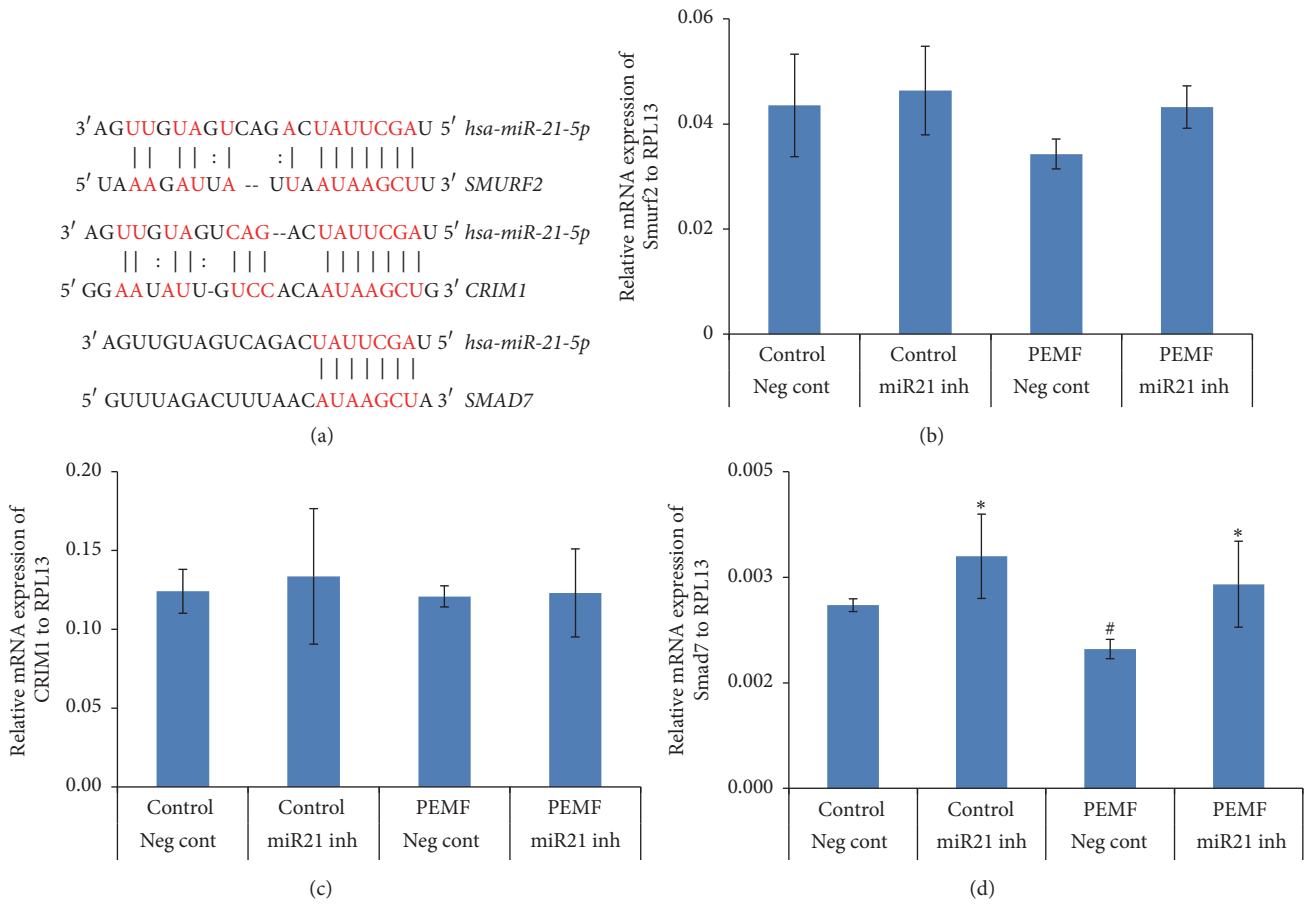

Figure 8: Putative target genes of miR21-5p and PEMF decreases Smad7 mRNA through miR21-5p. (a) The putative target region analysis was performed for Smurf2, Crim1, and Smad7 mRNAs 3′ UTR by miR21-5p seed sequence. ((b)–(d)) Human BMSCs from a 27-year-old female were transiently transfected with 50 nM of negative control miRNA or miR21-5p inhibitor for 72 h in osteogenic medium and PEMF treatment was carried out concurrently for 4 h each day for 3 days. Total RNA was isolated and RT-qPCR was carried out using the primers for (a) Smurf2, (b) Crim1, and (c) Smad7 genes. Expression of mRNAs is shown relative to that of the RPL13 gene. $n = 3$. $*$ indicates significant increase compared to negative control miRNA transfection or PEMF treatment with negative control miRNA transfection. # indicates significant decrease compared to PEMF treatment with miR21-5p inhibitor transfection. Analysis by one-way ANOVA.

of several signaling pathways such as TGF-β/BMP, Wnt/β-catenin, and transcription factors [41]. PEMF stimulated miR21-5p expression in differentiated hBMSCs from younger females (Figure 6) suggesting one of the ways PEMF mediates its osteogenic effect on these cells is via miR21-5p. MicroRNA 21 was one of the first miRNAs detected in the human genome and it was found to be overexpressed in several types of cancer tissues [42]. A role for miR21 in cell proliferation and apoptosis has been reported [43]. With regard to the regulation of bone formation, a number of miRNAs are expressed in the developing skeletal system and miRNA-dependent modulation of gene function can alter skeletal phenotypes across individuals and also within the same individual over time [44]. MicroRNAs might have direct or indirect effects for their regulatory functions in osteoblast differentiation.

To study the functional role of miR21-5p during osteoblast differentiation by PEMF treatment, it was necessary to alter its endogenous expression/activity. Overexpression of miR21-5p (mimic) in differentiated hBMSCs had no effect on mRNA expression of ALP and type I collagen (Figure 7) but required PEMF to have an enhanced effect on ALP mRNA expression which suggests that PEMF could also involve other pathways and molecules in addition to miR21-5p for its osteogenic effects in these cells. The putative targets of miR21-5p can be classified according to their negative contribution in osteogenic differentiation or positive contribution to other lineages using online software. Among them are some key regulators or antagonistic effectors of osteogenesis such as Smad7, Smurf2, and Crim1 and these genes are well documented in their antagonistic roles in osteogenesis [29, 45]. Expression of the putative target genes in the presence of the miR21-5p inhibitor showed a significant increase in Smad7 mRNA expression in differentiated hBMSCs (Figure 8). The inhibitory Smads (Smad6, Smad7) potentially act as suppressors of bone formation. While Smad7 inhibits TGF-β/BMP signaling, Smad6 is less effective in inhibiting TGF-β signaling. It has been reported that Smad7 can inhibit ALP activity and suppress type I collagen mRNA and protein levels [46]. MicroRNA 21 has been shown to be a key regulator

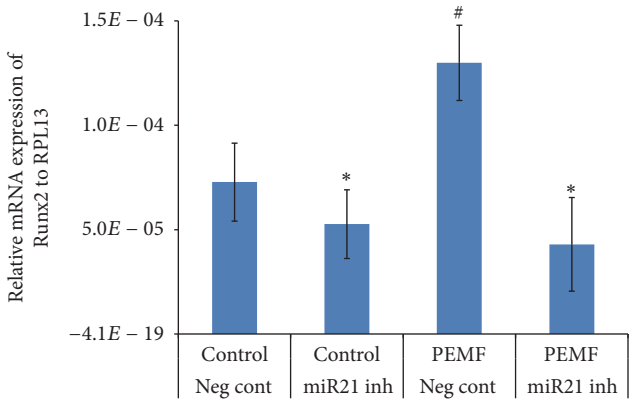

Figure 9: PEMF stimulated Runx2 expression and its effect was downregulated by miR21-5p inhibitor. Human BMSCs from a 27-year-old female were transiently transfected with 50 nM of negative control miRNA or miR21-5p inhibitor for 3 days in osteogenic medium and PEMF treatment was carried out concurrently for 4 h each day for 3 days. Total RNA was isolated and RT-qPCR was carried out using the primers for Runx2. Expression of Runx2 mRNA is shown relative to that of the RPL13 gene. $n = 3$. $*$ indicates significant decrease compared to negative control miRNA transfection or PEMF treatment with negative control miRNA transfection. # indicates significant increase compared to control treatment with negative control miRNA transfection. Analysis by one-way ANOVA.

of TGF-β signaling [47] and Smad7 was found to be one of its target genes [21, 40, 43]. Other target genes such as PTEN and STAT3 have also been reported for miR21 [48, 49]. Based on our results (Figures 7 and 8), we suggest that Smad7 is a target gene for miR21-5p during PEMF regulation of osteoblast differentiation.

Since PEMF stimulates miR21-5p expression in differentiated hBMSCs (Figure 6) and miR21-5p targets Smad7 (Figure 8(d)), the PEMF action on osteogenesis via miR21-5p and Smad7 was further investigated. Runx2 is essential for the commitment of multipotent mesenchymal cells to the osteoblastic lineage. In general, Runx2 activity can be altered by its interacting proteins and/or posttranslational modifications [17, 50–54]. The steady-state protein level of Runx2 can be regulated by E3 ubiquitin ligases, Smurf1 and Smurf2, and it has been reported that the degradation of endogenous Runx2 can be blocked by a proteasomal inhibitor or by Smurf2 siRNA [55]. PEMF stimulated Runx2 mRNA in differentiated hBMSCs, and miR21-5p inhibitor prevented the PEMF stimulation of Runx2 expression (Figure 9). It has already been reported that Smad7 interacts with Smurf2 but it does not interact with Runx2 [56]. Hence, targeting Smad7 through miR21-5p by PEMF could possibly decrease the Smad7-dependent Smurf2 activity, resulting in stabilization of Runx2 protein, and feedback to increased transcription of Runx2 in differentiated hBMSCs. A figure summarizing that the mechanisms we conclude are involved in PEMF stimulation of BMSCs and osteoblast differentiation is shown in Figure 10. We can only speculate as to how PEMF regulates miR21-5p, but others have shown that this microRNA

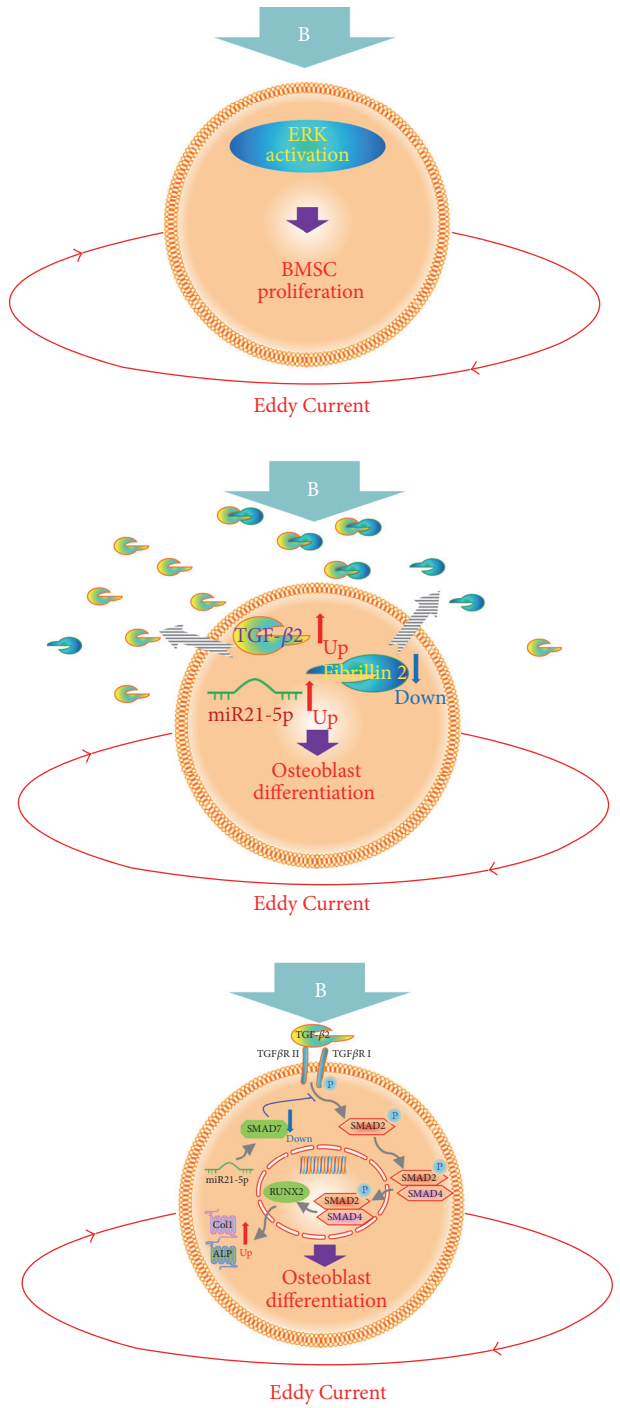

Figure 10: Schema of the mechanisms involved in PEMF stimulation of BMSC proliferation and osteoblast differentiation. The magnetic field (B) is thought to elicit Eddy Currents that act on BMSCs and cause activation of ERKs that are then involved in increased BMSC proliferation. After the BMSCs reach confluence and they are switched to differentiation medium, the magnetic field (B) and the resultant Eddy Currents cause a decrease in fibrillin 2 expression and an increase in TGF-β2 and miR21-5p expression. The decrease in fibrillin 2 would lead to an increase in the amount of available TGF-β2. The increase in miR21-5p appears to cause a decrease in inhibitory Smad7 expression, thus, enhancing TGF-β2 activation of Smad2 with resulting increase in Runx2, collagen I, and alkaline phosphatase expression in the cultures, that is, increased osteoblast differentiation.

is regulated by transcriptional mechanisms, such as by myocardin-related transcription factor-A (58) or by STAT3 (59), and such mechanisms could possibly be implicated in PEMF's actions.

5. Conclusions

Our results show that PEMF significantly stimulated the cell number of preosteoblasts from BMSCs of young women while not stimulating those from women older than 30. We also showed that PEMF regulates a range of genes in hBMSCs to stimulate their proliferation, differentiation, and mineralization. Our further investigation suggests a novel regulatory mechanism of PEMF action during differentiation and mineralization of hBMSCs by activation of the TGF-β signaling pathway. PEMF appears to activate this pathway in hBMSCs of younger women by inhibiting Smad7 expression through miR21-5p and in turn PEMF controls the function of Runx2 resulting in promotion of its osteogenic effect.

Conflicts of Interest

The authors declare that they have no conflicts of interest.

Authors' Contributions

Nagarajan Selvamurugan and Zhiming He contributed equally to the work; Nagarajan Selvamurugan drafted the paper; Nagarajan Selvamurugan, Zhiming He, Daniel Rifkin, and Branka Dabovic contributed to the research design, acquisition, analysis, and interpretation of data; Nicola C. Partridge designed the research, contributed to the analysis and interpretation of the data, and critically revised the paper. All authors have read and approved the final submitted manuscript.

Acknowledgments

This work was supported by a research contract to Dr. Partridge from Orthofix, Inc., Lewisville, TX, USA. Dr. Partridge also received honoraria and travel support from Orthofix, Inc. Dr. Selvamurugan and Mr. He received travel support from Orthofix, Inc. Drs. Rifkin and Dabovic received a subcontract from Dr. Partridge's Orthofix research contract. Drs. James T. Ryaby, Nianli Zhang, and Erik I. Waldorff of Orthofix, Inc., critically reviewed the paper.

References

[1] G. Victoria, B. Petrisor, B. Drew, and D. Dick, "Bone stimulation for fracture healing: what's all the fuss?" *Indian Journal of Orthopaedics*, vol. 43, no. 2, pp. 117–120, 2009.

[2] B. W. Kooistra, A. Jain, and B. Hanson, "Electrical stimulation: nonunions," *Indian Journal of Orthopaedics*, vol. 43, no. 2, pp. 149–155, 2009.

[3] D. E. Garland, B. Moses, and W. Salyer, "Long-term follow-up of fracture nonunions treated with PEMFs," *Contemporary Orthopaedics*, vol. 22, no. 3, pp. 295–302, 1991.

[4] R. J. Linovitz, M. Pathria, M. Bernhardt et al., "Combined magnetic fields accelerate and increase spine fusion: a double-blind, randomized, placebo controlled study," *Spine*, vol. 27, no. 13, pp. 1383–1389, 2002.

[5] V. Mooney, "A randomized double-blind prospective study of the efficacy of pulsed electromagnetic fields for interbody lumbar fusions," *Spine*, vol. 15, no. 7, pp. 708–712, 1990.

[6] T. Bodamyali, B. Bhatt, F. J. Hughes et al., "Pulsed electromagnetic fields simultaneously induce osteogenesis and upregulate transcription of bone morphogenetic proteins 2 and 4 in rat osteoblasts in vitro," *Biochemical and Biophysical Research Communications*, vol. 250, no. 2, pp. 458–461, 1998.

[7] N. Selvamurugan, S. Kwok, A. Vasilov, S. C. Jefcoat, and N. C. Partridge, "Effects of BMP-2 and pulsed electromagnetic field (PEMF) on rat primary osteoblastic cell proliferation and gene expression," *Journal of Orthopaedic Research*, vol. 25, no. 9, pp. 1213–1220, 2007.

[8] N. C. Partridge, Z. He, and N. Selvamurugan, "Microarray analysis of pulsed electromagnetic field (PEMF) stimulatory effects on human bone marrow stromal cells," *Journal of Bone and Mineral Research*, vol. 29, supplement 1, p. 432, 2014.

[9] R. K. Aaron, D. M. Ciombor, and B. J. Simon, "Treatment of nonunions with electric and electromagnetic fields," *Clinical Orthopaedics and Related Research*, no. 419, pp. 21–29, 2004.

[10] D. M. Ciombor and R. K. Aaron, "The role of electrical stimulation in bone repair," *Foot and Ankle Clinics*, vol. 10, no. 4, pp. 579–593, 2005.

[11] P. R. T. Kuzyk and E. H. Schemitsch, "The science of electrical stimulation therapy for fracture healing," *Indian Journal of Orthopaedics*, vol. 43, no. 2, pp. 127–131, 2009.

[12] R. J. Fitzsimmons, J. T. Ryaby, F. P. Magee, and D. J. Baylink, "Combined magnetic fields increased net calcium flux in bone cells," *Calcified Tissue International*, vol. 55, no. 5, pp. 376–380, 1994.

[13] F. M. Pavalko, S. M. Norvell, D. B. Burr, C. H. Turner, R. L. Duncan, and J. P. Bidwell, "A model for mechanotransduction in bone cells: the load-bearing mechanosomes," *Journal of Cellular Biochemistry*, vol. 88, no. 1, pp. 104–112, 2003.

[14] M.-T. Tsai, W. H.-S. Chang, K. Chang, R.-J. Hou, and T.-W. Wu, "Pulsed electromagnetic fields affect osteoblast proliferation and differentiation in bone tissue engineering," *Bioelectromagnetics*, vol. 28, no. 7, pp. 519–528, 2007.

[15] G. Ceccarelli, N. Bloise, M. Mantelli et al., "A comparative analysis of the in vitro effects of pulsed electromagnetic field treatment on osteogenic differentiation of two different mesenchymal cell lineages," *BioResearch Open Access*, vol. 2, no. 4, pp. 283–294, 2013.

[16] K. T. Foley, T. E. Mroz, P. M. Arnold et al., "Randomized, prospective, and controlled clinical trial of pulsed electromagnetic field stimulation for cervical fusion," *Spine Journal*, vol. 8, no. 3, pp. 436–442, 2008.

[17] S. Vimalraj, N. C. Partridge, and N. Selvamurugan, "A positive role of microRNA-15b on regulation of osteoblast differentiation," *Journal of Cellular Physiology*, vol. 229, no. 9, pp. 1236–1244, 2014.

[18] Y. F. Xie, W. G. Shi, J. Zhou et al., "Pulsed electromagnetic fields stimulate osteogenic differentiation and maturation of osteoblasts by upregulating the expression of BMPRII localized at the base of primary cilium," *Bone*, vol. 93, pp. 22–32, 2016.

[19] K. H. Wrighton, X. Lin, P. B. Yu, and X.-H. Feng, "Transforming growth factor β can stimulate Smad1 phosphorylation independently of bone morphogenic protein receptors," *Journal of Biological Chemistry*, vol. 284, no. 15, pp. 9755–9763, 2009.

[20] A. C. Daly, R. A. Randall, and C. S. Hill, "Transforming growth factor β-induced Smad1/5 phosphorylation in epithelial cells is mediated by novel receptor complexes and is essential for anchorage-independent growth," *Molecular and Cellular Biology*, vol. 28, no. 22, pp. 6889–6902, 2008.

[21] L. Lin, H. Gan, H. Zhang et al., "MicroRNA-21 inhibits SMAD7 expression through a target sequence in the 3′ untranslated region and inhibits proliferation of renal tubular epithelial cells," *Molecular Medicine Reports*, vol. 10, no. 2, pp. 707–712, 2014.

[22] Q. Li, D. Zhang, Y. Wang et al., "MiR-21/Smad 7 signaling determines TGF-β1-induced CAF formation," *Scientific Reports*, vol. 3, article 2038, 2013.

[23] F. Padilla, R. Puts, L. Vico, A. Guignandon, and K. Raum, "Stimulation of bone repair with ultrasound," *Advances in Experimental Medicine and Biology*, vol. 880, pp. 385–427, 2016.

[24] J. C. Chen, D. A. Hoey, M. Chua, R. Bellon, and C. R. Jacobs, "Mechanical signals promote osteogenic fate through a primary cilia-mediated mechanism," *FASEB Journal*, vol. 30, no. 4, pp. 1504–1511, 2016.

[25] N. Rosa, R. Simoes, F. D. Magalhães, and A. T. Marques, "From mechanical stimulus to bone formation: a review," *Medical Engineering and Physics*, vol. 37, no. 8, pp. 719–728, 2015.

[26] J. Gao, S. Fu, Z. Zeng et al., "Cyclic stretch promotes osteogenesis-related gene expression in osteoblast-like cells through a cofilin-associated mechanism," *Molecular Medicine Reports*, vol. 14, no. 1, pp. 218–224, 2016.

[27] M. Deng, P. Liu, H. Xiao et al., "Improving the osteogenic efficacy of BMP2 with mechano growth factor by regulating the signaling events in BMP pathway," *Cell and Tissue Research*, vol. 361, no. 3, pp. 723–731, 2015.

[28] M. S. Rahman, N. Akhtar, H. M. Jamil, R. S. Banik, and S. M. Asaduzzaman, "TGF-β/BMP signaling and other molecular events: regulation of osteoblastogenesis and bone formation," *Bone Research*, vol. 3, Article ID 15005, 2015.

[29] G. Chen, C. Deng, and Y.-P. Li, "TGF-β and BMP signaling in osteoblast differentiation and bone formation," *International Journal of Biological Sciences*, vol. 8, no. 2, pp. 272–288, 2012.

[30] Y.-C. Fu, C.-C. Lin, J.-K. Chang et al., "A novel single pulsed electromagnetic field stimulates osteogenesis of bone marrow mesenchymal stem cells and bone repair," *PLOS ONE*, vol. 9, no. 3, Article ID e91581, 2014.

[31] M. De Mattei, A. Caruso, G. C. Traina, F. Pezzetti, T. Baroni, and V. Sollazzo, "Correlation between pulsed electromagnetic fields exposure time and cell proliferation increase in human osteosarcoma cell lines and human normal osteoblast cells in vitro," *Bioelectromagnetics*, vol. 20, no. 3, pp. 177–182, 1999.

[32] K. Chang and W. H.-S. Chang, "Pulsed electromagnetic fields prevent osteoporosis in an ovariectomized female rat model: a prostaglandin E2-associated process," *Bioelectromagnetics*, vol. 24, no. 3, pp. 189–198, 2003.

[33] D. Jing, J. Cai, G. Shen et al., "The preventive effects of pulsed electromagnetic fields on diabetic bone loss in streptozotocin-treated rats," *Osteoporosis International*, vol. 22, no. 6, pp. 1885–1895, 2011.

[34] D. Jing, G. Shen, J. Huang et al., "Circadian rhythm affects the preventive role of pulsed electromagnetic fields on ovariectomy-induced osteoporosis in rats," *Bone*, vol. 46, no. 2, pp. 487–495, 2010.

[35] L. Guo, R. C. H. Zhao, and Y. Wu, "The role of microRNAs in self-renewal and differentiation of mesenchymal stem cells," *Experimental Hematology*, vol. 39, no. 6, pp. 608–616, 2011.

[36] A. Pan, L. Chang, A. Nguyen, and A. W. James, "A review of hedgehog signaling in cranial bone development," *Frontiers in Physiology*, vol. 4, article 61, 2013.

[37] D. Jing, F. Li, M. Jiang et al., "Pulsed electromagnetic fields improve bone microstructure and strength in ovariectomized rats through a Wnt/Lrp5/β-catenin signaling-associated mechanism," *PLoS ONE*, vol. 8, no. 11, Article ID e79377, 2013.

[38] L. Petecchia, F. Sbrana, R. Utzeri et al., "Electro-magnetic field promotes osteogenic differentiation of BM-hMSCs through a selective action on Ca^{2+}-related mechanisms," *Scientific Reports*, vol. 5, article 13856, 2015.

[39] S. Vimalraj and N. Selvamurugan, "MicroRNAs expression and their regulatory networks during mesenchymal stem cells differentiation toward osteoblasts," *International Journal of Biological Macromolecules*, vol. 66, pp. 194–202, 2014.

[40] H. Li, F. Yang, Z. Wang, Q. Fu, and A. Liang, "MicroRNA-21 promotes osteogenic differentiation by targeting small mothers against decapentaplegic 7," *Molecular Medicine Reports*, vol. 12, no. 1, pp. 1561–1567, 2015.

[41] V. Schramke and R. Allshire, "Hairpin RNAs and retrotransposon LTRs effect RNAi and chromatin-based gene silencing," *Science*, vol. 301, no. 5636, pp. 1069–1074, 2003.

[42] M. Ono, K. Yamada, F. Avolio, V. Afzal, D. Bensaddek, and A. I. Lamond, "Targeted knock-down of miR21 primary transcripts using snoMEN vectors induces apoptosis in human cancer cell lines," *PLoS ONE*, vol. 10, no. 9, Article ID e0138668, 2015.

[43] G. Jiao, B. Pan, Z. Zhou, L. Zhou, Z. Li, and Z. Zhang, "MicroRNA-21 regulates cell proliferation and apoptosis in H_2O_2-stimulated rat spinal cord neurons," *Molecular Medicine Reports*, vol. 12, no. 5, pp. 7011–7016, 2015.

[44] X. He, J. K. Eberhart, and J. H. Postlethwait, "MicroRNAs and micromanaging the skeleton in disease, development and evolution," *Journal of Cellular and Molecular Medicine*, vol. 13, no. 4, pp. 606–618, 2009.

[45] L. He, N. Yang, C. M. Isales, and X.-M. Shi, "Glucocorticoid-induced leucine zipper (GILZ) antagonizes TNF-α inhibition of mesenchymal stem cell osteogenic differentiation," *PLoS ONE*, vol. 7, no. 3, Article ID e31717, 2012.

[46] M. Yano, Y. Inoue, T. Tobimatsu et al., "Smad7 inhibits differentiation and mineralization of mouse osteoblastic cells," *Endocrine Journal*, vol. 59, no. 8, pp. 653–662, 2012.

[47] Y. Jeong Kim, S. Jin Hwang, Y. Chan Bae, and J. Sup Jung, "MiR-21 regulates adipogenic differentiation through the modulation of TGF-β signaling in mesenchymal stem cells derived from human adipose tissue," *Stem Cells*, vol. 27, no. 12, pp. 3093–3102, 2009.

[48] B. G. Zhang, J. F. Li, B. Q. Yu, Z. G. Zhu, B. Y. Liu, and M. Yan, "microRNA-21 promotes tumor proliferation and invasion in gastric cancer by targeting PTEN," *Oncology Reports*, vol. 27, no. 4, pp. 1019–1026, 2012.

[49] Y. J. Kim, S. H. Hwang, H. H. Cho, K. K. Shin, Y. C. Bae, and J. S. Jung, "MicroRNA 21 regulates the proliferation of human adipose tissue-derived mesenchymal stem cells and high-fat diet-induced obesity alters microRNA 21 expression in white adipose tissues," *Journal of Cellular Physiology*, vol. 227, no. 1, pp. 183–193, 2012.

[50] J. H. Jonason, G. Xiao, M. Zhang, L. Xing, and D. Chen, "Post-translational regulation of Runx2 in bone and cartilage," *Journal of Dental Research*, vol. 88, no. 8, pp. 693–703, 2009.

[51] N. Selvamurugan, E. Shimizu, M. Lee, T. Liu, H. Li, and N. C. Partridge, "Identification and characterization of Runx2

phosphorylation sites involved in matrix metalloproteinase-13 promoter activation," *FEBS Letters*, vol. 583, no. 7, pp. 1141–1146, 2009.

[52] Y. H. Choi, Y.-J. Kim, H. M. Jeong, Y.-H. Jin, C.-Y. Yeo, and K. Y. Lee, "Akt enhances Runx2 protein stability by regulating Smurf2 function during osteoblast differentiation," *FEBS Journal*, vol. 281, no. 16, pp. 3656–3666, 2014.

[53] C. Ge, W. P. Cawthorn, Y. Li, G. Zhao, O. A. Macdougald, and R. T. Franceschi, "Reciprocal control of osteogenic and adipogenic differentiation by ERK/MAP kinase phosphorylation of Runx2 and PPARγ transcription factors," *Journal of Cellular Physiology*, vol. 231, no. 3, pp. 587–596, 2016.

[54] C. Y. Wang, S. F. Yang, Z. Wang et al., "PCAF acetylates Runx2 and promotes osteoblast differentiation," *Journal of Bone and Mineral Metabolism*, vol. 31, no. 4, pp. 381–389, 2013.

[55] M. Vishal, R. Ajeetha, R. Keerthana, and N. Selvamurugan, "Regulation of Runx2 by histone deacetylases in bone," *Current Protein & Peptide Science*, vol. 17, no. 4, pp. 343–351, 2016.

[56] H. Kaneki, R. Guo, D. Chen et al., "Tumor necrosis factor promotes Runx2 degradation through up-regulation of Smurf1 and Smurf2 in osteoblasts," *Journal of Biological Chemistry*, vol. 281, no. 7, pp. 4326–4333, 2006.

Hindawi
Stem Cells International
Volume 2017, Article ID 3738071, 13 pages
https://doi.org/10.1155/2017/3738071

Research Article

A Conditioned Medium of Umbilical Cord Mesenchymal Stem Cells Overexpressing Wnt7a Promotes Wound Repair and Regeneration of Hair Follicles in Mice

Liang Dong, Haojie Hao, Jiejie Liu, Dongdong Ti, Chuan Tong, Qian Hou, Meirong Li, Jingxi Zheng, Gang Liu, Xiaobing Fu, and Weidong Han

Institute of Basic Medicine Science, College of Life Science, Chinese PLA General Hospital, Beijing 100853, China

Correspondence should be addressed to Xiaobing Fu; fuxiaobing@vip.sina.com and Weidong Han; hanwdrsw69@yahoo.com

Received 26 July 2016; Revised 25 September 2016; Accepted 5 October 2016; Published 27 February 2017

Academic Editor: Giacomina Brunetti

Copyright © 2017 Liang Dong et al. This is an open access article distributed under the Creative Commons Attribution License, which permits unrestricted use, distribution, and reproduction in any medium, provided the original work is properly cited.

Mesenchymal stem cells (MSCs) can affect the microenvironment of a wound and thereby accelerate wound healing. Wnt proteins act as key mediators of skin development and participate in the formation of skin appendages such as hair. The mechanisms of action of MSCs and Wnt proteins on skin wounds are largely unknown. Here, we prepared a Wnt7a-containing conditioned medium (Wnt-CM) from the supernatant of cultured human umbilical cord-MSCs (UC-MSCs) overexpressing Wnt7a in order to examine the effects of this CM on cutaneous healing. Our results revealed that Wnt-CM can accelerate wound closure and induce regeneration of hair follicles. Meanwhile, Wnt-CM enhanced expression of extracellular matrix (ECM) components and cell migration of fibroblasts but inhibited the migratory ability and expression of K6 and K16 in keratinocytes by enhancing expression of c-Myc. However, we found that the CM of fibroblasts treated with Wnt-CM ($HF^{Wnt\text{-}CM}$-CM) can also promote wound repair and keratinocyte migration; but there was no increase in the number of hair follicles of regeneration. These data indicate that Wnt7a and UC-MSCs have synergistic effects: they can accelerate wound repair and induce hair regeneration via cellular communication in the wound microenvironment. Thus, this study opens up new avenues of research on the mechanisms underlying wound repair.

1. Introduction

The skin is the largest organ and functions as a protective barrier against aggression of external microorganisms and dehydration [1]. Skin injury is very common and is associated with a high rate of mortality and morbidity because this type of injury not only abrogates the barrier function of the skin but also alters the perception of pain and temperature and the sense of touch [2, 3]. In humans, problems with wound healing can manifest themselves as delayed wound healing (e.g., in diabetes or radiation exposure), excessive healing (e.g., hypertrophic or keloid scars), or a lack of skin appendages (e.g., hair follicles or sweat glands) [4]. Previously, wound closure as early as possible was the main goal of treatment. With the increasing demand for quality repair of damaged skin, restoration of the anatomy and functions of the skin after wounding (to achieve perfect healing) has become the main focus in the field of wound repair [5, 6]. Thus, there is a need to identify an effective approach to enhancement of wound healing.

Cutaneous wound repair is similar to embryonic skin development in many respects and represents an attempt to restore integrity of the injured tissue [7–9]. However, in the middle and late phases of wound healing, cellular interactions are dominated by the interplay of keratinocytes and fibroblasts; these events gradually shift the microenvironment away from an inflammatory one to a microenvironment that promotes the formation of granulation tissue [10]. Fibroblasts are an important component of the skin and play a crucial role in wound repair by constructing and maintaining the extracellular matrix (ECM) through the production of matrix proteins, metalloproteinases, and relevant inhibitors [11]. However, these properties change in different microenvironments. Studies have shown differences between fibroblasts during development and in adult skin and between undamaged and wounded skin,

including differences in cell migration and in the expression of cytokines and growth factors. Under conditions of hair follicle development, the underlying dermis fibroblasts send signals to the epidermis to form a placode and to induce formation of hair follicles [10, 12]. On the other hand, adult skin does not normally show regeneration of hair follicles, but an exception has been documented in the case of adult mouse skin in response to transgenic Wnt/β-catenin or to wound-induced epidermal activation of Wnt/β-catenin [13]. Thus, a change in the microenvironment plays a key role in hair follicle regeneration. Regenerated hair follicles contain structures called dermal papillae (DP), implying crosstalk between the Wnt-activated epidermis and the dermis in the microenvironment of the wound. Thus, provision of an appropriate microenvironment for wound healing may enhance the crosstalk among cells and between cells and cytokines to achieve the goal of perfect repair.

Mesenchymal stem cells (MSCs) can create a favorable microenvironment for tissue regeneration through the secretion of a variety of prosurvival and promigratory cytokines and growth factors after MSC transplant [14–16]. Research shows that MSC-conditioned medium (MSC-CM) can enhance migration of fibroblasts and keratinocytes according to scratch assays in vitro [17]. Another study showed that MSC-CM by providing a type of pigment epithelium-derived factor (PEDF) can stimulate migration of fibroblasts to injured tissues; these cells release cytokines and ECM molecules modulating the growth of parenchymal cells and scar healing [18]. Furthermore, another study showed that MSC-CM can decrease high glucose (HG) and/or lipopolysaccharide- (LPS-) induced overproduction of reactive oxygen species and activation of the extracellular signal-regulated kinase (Erk) signaling pathway, thereby promoting proliferation and migration of keratinocytes by creating a diabetes-like microenvironment [19]. Thus, depending on various disease-related microenvironments, preconditioning of MSCs by physical, chemical, and genetic methods is necessary to maximize their therapeutic potential in wound repair.

Wnt proteins are key mediators of skin development and participate in various processes, from the development of the dermis to formation of skin appendages such as hair [20, 21]. The studies have shown that hair follicle neogenesis can be induced in 1 cm^2 (or larger) full-thickness wounds in mice: further, when Wnt7a is overexpressed, the number of hair follicles in the wound increases [13]. Thus, Wnt signaling in the process of wound repair may provide a microenvironment similar to that present at the developmental stage of the skin; several lines of evidence indirectly support a role for Wnt signaling in cutaneous repair [22]. In contrast, an inhibitory effect of β-catenin on reepithelialization has been suggested in a study that showed enhanced epidermal nuclear accumulation of β-catenin at the edge of chronic ulcers and that pharmacological stabilization of β-catenin inhibits keratinocyte migration by increasing c-Myc expression [23]. However, the combined effects of Wnt and MSCs in wound repair are still unclear.

Here, we prepared CM from the supernatant of cultured Wnt7a-overexpressing umbilical cord- (UC-) MSCs (Wnt-CM) and evaluated its effect on cutaneous healing in mice. Our results suggest that Wnt-CM can enhance the expression of ECM components and cell migration of fibroblasts and thereby accelerate wound closure and hair follicle regeneration, but it inhibits the migratory ability of keratinocytes. In contrast, $HF^{Wnt\text{-}CM}$-CM (fibroblasts treated with Wnt-CM) can accelerate wound closure and promote keratinocyte migration; however, the number of hair follicles did not increase compared to the control group. These results indicate that Wnt7a overexpression by UC-MSCs can enhance wound repair and induce hair regeneration through changes in the wound microenvironment that affect cell-cell interactions.

2. Materials and Methods

2.1. Ethics Statement. Human UC samples were obtained from a hospital after delivery of full-term infants. Human skin samples were selected by experienced plastic surgeons and collected during reconstructive procedures. All human skin tissues and human UCs were collected according to the protocol approved by the Ethics Committee of the Chinese PLA General Hospital, and informed consent forms were signed by the donors.

Six-week-old male C57BL/6 mice were obtained from the Chinese PLA General Hospital. The protocol of animal experiments was approved by the medical Ethics Committee of the Chinese PLA General Hospital.

2.2. Amplification and Purification of Retroviral Vectors. Human Wnt7a cDNA (NM_004625, Origene, BJ, CHN) was inserted between the *Mlu*I and *Sal*I sites of a retroviral vector (PWPT, from Shanghai Institute of Biochemistry and Cell Biology; researcher Xin Wang). Recombinant vectors were amplified in HEK 293T cells and then purified using polyethylene glycol (PEG) 6000 by the precipitation method. The viral particles expressing Wnt7a were resuspended in phosphate-buffered saline (PBS) and stored at −80°C.

2.3. Isolation of UC-MSCs and Preparation of Wnt-CM. Wharton's jelly from UCs was excised, minced into pieces of 0.5–1.0 mm^3 using scissors and scalpels, and washed twice with PBS. UC-MSCs were isolated and harvested as previously described [24]. The cells were then purified and identified. Passage-3 MSCs were cultured to 50–60% confluence in T-75 culture flasks and incubated with a medium containing the Wnt7a-expressing virus combined with polybrene (8 mg/mL). This medium was added to the flask, replenished with 12 mL of serum-free DMEM (Gibco, NY, USA) and incubated for 24 hours prior to harvesting of the CM of the cells infected with the Wnt7a-expressing virus (Wnt-CM). The culture supernatant was collected from passage-3 UC-MSCs and named MSC-CM. The CM was centrifuged at 3,000 rpm/min for 10 minutes at 4°C to remove the cell debris and then was concentrated 20-fold by dialysis in a bag of a tangential flow microfiltration membrane (4-kDa molecular weight cutoff; Sartorius, GER) at 4°C.

Table 1: List of sequences of forward and reverse primers.

Genes	Species	Forward primer	Reverse primer
α-SMA	Human	5′-CTATGAGGGCTATGCCTTGCC-3′	5′-GCTCAGCAGTAGTAACGAAGGA-3′
Collagen I	Human	5′-GTGCGATGACGTGATCTGTGA-3′	5′-CGGTGGTTTCTTGGTCGG-3
Collagen III	Human	5′-TTGAAGGAGGATGTTCCCATCT-3′	5′-ACAGACACATATTTGGCATGGT-3′
K6	Human	5′-ACGGAAACTACTACGGCGAC-3′	5′-GGCCTTCGTATCCACAGCAC-3′
K16	Human	5′-GACCGGCGGAGATGTGAAC-3′	5′-CTGCTCGTACTGGTCACGC-3′
C-Myc	Human	5′-AATAGAGCTGCTTCGCCTAGA-3′	5′-GAGGTGGTTCATACTGAGCAAG-3′
GAPDH	Human	5′-CTGGGCTACACTGAGCACC-3′	5′-AAGTGGTCGTTGAGGGCAATG-3′
α-SMA	Mouse	5′-GTCCCAGACATCAGGGAGTAA-3′	5′-TCGGATACTTCAGCGTCAGGA-3′
Collagen I	Mouse	5′-GCTCCTCTTAGGGGCCACT-3′	5′-CCACGTCTCACCATTGGGG-3′
Collagen III	Mouse	5′-CTGTAACATGGAAACTGGGGAAA-3′	5′-CCATAGCTGAACTGAAAACCACC-3′
GAPDH	Mouse	5′-AGGTCGGTGTGAACGGATTTG-3′	5′-TGTAGACCATGTAGTTGAGGTCA-3′

PCR amplification conditions on the Applied Biosystems 7500 Real-Time PCR System: 58°C for 5 minutes; 95°C for 2 minutes; 40 cycles of 95°C for 15 seconds and 60°C for 60 seconds.

2.4. ELISA. Wnt7a levels were measured by enzyme-linked immunosorbent assay (ELISA) according to the manufacturer's instructions (BioTek, VT, USA).

2.5. Preparation, Isolation, and Cultivation of Fibroblasts and Keratinocytes. Normal human skin keratinocytes and human fibroblasts (HFs) were derived from adult skin obtained from surgical waste, as previously described [25, 26]. Fibroblasts obtained from the outgrowth of explant cultures were grown in DMEM (Gibco, NY, USA) supplemented with 10% fetal bovine serum (Gibco, NY, USA), and cells from passage 3 were used for the experiments. Keratinocytes were cultured in the EpiLife medium (Gibco, NY, USA) at 37°C in a humidified atmosphere containing 5% of CO_2. The medium was replaced every 2 to 3 days.

2.6. Preparation of the CM of Fibroblasts. The culture supernatant was collected from HFs (passage 3) as HF-CM. We used MSC-CM and Wnt-CM for the treatment of fibroblasts for 24 hours after removal of the supernatant; we then added a fresh culture medium after 48 hours and collected the supernatant to prepare $HF^{MSC\text{-}CM}$-CM and 20-fold concentrated $HF^{Wnt\text{-}CM}$-CM.

2.7. The Use of the CM In Vitro. After cultivation of fibroblasts or keratinocytes, the CM (20-fold concentrated) was added to DMEM (the CM and DMEM were mixed in the 1 : 10 ratio, v/v).

2.8. RNA Isolation and Real-Time RT-PCR. Total RNA was isolated using the RNeasy Mini Kit (Qiagen, CA, USA). Single-stranded cDNA was synthesized using SuperScript II reverse transcriptase and oligo (dT) (Invitrogen, CA, USA). Quantitative RT-PCR was used to measure transcription of genes, and the data were normalized to glyceraldehyde 3-phosphate dehydrogenase (GAPDH). PCR was run on an ABI 7500 Real-Time PCR System (Applied Biosystems, USA) under the following cycling conditions: one cycle of 95°C for 10 min and 40 cycles of 95°C for 15 s and 60°C for 1 min, with the primers shown in Table 1. Relative mRNA expression was calculated by $2^{-\Delta\Delta Ct}$ method.

2.9. Western Blot Analysis. Western blotting was performed as previously described [27]. Total protein was isolated from MSCs and from retrovirally infected MSCs. Primary antibodies were a rabbit polyclonal antibody to Wnt7a, c-Myc, K6, and K16 and a mouse monoclonal antibody to GAPDH (Abcam, MA, UK). The secondary antibodies were goat anti-rabbit and goat anti-mouse IgG antibodies (horseradish peroxidase-conjugated; Abcam, MA, UK). The blots were analyzed by densitometry in the ImageJ software (NIH, MD, USA).

2.10. Immunocytochemistry. For the immunocytochemical analysis, cells were fixed in 4% paraformaldehyde for 30 min at 4°C and then permeabilized by 0.1% Triton X-100 for 15 min, followed by blocking with 3% fetal bovine serum for 30 min. Primary antibodies: rabbit polyclonal antibodies to Wnt7a and α-SMA (Abcam, MA, UK) were incubated with the cells overnight at 4°C. Secondary antibodies: an Alexa Fluor 594-conjugated goat anti-rabbit IgG antibody and an Alexa Fluor 488-conjugated goat anti-mouse IgG antibody (Invitrogen, CA, USA) were added to the cells and incubated for 1 h at 37°C. Finally, the cells were stained with Hoechst (Vector, Burlingame, CA) at a 1 : 3000 dilution and were examined under a fluorescence microscope (Olympus BX53, JP).

2.11. The Animal Model. We used 6-week-old C57BL/6 mice as a model of the full-thickness skin injury. After anesthesia, 1 cm diameter wounds were created on the back skin of the mice; then, 100 μL of Wnt-CM, MSC-CM, DMEM (Gibco BRL, NY, USA), $HF^{MSC\text{-}CM}$-CM, or $HF^{Wnt\text{-}CM}$-CM was injected at multiple points into the wound area.

2.12. Histological Analysis. The wounded skin from each mouse was collected for histological analysis. The samples were fixed in 10% formalin and then embedded in paraffin blocks to prepare paraffin sections (4 μm thick). The general histological features were visualized by hematoxylin and eosin (H&E) staining and were examined under a microscope (Olympus BX53JP).

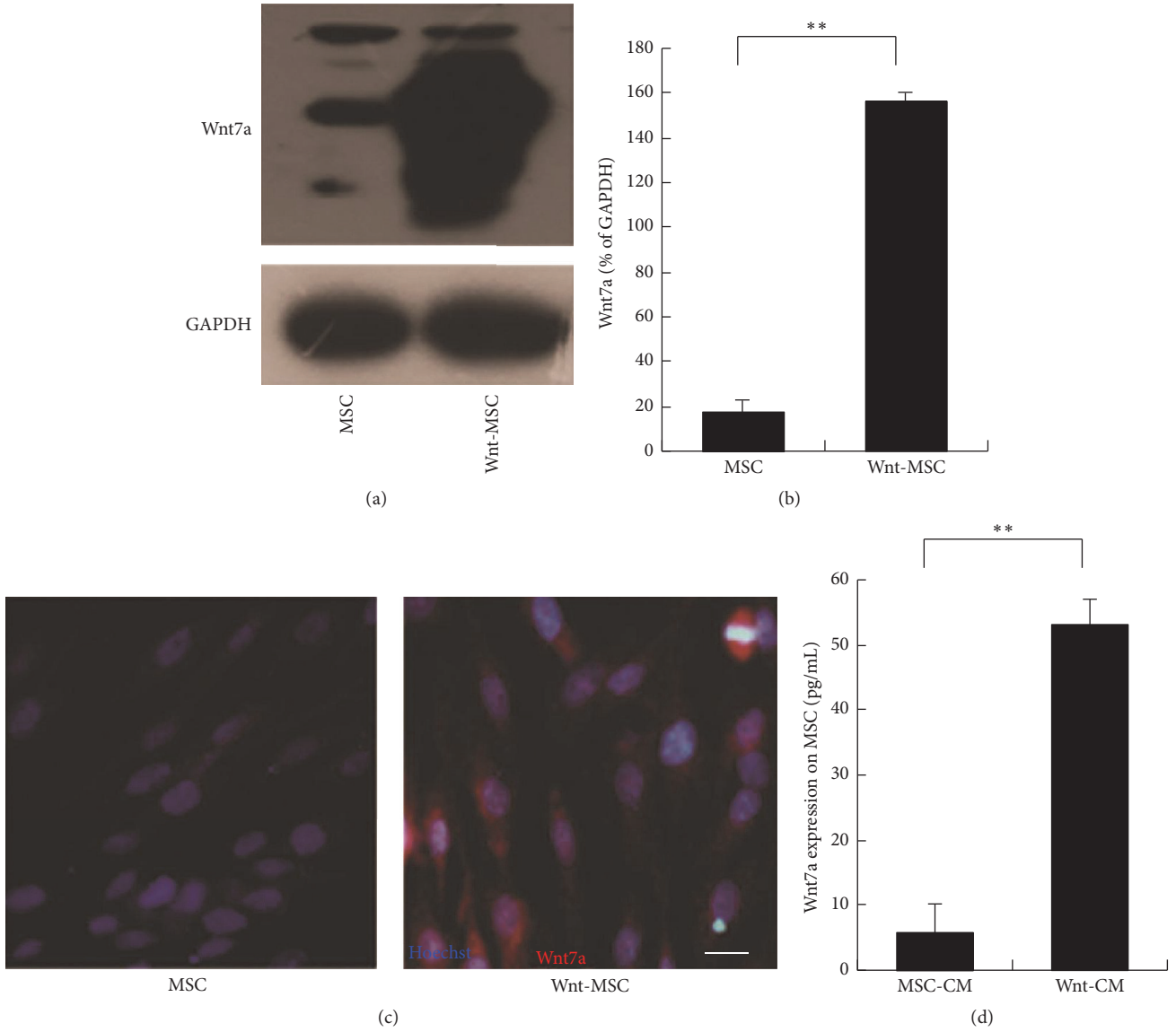

Figure 1: Wnt7a expression in human MSCs. (a, b) Western blots of Wnt7a and corresponding semiquantitative analysis. (c) Immunocytochemical analysis of MSCs overexpressing Wnt7a. The nuclei were counterstained with Hoechst. (d) Wnt7a was quantified in the CM by ELISA. The data are presented as mean ± SEM, $n = 3$; $^{**}P < 0.01$. In the images, Wnt7a (red fluorescence) and Hoechst (blue fluorescence) staining are shown. The scale bar in panel (b) is 20 μm.

2.13. The Cell Scratch Experiment. Fibroblasts and keratinocytes were seeded in 6-well plates at 5×10^5/well. When the cells covered the bottom of the well, a scratch was made with a sterilized P1000 pipette tip (width 1.0–1.2 mm), and the cells then were cultured in different media after a wash with PBS. After 24 h, the scratches were analyzed by microscopy (Olympus BX53, JP), and the scratch area was measured in the IPP software (Media Cybernetics).

2.14. Statistics. The results are expressed as mean ± SEM. All experiments were repeated three times with independent cultures, and similar results were obtained. Statistical significance was assessed using Student's *t*-test. Statistical significance was assumed for P values <0.05 or <0.01.

3. Results

3.1. Wnt7a Overexpression in UC-MSCs. A retroviral vector was constructed to express Wnt7a and was propagated in HEK293 cells. We purified the retrovirus to use it for the induction of Wnt7a expression in UC-MSCs by means of polybrene exposure. The retrovirus-mediated transduction of Wnt7a into UC-MSCs was confirmed by Western blotting and immunocytochemistry. Expression levels of the Wnt7a protein were higher in these UC-MSCs (Figures 1(a) and 1(b)). The immunocytochemical analysis also showed that the retrovirus-mediated transduction of Wnt7a into UC-MSCs made these cells positive for Wnt7a expression (Figure 1(c)). We detected the expression of Wnt7a in the culture supernatant by enzyme-linked immunosorbent assay (ELISA). The

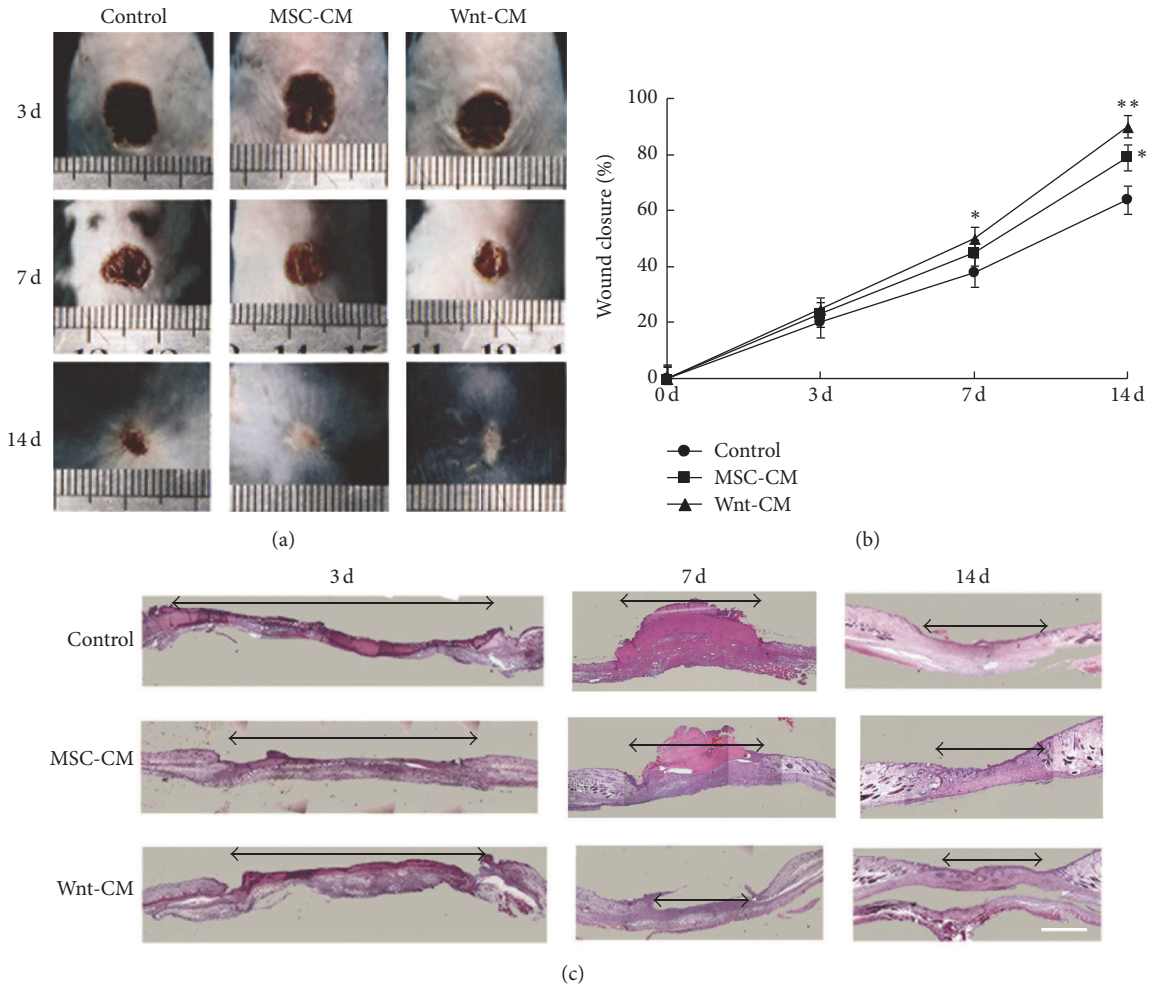

Figure 2: Topical injection of Wnt-CM accelerated healing of full-thickness skin wounds in mice. (a) Typical images of dorsal skin showing effectiveness of wound closure in the mice of treatments groups DMEM, MSC-CM, and Wnt-CM. (b) The percentage of wound closure on days 3, 7, and 14 after the surgical injury. (c) On postinjury days 3, 7, and 14, healing skin was examined by H&E staining of the tissue slices. The data are presented as mean ± SEM, $n = 3$; $^{*}P < 0.05$ and $^{**}P < 0.01$. The double arrow line denotes the wound area. The scale bar is 500 μm in panel (c).

results showed that the level of secreted Wnt7a protein (as a result of the retroviral-mediated transduction of Wnt7a into UC-MSCs) was significantly increased as compared to that in the control group (Figure 1(d)). These data showed that Wnt7a was successfully expressed in UC-MSCs and was secreted into the supernatant of the cultured UC-MSCs.

3.2. Wnt-CM Enhances Healing of Full-Thickness Skin Wounds in Mice. A model of healing of a full-thickness skin wound was used to estimate the effects of topical application of Wnt-CM on wound healing. We collected the culture medium from Wnt7a-overexpressing UC-MSCs and prepared Wnt-CM through tangential flow concentration (20-fold). Then, 100 μL of Wnt-CM was injected subcutaneously at multiple points into the wound area of each mouse, with the same dose of MSC-CM or Dulbecco's modified Eagle's medium (DMEM) serving as control. The wound closure rates in the Wnt-CM-treated mice on postinjury days 3, 7, and 14 were 25.3%, 51.6%, and 91.5%, respectively ($P < 0.05$, $n = 3$), whereas in MSC-CM-treated mice they were 22.9%, 44.3%, and 76.3% ($P < 0.05$, $n = 3$), and in DMEM-treated mice these rates were 20.1%, 38.7%, and 65.1% ($P < 0.05$, $n = 3$; Figures 2(a) and 2(b)). The results showed that Wnt-CM significantly enhanced the closure rates in comparison with MSC-CM, but the MSC-CM treatment group showed better results than did the DMEM treatment group. Similarly, H&E-stained histological slices of skin samples showed similar closure rates on postinjury days 3, 7, and 14 (Figure 2(c)). Thus, the results showed that Wnt-CM can enhance wound repair in mice.

3.3. Wnt-CM Enhances Expression of ECM Components and Migration of Fibroblasts. Injury to the skin resulting in a wound is known to trigger a repair process that is characterized by major alterations in both the composition and structure of the ECM. Accordingly, mRNA expression levels of ECM-related molecules were then evaluated. Compared to the DMEM treatment group, the MSC-CM and Wnt-CM

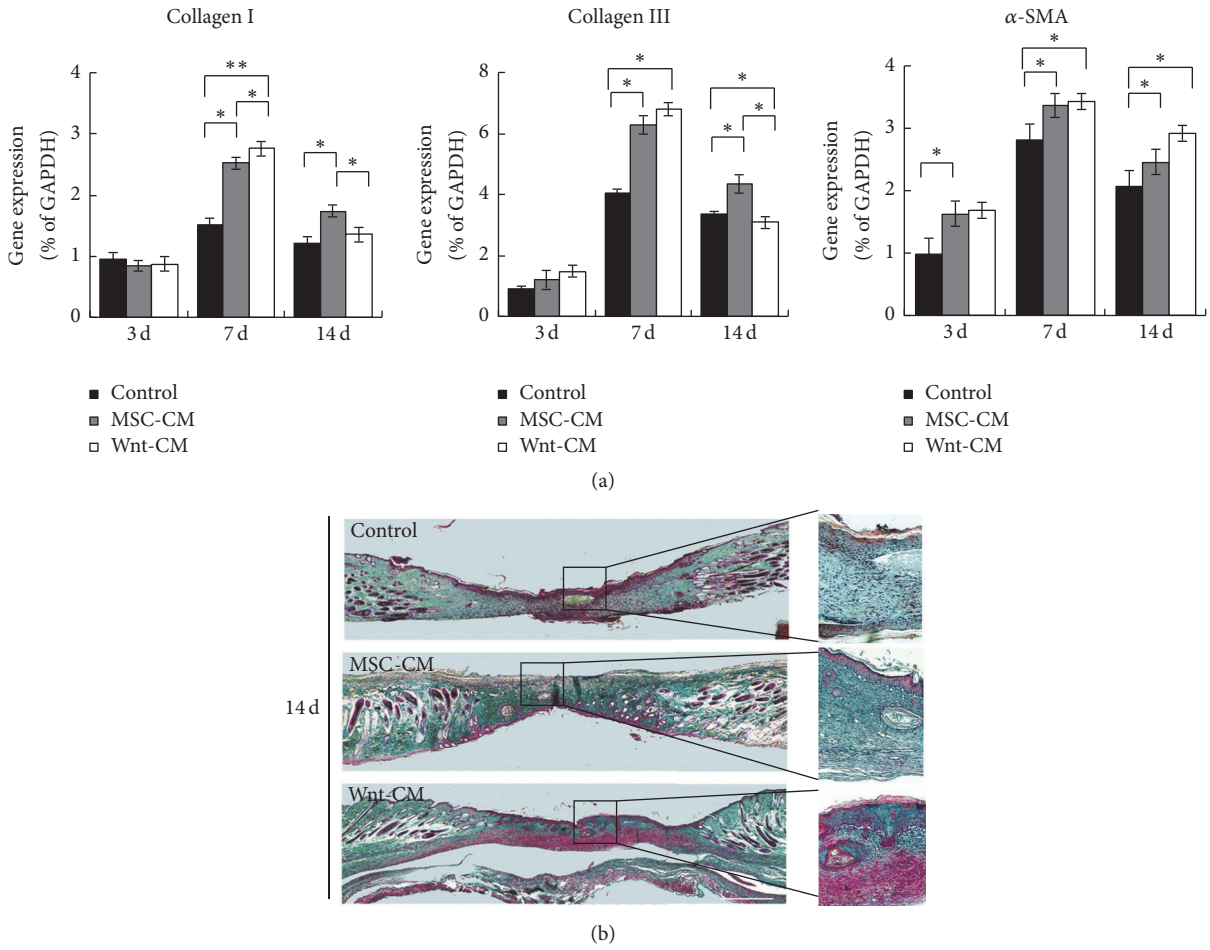

Figure 3: Expression of ECM components during the wound healing process in mice. (a) Expression levels of α-SMA, collagen III, and collagen I mRNA in mice of treatment groups DMEM, MSC-CM, and Wnt-CM were analyzed by real-time PCR and normalized to that of GAPDH. (b) Representative images of skin biopsy samples (obtained from mice of treatment groups DMEM, MSC-CM, and Wnt-CM), showing staining with Masson's trichrome. Statistical analysis involved unpaired t tests. The data are presented as mean ± SEM, $n = 3$; $^{*}P < 0.05$ and $^{**}P < 0.01$. The scale bar is 200 μm in panel (b).

treatment groups expressed significantly larger amounts of ECM molecules in the wound area, including α-SMA, collagen I, and collagen III (Figure 3(a)). To evaluate collagen accumulation in the skin, we used Masson's trichrome staining. The results showed that Wnt-CM markedly increased collagen deposition in the dermis compared with MSC-CM and DMEM (Figure 3(b)). Therefore, these findings indicate that Wnt-CM efficiently enhances wound healing-related events, such as collagen production.

The functional role of Wnt-CM in fibroblasts was analyzed in vitro. Human dermal fibroblasts (HFs) were obtained from surgical waste (adult skin samples) and were incubated with DMEM, MSC-CM, or Wnt-CM. A scratch wound assay showed that Wnt-CM accelerated migration of HFs into the wound area in comparison with MSC-CM and DMEM at 24 hours after scratching (Figures 4(a) and 4(c)). Therefore, we next tested the expression of migration-related genes of fibroblasts. We found that Wnt-CM can significantly increase expression of the smooth muscle cell actin isoform called -smooth muscle actin (α-SMA), collagen I, and collagen III in HFs as compared to DMEM and MSC-CM (Figures 4(b) and 4(d)). Overall, these results indicate that Wnt-CM significantly enhanced migration and ECM expression of fibroblasts.

3.4. Wnt-CM Enhances Reepidermalization during Skin Healing in Mice. To elucidate the effects of Wnt-CM on reepidermalization during skin healing, epithelial-tongue length and epidermal thickness of skin wounds were examined by histomorphological analysis on postinjury days 3, 7, and 14. The Wnt-CM treatment group yielded significantly better results than did the MSC-CM and DMEM groups on postinjury days 3 and 7, but the MSC-CM group showed better results than did the DMEM group (Figures 5(a) and 5(d)). Mice treated with Wnt-CM had a thicker epidermis with more organized cell layers as compared to the DMEM group on postinjury day 14 (Figures 5(b) and 5(e)). The Wnt-CM treatment group also showed regeneration of more hair follicles as compared to the MSC-CM treatment group (Figures 5(c) and 5(f)). These results confirmed that Wnt-CM can substantially increase epidermal thickness and the number of migrating cells in the epithelial-tongue area.

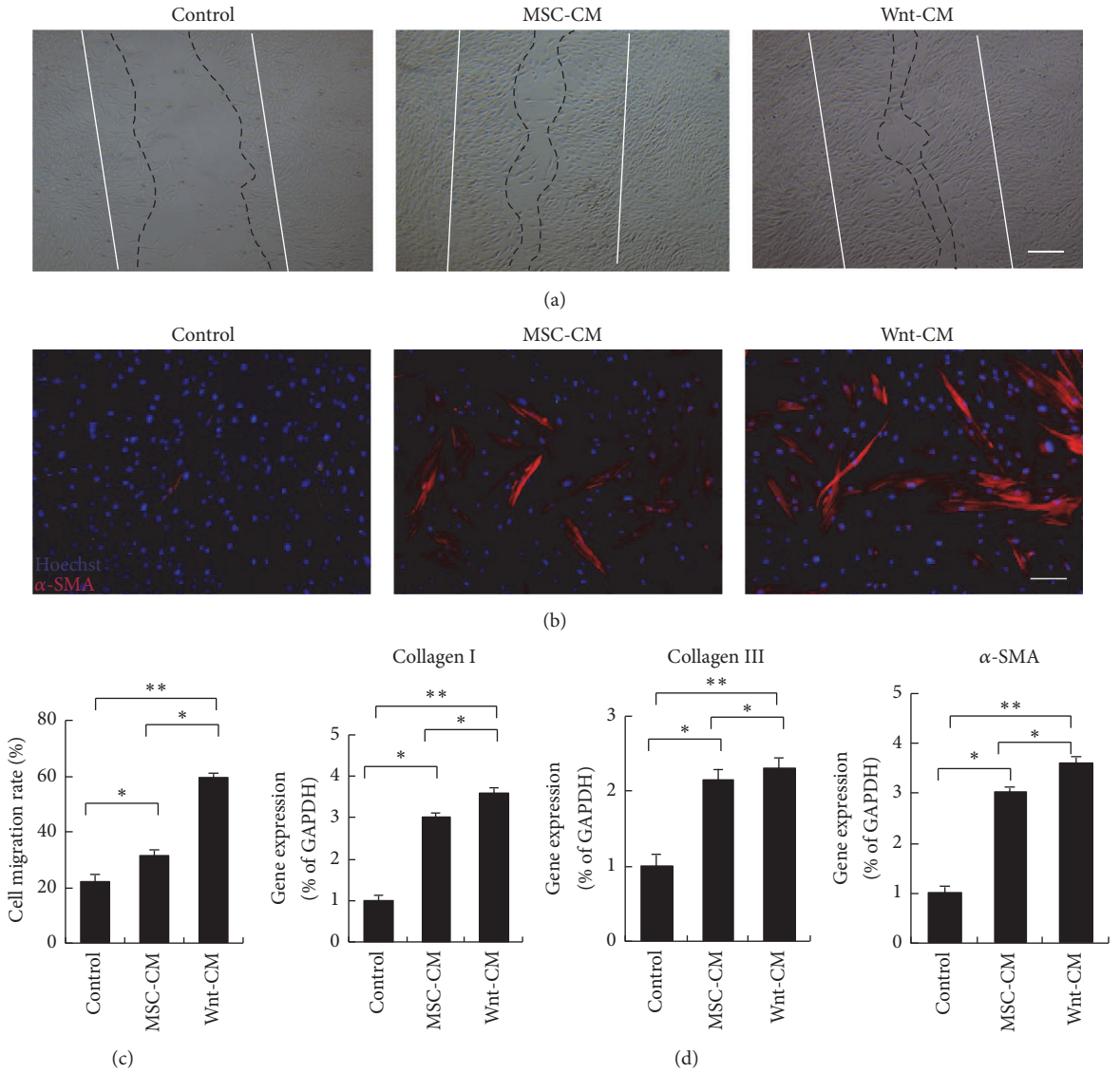

Figure 4: Wnt-CM stimulates migration and promotes expression of α-SMA and ECM components in fibroblasts. (a) Wnt-CM enhanced migration of primary human fibroblasts in a wound scratch assay (after 24 h) as compared to MSC-CM and DMEM. (b) Immunocytochemical staining for α-SMA shows upregulation of α-SMA induced by Wnt-CM. (c) Quantification of optical density of the immunocytochemical staining for α-SMA. (d) Expression levels of α-SMA, collagen III, and collagen I mRNA after treatment with DMEM, MSC-CM, or Wnt-CM were analyzed by RT-PCR and normalized to that of GAPDH. The data represent mean ± SEM, $n = 3$; $^{*}P < 0.05$ and $^{**}P < 0.01$. Solid lines indicate the initial wound area; dotted lines demarcate the migrating front of the cells. The scale bar is 100 μm in panel (a) and 50 μm in panel (b).

3.5. The Inhibitory Effects of Wnt-CM on Keratinocyte Migration Are Mediated by c-Myc. To demonstrate the effects of Wnt-CM on keratinocyte migration, scratch wound assays were performed. Keratinocyte migration was significantly retarded by Wnt-CM treatment as compared to either MSC-CM or DMEM treatment at 24 hours after scratching (Figures 6(a) and 6(b)). c-Myc can impair migration of basal keratinocytes and inhibit wound healing [23]. Accordingly, we assessed mRNA and protein expression levels of c-Myc at 48 hours (Figures 6(c) and 6(e)). Our results showed that c-Myc expression in the wound area was significantly higher in the Wnt-CM treatment group than in the MSC-CM and DMEM treatment groups at 48 hours. Next, the cytoskeletal components important for migration (K6 and K16) were analyzed by RT-PCR and Western blot. Wnt-CM significantly inhibited the expression of K6 and K16 at 48 h after scratching (Figures 6(d)–6(f)). These results suggested that Wnt-CM inhibits the migratory ability and cytoskeletal organization of keratinocytes by increasing the expression of c-Myc.

3.6. Wnt-CM Causes Fibroblasts to Promote Keratinocyte Migration and Expression of Cytoskeletal Proteins. The early stage of wound healing is infiltration of fibroblasts into the damaged area where they synthesize collagen and form the ECM; the crosstalk between fibroblasts and keratinocytes facilitates wound closure. Therefore, we tested whether

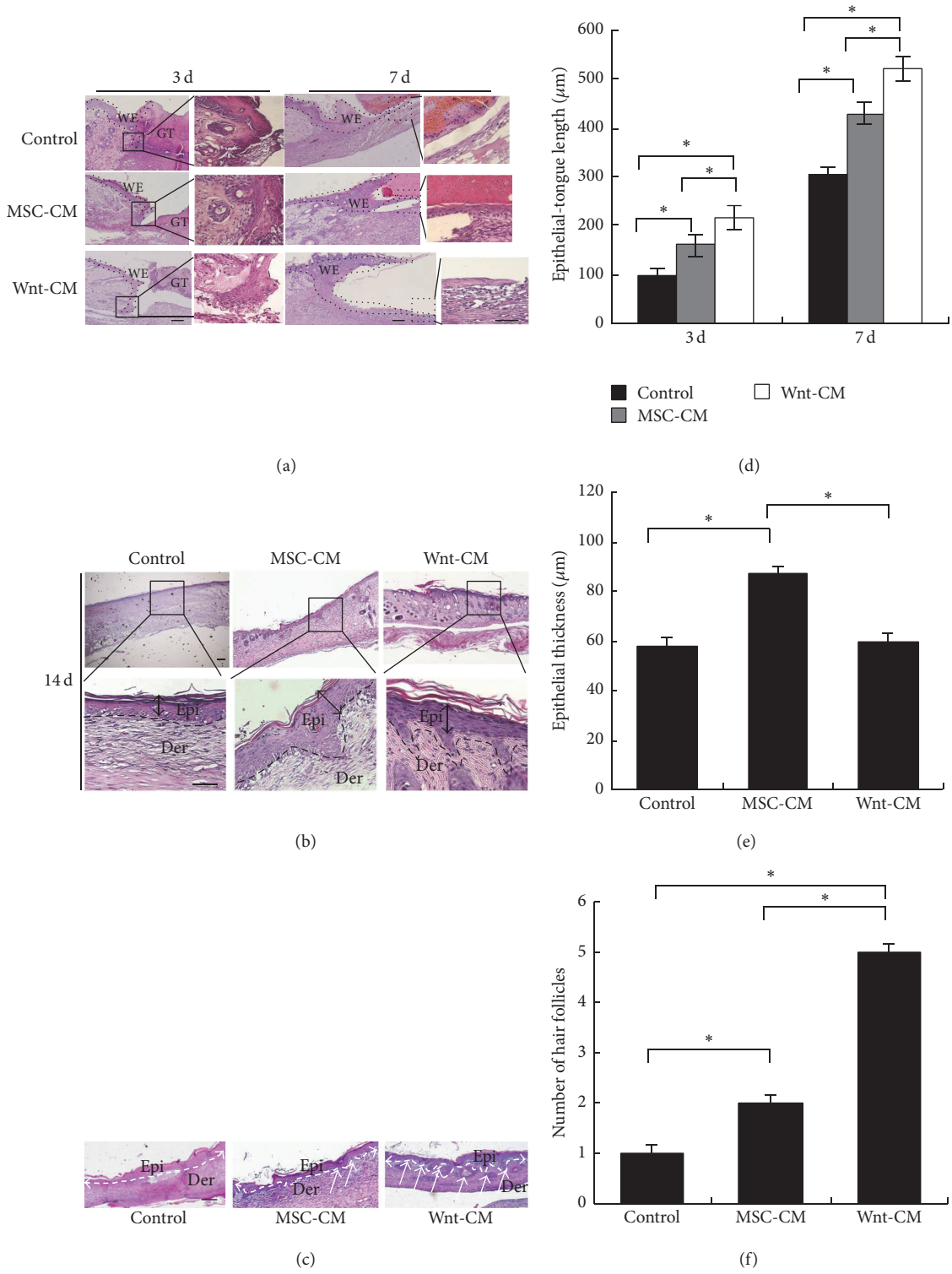

FIGURE 5: Histomorphological analysis of reepidermalization during skin healing in mice. (a, d) Histological analysis of wounds showed significantly increased length of the wound epithelial tongue in mice of treatment group Wnt-CM, as compared to the MSC-CM and DMEM treatment groups on postinjury days 3 and 5. (b, e) The epidermis thickness of the wounds treated with Wnt-CM, MSC-CM, or DMEM in mice on postinjury day 14. (c) The number of regeneration hair follicles in a wound. The data are presented as mean ± SEM, $n = 3$; $^{**}P < 0.01$. The arrow indicates hair follicle regeneration. GT, granulation tissue; WE, wound epithelium; Epi, epidermis; Der, dermis. The scale bar in panels (a), (b), and (c) is 100 μm.

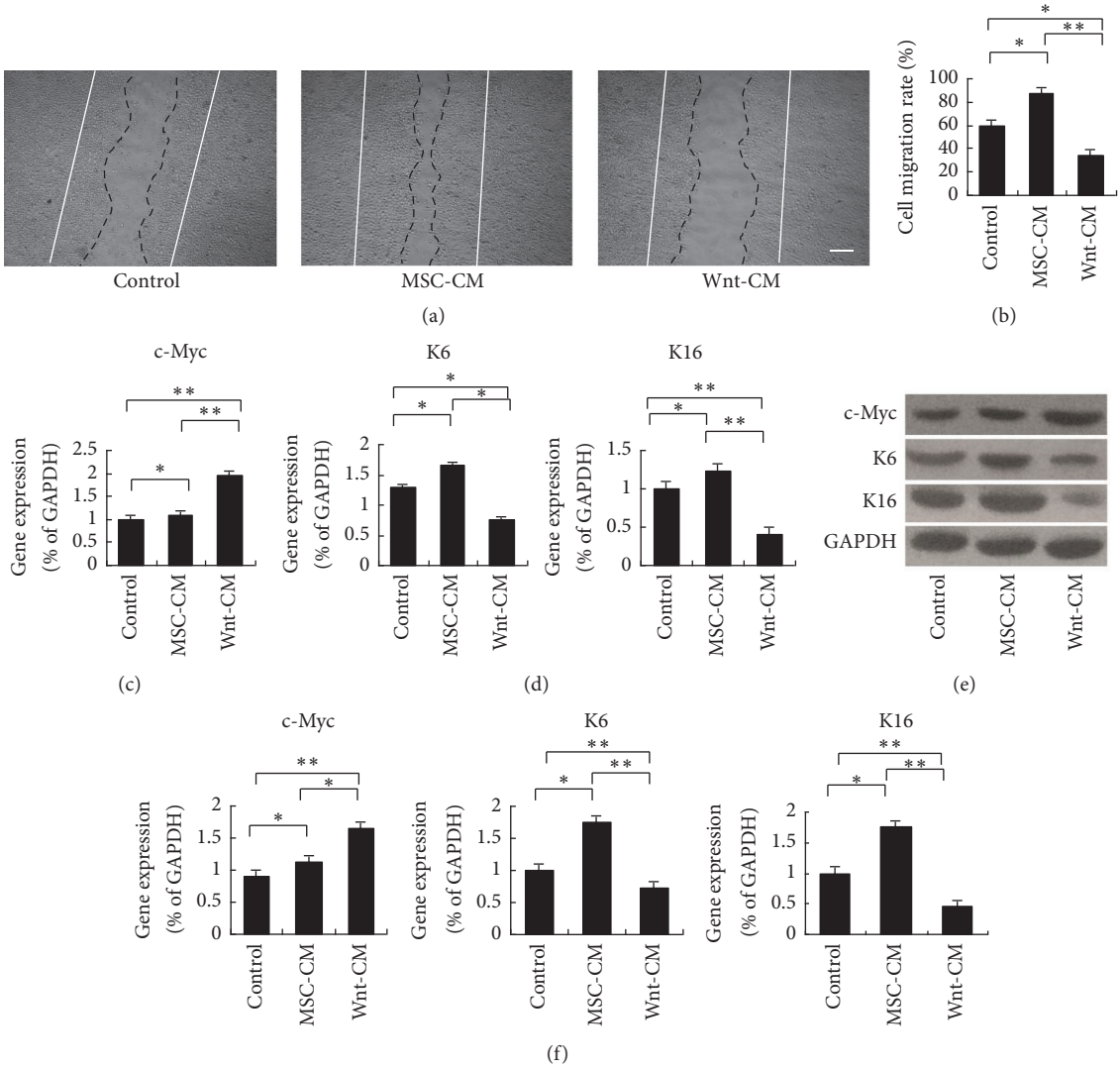

Figure 6: Wnt-CM inhibits migration and expression of the cytoskeletal components K6 and K16 via upregulation of c-Myc in human keratinocytes. (a and b) Wnt-CM inhibited migration of human keratinocytes in the wound scratch assay after 24 h as compared to MSC-CM and DMEM. (c) Expression levels of c-Myc mRNA after treatment with Wnt-CM, MSC-CM, or DMEM were analyzed by real-time PCR and normalized to that of GAPDH. (d) Expression levels of K6 and K16 mRNA after treatment with Wnt-CM, MSC-CM, and DMEM were analyzed by RT-PCR and normalized to that of GAPDH. (e, f) Western blots analysis of c-Myc, K6, K16, and corresponding semiquantitative analysis. The data represent mean ± SEM, $n = 3$; $^{*}P < 0.05$ and $^{**}P < 0.01$. Solid lines indicate the initial wound area; dotted lines demarcate the migrating front of the cells. The scale bar in panel (a) is 100 μm.

treatment of fibroblasts with Wnt-CM can affect the skin wound and keratinocyte migration. We used $HF^{MSC\text{-}CM}$-CM or $HF^{Wnt\text{-}CM}$-CM (treatment of fibroblasts with MSC-CM or Wnt-CM for 24 hours after removal of the supernatant; a fresh culture medium was added and the supernatant was collected after 48 hours) to treat the wound and cultured keratinocytes; the CM from nonactivated fibroblasts (HF-CM) and DMEM served as controls. We found that $HF^{Wnt\text{-}CM}$-CM significantly enhanced the closure rates (Figures 7(a) and 7(b)) and promoted keratinocyte migration and cytoskeletal-protein expression in comparison with $HF^{MSC\text{-}CM}$-CM, HF-CM, and DMEM (Figures 7(c)–7(g)). In contrast, $HF^{Wnt\text{-}CM}$-CM did not influence the expression of c-Myc according to RT-PCR and Western blot analysis of cultured keratinocytes (Figures 7(e)–7(g)). On the other hand, we found that $HF^{Wnt\text{-}CM}$-CM could not promote regeneration of hair follicles by H&E-stained histological slices analysis (Figure 7(a)). Thus, these results showed that Wnt-CM accelerates wound repair and enhances migration of keratinocytes by activating fibroblasts.

4. Discussion

In this study, we explored the effects of Wnt signaling in combination with UC-MSCs on wound repair. We found that Wnt-CM can promote wound repair and induce hair follicle regeneration. Moreover, Wnt-CM by activating fibroblasts enhanced secretory expression of ECM components, which interacted with keratinocytes to promote keratinocyte

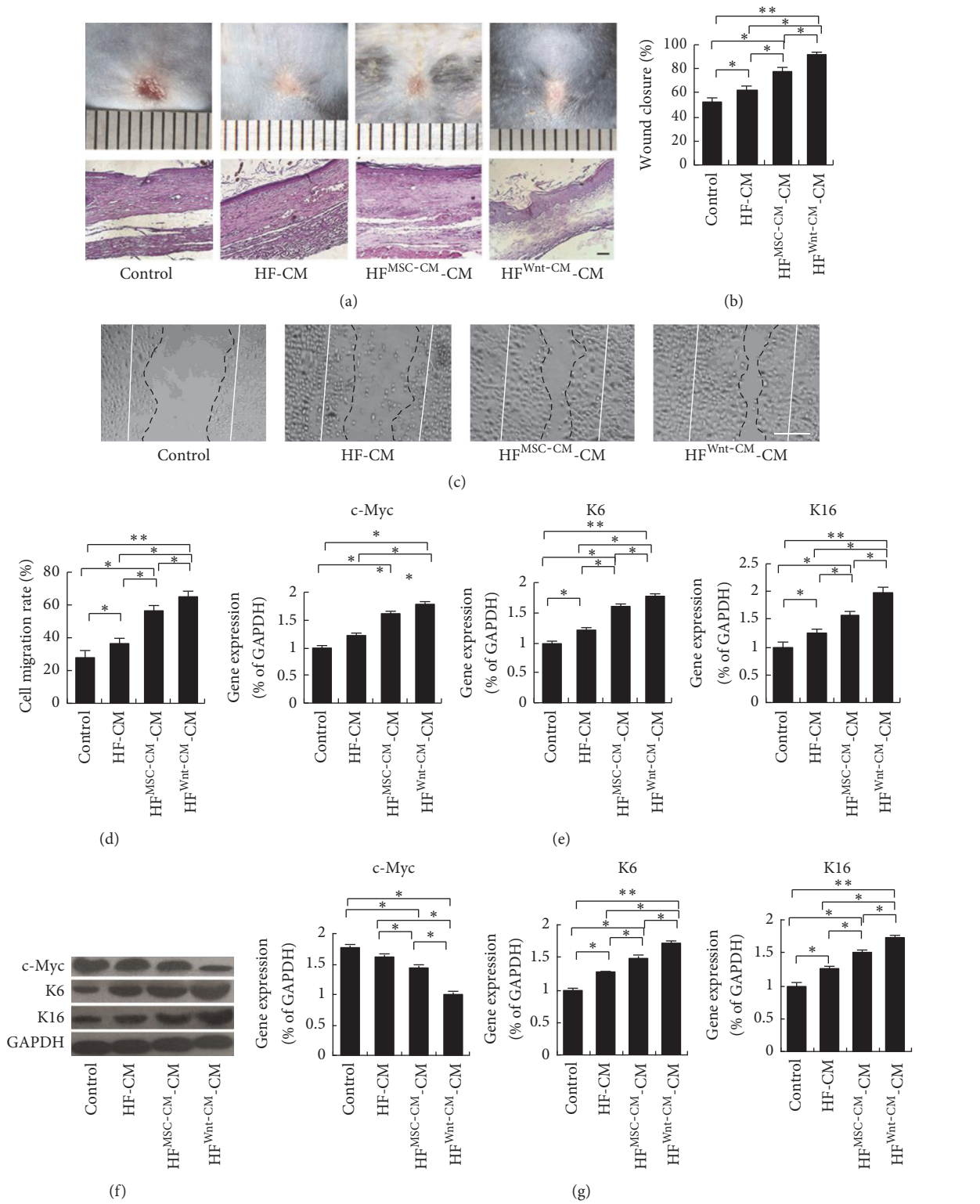

Figure 7: HF$^{Wnt\text{-}CM}$-CM enhances migration and expression of the cytoskeletal components K6 and K16 in human keratinocytes. (a) Typical images of dorsal skin showing effectiveness of wound closure in the mice and H&E-stained histological slices of treatments groups HF$^{Wnt\text{-}CM}$-CM, HF$^{MSC\text{-}CM}$-CM, and HF-CM. (b) Evaluation of wound closure by morphometrical analysis of wound areas (ImageJ, NIH). (c and d) HF$^{Wnt\text{-}CM}$-CM enhanced migration of human keratinocytes in a wound scratch assay after 24 h as compared to HF$^{MSC\text{-}CM}$-CM, HF-CM, and DMEM and corresponding semiquantitative analysis data. (e) Expression levels of c-Myc, K6, and K16 mRNA after treatment with HF$^{Wnt\text{-}CM}$-CM, HF$^{MSC\text{-}CM}$-CM, or HF-CM were analyzed by real-time PCR and normalized to that of GAPDH. (f, g) Western blots analysis of c-Myc, K6, K16, and corresponding semiquantitative analysis. The data represent mean ± SEM, $n = 3$; $^{*}P < 0.05$ and $^{**}P < 0.01$. Solid lines indicate the initial wound area; dotted lines demarcate the migrating front of the cells. The scale bar is 100 μm.

migration and to enhance reepidermalization. Moreover, our data indicate that Wnt-CM can enhance the crosstalk between cells and among cells in the complex wound microenvironment, thereby enhancing these multifaceted wound healing activities.

MSCs are increasingly studied as a potential treatment method for clinical application [28–30]. Recent studies showed that treatment of cutaneous wounds with MSCs accelerates wound healing kinetics, increases epithelialization, and promotes angiogenesis. Although MSCs may repair damaged tissue by direct induction of differentiation, they also have a second function: secretion of a broad repertoire of trophic factors and immunomodulatory cytokines [31, 32]. A large body of work has shown that MSCs can improve wound healing through adjustment of the local microenvironment by secreting various factors [33, 34]. Moreover, Wnt proteins are key mediators of wound regeneration and participate in various related processes, from the development of the dermis to formation of skin appendages [20]. Wnts can drive epidermal-mesenchymal interactions that enhance wound-induced follicle neogenesis in mouse models, and they are also important for maintenance of the hair induction activity of cultured DP cells [13, 35–37]. Overexpression of Wnt signaling molecules promotes cellular proliferation, migration, and ECM degradation; these changes reflect the basic phases of wound regeneration [38]. In this study, we injected Wnt-CM into skin wounds of mice and observed markedly accelerated wound closure and hair regeneration compared to those in mice that received injection of MSC-CM and a control group. MSC-CM can also accelerate wound closure and increase expression of ECM components in comparison with the DMEM treatment group, but MSC-CM causes significantly weaker regeneration of hair follicles as compared to Wnt-CM. The results proved that the synergy of MSCs with a Wnt protein can enhance wound healing and hair follicle regeneration.

Regeneration of hair follicles during wound repair is similar to the process of hair follicle initiation in the embryonic period. Various researchers have demonstrated that hair follicle neogenesis can be induced in a large wound through the overexpression of Wnt7a in the microenvironment [13]. We previously reported that Wnt-CM can induce regeneration and accelerate the cycling of hair follicles by activating DP cells in mice [39]. At the same time, Wnt-CM can maintain the ability of DP cells to induce hair regeneration when cotransplanted with epidermis cells in nude mice [37]. Here, we prepared CM from the culture supernatant of Wnt7a-overexpressing UC-MSCs (Wnt-CM) and used this CM to treat skin wounds in a mouse model. Newly formed hair follicles were observed in the basal epithelial tissues as well as an elevated number of hair follicles after Wnt-CM treatment as compared to the control group. Therefore, we can conclude that Wnt-CM stimulates wound healing and promotes hair follicle regeneration by stimulating the Wnt signing pathway.

Healing of full-thickness wounds involves migration of keratinocytes, fibroblasts, and endothelial cells to the wound bed prepared with deposition of appropriate ECM molecules and proliferation of these cells [5, 40]. Fibroblasts are the major stromal cells in the dermis and in many other tissues. They appear in the wound healing process and release numerous cytokines inducing production of ECM components and contributing to wound closure [41]. Our data here showed that Wnt-CM significantly promotes wound repair and expression of ECM molecules. In addition, Wnt-CM and MSC-CM (separately) can induce expression of α-SMA by fibroblasts in vitro. Nonetheless, the α-SMA expression implies that fibroblasts acquire the myofibroblastic phenotype [42]. Myofibroblasts perform a pivotal function in organogenesis during mesenchymal-epithelial interactions and accelerate wound healing by secreting components of the ECM and of the basement membrane [43]. Thus, our results suggest that Wnt-CM and MSC-CM can enhance ECM secretion and accelerate wound contraction.

Keratinocytes are a major cellular component of the epidermis during a normal wound healing process [10]. Research has shown that the overexpression of β-catenin and c-Myc impairs wound healing by inhibiting migration of keratinocytes and by altering their differentiation [23, 44]. Our results also confirmed that Wnt-CM inhibits cytoskeletal organization of keratinocytes and their migratory ability. In contrast, the results of the in vivo experiment showed that Wnt-CM increases reepidermalization during skin healing in mice. Thus, we can conclude that Wnt-CM may cause fibroblasts to promote reepithelialization. We found that $HF^{Wnt\text{-}CM}$-CM can promote migration of keratinocytes and expression of cytoskeletal proteins. We observed that this CM can promote wound healing in mice, but the number of regenerated hair follicles was not increased significantly. Consequently, we believe that $HF^{Wnt\text{-}CM}$-CM can effectively enhance wound healing and keratinocyte migration but cannot induce hair follicles without exogenous Wnt proteins. Therefore, Wnt proteins may be a useful and selective therapeutic target for hair regeneration during wound repair. Thus, coordinated expression of multiple genes in MSCs holds promise for stem cell-based therapy. Synergistic effects of treatment with Wnt7a and MSCs yield better results than MSC-CM treatment alone.

MSC therapy is a promising method to overcome the limitations of current therapies. Strategies to increase the efficacy of MSC properties through the use of gene engineering to enhance the natural production of specific proteins or to make their own requires the expression of protein, which can greatly broaden the spectrum of disease that can be treated and fully exploit their potential [45]. Enhancing the abilities of these cells to migrate, survive, and promote healing through immunomodulation, differentiation, and angiogenesis is the goal [46]. However, the mechanisms of action include two main aspects: (1) MSC only as a vehicle for transferring genes and drug delivery, but not to change the phenotypic and differentiation potential of MSC by using genetic modification [47] and (2) genes modified by MSC to enhance the expression of purpose genes and at the same time interact with cytokines, changing the secretion level to enhance the function [46, 48]. Thus, what role stem cells will play is something we need to continue to explore. Once these problems are solved, the coordinated expression of

more genes in MSCs using complex expression systems shows promise for clinical therapy.

5. Conclusion

In summary, Wnt-CM can enhance secretion of ECM components and migration of fibroblasts and then promote wound healing and induce hair regeneration. $HF^{Wnt\text{-}CM}$-CM also promotes wound healing and migration of keratinocytes, but, due to the lack of Wnt signals, the number of regenerated hair follicles is not increased. We believe that wound repair requires crosstalk among cells and between cells and cytokines, and any change in these processes will alter wound repair. Thus, the overexpression of Wnt7a by UC-MSCs can effectively accelerate wound healing and induce hair follicle regeneration by improving the wound microenvironment.

Competing Interests

The authors declare that there is no conflict of interests regarding publication of this paper.

Authors' Contributions

Liang Dong and Haojie Hao contributed equally to this work.

Acknowledgments

This research was supported in part by the National Basic Science and Development Program [2012CB518103, 2012CB518105], the 863 Projects of Ministry of Science and Technology of China [2013AA020105 and 2012AA020502], and National Natural Science Foundation of China (81121004, 81230041, and 31400822).

References

[1] T. Kondo and Y. Ishida, "Molecular pathology of wound healing," *Forensic Science International*, vol. 203, no. 1–3, pp. 93–98, 2010.

[2] T. Iqbal, M. Saaiq, and Z. Ali, "Epidemiology and outcome of burns: early experience at the country's first national burns Centre," *Burns*, vol. 39, no. 2, pp. 358–362, 2013.

[3] M. Blais, R. Parenteau-Bareil, S. Cadau, and F. Berthod, "Concise review: tissue-engineered skin and nerve regeneration in burn treatment," *Stem Cells Translational Medicine*, vol. 2, no. 7, pp. 545–551, 2013.

[4] G. C. Gurtner, S. Werner, Y. Barrandon, and M. T. Longaker, "Wound repair and regeneration," *Nature*, vol. 453, no. 7193, pp. 314–321, 2008.

[5] P. Martin, "Wound healing—aiming for perfect skin regeneration," *Science*, vol. 276, no. 5309, pp. 75–81, 1997.

[6] M. C. Y. Heng, "Wound healing in adult skin: aiming for perfect regeneration," *International Journal of Dermatology*, vol. 50, no. 9, pp. 1058–1066, 2011.

[7] R. Sennett and M. Rendl, "Mesenchymal-epithelial interactions during hair follicle morphogenesis and cycling," *Seminars in Cell and Developmental Biology*, vol. 23, no. 8, pp. 917–927, 2012.

[8] A. D. Metcalfe and M. W. J. Ferguson, "Bioengineering skin using mechanisms of regeneration and repair," *Biomaterials*, vol. 28, no. 34, pp. 5100–5113, 2007.

[9] P. Martin and S. M. Parkhurst, "Parallels between tissue repair and embryo morphogenesis," *Development*, vol. 131, no. 13, pp. 3021–3034, 2004.

[10] S. Werner, T. Krieg, and H. Smola, "Keratinocyte–fibroblast interactions in wound healing," *Journal of Investigative Dermatology*, vol. 127, no. 5, pp. 998–1008, 2007.

[11] R. Kalluri and M. Zeisberg, "Fibroblasts in cancer," *Nature Reviews Cancer*, vol. 6, no. 5, pp. 392–401, 2006.

[12] A. M. Wojtowicz, S. Oliveira, M. W. Carlson, A. Zawadzka, C. F. Rousseau, and D. Baksh, "The importance of both fibroblasts and keratinocytes in a bilayered living cellular construct used in wound healing," *Wound Repair and Regeneration*, vol. 22, no. 2, pp. 246–255, 2014.

[13] M. Ito, Z. Yang, T. Andl et al., "Wnt-dependent de novo hair follicle regeneration in adult mouse skin after wounding," *Nature*, vol. 447, no. 7142, pp. 316–320, 2007.

[14] V. W. Wong, B. Levi, J. Rajadas, M. T. Longaker, and G. C. Gurtner, "Stem cell niches for skin regeneration," *International Journal of Biomaterials*, vol. 2012, Article ID 926059, 8 pages, 2012.

[15] A. J. Wagers, "The stem cell niche in regenerative medicine," *Cell Stem Cell*, vol. 10, no. 4, pp. 362–369, 2012.

[16] A. Nuschke, "Activity of mesenchymal stem cells in therapies for chronic skin wound healing," *Organogenesis*, vol. 10, no. 1, pp. 29–37, 2014.

[17] M. N. M. Walter, K. T. Wright, H. R. Fuller, S. MacNeil, and W. E. B. Johnson, "Mesenchymal stem cell-conditioned medium accelerates skin wound healing: an in vitro study of fibroblast and keratinocyte scratch assays," *Experimental Cell Research*, vol. 316, no. 7, pp. 1271–1281, 2010.

[18] H. Sarojini, R. Estrada, H. Lu et al., "PEDF from mouse mesenchymal stem cell secretome attracts fibroblasts," *Journal of Cellular Biochemistry*, vol. 104, no. 5, pp. 1793–1802, 2008.

[19] M. Li, Y. Zhao, H. Hao et al., "Mesenchymal stem cell-conditioned medium improves the proliferation and migration of keratinocytes in a diabetes-like microenvironment," *The International Journal of Lower Extremity Wounds*, vol. 14, no. 1, pp. 73–86, 2015.

[20] R. B. Widelitz, "Wnt signaling in skin organogenesis," *Organogenesis*, vol. 4, no. 2, pp. 123–133, 2008.

[21] D. L. Zhang, L. J. Gu, L. Liu et al., "Effect of Wnt signaling pathway on wound healing," *Biochemical and Biophysical Research Communications*, vol. 378, no. 2, pp. 149–151, 2009.

[22] M. B. Labus, C. M. Stirk, W. D. Thompson, and W. T. Melvin, "Expression of Wnt genes in early wound healing," *Wound Repair and Regeneration*, vol. 6, no. 1, pp. 58–64, 1998.

[23] O. Stojadinovic, H. Brem, C. Vouthounis et al., "Molecular pathogenesis of chronic wounds: the role of β-catenin and c-myc in the inhibition of epithelialization and wound healing," *The American Journal of Pathology*, vol. 167, no. 1, pp. 59–69, 2005.

[24] H. Hao, G. Chen, J. Liu et al., "Culturing on Wharton's jelly extract delays mesenchymal stem cell senescence through p53 and p16INK4a/pRb pathways," *PLoS ONE*, vol. 8, no. 3, Article ID e58314, 2013.

[25] H. Smola, G. Thiekötter, and N. E. Fusenig, "Mutual induction of growth factor gene expression by epidermal-dermal cell interaction," *Journal of Cell Biology*, vol. 122, no. 2, pp. 417–429, 1993.

[26] H.-J. Stark, M. Baur, D. Breitkreutz, N. Mirancea, and N. E. Fusenig, "Organotypic keratinocyte cocultures in defined medium with regular epidermal morphogenesis and differentiation," *Journal of Investigative Dermatology*, vol. 112, no. 5, pp. 681–691, 1999.

[27] Z. Wu, Y. Li, X. Li et al., "LRP16 integrates into NF-κB transcriptional complex and is required for its functional activation," *PLoS ONE*, vol. 6, no. 3, Article ID e18157, 2011.

[28] M. Benderitter, P. Gourmelon, E. Bey et al., "New emerging concepts in the medical management of local radiation injury," *Health Physics*, vol. 98, no. 6, pp. 851–857, 2010.

[29] A. M. Hocking, "Mesenchymal stem cell therapy for cutaneous wounds," *Advances in Wound Care*, vol. 1, no. 4, pp. 166–171, 2012.

[30] E. B. Eaton and T. R. Varney, "Mesenchymal stem cell therapy for acute radiation syndrome: innovative medical approaches in military medicine," *Military Medical Research*, vol. 2, no. 1, article no. 2, 2015.

[31] D. Ti, H. Hao, C. Tong et al., "LPS-preconditioned mesenchymal stromal cells modify macrophage polarization for resolution of chronic inflammation via exosome-shuttled let-7b," *Journal of Translational Medicine*, vol. 13, no. 1, article 308, 2015.

[32] A. M. Hocking and N. S. Gibran, "Mesenchymal stem cells: paracrine signaling and differentiation during cutaneous wound repair," *Experimental Cell Research*, vol. 316, no. 14, pp. 2213–2219, 2010.

[33] A. Skardal, D. Mack, E. Kapetanovic et al., "Bioprinted amniotic fluid-derived stem cells accelerate healing of large skin wounds," *Stem Cells Translational Medicine*, vol. 1, no. 11, pp. 792–802, 2012.

[34] A. Gebler, O. Zabel, and B. Seliger, "The immunomodulatory capacity of mesenchymal stem cells," *Trends in Molecular Medicine*, vol. 18, no. 2, pp. 128–134, 2012.

[35] S. Sick, S. Reinker, J. Timmer, and T. Schlake, "WNT and DKK determine hair follicle spacing through a reaction-diffusion mechanism," *Science*, vol. 314, no. 5804, pp. 1447–1450, 2006.

[36] C. L. Celso, D. M. Prowse, and F. M. Watt, "Transient activation of β-catenin signalling in adult mouse epidermis is sufficient to induce new hair follicles but continuous activation is required to maintain hair follicle tumours," *Development*, vol. 131, no. 8, pp. 1787–1799, 2004.

[37] L. Dong, H. Hao, J. Liu et al., "Wnt1a maintains characteristics of dermal papilla cells that induce mouse hair regeneration in a 3D preculture system," *Journal of Tissue Engineering and Regenerative Medicine*, 2015.

[38] S. S. Cheon, A. Y. L. Cheah, S. Turley et al., "β-Catenin stabilization dysregulates mesenchymal cell proliferation, motility, and invasiveness and causes aggressive fibromatosis and hyperplastic cutaneous wounds," *Proceedings of the National Academy of Sciences of the United States of America*, vol. 99, no. 10, pp. 6973–6978, 2002.

[39] L. Dong, H. Hao, L. Xia et al., "Treatment of MSCs with Wnt1a-conditioned medium activates DP cells and promotes hair follicle regrowth," *Scientific Reports*, vol. 4, article no. 5432, 2014.

[40] A. J. Singer and R. A. F. Clark, "Cutaneous wound healing," *The New England Journal of Medicine*, vol. 341, no. 10, pp. 738–746, 1999.

[41] R. R. Driskell, B. M. Lichtenberger, E. Hoste et al., "Distinct fibroblast lineages determine dermal architecture in skin development and repair," *Nature*, vol. 504, no. 7479, pp. 277–281, 2013.

[42] A. Desmoulière, C. Chaponnier, and G. Gabbiani, "Tissue repair, contraction, and the myofibroblast," *Wound Repair and Regeneration*, vol. 13, no. 1, pp. 7–12, 2005.

[43] V. Moulin, F. A. Auger, D. Garrel, and L. Germain, "Role of wound healing myofibroblasts on re-epithelialization of human skin," *Burns*, vol. 26, no. 1, pp. 3–12, 2000.

[44] F.-L. Li, X. Li, Y.-F. Wang et al., "Astragaloside IV downregulates β-Catenin in rat keratinocytes to counter LiCl-induced inhibition of proliferation and migration," *Evidence-based Complementary and Alternative Medicine*, vol. 2012, Article ID 956107, 12 pages, 2012.

[45] A. Nowakowski, P. Walczak, B. Lukomska, and M. Janowski, "Genetic engineering of mesenchymal stem cells to induce their migration and survival," *Stem Cells International*, vol. 2016, Article ID 4956063, 9 pages, 2016.

[46] A. Nowakowski, A. Andrzejewska, M. Janowski, P. Walczak, and B. Lukomska, "Genetic engineering of stem cells for enhanced therapy," *Acta Neurobiologiae Experimentalis*, vol. 73, no. 1, pp. 1–18, 2013.

[47] C. D. Porada and G. Almeida-Porada, "Mesenchymal stem cells as therapeutics and vehicles for gene and drug delivery," *Advanced Drug Delivery Reviews*, vol. 62, no. 12, pp. 1156–1166, 2010.

[48] Z. Du, C. Wei, J. Yan et al., "Mesenchymal stem cells overexpressing C-X-C chemokine receptor type 4 improve early liver regeneration of small-for-size liver grafts," *Liver Transplantation*, vol. 19, no. 2, pp. 215–225, 2013.

Hindawi
Stem Cells International
Volume 2017, Article ID 4585401, 11 pages
https://doi.org/10.1155/2017/4585401

Review Article

Emerging Perspectives in Scaffold for Tissue Engineering in Oral Surgery

Gabriele Ceccarelli,[1,2] Rossella Presta,[3] Laura Benedetti,[1,2] Maria Gabriella Cusella De Angelis,[1,2] Saturnino Marco Lupi,[3] and Ruggero Rodriguez y Baena[3]

[1]*Department of Public Health, Experimental Medicine and Forensic, Human Anatomy Unit, University of Pavia, Via Forlanini 8, 27100 Pavia, Italy*
[2]*Centre for Health Technologies (CHT), University of Pavia, Via Ferrata 5, 27100 Pavia, Italy*
[3]*Department of Clinico-Surgical, Diagnostic and Pediatric Sciences, School of Dentistry, University of Pavia, P.le Golgi 2, 27100 Pavia, Italy*

Correspondence should be addressed to Ruggero Rodriguez y Baena; ruggero.rodriguez@unipv.it

Received 22 September 2016; Accepted 2 February 2017; Published 26 February 2017

Academic Editor: Filiberto Mastrangelo

Copyright © 2017 Gabriele Ceccarelli et al. This is an open access article distributed under the Creative Commons Attribution License, which permits unrestricted use, distribution, and reproduction in any medium, provided the original work is properly cited.

Bone regeneration is currently one of the most important and challenging tissue engineering approaches in regenerative medicine. Bone regeneration is a promising approach in dentistry and is considered an ideal clinical strategy in treating diseases, injuries, and defects of the maxillofacial region. Advances in tissue engineering have resulted in the development of innovative scaffold designs, complemented by the progress made in cell-based therapies. In vitro bone regeneration can be achieved by the combination of stem cells, scaffolds, and bioactive factors. The biomimetic approach to create an ideal bone substitute provides strategies for developing combined scaffolds composed of adult stem cells with mesenchymal phenotype and different organic biomaterials (such as collagen and hyaluronic acid derivatives) or inorganic biomaterials such as manufactured polymers (polyglycolic acid (PGA), polylactic acid (PLA), and polycaprolactone). This review focuses on different biomaterials currently used in dentistry as scaffolds for bone regeneration in treating bone defects or in surgical techniques, such as sinus lift, horizontal and vertical bone grafts, or socket preservation. Our review would be of particular interest to medical and surgical researchers at the interface of cell biology, materials science, and tissue engineering, as well as industry-related manufacturers and researchers in healthcare, prosthetics, and 3D printing, too.

1. Introduction

Bone tissue engineering aims to restore tissues damaged due to trauma, diseases, or congenital abnormalities. This tissue engineering approach can be developed by combining stem cells with innovative scaffolds designed to produce the required extracellular matrix in an adequate manner and ultimately a healthy bone tissue with acceptable geometry, size, and composition [1–3]. Thus, regenerative medicine can be successfully combined with tissue engineering to recreate the appropriate cellular microenvironment that can rebuild whole organs [4, 5].

In the last 20 years, there has been increasing interest in tissue regeneration in the craniofacial region as well as for whole teeth and periodontal structures in dentistry [6]. The principles of tissue engineering have found widespread application in several branches of dentistry, such as periodontics, oral maxillofacial surgery, and implant dentistry [2, 7]. Tooth engineering attempts to enhance the creation of osseointegrated implants with specific, biocompatible materials that replace the missing tooth or provide support to the regenerated maxillary bone. In implant dentistry, the lack of adequate bone tissue and proximity to important anatomical structures (such as the maxillary sinus and the

inferior alveolar nerve) are the most frequently observed problems at the implantation site [7].

To avoid iatrogenic damage to sensitive structures, the sinus lift, horizontal and vertical bone grafts, and socket preservation are the conventionally used surgical techniques [8, 9]. These techniques have been considerably improved in the last 5 years to achieve the regeneration of increasingly larger and higher bone volume [10, 11] and will ensure the best prosthetic rehabilitation for each patient. For successful outcomes in regenerative dentistry, the combination of stem cells of mesenchymal origin and scaffolds has been regarded to have considerable potential in regenerative medicine at the maxillary bone level [12–14].

For these reasons, bone tissue engineering represents an important and promising approach to treat various pathological conditions in the oral cavity. Bone tissue engineering for pathological bone conditions requires an appropriate source of mesenchymal stem cells, such as dental pulp stem cells (DPSCs) or periosteal stem cells (PSCs), and a suitable scaffold on which the stem cells can be seeded and growth factors/molecular signals can be provided in order to facilitate bone regeneration [1–5, 15]. Several studies have reported different scaffolds for different types of tissue regeneration; for example, some scaffolds used in plastic surgery attract the epidermal and connective substitutes, while others are specifically used for bone regeneration [16, 17].

This review will focus on the significant advancements that have been made in the field of dentistry-based tissue engineering with emphasis on the different biomaterials currently available in clinical therapy for surgical procedures in the oral cavity. Moreover, it would be of particular interest to medical and surgical researchers at the interface of cell biology, materials science, and tissue engineering, as well as industry-related manufacturers and researchers in healthcare, prosthetics, and 3D printing, too.

2. Stem Cells in Dentistry-Based Tissue Engineering

Stem cells can be classified as totipotent, pluripotent, or multipotent according to their abilities to differentiate into other cell types [2, 6, 49]. Totipotent cells can give rise to the whole organism; pluripotent cells (iPSC, such as embryonic stem (ES) cells) can give rise to every cell type of an organism except its extraembryonic tissues, such as the placenta. Multipotent stem cells (MSC) are adult stem cells, which can differentiate into a specific cell lineage [50]. Owing to ethical reasons and technical issues associated with ES cells and iPSC, MSCs are the most commonly used stem cells in tissue engineering, including dentistry-based tissue engineering [49]. MSCs can be isolated from several tissues, such as bone marrow, peripheral blood, umbilical cord blood, adult connective tissue, dental tissues, placenta, and amniotic membrane [1, 2, 50, 51]. Morphologically, MSCs adhere to plastic, have fibroblast-like appearance, and are able to differentiate into osteocytes, chondrocytes, and adipocytes [52, 53]. MSCs express surface-specific antigens, such as CD105, CD73, and CD90, and they are negative for the leukocyte marker (CD45) and the primitive hematopoietic progenitor and endothelial cell marker, CD34 [54]. Several types of adult stem cells with mesenchymal origin have been isolated from the oral cavity, including DPSCs [55, 56], stem cells from human exfoliated deciduous teeth (SHED) [57], periodontal ligament stem cells (PDLSCs) [58], dental follicle progenitor stem cells (DFPCs) [6], and stem cells from apical papilla (SCAP) [6, 59].

Gronthos et al. first identified DPSCs with a high cell proliferation capacity and the ability to differentiate into osteoblasts and chondroblasts [60]. In addition, when transplanted in host mice, DPSCs can differentiate into odontoblast-like cells and form some important tooth structures, such as dentin-like structure or cementum, when cultured on ceramic substrates (such as hydroxyapatite or tricalcium phosphate) [61]. Several in vivo applications of DPSCs have improved bone regeneration, as demonstrated by D'Aquino et al. based on radiographic evidence [56] and by Graziano et al. based on histology [62]. Moreover, DPSCs seeded onto collagen scaffolds in the presence of dentin matrix protein 1 formed an organized matrix [61, 62], which could induce the formation of hard tissue.

Exfoliated deciduous teeth are another important source for stem cells, from which Miura et al. isolated stem cells with mesenchymal properties [63]. Similar to DPSCs, SHED express MSC markers, including CD105, CD146, Stro-1, and CD29 and when transplanted, they form a dentin-like structure [63]. SCAP (from apical papilla) were isolated from the root apex of a developing tooth and showed MSC properties, such as the expression of surface antigen markers (they also express CD24); SCAP can undergo differentiation to form odontoblasts and chondroblasts [64]. PDLSCs, isolated from the dental follicle during tooth development, are highly positive for mesenchymal markers; they can differentiate into osteoblasts, chondrocytes, adipocytes, neurons, and even hepatocytes [6, 58].

Finally, the periosteum from craniofacial bones has also been proposed to be a source of progenitor cells responsible for injury repair in adult bones. In fact, periosteal cells (PCs), described by Mattioli-Belmonte et al. as cells with MSC-like properties, are involved in cell mechanosensing and contribute to matrix organization, bone microarchitecture, and bone strength [65, 66]. In addition, it has been demonstrated that PCs could replace mesenchymal cells from bone marrow in oral tissue engineering applications owing to the ease of collecting and the rapid in situ engraftment of PCs [66]. It has been proposed to culture PCs ex vivo and subsequently seed them into a natural or synthetic scaffold [67]. However, the success of this approach is strictly limited to the use of an appropriate material that is able to enhance the differentiation of PCs.

Thus, in dentistry-based bone tissue engineering, scaffolds in combination with the appropriate stem cell are considered to be the most important factors to create substitutes for the original tissue after any injury.

3. Scaffolds

3.1. Classification of Scaffolds. In scientific literature, the term "scaffold" has been adopted to indicate a biomaterial that

can provide support. Here, "support" is used to describe the biomaterial as a biological platform that facilitates the appropriate repair and restoration of the physiological/histological features of injured tissues during the healing process [16, 17, 23, 62].

In tissue regeneration, a biocompatible scaffold will allow cell adhesion and induce cell proliferation and differentiation without triggering any inflammatory responses or rejection from the body [23]. Currently, the ultimate goal of tissue engineering is to create a three-dimensional (3D) biocompatible support that can be inserted into a tissue to repair a lesion or correct a defect by allowing the adhesion and proliferation of a specific cell type [23].

An ideal bone scaffold must have three fundamental features: it should be osteogenic, osteoconductive, and osteoinductive. An osteogenic material can generate bone tissue, which is a characteristic unique to osteoblasts. Thus, the "living" bone can be considered the only real osteogenic scaffold. Moreover, to ensure that the osteogenic feature is retained in bone grafts, the graft must be collected and used as quickly as possible to facilitate cell survival after surgical trauma [17]. An ideal scaffold should also be an osteoconductive material that stimulates bone cells to grow on its surface. Moreover, the osteoinductive capacity (the ability of the biomaterial to induce proliferation and differentiation of MSCs in preosteoblasts, which produce matrix) is essential for bone healing.

These fundamental characteristics alone are insufficient for the successful in vivo application of the bone scaffold. To fabricate a bone scaffold, an ideal biomaterial must also possess other properties, such as being bioinert, biocompatible, bioactive, and biodegradable with suitable mechanical properties. Furthermore, the biomaterial should also be able to withstand sterilization to prevent infections and be interconnected and demonstrate controlled porosity [17]. Moreover, it should be able to undergo efficient resorption at the same time that the bone regenerates.

The scaffold-cell interaction must also ensure easy penetration, distribution, and proliferation. The biomaterial should be 90% porous with a suitable pore diameter to enable the cells to penetrate the biomaterial, thus, ensuring the growth of new bone tissue and optimal vascularization [17]. Biocompatibility, however, remains the most essential property that scaffolds must possess; in fact, the biomaterials should not induce inflammatory responses in the body or show any immunogenicity or cytotoxicity [24]. Furthermore, from the industrial point of view, the manufacturing process should be simple, fast, and cost-effective. However, it has been considered difficult and challenging to fabricate a single ideal biomaterial that encompasses all these features.

Finally, it is also essential that the scaffold biomaterial must be efficiently resorbed with the deposition of new bone tissue so that the new bone can replace it entirely, while maintaining the shape and thickness [68]. Craniofacial scaffolds (having several applications in dentistry) must fill three-dimensionally complex defects and provide adequate resistance to temporary load during regeneration. To meet these requirements, it is fundamental to apply the modulus of elasticity (or Young's modulus "E"), described as the ratio between the stress applied and the resulting deformation in the biomaterial [18, 69, 70]. Since skull bones have an elastic modulus between 100 and 30000 MPa (which can be variable in relation to the bone type and load zone), craniofacial scaffolds must have a similar elastic modulus to ensure resistance to the load without breaking [68]. The modulus of elasticity of the material increases with its volume fraction, but increased volume can decrease the permeability and, consequently, the porosity of the material. Then, the volume (and density) of the material will be directly proportional to its elasticity and inversely proportional to its permeability. This indicates that it is difficult to provide good elasticity and resistance to the biomaterial, while concomitantly maintaining an optimal permeability for cell colonization [19].

The numerous and different types of scaffolds have been predominantly classified according to the intrinsic characteristics of the biomaterials and placed in macrogroups [20]. For simplicity, we will discuss bone grafts, matrices, polymeric materials, and combined (composite) scaffolds.

3.2. Bone Grafts. Bone grafts are classified as autologous, homologous, heterologous (xenografts), and alloplastic grafts. Currently, autologous bone graft is considered as the gold standard among all bone grafts. In autologous bone grafting, the donor's own bone is taken from a healthy part of the donor's body and grafted in the affected region, minimizing rejection issues. The donor sites can be intraoral or extraoral [21, 70]. It is interesting to note the different properties of the cortical and cancellous bone grafts. A cortical bone graft provides good structural support and reduced resorption. Nevertheless, due to its high density, revascularization of the newly formed tissue is slow and difficult resulting in engraftment delay. In contrast, a cancellous bone graft ensures early revascularization, resulting in faster engraftment, lesser risk of infection, and a shorter time for implant placement.

The allografts or allogeneic grafts are derived from donors of the same species (usually from bone banks) but lose many of their characteristics during the long and expensive process of sterilization and decellularization. Although these processes are necessary to minimize rejection or disease transmission, they deprive the bone of its osteogenic properties, making it a simple, empty scaffold. These grafts can be further classified as freeze-dried bone allograft (FDBA) and demineralized freeze-dried bone allograft (DFDBA) [22]. Due to their high manufacturing costs and increased rate of resorption these types of grafts are limited to small and medium defects used [25].

Xenografts are a cheaper alternative to allografts but undergo similar sterilization procedures. They are animal-derived grafts, mainly obtained from cattle, pigs, and horses. Various studies have shown that these materials provide support and survival similar to those of autologous bone grafts, but without the osteogenic properties. The deproteinized bovine bone in sterilized granules or blocks is an example of a xenograft commonly used in bone regeneration [26, 27].

Several alloplastic grafts, such as β-tricalcium phosphate (β-TCP), bioceramics, and hydroxyapatite (HA), have been used for bone regeneration. They can be manufactured at lesser costs compared to heterologous biomaterials; however,

their resorption is not always ideal. Although inadequate resorption does not cause problems in bone grafting for mucosa-supported prosthesis, in preimplant grafting, the residual grafted material could affect the osseointegration.

3.3. Matrices. A matrix is defined as a microscopic structure inserted into the body to give form to a macroscopic and organized structure [28]. Matrices are divided as organic and inorganic matrices.

Organic matrices include collagen type I—the most abundant protein in human and animal tissues, which is required for the structural maintenance of tissues. Collagen has also been included in the group of polymeric materials in a subsequent section, where it will be discussed in detail.

All inorganic matrices have common features, such as fragility, no susceptibility to corrosion, and small fatigue resistance. The most significant property of inorganic matrices is their long resorption time in the body associated with the absence of any induced inflammatory response. These materials have been used in dentistry since the 1980s; however, none of them possesses the properties of osteogenesis and bone induction [17]. HA and calcium phosphate (CaP) are the commonly used inorganic matrices. CaP-based inorganic matrices can be further classified as ceramic and cement matrices. Ceramic matrices are divided into bioglass (BG) and HA ceramics, whereas β-TCP is included in a subgroup of cement matrices [17].

HA can be derived from animal bone, coral, or be manufactured as purely synthetic HA. HA has several disadvantages that include reduced mechanical resistance, long resorption time, and difficulty in controlling pore size [24]. The β-TCP-based scaffolds are preferred to HA-based scaffolds as they are easier to manufacture and can be shaped with suitable morphologies and controlled pore sizes. Moreover, the resorption rate of β-TCP-based scaffolds is 3–12-fold faster than that of HA-based ones, but it is also equally difficult to precisely predict the time taken for their resorption. β-TCP-based scaffolds have low mechanical strength, which further decreases with the increase in pore size and texture. For these reasons, CaP cannot be used alone as a scaffold in conditions of immediate loading [17].

The BG ceramics are biocompatible glass (approved by the FDA) and entirely synthetic [29]. BG is composed of oxides of silicon, sodium, calcium, phosphorus, and boron, although the final chemical composition is extremely variable according to the percentage of the various elements present. For this reason, the final characteristics of the product will differ in BGs, and it may be very difficult to clearly obtain the final product properties, even after lengthy industrial and chemical studies. It has also been shown that the high percentage of ions released by the insertion of BG in the body induces intra- and extracellular responses by stimulating osteoblast differentiation and revascularization [30, 31, 33]. Moreover, BGs demonstrate controlled resorption in optimal time, efficient bioactivity, and the ability to modulate cell migration and can form chemical bonds with the tissues with which they come in contact. If placed in contact with a liquid medium, they form a layer of a hydroxycarbonate gel of calcium and silica, which facilitates the absorption of proteins used by osteoblasts to produce matrix [32]. Furthermore, BGs have an advantageous peculiarity in their cortical bone-like modulus of elasticity [24], which can support the revascularization, enzyme activity, adhesion, growth, and differentiation of osteoblasts [17, 26]. Despite these exceptional characteristics, this biomaterial has low resistance to load, similar to other inorganic matrices [24, 32].

3.4. Polymeric Materials. Polymeric materials are classified as natural and synthetic polymers. Natural polymers are organic in origin and the most representative organic polymer is collagen. Collagen is used in bone and periodontal regeneration, often in combination with other grafting materials such as HA and β-TCP. Other organic polymers used as scaffolds (but less frequently for bone regeneration) include alginate, hyaluronic acid, chitosan, and peptide hydrogel [17]. Although these materials are biocompatible, they have a major disadvantage in being water soluble. For this reason, their use in bone regeneration is limited and they can be used only in combination with other materials, such as HA and TCP [17].

Synthetic polymers are manufactured industrially from inorganic sources. They are classified as absorbable and nonabsorbable polymers. The resorbable polyesters are predominant among synthetic polymers. They include polylactic acid (PLA), polyglycolic acid (PGA), polylactic-polyglycolic acid (PLGA), polyethylene glycol (PEG), PEG with PLGA (PEG-PLGA), and polycaprolactone (PCL) [25].

The most nonabsorbable polymer used in bone regeneration is polytetrafluoroethylene-expanded (e-PTFE). This polymer is used in the form of a membrane to cover bone grafts and it is used as a barrier between the graft material and the soft tissues of the flap to inhibit the early onset of gingiva-derived fibroblast formation, which could provoke scar tissue formation, before the proliferation of osteoblasts. e-PTFE is commonly anchored with metallic or synthetic absorbable pins and subsequently removed before the implant placement [32].

Collagen is a part of the bone matrix before primary ossification. It is biocompatible and biodegradable and has poor mechanical properties. Since it is already present in the body, it does not induce toxicity-based inflammatory or immunological responses when grafted [34]. It can be easily manipulated for the formation of 3D scaffolds with controlled porosity. The increase in scaffold porosity diminishes its mechanical characteristics [34]. The cytocompatibility of this polymer also makes it an excellent substrate for the proliferation of MSCs in vitro [35]. It is a hydrophilic material, whose permeability is essential for cell migration. The term permeability refers to the capacity of fluids to pass through tissues or membranes, and thus, the higher the scaffold compression, the greater the reduction in its permeability. Consequently, collagen is not suitable as a scaffold that can tolerate excessive loads, because as it gets squeezed or compressed, the quality of the collagen scaffold gets reduced [36]. Owing to its malleability, collagen is often combined with other materials (PLA, PGA, BG, and HA) in order to improve its mechanical characteristics, thus forming a complex or composite scaffold. This material can also

promote engraftment and cell differentiation [34]. Collagen scaffolds have also been used to efficiently vehicle growth factors, but this field of research is still under development [17, 35].

PLA and PGA are synthetic polymers with excellent biomaterial characteristics that are dependent on the ability to control their synthesis, which influences the final surface characteristics [37]. Quantitatively, there are no limitations to their production and they are degraded in the body by chemicals and not cell-mediated processes [38]. The PLA and PGA polymers are cleaved into their respective monomers (lactic acid and glycolic acid, resp.) that are eliminated through different metabolic pathways. Their rapid degradation is also a disadvantage as it could cause early failure of the graft. Additionally, intracellular degradation of an acid can induce an inflammatory response [37, 39]. To reduce inflammation, hybrid scaffolds have been created, combining PLA and PGA with BGs and CaP [38, 40]. These polymers also have other disadvantages, such as low mechanical strength, difficulties associated with their production, and their uncertain interaction with cells. PGA degrades more rapidly than PLA. However, both are degraded too quickly for bone regeneration. Due to this reason, they are never used individually, but only as a combination in the form of PLGA 12 : 13 [24].

The polylactic-polyglycolic acid (PLGA) is a copolymer obtained by the union of lactic and glycolic acid through ester bonds. The composition of the final polymer chains will influence the degradation time, prolonging the half-life of the composite polymer in the oral cavity once applied in situ [35]. The different relationships between the two monomers and the different sequences that can be obtained greatly increase the variability of the final scaffold used in clinical practice, with several different formulations and resorption times. The 50 : 50 combination of PLA and PGA is less resistant, while the presence of the right- and left-handed monomers increases the resistance of the biomaterial [24]. The relationship between hydrophilicity and hydrophobicity and the balance of the crystalline structure, in turn, increases resorption times. It is also possible to control the morphology and diameter of the pores, as well as all other surface features [37, 39]. Currently, this polymeric bone substitute is extensively used for bone regeneration in dentistry and it has been combined with growth factors and MSCs to obtain good results [37]. Moreover, it can be fabricated in different forms: hydrogels, microspheres, blocks, and fibers [37, 39].

PEG is a polyether with a high molecular weight and is very resistant to resorption. It has been used in combination with MSCs and peptides with good results; in addition, it has been used as a scaffold for neuronal regeneration in the treatment of pathologies of the central nervous system [35].

PCL is an aliphatic polyester that is lesser known among the synthetic polymers. It has good mechanical characteristics and very long resorption times (of up to three years) and degrades via hydrolysis of the ester bonds [24]. It has been combined with HA and chitosan to form hybrid scaffolds with better mechanical resistance and has also been used in association with MSCs and growth factors [24, 41, 42].

3.5. Composite Scaffolds. The scaffolds described in the preceding sections are the most commonly used scaffolds in bone regeneration in dentistry. In some cases, it is possible to combine some of these materials to improve their mechanical characteristics and osteoconductivity. In fact, the wide range of biomaterials can be further widened if we consider combined (composite) scaffolds, obtained by the union of several components. Composite scaffolds obtained when PLA is enriched with dicalcium phosphate [38] or PGA and PLGA are combined with HA or β-TCP and can increase the degradation time and improve the mechanical properties of the scaffolds [36, 43, 44]. Scaffolds containing HA reinforced with collagen have been developed to overcome the mechanical strength limitations of collagen and stimulate the differentiation of stromal cells in vitro and in vivo [45]. Collagen was also enriched with growth factors to induce osteogenesis or associated with MSCs and polypeptides in order to improve cellular colonization [35, 46, 47]. Furthermore, other novel combined scaffolds have also been developed, such as PCL and bioactive glass coated with magnesium to implement bioactivity [48]. Metallic magnesium was also used in association with PLGA in order to stimulate in vitro stromal cells proliferation [71]. Even though the combination of different materials is usually convenient, it is essential that the design of these combined scaffolds must be accurate in order to optimize the results, minimize the disadvantages of each material, and enhance the advantageous properties.

Scaffolds enriched with HA have had the best outcomes in maxillofacial surgery [43]. In particular, different collagen formulations enriched with nano-HA have been created to increase migration and differentiation of progenitor cells involved in bone regeneration [45, 72]. These scaffolds were also tested in vitro with MSCs with the aim to graft bioactive scaffolds enriched with them [71]. PLGA scaffolds have been enriched with HA to slow the graft resorption time and enhance the mechanical properties; surprisingly, this combination also increased cell engraftment and the amount of newly formed bone tissue [43, 44].

4. Scaffolds with Stem Cells

Several scaffolds currently used in dental tissue engineering have been discussed in this review. Each biomaterial has a specific chemistry, composition and structure, and degradation profile and offers the possibility for modification. The combination of these scaffolds with stem cells represents the gold standard for future clinical treatments in dentistry-based bone regeneration approaches [1]. Different research groups and researchers have extensively described the positive association between scaffold and stem cells for bone regeneration. For this reason, the in-depth understanding of the molecular interactions between different scaffolds, stem cells, and their in situ microenvironment remains the main objective that needs to be achieved in regenerative medicine.

Among the organic scaffolds, collagen, despite its poor mechanical properties, is one of the most investigated materials. Its cytocompatibility and hydrophilicity make it perfect for cell adhesion in short time periods and, as an organic

Table 1: Properties of scaffolds designed for dentistry tissue engineering.

Scaffolds	Advantages	Disadvantages	Preclinical and clinical studies
Bone graft	(i) Autologous bone is the gold standard (ii) A graft of cortical bone guarantees a good structural support and a reduced resorption (iii) A cancellous bone graft ensures an early revascularization resulting in rapid engraftment, less infection risk, and a shorter time for implant placement (iv) The allograft has no rejection or diseases transmission's risk (v) The xenografts costs are reduced compared with heterologous	(i) Newly formed tissue is slow and difficult (ii) The allograft has long and expensive process of sterilization and decellularization (iii) The xenografts do not have the best resorption time	(i) Autologous bone graft [18] (ii) Allografts [19, 20] (iii) Xenografts [21, 22]
Inorganic matrices			
(1) Hydroxyapatite (HA)	(i) Long resorption time in the body (ii) Absence of inflammatory response	(i) Fragility (ii) No susceptibility to corrosion (iii) Difficulty of controlling the size of pores (iv) Reduced mechanical resistance (v) Long resorption time in the body	Inorganic matrix [23–25]
(2) β-Tricalcium-phosphate (β-TCP)	(i) They are more easily produced and shaped in contrast to HA (ii) Suitable morphology (iii) Controlled pore sizes (iv) Resorption is 3–12 times faster than the HA	(i) Fragility (ii) No susceptibility to corrosion (iii) Difficult to predict precisely how long resorption will take (iv) Low mechanical strength, which decreases with the augment of the pores size and texture	[25]
(3) Bioglasses (BG)	(i) Accepted by the FDA (ii) Totally synthetic (iii) The final chemical composition is extremely variable (iv) Intra- and extracellular responses by stimulating osteoblast differentiation and revascularization (v) Controlled resorption time (vi) Bioactivity: good interaction with osteoblasts (vii) Modulate cell migration (viii) Form chemical bonds with the nearby tissue (ix) Cortical bone-like modulus of elasticity	(i) Low load resistance (ii) Fragility	[23, 24, 26–32]

Table 1: Continued.

Scaffolds	Advantages	Disadvantages	Preclinical and clinical studies
Polymeric materials			
(1) Collagen	(i) Natural polymer (ii) Biocompatible (iii) Biodegradable (iv) Does not induce toxicity or inflammatory or immunological response (v) Easy to manipulate (vi) Porosity (vii) Permeability (viii) Malleability (ix) Used to vehicle growth factors	(i) Water soluble (ii) Limited bone regeneration (iii) Low mechanical properties	[23, 31–33]
(2) Polytetrafluoroethylene-expanded (e-PTFE)	Nonabsorbable synthetic polymer	Anchored with metal or synthetic absorbable pins	[30]
(3) Polylactic acid (PLA)	(i) No limits to their production (ii) Absorbable synthetic polymer (iii) Degraded in the body with chemical non-cell-mediated processes	(i) Rapid degradation (ii) Degradation of an acid causes an inflammatory response (iii) Low mechanical strength (iv) Difficulty of production (v) Dubious interaction with cells	[34–36]
(4) Polyglycolic acid (PGA)	(i) No limits to their production (ii) Absorbable synthetic polymer (iii) Degraded in the body with chemical non-cell-mediated processes	(i) Rapid degradation (ii) Degradation of an acid causes an inflammatory response (iii) Low mechanical strength (iv) Difficulty of production (v) Dubious interaction with cells	[34–36]
(5) Polylactic-polyglycolic acid (PLGA)	(i) Absorbable synthetic polymer (ii) Copolymer of PLA and PGA (iii) Control the morphology, diameter of the pores, and all surface features (iv) Combined with growth factors and MSCs	(i) The different relationships between the two monomers and the different sequences obtainable increase the variability of the final scaffold (ii) Hydrophobicity	[24, 36, 37]
(6) Polyethylene glycol (PEG)	(i) Resistant to resorption (ii) Used in combination with MSCs and peptides	Not used frequently in dentistry	[32]
(7) Polycaprolactone (PCL)	(i) Good mechanical characteristics (ii) Long resorption times (up to three years) (iii) Degrades by hydrolysis of the ester bonds (iv) Used with stem cells and polypeptides	Less studied	[24, 38, 39]
(8) Composite scaffolds	(i) The combination improves mechanical characteristics and osteoconductivity (ii) Overcome strength limitations and stimulate the differentiation of stromal cells in vitro and in vivo (iii) Implement bioactivity (iv) Increase migration and differentiation of progenitor cells	The design of these combined scaffolds must be necessarily accurate	[32–34, 40–48]

matrix, it effectively promotes cell viability, proliferation, and adhesion to the scaffold material [15]. The association between collagenous scaffold and stem cells has been extensively studied in vitro by evaluating the specific cell behavior, as well as in vivo both in animal studies and in human clinical trials. In particular, Kawase et al. demonstrated that the periosteum sheets coated with collagen enhanced initial adhesion of periosteum segments, improved cell growth, and increased the efficiency of implantation in periodontal therapy [47]. Moreover, the combination of poly-dL-lactic acid (PDLLA) and collagen promoted cell proliferation and osteogenic differentiation of MSCs as compared to MSCs seeded on the simple PDLLA/gelatine scaffolds [46, 47]. Zhang et al. showed that newly formed tissue, regenerated by DPSCs seeded on collagen sponges in vivo, appeared to be similar to connective tissues rather than dentin-like tissues [32, 73]. For this reason, collagen sponges are frequently used in combination with other materials, such as HA or PLGA, in order to enhance the mechanical properties of the scaffold and to overcome the inadequate production of mineral matrix deposition [31–33]. However, further studies will be necessary in this field before human clinical trials can be conducted.

Inorganic matrices have been studied in vivo and in vitro. HA is a commonly used scaffold in regenerative oral surgery in combination with stem cells. Several studies have shown that a scaffold composed of porous HA and MSCs with controlled and interconnected porosity facilitate bone regeneration, promoting the deposition of more bone matrix than simple HA [4, 41, 72]. However, poor cell adhesion and fast resorption remained the major problems associated with this biomaterial.

Calcium phosphate, dicalcium phosphate, and TCP are inorganic matrices widely used as scaffolds for their excellent mechanical and physical properties [27]. Their slow resorption and the ability to form chemical bonds with tissues make them suitable for bone regeneration. Gandhimathi et al. demonstrated that the physicochemical characteristics of these matrices promote cell communication, which results in matrix production [74]. In contrast, other studies [28, 74–77] have shown that, owing to the strong hydrophobicity of this material, it does not promote cell adhesion. Surface treatments or association with biomolecules, such as collagen, alginate, or polypeptides, are therefore necessary to facilitate the interaction between the cells and the biomaterial [75]. In fact, Wang et al. demonstrated that the incorporation of MSCs in nanoparticles mixed with calcium phosphate cements (CPC), inserted into cranial defects in nude rats, promoted bone regeneration [28]. Thus, these scaffolds are suitable for bone regeneration, showing good results in newly formed bone volumes in animal studies [75, 78].

Among many polymeric materials that have been widely studied and used in dentistry, PLGA has shown biocompatibility and good physical properties with suitable resorption times. For this reason, it is extensively used in dental procedure for bone healing [4]. Similar to calcium-based scaffolds, PLGA shows high hydrophobicity that entails the modification of PLGA surface in order to improve cell adhesion [79–81]. In fact, Chuenjitkuntaworn et al. showed that a novel fabricated 3D-PCL/HA scaffold possessed a good biocompatibility for osteoblasts, supporting cell growth and calcium deposition of three kinds of mesenchymal stem cells (DPSCs, BMSCs, and SHED) [79]. Other studies have suggested the potential roles of combined scaffolds of PLGA and PCL and organic matrices of collagen and MSCs in bone restoration by the creation of functional synthetic substitutes [45, 62, 81]. Graziano et al. demonstrated that the concave surface of PLGA 85 : 15, HA chips, and titanium increase cellular activity, matrix deposition, and the expression of bone-specific genes of human DPSCs in vitro [81]. Ryan et al. demonstrated that PLGA/PCL and HA/TCP scaffolds promoted in vitro cartilage matrices, whereas the in vivo application of these scaffolds supported progressive lamellar-like bone formation with mature bone marrow development for up to 8 weeks in mice [82].

We reviewed the most widely used biomaterials for scaffolds in oral implantology and oral surgery that are detailed in Table 1. Thus far, the literature suggests that it has not been possible to develop the "perfect" scaffold for maxillary bone regeneration. However, we can infer that the combination of different biomaterials represents the goal for future tissue engineering studies and clinical trials in dentistry.

5. Conclusion

Currently, dentists can select from among several biomaterials with different characteristics for bone regenerative surgery. Recent studies have shown that the use of combined scaffolds supplemented with mesenchymal stem cells is a safe procedure with predictable successful outcomes. In fact, several studies have demonstrated a good interaction between organic or inorganic scaffolds and adult stem cells in vitro. Thus, tissue engineering approaches have significantly and successfully enhanced the potential for bone regeneration in in vivo grafts. In the future, we will be able to develop custom-made 3D composite scaffolds that can be grafted with stem cells and precisely tailored to complement the exact shape of the bone defect. Therefore, future studies are needed to optimize approaches to facilitate complete restoration of defects in both hard and soft tissues.

Competing Interests

The authors declare that there is no conflict of interests regarding the publication of this paper.

Acknowledgments

The authors would like to thank Editage (https://www.editage.com) for English language editing.

References

[1] L. Rimondini and S. Mele, "Stem cell technologies for tissue regeneration in dentistry," *Minerva Stomatologica*, vol. 58, no. 10, pp. 483–500, 2009.

[2] H. Zhao and Y. Chai, "Stem cells in teeth and craniofacial bones," *Journal of Dental Research*, vol. 94, no. 11, pp. 1495–1501, 2015.

[3] R. Rai, R. Raval, R. V. S. Khandeparker, S. K. Chidrawar, A. A. Khan, and M. S. Ganpat, "Tissue engineering: step ahead in maxillofacial reconstruction," *Journal of International Oral Health*, vol. 7, no. 9, pp. 138–142, 2015.

[4] L. Larsson, A. M. Decker, L. Nibali, S. P. Pilipchuk, T. Berglundh, and W. V. Giannobile, "Regenerative medicine for periodontal and peri-implant diseases," *Journal of Dental Research*, vol. 95, no. 3, pp. 255–266, 2016.

[5] S. Liu, J. Zhou, X. Zhang et al., "Strategies to optimize adult stem cell therapy for tissue regeneration," *International Journal of Molecular Sciences*, vol. 17, no. 6, article no. 982, 2016.

[6] D. Hughes and B. Song, "Dental and nondental stem cell based regeneration of the craniofacial region: a tissue based approach," *Stem Cells International*, vol. 2016, Article ID 8307195, 20 pages, 2016.

[7] G. Juodzbalys and M. Kubilius, "Clinical and radiological classification of the jawbone anatomy in endosseous dental implant treatment," *Journal of Oral and Maxillofacial Research*, vol. 4, no. 2, article no. e2, 2013.

[8] R. Rodriguez y Baena, S. M. Lupi, R. Pastorino, C. Maiorana, A. Lucchese, and S. Rizzo, "Radiographic evaluation of regenerated bone following poly(Lactic-Co- Glycolic) acid/hydroxyapatite and deproteinized bovine bone graft in sinus lifting," *Journal of Craniofacial Surgery*, vol. 24, no. 3, pp. 845–848, 2013.

[9] R. Rodriguez y Baena, R. Pastorino, E. Gherlone, L. Perillo, S. Saturnino, and A. Lucchese, "Histomorphometric evaluation of two different bone substitutes in sinus augmentation procedures: a randomized controlled trial in humans," *The International Journal of Oral & Maxillofacial Implants*, vol. 32, no. 1, pp. 188–194, 2017.

[10] R. F. Neiva, G. F. Neiva, and H.-L. Wang, "Utilization of mandibular tori for alveolar ridge augmentation and maxillary sinus lifting: a case report," *Quintessence International*, vol. 37, no. 2, pp. 131–137, 2006.

[11] A. S. T. AlGhamdi, "Management of combined ridge defect and osteotome sinus floor elevation with simultaneous implant placement—a 36-month follow-up case report," *The Journal of Oral Implantology*, vol. 35, no. 5, pp. 225–231, 2009.

[12] M. Monti, A. Graziano, S. Rizzo et al., "In vitro and in vivo differentiation of progenitor stem cells obtained after mechanical digestion of human dental pulp," *Journal of Cellular Physiology*, vol. 232, no. 3, pp. 548–555, 2016.

[13] L. Trovato, M. Monti, C. del Fante et al., "A new medical device rigeneracons allows to obtain viable micro-grafts from mechanical disaggregation of human tissues," *Journal of Cellular Physiology*, vol. 230, no. 10, pp. 2299–2303, 2015.

[14] M. T. P. Albuquerque, M. C. Valera, M. Nakashima, J. E. Nör, and M. C. Bottino, "Tissue-engineering-based strategies for regenerative endodontics," *Journal of Dental Research*, vol. 93, no. 12, pp. 1222–1231, 2014.

[15] N. Monteiro and P. C. Yelick, "Advances and perspectives in tooth tissue engineering," *Journal of Tissue Engineering and Regenerative Medicine*, 2016.

[16] A. Khojasteh, S. R. Motamedian, M. R. Rad, M. H. Shahriari, and N. Nadjmi, "Polymeric vs hydroxyapatite-based scaffolds on dental pulp stem cell proliferation and differentiation," *World Journal of Stem Cells*, vol. 7, no. 10, pp. 1215–1221, 2015.

[17] L. Polo-Corrales, M. Latorre-Esteves, and J. E. Ramirez-Vick, "Scaffold design for bone regeneration," *Journal of Nanoscience and Nanotechnology*, vol. 14, no. 1, pp. 15–56, 2014.

[18] M. Kadkhodazadeh, A. Lafzi, S. Raoofi et al., "Comparison of the effects of different implant apical designs on the magnitude and distribution of stress and strain in bone: a finite element analysis study," *Journal of Long-Term Effects of Medical Implants*, vol. 24, no. 2-3, pp. 109–119, 2014.

[19] S. J. Hollister, C. Y. Lin, E. Saito et al., "Engineering craniofacial scaffolds," *Orthodontics & Craniofacial Research*, vol. 8, no. 3, pp. 162–173, 2005.

[20] L. L. Hench and J. M. Polak, "Third-generation biomedical materials," *Science*, vol. 295, no. 5557, pp. 1014–1017, 2002.

[21] A. Kinaci, V. Neuhaus, and D. C. Ring, "Trends in bone graft use in the United States," *Orthopedics*, vol. 37, no. 9, pp. e783–e788, 2014.

[22] N. P. Lang and J. Lindhe, *Clinical Periodontology and Implant Dentistry*, John Wiley and Sons, Chichester, UK, 6th edition, 2015.

[23] N. D. Evans, E. Gentleman, and J. M. Polak, "Scaffolds for stem cells," *Materials Today*, vol. 9, no. 12, pp. 26–33, 2006.

[24] K. Rezwan, Q. Z. Chen, J. J. Blaker, and A. R. Boccaccini, "Biodegradable and bioactive porous polymer/inorganic composite scaffolds for bone tissue engineering," *Biomaterials*, vol. 27, no. 18, pp. 3413–3431, 2006.

[25] S. P. Pilipchuk, A. B. Plonka, A. Monje et al., "Tissue engineering for bone regeneration and osseointegration in the oral cavity," *Dental Materials*, vol. 31, no. 4, pp. 317–338, 2015.

[26] R. Manfro, F. S. Fonseca, M. C. Bortoluzzi, and W. R. Sendyk, "Comparative, histological and histomorphometric analysis of three anorganic bovine xenogenous bone substitutes: bio-oss, bone-fill and gen-ox anorganic," *Journal of Maxillofacial and Oral Surgery*, vol. 13, no. 4, pp. 464–470, 2014.

[27] M. E. Aichelmann-Reidy and R. A. Yukna, "Bone replacement grafts. The bone substitutes.," *Dental clinics of North America*, vol. 42, no. 3, pp. 491–503, 1998.

[28] *Collins English Dictionary—Complete & Unbridged*, HarperCollins Publishers, Glasgow, UK, 6th edition, 2016.

[29] H.-S. Yun, J.-W. Park, S.-H. Kim, Y.-J. Kim, and J.-H. Jang, "Effect of the pore structure of bioactive glass balls on biocompatibility in vitro and in vivo," *Acta Biomaterialia*, vol. 7, no. 6, pp. 2651–2660, 2011.

[30] K. Omata, T. Matsuno, K. Asano, Y. Hashimoto, Y. Tabata, and T. Satoh, "Enhanced bone regeneration by gelatin-β-tricalcium phosphate composites enabling controlled release of bFGF," *Journal of Tissue Engineering and Regenerative Medicine*, vol. 8, no. 8, pp. 604–611, 2014.

[31] E. J. G. Schepers, P. Ducheyne, L. Barbier, and S. Schepers, "Bioactive glass particles of narrow size range: a new material for the repair of bone defects," *Implant Dentistry*, vol. 2, no. 3, pp. 151–156, 1993.

[32] M. Simion, U. Misitano, L. Gionso, and A. Salvato, "Treatment of dehiscences and fenestrations around dental implants using resorbable and nonresorbable membranes associated with bone autografts: a comparative clinical study," *The International Journal of Oral & Maxillofacial Implants*, vol. 12, no. 2, pp. 159–167, 1997.

[33] E. Schepers, M. D. Clercq, P. Ducheyne, and R. Kempeneers, "Bioactive glass particulate material as a filler for bone lesions," *Journal of Oral Rehabilitation*, vol. 18, no. 5, pp. 439–452, 1991.

[34] V. A. Kumar, J. M. Caves, C. A. Haller et al., "Acellular vascular grafts generated from collagen and elastin analogs," *Acta Biomaterialia*, vol. 9, no. 9, pp. 8067–8074, 2013.

[35] S. Willerth and S. Sakiyama-Elbert, "Combining stem cells and biomaterial scaffolds for constructing tissues and cell delivery," in *StemBook*, S. Willerth and S. Sakiyama-Elbert, Eds., Harvard Stem Cell Institute, Cambridge, UK, 2008.

[36] T. Matsuno, K. Omata, Y. Hashimoto, Y. Tabata, and T. Satoh, "Alveolar bone tissue engineering using composite scaffolds for drug delivery," *Japanese Dental Science Review*, vol. 46, no. 2, pp. 188–192, 2010.

[37] P. Gentile, V. Chiono, I. Carmagnola, and P. V. Hatton, "An overview of poly(lactic-co-glycolic) Acid (PLGA)-based biomaterials for bone tissue engineering," *International Journal of Molecular Sciences*, vol. 15, no. 3, pp. 3640–3659, 2014.

[38] N. Tanataweethum, W. Liu, W. Goebel, D. Li, and T. Chu, "Fabrication of Poly-l-lactic acid/dicalcium phosphate dihydrate composite scaffolds with high mechanical strength—implications for bone tissue engineering," *Journal of Functional Biomaterials*, vol. 6, no. 4, pp. 1036–1053, 2015.

[39] R. A. Jain, "The manufacturing techniques of various drug loaded biodegradable poly(lactide-co-glycolide) (PLGA) devices," *Biomaterials*, vol. 21, no. 23, pp. 2475–2490, 2000.

[40] H. Cao and N. Kuboyama, "A biodegradable porous composite scaffold of PGA/β-TCP for bone tissue engineering," *Bone*, vol. 46, no. 2, pp. 386–395, 2010.

[41] V. D'Antò, M. G. Raucci, V. Guarino, S. Martina, R. Valletta, and L. Ambrosio, "Behaviour of human mesenchymal stem cells on chemically synthesized HA-PCL scaffolds for hard tissue regeneration," *Journal of Tissue Engineering and Regenerative Medicine*, vol. 10, no. 2, pp. E147–E154, 2016.

[42] N. Thuaksuban, T. Nuntanaranont, W. Pattanachot, S. Suttapreyasri, and L. K. Cheung, "Biodegradable polycaprolactone-chitosan three-dimensional scaffolds fabricated by melt stretching and multilayer deposition for bone tissue engineering: assessment of the physical properties and cellular response," *Biomedical Materials*, vol. 6, no. 1, Article ID 015009, 2011.

[43] S.-S. Kim, M. Sun Park, O. Jeon, C. Yong Choi, and B.-S. Kim, "Poly(lactide-co-glycolide)/hydroxyapatite composite scaffolds for bone tissue engineering," *Biomaterials*, vol. 27, no. 8, pp. 1399–1409, 2006.

[44] Y. X. Huang, J. Ren, C. Chen, T. B. Ren, and X. Y. Zhou, "Preparation and properties of poly(lactide-co-glycolide) (PLGA)/Nano-Hydroxyapatite (NHA) scaffolds by thermally induced phase separation and rabbit MSCs culture on scaffolds," *Journal of Biomaterials Applications*, vol. 22, no. 5, pp. 409–432, 2008.

[45] R. J. Kane, H. E. Weiss-Bilka, M. J. Meagher et al., "Hydroxyapatite reinforced collagen scaffolds with improved architecture and mechanical properties," *Acta Biomaterialia*, vol. 17, pp. 16–25, 2015.

[46] X. Qiao, S. Russell, X. Yang, G. Tronci, and D. Wood, "Compositional and in vitro evaluation of nonwoven type I collagen/poly-dl-lactic acid scaffolds for bone regeneration," *Journal of Functional Biomaterials*, vol. 6, no. 3, pp. 667–686, 2015.

[47] T. Kawase, K. Yamanaka, Y. Suda et al., "Collagen-coated poly(L-lactide-co-ε-caprolactone) film: a promising scaffold for cultured periosteal sheets," *Journal of Periodontology*, vol. 81, no. 11, pp. 1653–1662, 2010.

[48] M. Yazdimamaghani, M. Razavi, D. Vashaee, and L. Tayebi, "Surface modification of biodegradable porous Mg bone scaffold using polycaprolactone/bioactive glass composite," *Materials Science and Engineering: C*, vol. 49, pp. 436–444, 2015.

[49] K. M. Fawzy El-Sayed and C. E. Dörfer, "Gingival mesenchymal stem/progenitor cells: a unique tissue engineering gem," *Stem Cells International*, vol. 2016, Article ID 7154327, 16 pages, 2016.

[50] G. Asatrian, D. Pham, W. R. Hardy, A. W. James, and B. Peault, "Stem cell technology for bone regeneration: current status and potential applications," *Stem Cells and Cloning: Advances and Applications*, vol. 8, pp. 39–48, 2015.

[51] F.-J. Rodríguez-Lozano, C.-L. Insausti, F. Iniesta et al., "Mesenchymal dental stem cells in regenerative dentistry," *Medicina Oral, Patologia Oral y Cirugia Bucal*, vol. 17, no. 6, pp. e1062–e1067, 2012.

[52] A. R. Sanz, F. S. Carrión, and A. P. Chaparro, "Mesenchymal stem cells from the oral cavity and their potential value in tissue engineering," *Periodontology 2000*, vol. 67, no. 1, pp. 251–267, 2015.

[53] P. Bianco, P. G. Robey, and P. J. Simmons, "Mesenchymal stem cells: revisiting history, concepts, and assays," *Cell Stem Cell*, vol. 2, no. 4, pp. 313–319, 2008.

[54] M. E. Bernardo, M. A. Avanzini, C. Perotti et al., "Optimization of in vitro expansion of human multipotent mesenchymal stromal cells for cell-therapy approaches: further insights in the search for a fatal calf serum substitute," *Journal of Cellular Physiology*, vol. 211, no. 1, pp. 121–130, 2007.

[55] T. Yasui, Y. Mabuchi, H. Toriumi et al., "Purified human dental pulp stem cells promote osteogenic regeneration," *Journal of Dental Research*, vol. 95, no. 2, pp. 206–214, 2016.

[56] R. D'Aquino, A. De Rosa, V. Lanza et al., "Human mandible bone defect repair by the grafting of dental pulp stem/progenitor cells and collagen sponge biocomplexes," *European Cells and Materials*, vol. 18, pp. 75–83, 2009.

[57] D. Kaigler, G. Pagni, C. H. Park et al., "Stem cell therapy for craniofacial bone regeneration: a randomized, controlled feasibility trial," *Cell Transplantation*, vol. 22, no. 5, pp. 767–777, 2013.

[58] Y. Cha, M. Jeon, H.-S. Lee et al., "Effects of in vitro osteogenic induction on in vivo tissue regeneration by dental pulp and periodontal ligament stem cells," *Journal of Endodontics*, vol. 41, no. 9, pp. 1462–1468, 2015.

[59] S. Lee, Q. Zhang, and A. D. Le, "Dental stem cells: sources and potential applications," *Current Oral Health Reports*, vol. 1, no. 1, pp. 34–42, 2014.

[60] S. Gronthos, M. Mankani, J. Brahim, P. G. Robey, and S. Shi, "Postnatal human dental pulp stem cells (DPSCs) in vitro and in vivo," *Proceedings of the National Academy of Sciences of the United States of America*, vol. 97, no. 25, pp. 13625–13630, 2000.

[61] N. Nuti, C. Corallo, B. M. F. Chan, M. Ferrari, and B. Gerami-Naini, "Multipotent differentiation of human dental pulp stem cells: a literature review," *Stem Cell Reviews and Reports*, vol. 12, no. 5, pp. 511–523, 2016.

[62] A. Graziano, R. D'Aquino, M. G. Cusella-De Angelis et al., "Scaffold's surface geometry significantly affects human stem cell bone tissue engineering," *Journal of Cellular Physiology*, vol. 214, no. 1, pp. 166–172, 2008.

[63] M. Miura, S. Gronthos, M. Zhao et al., "SHED: stem cells from human exfoliated deciduous teeth," *Proceedings of the National Academy of Sciences of the United States of America*, vol. 100, no. 10, pp. 5807–5812, 2003.

[64] W. Sonoyama, Y. Liu, D. Fang et al., "Mesenchymal stem cell-mediated functional tooth regeneration in Swine," *PLoS ONE*, vol. 1, no. 1, article no. e79, 2006.

[65] C. Ferretti and M. Mattioli-Belmonte, "Periosteum derived stem cells for regenerative medicine proposals: boosting current knowledge," *World Journal of Stem Cells*, vol. 6, no. 3, pp. 266–277, 2014.

[66] G. Ceccarelli, A. Graziano, L. Benedetti et al., "Osteogenic potential of human oral-periosteal cells (PCs) isolated from different oral origin: an in vitro study," *Journal of Cellular Physiology*, vol. 231, no. 3, pp. 607–612, 2016.

[67] M. Mattioli-Belmonte, G. Teti, V. Salvatore et al., "Stem cell origin differently affects bone tissue engineering strategies," *Frontiers in Physiology*, vol. 6, article no. 266, 2015.

[68] H. Abukawa, M. Papadaki, M. Abulikemu et al., "The engineering of craniofacial tissues in the laboratory: a review of biomaterials for scaffolds and implant coatings," *Dental Clinics of North America*, vol. 50, no. 2, pp. 205–216, 2006.

[69] J. D. Currey, "Effects of differences in mineralization on the mechanical properties of bone," *Philosophical Transactions of the Royal Society of London B: Biological Sciences*, vol. 304, no. 1121, pp. 509–518, 1984.

[70] Y. Fillingham and J. Jacobs, "Bone grafts and their substitutes," *The bone & joint journal*, vol. 98-B, no. 1, SA, pp. 6–9, 2016.

[71] A. Brown, S. Zaky, H. Ray, and C. Sfeir, "Porous magnesium/PLGA composite scaffolds for enhanced bone regeneration following tooth extraction," *Acta Biomaterialia*, vol. 11, pp. 543–553, 2015.

[72] Y. Wang, N. Van Manh, H. Wang, X. Zhong, X. Zhang, and C. Li, "Synergistic intrafibrillar/extrafibrillar mineralization of collagen scaffolds based on a biomimetic strategy to promote the regeneration of bone defects," *International Journal of Nanomedicine*, vol. 11, pp. 2053–2067, 2016.

[73] W. Zhang, X. Frank Walboomers, T. H. van Kuppevelt, W. F. Daamen, Z. Bian, and J. A. Jansen, "The performance of human dental pulp stem cells on different three-dimensional scaffold materials," *Biomaterials*, vol. 27, no. 33, pp. 5658–5668, 2006.

[74] C. Gandhimathi, J. Venugopal, R. Ravichandran, S. Sundarrajan, S. Suganya, and S. Ramakrishna, "Mimicking nanofibrous hybrid bone substitute for mesenchymal stem cells differentiation into osteogenesis," *Macromolecular Bioscience*, vol. 13, no. 6, pp. 696–706, 2013.

[75] H. Namli, Ö. Erdogan, G. Gönlüşen et al., "Vertical bone augmentation using bone marrow-derived stem cells: an in vivo study in the rabbit calvaria," *Implant Dentistry*, vol. 25, no. 1, pp. 54–62, 2016.

[76] M. A. Lopes, F. J. Monteiro, J. D. Santos, A. P. Serro, and B. Saramago, "Hydrophobicity, surface tension, and zeta potential measurements of glass-reinforced hydroxyapatite composites," *Journal of Biomedical Materials Research*, vol. 45, no. 4, pp. 370–375, 1999.

[77] A. Polini, D. Pisignano, M. Parodi, R. Quarto, and S. Scaglione, "Osteoinduction of human mesenchymal stem cells by bioactive composite scaffolds without supplemental osteogenic growth factors," *PLoS ONE*, vol. 6, no. 10, Article ID e26211, 2011.

[78] H. Semyari, M. Rajipour, S. Sabetkish, N. Sabetkish, F. M. Abbas, and A.-M. Kajbafzadeh, "Evaluating the bone regeneration in calvarial defect using osteoblasts differentiated from adipose-derived mesenchymal stem cells on three different scaffolds: an animal study," *Cell and Tissue Banking*, vol. 17, no. 1, pp. 69–83, 2016.

[79] B. Chuenjitkuntaworn, T. Osathanon, N. Nowwarote, P. Supaphol, and P. Pavasant, "The efficacy of polycaprolactone/hydroxyapatite scaffold in combination with mesenchymal stem cells for bone tissue engineering," *Journal of Biomedical Materials Research A*, vol. 104, no. 1, pp. 264–271, 2016.

[80] J. M. Curran, S. Fawcett, L. Hamilton et al., "The osteogenic response of mesenchymal stem cells to an injectable PLGA bone regeneration system," *Biomaterials*, vol. 34, no. 37, pp. 9352–9364, 2013.

[81] A. Graziano, R. d'Aquino, M. G. Cusella-De Angelis et al., "Concave pit-containing scaffold surfaces improve stem cell-derived osteoblast performance and lead to significant bone tissue formation," *PLoS ONE*, vol. 2, no. 6, article e496, 2007.

[82] A. J. Ryan, J. P. Gleeson, A. Matsiko, E. M. Thompson, and F. J. O'Brien, "Effect of different hydroxyapatite incorporation methods on the structural and biological properties of porous collagen scaffolds for bone repair," *Journal of Anatomy*, vol. 227, no. 6, pp. 732–745, 2015.

Hindawi
Stem Cells International
Volume 2017, Article ID 3945403, 13 pages
https://doi.org/10.1155/2017/3945403

Review Article

Promising Therapeutic Strategies for Mesenchymal Stem Cell-Based Cardiovascular Regeneration: From Cell Priming to Tissue Engineering

Seung Taek Ji,[1] Hyunyun Kim,[1] Jisoo Yun,[1] Joo Seop Chung,[2] and Sang-Mo Kwon[1]

[1]*Laboratory for Vascular Medicine and Stem Cell Biology, Convergence Stem Cell Research Center, Medical Research Institute, Pusan National University School of Medicine, Yangsan, Republic of Korea*
[2]*Department of Internal Medicine, Medical Research Institute, Pusan National University School of Medicine, Busan, Republic of Korea*

Correspondence should be addressed to Joo Seop Chung; hemon@pusan.ac.kr and Sang-Mo Kwon; smkwon323@hotmail.com

Received 15 September 2016; Revised 2 December 2016; Accepted 13 December 2016; Published 20 February 2017

Academic Editor: Elisabetta A. Cavalcanti-Adam

Copyright © 2017 Seung Taek Ji et al. This is an open access article distributed under the Creative Commons Attribution License, which permits unrestricted use, distribution, and reproduction in any medium, provided the original work is properly cited.

The primary cause of death among chronic diseases worldwide is ischemic cardiovascular diseases, such as stroke and myocardial infarction. Recent evidence indicates that adult stem cell therapies involving cardiovascular regeneration represent promising strategies to treat cardiovascular diseases. Owing to their immunomodulatory properties and vascular repair capabilities, mesenchymal stem cells (MSCs) are strong candidate therapeutic stem cells for use in cardiovascular regeneration. However, major limitations must be overcome, including their very low survival rate in ischemic lesion. Various attempts have been made to improve the poor survival and longevity of engrafted MSCs. In order to develop novel therapeutic strategies, it is necessary to first identify stem cell modulators for intracellular signal triggering or niche activation. One promising therapeutic strategy is the priming of therapeutic MSCs with stem cell modulators before transplantation. Another is a tissue engineering-based therapeutic strategy involving a cell scaffold, a cell-protein-scaffold architecture made of biomaterials such as ECM or hydrogel, and cell patch- and 3D printing-based tissue engineering. This review focuses on the current clinical applications of MSCs for treating cardiovascular diseases and highlights several therapeutic strategies for promoting the therapeutic efficacy of MSCs in vitro or in vivo from cell priming to tissue engineering strategies, for use in cardiovascular regeneration.

1. Introduction

The World Health Organization (WHO) announced that the leading cause of death among chronic diseases worldwide is ischemic cardiovascular diseases, such as stroke and myocardial infarction (MI) [1]. Cardiovascular disease is caused by fat accumulation, platelet aggregation, and blood clots formation in the lining of blood vessels. Cardiovascular disease encompasses a very broad range of conditions, such as heart diseases, including MI, hypertension, heart failure, arrhythmias, cardiomyopathy, and ischemic heart disease due to atherosclerosis progression and vascular disease including peripheral vascular disease and stroke [2].

The treatment approach for the majority of cardiovascular disease is to administer drugs, and some cases may require surgery such as coronary angioplasty with stent insertion into the narrowed blood vessel to normalize blood flow through the coronary artery and coronary artery bypass [3]. In addition, gene therapy has been applied to treat cardiovascular disease [4]. In particular, phase II clinical trials of therapeutic angiogenesis using gene therapy are in progress, and the method is expected to be available soon for clinical use. The incidence of cardiovascular disease has continued to increase, and aside from transplantation, other therapies, despite recent advances in heart treatments, cannot fundamentally remedy the major etiology of cardiovascular disease; thus, there is a limit to how much treatment outcomes can be improved with the current approaches [5]. Although various studies have been conducted to overcome the limitations of cardiovascular therapies, stem cell therapy using several types of stem cells such as hematopoietic stem cells (HSCs), mesenchymal stem cells (MSCs), cardiac stem cells

(CSCs), and endothelial progenitor cells (EPCs) provides an alternative approach, and remarkable advances have been made in clinical and basic research [6].

Several reasons favor the clinical and therapeutic application of adult stem cells over embryonic stem cells (ESCs), including controlled proliferation, exceptional reliability, and a site-specific differentiation ability [7]. Among adult stem cells, MSCs are frequently used to treat the most common cardiovascular diseases. MSCs can be found in the bone marrow (BM), adipose tissue, umbilical cord blood (UCB), and many other tissues. They have self-renewing properties and are multipotent progenitor cells that can differentiate into various lineages such as osteocytes, chondrocytes, adipocytes, and myocytes [8–11]. MSCs also have immunomodulatory properties [12, 13]. In addition, MSCs are unlikely to lead to immune rejection because of their low expression of CD40, CD80, and CD86, as well as MHC class I molecules [14, 15]. The therapeutic benefit of this approach is based on the potency of secretion of beneficial cytokines and growth factors for tissue repair/regeneration, as well as the immunomodulation effect and/or their differentiation for regenerating damaged organs [16].

MSCs can be applied for cardiovascular regeneration and provide therapeutic benefit for cardiovascular disease. However, MSCs have several disadvantages regarding their therapeutic application, including their very low survival rate in vivo and integration rate into the host cells after transplantation [17]. Another limitation is the low accuracy in delivering the stem cells to the damaged site [18]. Various attempts have been made to improve the poor survival and longevity of engrafted MSCs. The first step in developing therapeutic strategies is the identification of more effective reagents for promoting the ability of stem cells via understanding stem cell niche modulators. An emerging promising therapeutic strategy is the preconditioning of MSCs before transplantation using cytokines and natural compounds that induce intracellular signaling or niche stimulation through paracrine mechanisms [19]. Another is a tissue engineering-based therapeutic strategy involving a cell scaffold, a cell-protein-scaffold architecture made of biomaterials such as ECM or hydrogel, and cell patch- and 3D printing-based tissue engineering, to enhance cell survival via cell-cell communication or cell-scaffold interactions [20].

This review focuses on promising cell therapeutic strategies for MSC therapy against cardiovascular diseases and introduces a variety of studies designed to promote the therapeutic efficacy of MSCs in vitro or in vivo from cell priming strategies to tissue engineering strategies for cardiovascular regeneration.

2. Characterization of MSCs

The term "mesenchymal stem cells" was introduced by Caplan in the early 1990s [21], although nonhematopoietic, "mesenchymal" precursor cells were first described in the 1970s by Friedenstein et al. as a population of bone marrow stromal cells capable of mesodermal differentiation and trophic support of hematopoiesis [22, 23].

MSCs are present in almost all tissues of the body and are located in the perivascular space [24]. They can also be isolated from other sources, such as adipose tissue [25–30], cartilage [31, 32], umbilical cord blood [33–36], and peripheral blood [37]. In addition, MSCs can be derived from many different organs and tissues, including the brain, spleen, liver, kidney, lung, bone marrow, muscle, thymus, and pancreas [38].

The Mesenchymal and Tissue Stem Cell Committee of the International Society for Cellular Therapy (ISCT) set minimal criteria in 2001 for defining MSCs. They must be plastic-adherent when maintained in standard culture conditions. Second, MSCs must express CD105, CD73, and CD90 and lack the expression of CD45, CD34, CD14, or CD11b; CD79α or CD19; and HLA-DR surface molecules as assessed by fluorescence-activated cell sorter analysis. Third, MSCs must be able to differentiate into osteoblasts, adipocytes and chondroblasts in vitro [39, 40]. Other surface markers generally expressed by MSCs include CD9, CD105 (SH2), CD73 (SH3/4), CD44, CD90 (Thy-1), CD71, CD106 (vascular cell adhesion molecule- [VCAM-] 1), CD166 (activated leukocyte cell adhesion molecule [ALCAM]), intercellular adhesion molecule- (ICAM-) 1, and CD29 [9, 14, 41, 42]. Stem cells are characterized by their ability to self-renew, clone, and differentiate into multiple tissues [6]. MSCs are a pluripotent cell type that can differentiate into several distinct lineages, including mesodermal lineage cells (osteoblasts, chondrocytes, and adipocytes) [9, 43, 44] and myogenic lineage [45]. Adipogenic differentiation is induced with FBS in medium supplemented with dexamethasone, insulin, isobutyl methyl xanthine, and indomethacin. The differentiation can be confirmed by the staining of lipid vacuoles with oil red O [46, 47] and measuring the levels of several proteins, including PPAR γ, fatty acid-binding protein aP2, and lipoprotein lipase [27]. For osteogenic differentiation, MSCs are treated with ascorbic acid, beta-glycerophosphate, and dexamethasone. The differentiation is confirmed increase in alkaline phosphatase activity and calcium deposition [47, 48]. Chondrogenic differentiation is induced by culture with serum-free medium supplemented with transforming growth factor-beta (TGF-β), resulting in an increase in the levels of highly glycosaminoglycan and type II collagen [46, 49].

Recently, in vivo studies demonstrated that human MSCs transdifferentiate into endoderm-derived cells and cardiomyocytes [50–52], and MSCs transdifferentiated into a cardiomyocyte-phenotype [53]. Animal preclinical studies of MSC administration in post-MI hearts revealed the ability of MSCs to engraft, differentiate, and produce substantial functional recovery [54–57]. In recent years, MSCs therapy has been translated to clinical trials for ischemic heart disease [58–60].

3. Clinical Trials Using MSCs against Cardiovascular Diseases

Cell-based treatments represent a new generation in the evolution of biological therapeutics. A prototypic cell-based therapy for heart failure using MSCs has successfully reached

the pivotal phase III trials, indicating adequate safety and efficacy data from phases I and II trials. Successful phase III trials can lead to the approval of a new biologic therapy for regenerative medicine [61]. There have been about 43 clinical trials using MSCs in relation to cardiovascular regeneration registered with clinicaltrials.gov (Table 1, a web-based service by the US National Institute of Health). Among the MSC-based clinical trials, studies designed to treat cardiovascular disease represent a substantial proportion (14.8%) [62]. On the basis of the rigorous preclinical testing highlighted above that demonstrated the safety of MSC delivery to patients with cardiac disease, clinical trials have been initiated for both acute MI and ischemic cardiomyopathy. The results of a clinical trial of autologous MSC transplantation might aid in improving the long-term survival of patients with severe heart failure and significantly reduce hospitalizations for worsening angina [63]. A much smaller study revealed that both autologous BM MNCs and expanded BM MSCs reduced myocardial scarring by 3 months, indicating the stimulation of beneficial tissue remodeling [64]. The intracoronary administration of MSCs has been shown to have a minor benefit on the left ventricular ejection fraction [65], and a meta-analysis of cell therapies involving intracoronary administration found that there was no clinical benefit for left ventricular function [66]. The four clinical trials of plasmonic photothermal therapy (PPTT) using silica-gold nanoparticles demonstrated the significant regression of coronary atherosclerosis [67]. In an early stage study of patients with ICM, the transendocardial injections of allogeneic and autologous MSCs without a placebo control were both associated with low rates of treatment-emergent SAEs, including immunologic reactions [68]. Transendocardial stem cell injection with MSCs or BMCs appeared to be safe for patients with chronic ischemic cardiomyopathy and LV dysfunction [69]. The intramyocardial injection of autologous MSCs into akinetic but nonrevascularized segments produced comprehensive regional functional restitution, which in turn drove improvement in global LV function. These findings, although inconclusive because of the lack of a placebo group, have important therapeutic and mechanistic hypothesis-generating implications [70].

4. Understanding MSC Biology for Tissue Regeneration

4.1. Enhancing MSC Survival for Cardiovascular Regeneration. In ischemic sites of ischemia-reperfusion injuries, cardiomyocytes undergo apoptosis [71]. Accumulating evidence clearly indicates that activated Akt signals protect cardiomyocytes from apoptosis. Similarly, transduced Akt in MSCs significantly enhanced their stem cell function in an in vivo rat model [72]. Lim et al. investigated the pivotal role of Akt-transduced MSCs in the ischemic porcine heart [55]. When applied to MI, Akt-MSCs administration increased the left ventricular ejection fraction and decreased the area of MI. Notably, Akt-MSCs have an enhanced cell survival ratio with augmented expression levels of ERK and VEGF, suggesting that administering Akt-transduced MSCs might be a promising therapeutic strategy for treating human patients with cardiovascular diseases.

Epidermal growth factor (EGF) is a well-known cytokine involved in cell growth and vascular tissue repair. In general, EGF binds to the EGF receptor (EGFR) and activates extracellular-regulated kinase (ERK) and Akt-mediated intracellular signaling pathways, resulting in increased cellular activities, including cell adhesion, migration, proliferation, and cell survival. Recently, it was reported that MSCs stimulated by soluble EGF induced EGFR signaling and promoted the upregulation of migration and proliferation [73]. Fan et al. also studied the pivotal role of surface-tethered EGF in MSC survival [74]. The proportion of total ERK that was phosphorylated was strongly linked to improved cell spreading and cell survival in tEGF-polymer conditions. Under these severe culture conditions, tEGF-polymer protected MSCs from FasL and eventually increased the survival rate, suggesting that tethered EGF might have protective functions in transplanted MSCs during acute inflammatory reactions.

Vascular endothelial growth factor (VEGF) has a pivotal role in cardiovascular regeneration. When MSCs isolated from B6 mice were cocultured with VEGF peptide, the primed MSCs exhibited reduced levels of cellular stress and higher expression of prosurvival factors via phosphorylation of Akt and Bcl-xL. The administration of MSCs primed with VEGF peptide in an MI disease model resulted in improved cardiac function via enhanced cell engraftment and cell survival capabilities, indicating that VEGF protects MSCs from cellular stress, leading to enhanced cardiac function and cardiovascular regeneration.

4.2. Enhancing MSC Proliferation for Cardiovascular Regeneration. In the human body, the subpopulations of MSCs are very small. Healthy MSCs dramatically activate their self-renewal signaling pathway when required. After the onset of an injury caused by ischemic cardiovascular diseases, an insufficient MSC number leads to impaired tissue regeneration. Furthermore, the clinical use of MSCs for tissue regeneration has been limited mainly because they have a low proliferation rate and progressively lose their stem cell properties during in vitro expansion. To overcome these limitations, many research groups have studied the signaling cascades associated with MSC proliferation and identified pivotal modulators for MSC proliferation for use in the treatment of cardiovascular diseases [75].

Octamer-binding transcription factor 4 (Oct4) and sex determining region Y-box 2 (Sox2) are pluripotent stem cell-specific factors. The pivotal roles of these two factors in maintaining MSC stemness and proliferation have been studied [76, 77]. Although early passage MSCs express Oct4 and Sox2 at low levels, their expression levels decrease as the passage number increases. To improve MSC proliferation and stemness, human adipose tissue MSCs (ATMSCs) were transfected with Oct4 and Sox2 [78], and the MSCs that expressed Oct4 and Sox2 exhibited enhanced proliferative activity. This result was mediated by the upregulation of cyclin D1, indicating that the transition of cells from G1 to S phase might be accelerated.

Table 1: Clinical trials with mesenchymal stem cells (https://clinicaltrials.gov/).

	Study	Year (country)	Study status	Age	Number treated	Phase	Study ID
1	Mesenchymal Stem Cells and Myocardial Ischemia	2010–2014 (France)	Completed	18 years and older	10	Phase 1 Phase 2	NCT01076920
2	Administration of Mesenchymal Stem Cells in Patients with Chronic Ischemic Cardiomyopathy (MESAMI2)	2015-2016 (France)	Ongoing	18 years to 75 years	90	Phase 2	NCT02462330
3	Stem Cell Therapy for Vasculogenesis in Patients with Severe Myocardial Ischemia	2009–2013 (Denmark)	Completed	30 years to 80 years	31	Phase 1 Phase 2	NCT00260338
4	Human Umbilical-Cord-Derived Mesenchymal Stem Cell Therapy in Ischemic Cardiomyopathy	2015–2018 (China)	Ongoing	18 years to 80 years	40	Phase 1 Phase 2	NCT02439541
5	MesenchYmal STROMAL CELL Therapy in Patients with Chronic Myocardial Ischemia (MyStromalCell Trial)	2010–2014 (Denmark)	Completed	30 years to 80 years	60	Phase 2	NCT01449032
6	Safety and Exploratory Efficacy Study of UCMSCs in Patients With Ischemic Heart Disease (SEESUPIHD)	2016-2017 (China)	Ongoing	18 years to 70 years	64	Phase 1 Phase 2	NCT02666391
7	Intracoronary Autologous Mesenchymal Stem Cells Implantation in Patients with Ischemic Dilated Cardiomyopathy	2012–2015 (Malaysia)	Ongoing	35 years to 75 years	80	Phase 2	NCT01720888
8	Therapy of Preconditioned Autologous BMMSCs for Patients With Ischemic Heart Disease	2015–2017 (China)	Ongoing	up to 75 years	200	Phase 1 Phase 2	NCT02504437
9	The TRansendocardial Stem Cell Injection Delivery Effects on Neomyogenesis STudy (The TRIDENT Study)	2013–2017 (USA)	Ongoing	21 years to 90 years	30	Phase 2	NCT02013674
10	Mesenchymal Stem Cell Administration in the Treatment of Coronary Graft Disease in Heart Transplant Patients	2014–2017 (France)	Ongoing	18 years to 80 years	14	Phase 1 Phase 2	NCT02472002
11	Safety and Efficacy of Intracoronary Adult Human Mesenchymal Stem Cells after Acute Myocardial Infarction	2007–2011 (Korea)	Completed	18 years to 70 years	80	Phase 2 Phase 3	NCT01392105
12	Human Umbilical Cord Stroma MSC in Myocardial Infarction	2014–2017 (Turky)	Ongoing	30 years to 80 years	79	Phase 1 Phase 2	NCT02323477
13	Stem Cell Injection to Treat Heart Damage during Open Heart Surgery	2012–2020 (USA)	Ongoing	18 years to 85 years	60	Phase 1	NCT01557543
14	Safety Study of Adult Mesenchymal Stem Cells (MSC) to Treat Acute Myocardial Infarction	2005–2014 (Australia)	Completed	21 years to 85 years	53	Phase 1	NCT00114452
15	RELIEF (A Randomized, Open labEled, muLticenter Trial for Safety and Efficacy of Intracoronary Adult Human Mesenchymal stEm Cells Acute Myocardial inFarction)	2012–2016 (Korea)	Ongoing	20 years to 70 years	135	Phase 3	NCT01652209
16	Intracoronary Human Wharton's Jelly-Derived Mesenchymal Stem Cells (WJ-MSCs) Transfer in Patients with Acute Myocardial Infarction (AMI)	2011–2015 (China)	Completed	18 years and older	160	Phase 2	NCT01291329
17	Ex Vivo Cultured Bone Marrow Derived Allogenic MSCs in AMI	2009–2013 (India)	Completed	20 years to 70 years	20	Phase 1 Phase 2	NCT00883727
18	"ESTIMATION Study" for Endocardial Mesenchymal Stem Cells Implantation in Patients after Acute Myocardial Infarction	2011–2016 (Russia)	Ongoing	30 years to 75 years	50	Phase 3	NCT01394432
19	Prochymal® (Human Adult Stem Cells) Intravenous Infusion following Acute Myocardial Infarction (AMI)	2009–2016 (Australia)	Ongoing	21 years to 85 years	220	Phase 2	NCT00877903
20	Plasmonic Nanophotothermic Therapy of Atherosclerosis	2007–2015 (Russia)	Completed *Has results*	45 years to 65 years	180	Phase 1 Phase 2	NCT01270139
21	The Percutaneous Stem Cell Injection Delivery Effects on Neomyogenesis Pilot Study (The POSEIDON-Pilot Study)	2010–2015 (USA)	Completed *Has results*	21 years to 90 years	31	Phase 1 Phase 2	NCT01087996
22	The Transendocardial Autologous Cells (hMSC or hBMC) in Ischemic Heart Failure Trial (TAC-HFT)	2008–2015 (USA)	Completed *Has results*	21 years to 90 years	65	Phase 1 Phase 2	NCT00768066
23	Safety and Efficacy Study of Stem Cell Transplantation to Treat Dilated Cardiomyopathy	2013–2015 (Slovenia, USA)	Completed	18 years to 80 years	110	Phase 2	NCT00629018

Table 1: Continued.

	Study	Year (country)	Study status	Age	Number treated	Phase	Study ID
24	Prospective Randomized Study of Mesenchymal Stem Cell Therapy in Patients Undergoing Cardiac Surgery (PROMETHEUS)	2007–2015 (USA)	Completed *Has results*	21 years to 80 years	9	Phase 1 Phase 2	NCT00587990
25	Human Umbilical Cord-derived Mesenchymal Stem Cells with Injectable Collagen Scaffold Transplantation for Chronic Ischemic Cardiomyopathy	2015–2018 (China)	Ongoing	35 years to 65 years	45	Phase 1 Phase 2	NCT02635464
26	The Effect of Mobilized Stem Cell by G-CSF and VEGF Gene Therapy in Patients with Stable Severe Angina Pectoris	2003–2011 (Denmark)	Completed	20 years to 80 years	48	Phase 1 Phase 2	NCT00135850
27	Plasmonic Photothermal and Stem Cell Therapy of Atherosclerosis versus Stenting	2010–2015 (Russia)	Terminated	45 years to 65 years	62	Phase 1	NCT01436123
28	Clinical Trial of Autologous Adipose Tissue Derived Stromal Cell Therapy for Ischemic Heart Failure	2012–2014 (Japan)	Enrolling by invitation	20 years and older	6	—	NCT01709279
29	Safety Study of Allogeneic Mesenchymal Precursor Cell Infusion in MyoCardial Infarction	2012–2015 (USA)	Ongoing	18 years and older	225	Phase 2	NCT01781390
30	PercutaneOus StEm Cell Injection Delivery Effects On Neomyogenesis in Dilated CardioMyopathy (The POSEIDON-DCM Study)	2011–2016 (USA)	Ongoing	18 years to 95 years	36	Phase 1 Phase 2	NCT01392625

The Wnt signaling pathway regulates cell proliferation and cell fate determination [79]. The canonical Wnt signaling pathway is a well-known Wnt signaling pathway involved in stem cell biology. Wnt ligands secreted from a cell can affect the cell itself (autocrine) or neighboring cells (paracrine), and they bind to their receptor, low-density lipoprotein receptor-related protein (LRP) 5/6. As a result, stabilized β-catenin is translocated to the nucleus, where it upregulates its downstream genes. Activation of the canonical Wnt signaling pathway in stem cells results in increased proliferation or self-renewal activity in ESCs, neural stem cells (NSCs) [80], and HSCs [81]. In addition to previous studies on stem cells, MSC regulation by Wnt signaling pathways has been investigated. When adult MSCs are treated with Wnt3a ligand, a typical ligand for the canonical Wnt signaling pathway, the MSCs exhibit enhanced proliferation, but decreased apoptosis [82]. However, treatment with secreted frizzled-related protein 3, a canonical Wnt signaling inhibitor, had opposite effects on MSCs. Another research group used lithium as a proliferation activator [83] to target glycogen synthase kinase-3β (GSK-3β), a downstream protein in the canonical Wnt signaling pathway. When BM-derived MSCs were treated with lithium, the proportion of cells in S phase and expression levels of cyclin D1 were significantly increased. In contrast, Wnt5a, a noncanonical Wnt member, has been reported to promote MSC differentiation [84, 85], suggesting that a distinct mechanism of Wnt ligand-mediated MSC signaling might be involved.

Estrogen is the primary female sex hormone and controls the female reproductive system and secondary sex characteristics, indicating its multifunctional roles in many tissues. Similar to many other types of cells, MSCs have estrogen receptor (α and β), suggesting that estrogen might affect MSC function. Estradiol (E2), a major form of estrogen, was found to affect MSC proliferation [86]. 17-β estradiol-pretreated MSCs exhibited a significantly increased proliferation rate in vitro, although it did not alter the MSC phenotypes, including the surface marker expression of MSCs such as CD105 and CD166. Based on these data, 17-β estradiol might be a priming agent for enhancing MSC function in practical applications.

4.3. Enhancing MSC Homing for Cardiovascular Regeneration. The process of delivering cells to injured tissues is called "homing," which is induced in response to a diverse array of molecules including chemokines and growth factors. To overcome the insufficient number of homed MSCs, many researchers have investigated the pivotal regulators of MSC homing to ischemic sites.

MSCs strongly express CXC chemokine receptor 4 (CXCR4) on their surface. Stromal-derived factor-1 (SDF-1), which is secreted from ischemic tissues, binds to CXCR4 on the MSC surface, inducing MSC migration to injured sites. In line with this mechanism, MSCs were retrovirally transduced with a CXCR4 overexpression vector and pre-clinically applied to an MI disease model [87]. As a result, there were an increased cell number of transplanted cells, and echocardiographic imaging of the MI area showed less anterior wall thinning and improvement in the left ventricular (LV) chamber dimensions.

Arachidonic acid (AA) is a polyunsaturated omega-6 fatty acid found in the cell's membrane, and it plays a critical role as a lipid second messenger. Although it has been reported that injured tissues release large amounts of AA, the detailed and precise mechanism is not fully understood. The effect of AA on skin wound healing was studied with human umbilical cord blood-derived MSCs (hUCB-MSCs) [88], and preconditiong hUCB-MSCs with AA improved wound healing, reepithelization, and angiogenesis. AA activates mammalian target of rapamycin complex

2 (mTORC2) and Akt via the GPR40/phosphoinositide 3-kinase (PI3K) signaling pathway. p38 is phosphorylated by PKCζ and it activates Sp1. As a result, membrane type 3-matrix metalloproteinase (MT3-MMP) is stimulated, and eventually the secreted MT3-MMPs degrade fibronectin and facilitate hUCB-MSC migration, suggesting that skin wound healing might be promoted by priming MSCs with AA via MT3-MMP-dependent fibronectin degradation.

An effective cell therapy for MI requires accurate MSC delivery. To enhance MSC homing activity, phage display approaches have been used to screen MI-specific peptide sequences [89]. In a mouse MI model, four peptide sequences were identified, CRPPR, CRKDKC, KSTRKS, and CARSKNKDC, which are synthesized as palmitated derivatives. MI homing peptides-coated MSCs were injected into a mouse model of MI, and the number of migrated MSCs was greater in the coated groups than in the noncoated groups, indicating that the coating of MSCs with homing peptides is a promising therapeutic methodology for treating cardiovascular diseases including MI.

5. Priming Strategies for Therapeutic MSCs for Cardiovascular Regeneration

In general, the low survival rate of transplanted stem cells in ischemic myocardium has limited their therapeutic efficacy against ischemic cardiovascular diseases. Accumulating evidence indicates that the pharmacological pretreatment of MSCs ex vivo is a rational approach to reinforce the cells so that they can withstand the ischemic and reperfusion injury environment [90–92], although researchers first should define and clarify potential priming molecules and agents for cardiovascular regeneration.

Curcumin effectively protects MSCs from oxidative stress via regulation of PTEN/Akt/p53 and HO-1 signaling proteins and thereby promotes VEGF release from MSCs, facilitating the enhancement of cardiac function, improving cells retention, and reducing fibrosis in MI hearts [90]. As a conventional inductor, 5-azacytidine (5-AZA) has been used to induce MSC differentiation into cardiomyocytes [53, 93, 94]. Similarly, BMP-2 present in the embryonic heart was used to differentiate ESCs or induce pluripotent stem cells (iPS) into cardiomyocyte-like cells [95, 96], which opens up new possibilities for cardiomyocyte differentiation from MSCs [97].

Angiotensin-II (Ang-II) is peptide hormone that is produced from angiotensin-I (Ang-I) through modifications by angiotensin-converting enzyme (ACE). It is well-known that Ang-II increases blood volume and pressure. MSCs pretreated with Ang-II trigger VEGF production. Based on the effect of Ang-II on VEGF production, the therapeutic efficacy of Ang-II-preconditioned MSCs was investigated [98]. MSCs, isolated from Sprague-Dawley rats, were pretreated with 100 nM of Ang-II for 24 hours and injected into the border zone of the ischemic heart. After 30 days, the restoration efficacy of MSCs was evaluated by measuring angiogenesis, cardiac function, cell differentiation fibrosis, infarct size, and VEGF expression. Ang-II-MSCs exhibited better cardiac function, higher expression of VEGF and von Willebrand factor (vWF), less cardiac fibrosis, and a smaller infarct size. In addition, preconditioning MSCs with Ang-II resulted in an increased survival rate and enhanced tube formation via the upregulation of connexin-43 (Cx43), suggesting that priming MSCs with Ang-II improved their therapeutic efficacy by enhancing angiogenesis and gap junction formation, in addition to the paracrine effect of VEGF against MI.

Fucoidan, a natural compound found in brown algae and seaweed, has various functional properties in biological processes. This sulfated polysaccharide reacts with cytokines and contributes to improving cell functional activity, including antioxidant effects, proliferation, and differentiation. The effects of fucoidan on preconditioned adipose tissue-derived MSCs (ADSCs) were evaluated in a chronic kidney disease (CKD) model [99]. Fucoidan-ADSCs exhibited increased proliferation potential with a significant increase in cell cycle-associated proteins such as cyclin E, cyclin D1, cyclin dependent kinase 2 (CDK 2), and CDK4. When applied to a CKD disease model, the in vivo transplantation of fucoidan-ADSCs enhanced the proliferation, incorporation, and endothelial differentiation of transplanted MSCs in ischemic sites, revealing a novel therapeutic strategy of using MSCs for cardiovascular regeneration.

6. Tissue Engineering Strategies: A Powerful Application of MSC-Mediated Vascular Regeneration

Stem cells derived from healthy tissue can be used for tissue regeneration. In studies of cardiac tissue regeneration, researchers originally focused on organ transplantation. However, with the development of stem cell-based technics, stem cells are predicted to be useful for cardiac tissue regeneration. Particularly, MSCs are promising candidates for heart failure treatment because of their unique characteristics. Over the past decade, MSCs have gained attention as a therapeutic approach for treating MI compared with other cell types considered for cardiomyoplasty. MSCs have unique properties that may translate into convenient and extremely effective cell therapy [8, 100]. Recent reports have questioned their "transdifferentiation" potential after injection into the myocardium and suggested the benefits of MSC mechanisms [101]. However, the tissues regenerated by this tissue engineering and widely applied to patients are still very limited, including skin, bone, cartilage, capillary, and periodontal tissues. What are the reasons for such slow advances in clinical applications of tissue engineering? This article gives the brief overview on the current tissue engineering, covering the fundamentals and applications.

6.1. Biomaterial-Based Tissue Engineering for Cardiovascular Regeneration. Biomaterials are biofriendly materials that have been engineered to interact with biological systems, and they are capable of protecting transplanted cells against harsh ischemic environments, including low oxygen, nutrient depletion, and severe attack by inflammatory cells [102].

Scaffolds containing silicon dioxide for tissue engineering enhance MSC growth through ERK1/2 activation [103].

Another study showed that the proliferation of hMSCs cultured in media containing 2 or 4 μM silicon was significantly higher than that in control medium, suggesting the enhanced mechanical strength of the medium with silicon may have contribute to this result [104]. Other scaffolds, such as collagen-HA, also enhance MSC attachment and proliferation [105], and collagen I scaffolds exhibit excellent cellular compatibility [106]. Similarly, nanoparticle-containing liposomes were cultured with MSCs to make sheet-like structures [107]. The MSC sheets were layered on the ischemic tissues, and the recovery efficiency was evaluated. The organized structure of MSC sheets provided protection against ischemic limb diseases due to increased blood flow and recovery of angiogenesis, suggesting that tissue engineering scaffolds containing nanoparticles might improve MSC growth and that single-component silica-derived nanoparticles could be advantageous for scaffolds used in stem cell therapy [103, 108]. In addition, various biomaterials have been employed in 3D scaffolds for cultured MSCs, such as chitosan, silk, and alginate [109–111].

Cell-based gene therapy combined with biomaterial-based tissue engineering offers an alternative strategy for therapeutic angiogenesis. Chinese hamster ovary (CHO) cells were transfected with pCDNA3-VEGF-hemagglutinin (HA) vector [112]. The genetically modified CHO cells secreted VEGF and they were enveloped into semipermeable microcapsules. When the microencapsulated VEGF-CHO cells were transplanted into the MI region of rats, the capillary density of the microencapsulated VEGF-CHO cell group was significantly higher than that of the control group, with functional improvement of the injured heart. Wang et al. also examined the effect of the transplantation of microencapsulated Schwann cells with MSCs on angiogenesis [113]. In the harsh microenvironment of the nervous system, Schwann cells secrete VEGF, which enhances neuronal survival [114]. When semipermeable alginate-poly-L-lysine-alginate microcapsules containing Schwann cells and MSCs were applied to an acute myocardial infarction (AMI) rat model, they improved cardiac function because the recipient cells avoided the immune reaction due to the microencapsulation, and they secreted VEGF through small pores on their surface. Another research group investigated genetically modified MSCs that secreted glucagon-like peptide 1 (GLP-1) [115], which regulates blood glucose homeostasis and has a cardioprotective effect in heart disease. When Bead-GLP-1 MSCs were delivered to coronary artery branches in a porcine MI model, the echocardiography results showed improved left ventricular (LV) function, whereas histological analysis showed reduced inflammation and a lower apoptosis rate, indicating that combining the therapeutic strategies of utilizing recombinant GLP-1 and the inherent paracrine stem cell factors of MSCs might be beneficial for clinical application against MI.

Recently, cardiac patch-based therapeutics have been suggested as novel noninvasive methods functional strategies for cardiac regeneration because they can overcome the negative aspects of invasive surgery including complications resulting from the altered mechanics of the infarcted heart [116]. Bioengineered cardiac patches are made from a stem cell seeded multilayered scaffold. Briefly, stem cells, including MSCs, cardiac progenitor cells (CPCs), and endothelial progenitor cells (EPCs), grow on the cell-sheet culture system and generate a cell-sheet structure that can be cultured multiple times. Recently, MSC patches were applied to infarcted hearts with a previously described protocol [117]. The engineered MSC sheets represent a tightly adhered meshwork with adhesive agents, including fibronectin and laminin. MSC patches were attached to the ligated left coronary artery (LCA) in rats. Twelve weeks after patch implantation, echocardiography and heart catheterization were performed. The MSC patch implanted group exhibited improved heart function. In addition, neomuscle fibers and neomicrovessels were observed in the ligated LCA, as well as increased levels of angiogenic cytokines (bFGF, vWF, and PDGF-B) and cardioprotective factors (IGF-1 and HGF) in the MSC patch group, indicating the effectiveness of the bioengineered MSC patch as a therapeutic strategy against cardiovascular diseases including MI. (Figure 1). Taken together, studies of potential bioengineered cardiac patches-based therapeutics may improve the therapeutic efficacy of transplanted MSCs to overcome the limited number of multilayer of cardiac patches for cell survival and complications resulting from the altered mechanics of the infarcted heart and improve cell infiltration and migration of transplanted patch-derived MSCs.

6.2. Emerging 3D Printing-Based Tissue Engineering for Cardiovascular Regeneration. 3D printing is a novel manufacturing technique in which 3D objects can be synthesized. Objects that researchers want to make are captured with computed tomography (CT) or magnetic resonance imaging (MRI). Then, a 3D computer assisted design (CAD) model is developed from the captured objects. Digitally sliced images are generated by a visualized motion program. Finally, the captured objects are printed with a 3D printer, and they can be reprinted as needed [118]. Similar to commercial personal printers, 3D printers require ink. 3D printers, however, can use many types of ink. The human body is composed of various types of tissue. These tissue structures cover a wide range of sizes and stiffness. To meet these different demands, many types of ink have been developed. To develop functional 3D-engineered tissue constructs, various key components should be evaluated.

3D-engineered tissue constructs require several key components, such as cells, extracellular matrix (ECM), and vasculature. Each component supports a biomimetic function of the engineered tissue constructs. Thick vascularized tissues were made by bioprinting with 3D cell-laden ink [119] using two types of ink. Fugitive (vascular) ink contains pluronic and thrombin, and cell-laden ink contains gelatin, fibrinogen, thrombin, transglutaminase, and cells. Fugitive ink is printed on a 3D perfusion chip. Then, cell-laden ink is cast over the printed inks. Gelatin and fibrins are cross-linked by diffused transglutaminase from the molten casting matrix. Upon cooling, the fugitive ink liquefies and is evacuated, leaving behind a pervasive vascular network. hMSCs and human neonatal dermal fibroblasts (hNDFs) are subsequently lined with human umbilical vein endothelial cells (HUVECs).

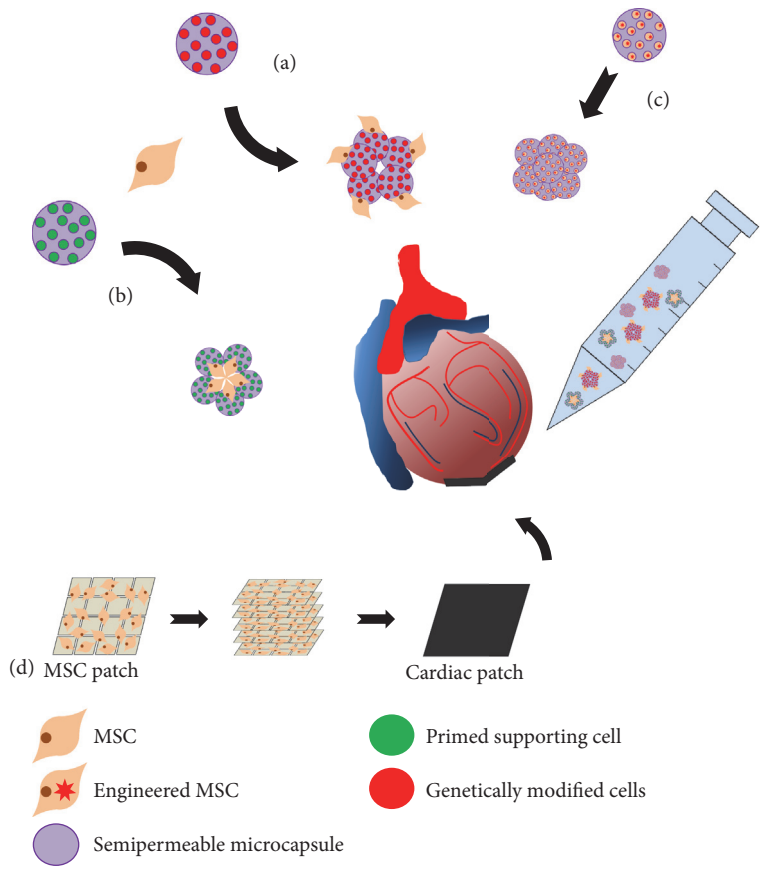

Figure 1: Therapeutic strategies of MSC-based tissue engineering. (a) Genetically modified MSCs are encapsulated into semipermeable microcapsules. This modified MSC secrete cytokine for homed stem cell. (b) Semipermeable microcapsules containing primed supporting cells. Secreted cytokines from primed supporting cells enhance MSC cellular function. (c) Engineered MSCs encapsulated into semipermeable microcapsules. MSCs secreted recombinant hormone such as glucagon-like peptide 1. Each semipermeable microcapsule is transplanted into infracted region of heart. (d) MSCs seeded on biomaterial-based patch. Multilayered cells as a cardiac patch for myocardial infraction.

These thick vascularized tissues are actively perfused with growth factors necessary for differentiation of hMSCs. Taken together, 3D printing has gained a considerable amount of attention owing to its ability to provide precise control of the initial structure of tissue-engineered constructs [102], indicating that 3D scaffold architecture and geometric cues play a major role in dictating cell behavior and tissue regeneration (Figure 2).

7. Conclusion

MSCs can be readily isolated from various sources in the human body. In addition, MSCs are able to self-replicate for many passages and differentiate into multiple cell lineages, such as osteoblasts, myoblasts, and fibroblasts. Thus, MSCs have become the most practical and prominent therapeutic stem cell. Recently, a number of research groups have focused on applying MSC-based therapies clinically relevant disease models. Based on MSC signaling pathways, natural compounds or chemical drugs are used to improve of MSC functions. Moreover, scientists are working to develop novel materials that are biologically inert. With the advances in technology, it is possible to modulate the microstructure of biomaterials to enable their practical use in medicine. An artificial structure composed of modified biomaterials can enhance MSC proliferation, survival, and differentiation. Tissue engineering technologies such as cell-scaffolds, cell-protein-scaffold architectures made of biomaterials including ECM or hydrogel, and cell patch- and 3D printing-based tissue techniques allow researchers to make artificial versions of human tissues and organs. Because of its numerous applications, a combined therapeutic strategy that includes cell priming and tissue engineering technology is a promising therapeutic approach for cardiovascular regeneration.

Competing Interests

The authors declare that they do not have any conflict of interests.

Authors' Contributions

Seung Taek Ji, Hyunyun Kim, and Jisoo Yun contributed equally to this study.

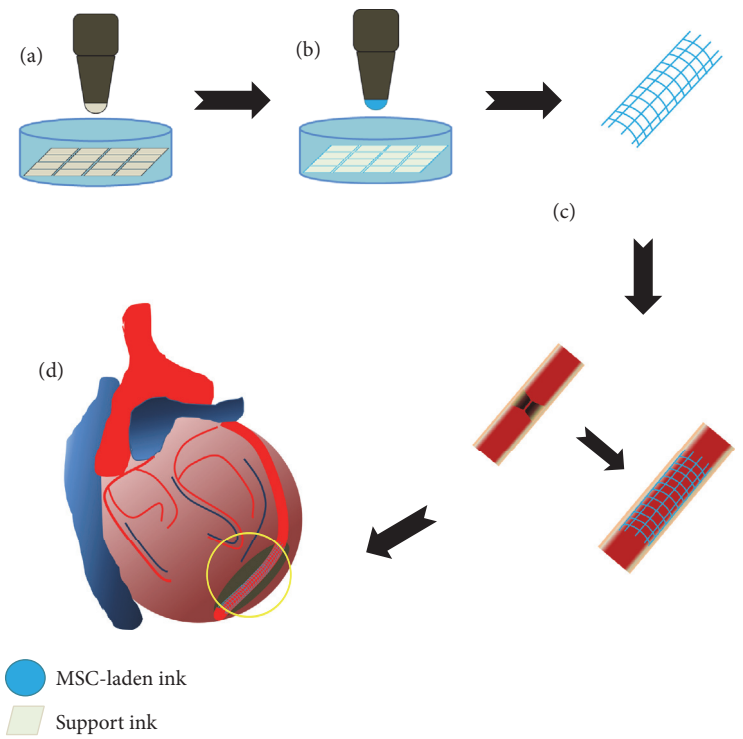

Figure 2: 3D printing-based tissue engineering for myocardiac infarction. (a) Casting a support frame with support ink. (b) MSC-laden ink is cast over the support ink. (c)-(d) 3D printing-based engineered tissues could be used for myocardiac infarction treatment.

Acknowledgments

This work was supported by a grant from the National Research Foundation (NRF-2015M3A9B4051053, NRF-2015R1A5A2009656, NRF-2015M3A9B4066493, NRF-2014R1A1 A2056907, and NRF-2015R1A2A2A01004908) and the Brain Busan 21 (BB21) program.

References

[1] GBD 2013 Mortality and Causes of Death Collaborators, "Global, regional, and national age-sex specific all-cause and cause-specific mortality for 240 cause of death, 1990–2013: a systematic analysis for the global burden of disease study 2013," *The Lancet*, vol. 385, no. 9963, pp. 117–171, 2015.

[2] A. E. Guttmacher, F. S. Collins, and E. G. Nabel, "Cardiovascular disease," *New England Journal of Medicine*, vol. 349, no. 1, pp. 60–72, 2003.

[3] C. Meads, C. Cummins, K. Jolly, A. Stevens, A. Burls, and C. Hyde, "Coronary artery stents in the treatment of ischaemic heart disease: a rapid and systematic review," *Health Technology Assessment*, vol. 4, no. 23, pp. 1–153, 2000.

[4] T. D. Henry, B. H. Annex, G. R. McKendall et al., "The VIVA trial: vascular endothelial growth factor in ischemia for vascular angiogenesis," *Circulation*, vol. 107, no. 10, pp. 1359–1365, 2003.

[5] A. Rozanski, J. A. Blumenthal, and J. Kaplan, "Impact of psychological factors on the pathogenesis of cardiovascular disease and implications for therapy," *Circulation*, vol. 99, no. 16, pp. 2192–2217, 1999.

[6] V. F. M. Segers and R. T. Lee, "Stem-cell therapy for cardiac disease," *Nature*, vol. 451, no. 7181, pp. 937–942, 2008.

[7] K. W. Liechty, T. C. MacKenzie, A. F. Shaaban et al., "Human mesenchymal stem cells engraft and demonstrate site-specific differentiation after in utero transplantation in sheep," *Nature Medicine*, vol. 6, no. 11, pp. 1282–1286, 2000.

[8] M. F. Pittenger and B. J. Martin, "Mesenchymal stem cells and their potential as cardiac therapeutics," *Circulation Research*, vol. 95, no. 1, pp. 9–20, 2004.

[9] M. F. Pittenger, A. M. Mackay, S. C. Beck et al., "Multilineage potential of adult human mesenchymal stem cells," *Science*, vol. 284, no. 5411, pp. 143–147, 1999.

[10] I. Ullah, R. B. Subbarao, and G. J. Rho, "Human mesenchymal stem cells—current trends and future prospective," *Bioscience Reports*, vol. 35, Article ID e00191, 2015.

[11] C. Nombela-Arrieta, J. Ritz, and L. E. Silberstein, "The elusive nature and function of mesenchymal stem cells," *Nature Reviews Molecular Cell Biology*, vol. 12, no. 2, pp. 126–131, 2011.

[12] R. Atoui and R. C. J. Chiu, "Mesenchymal stromal cells as universal donor cells," *Expert Opinion on Biological Therapy*, vol. 12, no. 10, pp. 1293–1297, 2012.

[13] W. Faiella and R. Atoui, "Therapeutic use of stem cells for cardiovascular disease," *Clinical and Translational Medicine*, vol. 5, no. 1, article 34, 2016.

[14] K. Le Blanc, C. Tammik, K. Rosendahl, E. Zetterberg, and O. Ringdén, "HLA expression and immunologic properties of differentiated and undifferentiated mesenchymal stem cells," *Experimental Hematology*, vol. 31, no. 10, pp. 890–896, 2003.

[15] J. Stagg, S. Pommey, N. Eliopoulos, and J. Galipeau, "Interferon-γ-stimulated marrow stromal cells: a new type of non-hematopoietic antigen-presenting cell," *Blood*, vol. 107, no. 6, pp. 2570–2577, 2006.

[16] D. M. Patel, J. Shah, and A. S. Srivastava, "Therapeutic potential of mesenchymal stem cells in regenerative medicine," *Stem Cells International*, vol. 2013, Article ID 496218, 15 pages, 2013.

[17] L. Li, X. Chen, W. E. Wang, and C. Zeng, "How to improve the survival of transplanted mesenchymal stem cell in ischemic heart?" *Stem Cells International*, vol. 2016, Article ID 9682757, 14 pages, 2016.

[18] J. M. Karp and G. S. L. Teo, "Mesenchymal stem cell homing: the devil is in the details," *Cell Stem Cell*, vol. 4, no. 3, pp. 206–216, 2009.

[19] P. R. Baraniak and T. C. McDevitt, "Stem cell paracrine actions and tissue regeneration," *Regenerative Medicine*, vol. 5, no. 1, pp. 121–143, 2010.

[20] N. Zippel, M. Schulze, and E. Tobiasch, "Biomaterials and mesenchymal stem cells for regenerative medicine," *Recent patents on biotechnology*, vol. 4, no. 1, pp. 1–22, 2010.

[21] A. I. Caplan, "Mesenchymal stem cells," *Journal of Orthopaedic Research*, vol. 9, no. 5, pp. 641–650, 1991.

[22] A. J. Friedenstein, R. K. Chailakhjan, and K. S. Lalykina, "The development of fibroblast colonies in monolayer cultures of guinea-pig bone marrow and spleen cells," *Cell and Tissue Kinetics*, vol. 3, no. 4, pp. 393–403, 1970.

[23] A. J. Friedenstein, U. F. Gorskaja, and N. N. Kulagina, "Fibroblast precursors in normal and irradiated mouse hematopoietic organs," *Experimental Hematology*, vol. 4, no. 5, pp. 267–274, 1976.

[24] R. Hass, C. Kasper, S. Böhm, and R. Jacobs, "Different populations and sources of human mesenchymal stem cells (MSC): a comparison of adult and neonatal tissue-derived MSC," *Cell Communication and Signaling*, vol. 9, article 12, 2011.

[25] A. P. Franco Lambert, A. Fraga Zandonai, D. Bonatto, D. Cantarelli Machado, and J. A. Pêgas Henriques, "Differentiation of human adipose-derived adult stem cells into neuronal tissue: does it work?" *Differentiation*, vol. 77, no. 3, pp. 221–228, 2009.

[26] S. Gronthos, D. M. Franklin, H. A. Leddy, P. G. Robey, R. W. Storms, and J. M. Gimble, "Surface protein characterization of human adipose tissue-derived stromal cells," *Journal of Cellular Physiology*, vol. 189, no. 1, pp. 54–63, 2001.

[27] A.-M. Rodriguez, C. Elabd, E.-Z. Amri, G. Ailhaud, and C. Dani, "The human adipose tissue is a source of multipotent stem cells," *Biochimie*, vol. 87, no. 1, pp. 125–128, 2005.

[28] B. Lindroos, S. Boucher, L. Chase et al., "Serum-free, xeno-free culture media maintain the proliferation rate and multipotentiality of adipose stem cells in vitro," *Cytotherapy*, vol. 11, no. 7, pp. 958–972, 2009.

[29] S. Schreml, P. Babilas, S. Fruth et al., "Harvesting human adipose tissue-derived adult stem cells: resection versus liposuction," *Cytotherapy*, vol. 11, no. 7, pp. 947–957, 2009.

[30] L. Sensebé and P. Bourin, "Mesenchymal stem cells for therapeutic purposes," *Transplantation*, vol. 87, no. 9S, pp. S49–53, 2009.

[31] S. Alsalameh, R. Amin, T. Gemba, and M. Lotz, "Identification of mesenchymal progenitor cells in normal and osteoarthritic human articular cartilage," *Arthritis and Rheumatism*, vol. 50, no. 5, pp. 1522–1532, 2004.

[32] K. Hiraoka, S. Grogan, T. Olee, and M. Lotz, "Mesenchymal progenitor cells in adult human articular cartilage," *Biorheology*, vol. 43, no. 3-4, pp. 447–454, 2006.

[33] M. Secco, Y. B. Moreira, E. Zucconi et al., "Gene expression profile of mesenchymal stem cells from paired umbilical cord units: cord is different from blood," *Stem Cell Reviews and Reports*, vol. 5, no. 4, pp. 387–401, 2009.

[34] M. Jäger, C. Zilkens, B. Bittersohl, and R. Krauspe, "Cord blood—an alternative source for bone regeneration," *Stem Cell Reviews and Reports*, vol. 5, no. 3, pp. 266–277, 2009.

[35] K. Bieback and H. Klüter, "Mesenchymal stromal cells from umbilical cord blood," *Current Stem Cell Research and Therapy*, vol. 2, no. 4, pp. 310–323, 2007.

[36] C. Campagnoli, I. A. G. Roberts, S. Kumar, P. R. Bennett, I. Bellantuono, and N. M. Fisk, "Identification of mesenchymal stem/progenitor cells in human first-trimester fetal blood, liver, and bone marrow," *Blood*, vol. 98, no. 8, pp. 2396–2402, 2001.

[37] N. J. Zvaifler, L. Marinova-Mutafchieva, G. Adams et al., "Mesenchymal precursor cells in the blood of normal individuals," *Arthritis Research*, vol. 2, no. 6, pp. 477–488, 2000.

[38] L. da Silva Meirelles, P. C. Chagastelles, and N. B. Nardi, "Mesenchymal stem cells reside in virtually all post-natal organs and tissues," *Journal of Cell Science*, vol. 119, no. 11, pp. 2204–2213, 2006.

[39] M. Dominici, K. Le Blanc, I. Mueller et al., "Minimal criteria for defining multipotent mesenchymal stromal cells. The International Society for Cellular Therapy position statement," *Cytotherapy*, vol. 8, no. 4, pp. 315–317, 2006.

[40] E. M. Horwitz, K. Le Blanc, M. Dominici et al., "Clarification of the nomenclature for MSC: the International Society for Cellular Therapy position statement," *Cytotherapy*, vol. 7, no. 5, pp. 393–395, 2005.

[41] S. E. Haynesworth, M. A. Barer, and A. I. Caplan, "Cell surface antigens on human marrow-derived mesenchymal cells are detected by monoclonal antibodies," *Bone*, vol. 13, no. 1, pp. 69–80, 1992.

[42] P. A. Conget and J. J. Minguell, "Phenotypical and functional properties of human bone marrow mesenchymal progenitor cells," *Journal of Cellular Physiology*, vol. 181, no. 1, pp. 67–73, 1999.

[43] J.-H. Hong, E. S. Hwang, M. T. McManus et al., "TAZ, a transcriptional modulator of mesenchymal stem cell differentiation," *Science*, vol. 309, no. 5737, pp. 1074–1078, 2005.

[44] A. I. Caplan and S. P. Bruder, "Mesenchymal stem cells: building blocks for molecular medicine in the 21st century," *Trends in Molecular Medicine*, vol. 7, no. 6, pp. 259–264, 2001.

[45] B. Short, N. Brouard, T. Occhiodoro-Scott, A. Ramakrishnan, and P. J. Simmons, "Mesenchymal stem cells," *Archives of Medical Research*, vol. 34, no. 6, pp. 565–571, 2003.

[46] A. Augello and C. De Bari, "The regulation of differentiation in mesenchymal stem cells," *Human Gene Therapy*, vol. 21, no. 10, pp. 1226–1238, 2010.

[47] H. Song, W. Chang, B. W. Song, and K. C. Hwang, "Specific differentiation of mesenchymal stem cells by small molecules," *American Journal of Stem Cells*, vol. 1, no. 1, pp. 22–30, 2012.

[48] I. Mahjneh, M.-R. Passos-Bueno, M. Zatz et al., "The phenotype of chromosome 2p-linked limb-girdle muscular dystrophy," *Neuromuscular Disorders*, vol. 6, no. 6, pp. 483–490, 1996.

[49] A. M. Mackay, S. C. Beck, J. M. Murphy, F. P. Barry, C. O. Chichester, and M. F. Pittenger, "Chondrogenic differentiation of cultured human mesenchymal stem cells from marrow," *Tissue Engineering*, vol. 4, no. 4, pp. 415–428, 1998.

[50] Y. Sato, H. Araki, J. Kato et al., "Human mesenchymal stem cells xenografted directly to rat liver are differentiated into human hepatocytes without fusion," *Blood*, vol. 106, no. 2, pp. 756–763, 2005.

[51] C. Toma, M. F. Pittenger, K. S. Cahill, B. J. Byrne, and P. D. Kessler, "Human mesenchymal stem cells differentiate to a cardiomyocyte phenotype in the adult murine heart," *Circulation*, vol. 105, no. 1, pp. 93–98, 2002.

[52] A. R. Williams and J. M. Hare, "Mesenchymal stem cells: biology, pathophysiology, translational findings, and therapeutic implications for cardiac disease," *Circulation Research*, vol. 109, no. 8, pp. 923–940, 2011.

[53] W. Xu, X. Zhang, H. Qian et al., "Mesenchymal stem cells from adult human bone marrow differentiate into a cardiomyocyte phenotype in vitro," *Experimental Biology and Medicine*, vol. 229, no. 7, pp. 623–631, 2004.

[54] Y. S. Kim, J. S. Kwon, M. H. Hong et al., "Promigratory activity of oxytocin on umbilical cord blood-derived mesenchymal stem cells," *Artificial Organs*, vol. 34, no. 6, pp. 453–461, 2010.

[55] S. Y. Lim, Y. S. Kim, Y. Ahn et al., "The effects of mesenchymal stem cells transduced with Akt in a porcine myocardial infarction model," *Cardiovascular Research*, vol. 70, no. 3, pp. 530–542, 2006.

[56] H. C. Quevedo, K. E. Hatzistergos, B. N. Oskouei et al., "Allogeneic mesenchymal stem cells restore cardiac function in chronic ischemic cardiomyopathy via trilineage differentiating capacity," *Proceedings of the National Academy of Sciences of the United States of America*, vol. 106, no. 33, pp. 14022–14027, 2009.

[57] D. Wang, F. Zhang, W. Shen et al., "Mesenchymal stem cell injection ameliorates the inducibility of ventricular arrhythmias after myocardial infarction in rats," *International Journal of Cardiology*, vol. 152, no. 3, pp. 314–320, 2011.

[58] J. M. Hare, J. H. Traverse, T. D. Henry et al., "A randomized, double-blind, placebo-controlled, dose-escalation study of intravenous adult human mesenchymal stem cells (prochymal) after acute myocardial infarction," *Journal of the American College of Cardiology*, vol. 54, no. 24, pp. 2277–2286, 2009.

[59] B. Trachtenberg, D. L. Velazquez, A. R. Williams et al., "Rationale and design of the transendocardial injection of autologous human cells (bone marrow or mesenchymal) in chronic ischemic left ventricular dysfunction and heart failure secondary to myocardial infarction (TAC-HFT) trial: a randomized, double-blind, placebo-controlled study of safety and efficacy," *American Heart Journal*, vol. 161, no. 3, pp. 487–493, 2011.

[60] J. M. Hare, "Translational development of mesenchymal stem cell therapy for cardiovascular diseases," *Texas Heart Institute Journal*, vol. 36, no. 2, pp. 145–147, 2009.

[61] C. Sanina and J. M. Hare, "Mesenchymal stem cells as a biological drug for heart disease: where are we with cardiac cell-based therapy?" *Circulation Research*, vol. 117, no. 3, pp. 229–233, 2015.

[62] T. Squillaro, G. Peluso, and U. Galderisi, "Clinical trials with mesenchymal stem cells: an update," *Cell Transplantation*, vol. 25, no. 5, pp. 829–848, 2016.

[63] A. B. Mathiasen, M. Haack-Sørensen, E. Jørgensen, and J. Kastrup, "Autotransplantation of mesenchymal stromal cells from bone-marrow to heart in patients with severe stable coronary artery disease and refractory angina—final 3-year follow-up," *International Journal of Cardiology*, vol. 170, no. 2, pp. 246–251, 2013.

[64] A. R. Williams, B. Trachtenberg, D. L. Velazquez et al., "Intramyocardial stem cell injection in patients with ischemic cardiomyopathy: functional recovery and reverse remodeling," *Circulation Research*, vol. 108, no. 7, pp. 792–796, 2011.

[65] J.-W. Lee, S.-H. Lee, Y.-J. Youn et al., "A randomized, open-label, multicenter trial for the safety and efficacy of adult mesenchymal stem cells after acute myocardial infarction," *Journal of Korean Medical Science*, vol. 29, no. 1, pp. 23–31, 2014.

[66] M. Gyöngyösi, W. Wojakowski, P. Lemarchand et al., "Meta-analysis of cell-based CaRdiac stUdiEs (ACCRUE) in patients with acute myocardial infarction based on individual patient data," *Circulation Research*, vol. 116, no. 8, pp. 1346–1360, 2015.

[67] A. N. Kharlamov, A. E. Tyurnina, V. S. Veselova, O. P. Kovtun, V. Y. Shur, and J. L. Gabinsky, "Silica-gold nanoparticles for atheroprotective management of plaques: results of the NANOM-FIM trial," *Nanoscale*, vol. 7, no. 17, pp. 8003–8015, 2015.

[68] J. M. Hare, J. E. Fishman, G. Gerstenblith et al., "Comparison of allogeneic vs autologous bone marrow-derived mesenchymal stem cells delivered by transendocardial injection in patients with ischemic cardiomyopathy: the POSEIDON randomized trial," *The Journal of the American Medical Association*, vol. 308, no. 22, pp. 2369–2379, 2012.

[69] A. W. Heldman, D. L. DiFede, J. E. Fishman et al., "Transendocardial mesenchymal stem cells and mononuclear bone marrow cells for ischemic cardiomyopathy: the TAC-HFT randomized trial," *JAMA*, vol. 311, no. 1, pp. 62–73, 2014.

[70] V. Karantalis, D. L. Difede, G. Gerstenblith et al., "Autologous mesenchymal stem cells produce concordant improvements in regional function, tissue perfusion, and fibrotic burden when administered to patients undergoing coronary artery bypass grafting: the Prospective Randomized Study of Mesenchymal Stem Cell Therapy in Patients Undergoing Cardiac Surgery (PROMETHEUS) trial," *Circulation Research*, vol. 114, no. 8, pp. 1302–1310, 2014.

[71] T. Matsui, J. Tao, F. Del Monte et al., "Akt activation preserves cardiac function and prevents injury after transient cardiac ischemia in vivo," *Circulation*, vol. 104, no. 3, pp. 330–335, 2001.

[72] A. A. Mangi, N. Noiseux, D. Kong et al., "Mesenchymal stem cells modified with Akt prevent remodeling and restore performance of infarcted hearts," *Nature Medicine*, vol. 9, no. 9, pp. 1195–1201, 2003.

[73] K. Tamama, V. H. Fan, L. G. Griffith, H. C. Blair, and A. Wells, "Epidermal growth factor as a candidate for ex vivo expansion of bone marrow-derived mesenchymal stem cells," *Stem Cells*, vol. 24, no. 3, pp. 686–695, 2006.

[74] V. H. Fan, A. Au, K. Tamama et al., "Tethered epidermal growth factor provides a survival advantage to mesenchymal stem cells," *Stem Cells*, vol. 25, no. 5, pp. 1241–1251, 2007.

[75] H. L. Michalis Mastri and T. Lee, "Enhancing the efficacy of mesenchymal stem cell therapy," *World Journal of Stem Cells*, vol. 6, no. 2, pp. 82–93, 2014.

[76] D. S. Yoon, Y. H. Kim, H. S. Jung, S. Paik, and J. W. Lee, "Importance of Sox2 in maintenance of cell proliferation and multipotency of mesenchymal stem cells in low-density culture," *Cell Proliferation*, vol. 44, no. 5, pp. 428–440, 2011.

[77] T. M. Liu, Y. N. Wu, X. M. Guo, J. H. P. Hui, E. H. Lee, and B. Lim, "Effects of ectopic nanog and Oct4 overexpression on mesenchymal stem cells," *Stem Cells and Development*, vol. 18, no. 7, pp. 1013–1022, 2009.

[78] S.-M. Han, S.-H. Han, Y.-R. Coh et al., "Enhanced proliferation and differentiation of Oct4- And Sox2-overexpressing human adipose tissue mesenchymal stem cells," *Experimental and Molecular Medicine*, vol. 46, no. 6, article no. e101, 2014.

[79] Y. Komiya and R. Habas, "Wnt signal transduction pathways," *Organogenesis*, vol. 4, no. 2, pp. 68–75, 2008.

[80] R. Nusse, "Wnt signaling and stem cell control," *Cell Research*, vol. 18, no. 5, pp. 523–527, 2008.

[81] F. J. T. Staal and T. C. Luis, "Wnt signaling in hematopoiesis: crucial factors for self-renewal, proliferation, and cell fate decisions," *Journal of Cellular Biochemistry*, vol. 109, no. 5, pp. 844–849, 2010.

[82] G. M. Boland, G. Perkins, D. J. Hall, and R. S. Tuan, "Wnt 3a promotes proliferation and suppresses osteogenic differentiation of adult human mesenchymal stem cells," *Journal of Cellular Biochemistry*, vol. 93, no. 6, pp. 1210–1230, 2004.

[83] Z. Zhu, J. Yin, J. Guan et al., "Lithium stimulates human bone marrow derived mesenchymal stem cell proliferation through GSK-3β-dependent β-catenin/Wnt pathway activation," *FEBS Journal*, vol. 281, no. 23, pp. 5371–5389, 2014.

[84] S. Guan, Z. Wang, F. Xin, and H. Xin, "Wnt5a is associated with the differentiation of bone marrow mesenchymal stem cells in vascular calcification by connecting with different receptors," *Molecular Medicine Reports*, vol. 10, no. 4, pp. 1985–1991, 2014.

[85] R. Bilkovski, D. M. Schulte, F. Oberhauser et al., "Role of Wnt-5a in the determination of human mesenchymal stem cells into preadipocytes," *The Journal of Biological Chemistry*, vol. 285, no. 9, pp. 6170–6178, 2010.

[86] L. Hong, G. Zhang, H. Sultana, Y. Yu, and Z. Wei, "The effects of 17-β estradiol on enhancing proliferation of human bone marrow mesenchymal stromal cells in vitro," *Stem Cells and Development*, vol. 20, no. 5, pp. 925–931, 2011.

[87] Z. Cheng, L. Ou, X. Zhou et al., "Targeted migration of mesenchymal stem cells modified with CXCR4 gene to infarcted myocardium improves cardiac performance," *Molecular Therapy*, vol. 16, no. 3, pp. 571–579, 2008.

[88] S. Y. Oh, S.-J. Lee, Y. H. Jung, H. J. Lee, and H. J. Han, "Arachidonic acid promotes skin wound healing through induction of human MSC migration by MT3-MMP-mediated fibronectin degradation," *Cell Death and Disease*, vol. 6, no. 5, 2015.

[89] T. J. Kean, L. Duesler, R. G. Young et al., "Development of a peptide-targeted, myocardial ischemia-homing, mesenchymal stem cell," *Journal of Drug Targeting*, vol. 20, no. 1, pp. 23–32, 2012.

[90] J. Liu, P. Zhu, P. Song et al., "Pretreatment of adipose derived stem cells with curcumin facilitates myocardial recovery via antiapoptosis and angiogenesis," *Stem Cells International*, vol. 2015, Article ID 638153, 12 pages, 2015.

[91] X.-B. Liu, H. Chen, H.-Q. Chen et al., "Angiopoietin-1 preconditioning enhances survival and functional recovery of mesenchymal stem cell transplantation," *Journal of Zhejiang University: Science B*, vol. 13, no. 8, pp. 616–623, 2012.

[92] H. K. Haider and M. Ashraf, "Preconditioning and stem cell survival," *Journal of Cardiovascular Translational Research*, vol. 3, no. 2, pp. 89–102, 2010.

[93] B. Balana, C. Nicoletti, I. Zahanich et al., "5-Azacytidine induces changes in electrophysiological properties of human mesenchymal stem cells," *Cell Research*, vol. 16, no. 12, pp. 949–960, 2006.

[94] Y. Liu, J. Song, W. Liu, Y. Wan, X. Chen, and C. Hu, "Growth and differentiation of rat bone marrow stromal cells: does 5-azacytidine trigger their cardiomyogenic differentiation?" *Cardiovascular Research*, vol. 58, no. 2, pp. 460–468, 2003.

[95] H. Gai, E. L.-H. Leung, P. D. Costantino et al., "Generation and characterization of functional cardiomyocytes using induced pluripotent stem cells derived from human fibroblasts," *Cell Biology International*, vol. 33, no. 11, pp. 1184–1193, 2009.

[96] Z. Bin, L.-G. Sheng, Z.-C. Gang et al., "Efficient cardiomyocyte differentiation of embryonic stem cells by bone morphogenetic protein-2 combined with visceral endoderm-like cells," *Cell Biology International*, vol. 30, no. 10, pp. 769–776, 2006.

[97] J. Hou, A.-L. Lü, B.-W. Liu et al., "Combination of BMP-2 and 5-AZA is advantageous in rat bone marrow-derived mesenchymal stem cells differentiation into cardiomyocytes," *Cell Biology International*, vol. 37, no. 12, pp. 1291–1299, 2013.

[98] C. Liu, Y. Fan, L. Zhou et al., "Pretreatment of mesenchymal stem cells with angiotensin II enhances paracrine effects, angiogenesis, gap junction formation and therapeutic efficacy for myocardial infarction," *International Journal of Cardiology*, vol. 188, no. 1, pp. 22–32, 2015.

[99] J. H. Lee, J. M. Ryu, Y.-S. Han et al., "Fucoidan improves bioactivity and vasculogenic potential of mesenchymal stem cells in murine hind limb ischemia associated with chronic kidney disease," *Journal of Molecular and Cellular Cardiology*, vol. 97, pp. 169–179, 2016.

[100] M. T. Elnakish, F. Hassan, D. Dakhlallah, C. B. Marsh, I. A. Alhaider, and M. Khan, "Mesenchymal stem cells for cardiac regeneration: translation to bedside reality," *Stem Cells International*, vol. 2012, Article ID 646038, 14 pages, 2012.

[101] M. Breitbach, T. Bostani, W. Roell et al., "Potential risks of bone marrow cell transplantation into infarcted hearts," *Blood*, vol. 110, no. 4, pp. 1362–1369, 2007.

[102] J. C. Bernhard and G. Vunjak-Novakovic, "Should we use cells, biomaterials, or tissue engineering for cartilage regeneration?" *Stem Cell Research and Therapy*, vol. 7, no. 1, article 56, 2016.

[103] K. J. Kim, Y. A. Joe, M. K. Kim et al., "Silica nanoparticles increase human adipose tissue-derived stem cell proliferation through ERK1/2 activation," *International Journal of Nanomedicine*, vol. 10, pp. 2261–2272, 2015.

[104] K. J. Kim, Y.-J. Jeon, J. H. Lee, and J.-W. Rhie, "The effect of silicon ion on proliferation and osteogenic differentiation of human ADSCs," *Korean Tissue Engineering and Regenerative Medicine Society*, vol. 7, no. 2, pp. 171–177, 2010.

[105] L. Ning, H. Malmström, and Y.-F. Ren, "Porous collagen-Hydroxyapatite scaffolds with mesenchymal stem cells for bone regeneration," *Journal of Oral Implantology*, vol. 41, no. 1, pp. 45–49, 2015.

[106] Y.-S. Zhang, J.-H. Gao, F. Lu, M. Zhu, and Y.-J. Liao, "Cellular compatibility of type collagen I scaffold and human adipose-derived stem cells," *Nan Fang Yi Ke Da Xue Xue Bao*, vol. 27, no. 2, pp. 223–225, 2007.

[107] M. Ishii, R. Shibata, Y. Numaguchi et al., "Enhanced angiogenesis by transplantation of mesenchymal stem cell sheet created by a novel magnetic tissue engineering method," *Arteriosclerosis, Thrombosis, and Vascular Biology*, vol. 31, no. 10, pp. 2210–2215, 2011.

[108] I.-S. Yoon, C. W. Chung, J.-H. Sung et al., "Proliferation and chondrogenic differentiation of human adipose-derived mesenchymal stem cells in porous hyaluronic acid scaffold," *Journal of Bioscience and Bioengineering*, vol. 112, no. 4, pp. 402–408, 2011.

[109] R. Yao, R. Zhang, J. Luan, and F. Lin, "Alginate and alginate/gelatin microspheres for human adipose-derived stem cell encapsulation and differentiation," *Biofabrication*, vol. 4, no. 2, Article ID 025007, 2012.

[110] N.-C. Cheng, S. Wang, and T.-H. Young, "The influence of spheroid formation of human adipose-derived stem cells on chitosan films on stemness and differentiation capabilities," *Biomaterials*, vol. 33, no. 6, pp. 1748–1758, 2012.

[111] J. R. Mauney, T. Nguyen, K. Gillen, C. Kirker-Head, J. M. Gimble, and D. L. Kaplan, "Engineering adipose-like tissue in vitro and in vivo utilizing human bone marrow and adipose-derived mesenchymal stem cells with silk fibroin 3D scaffolds," *Biomaterials*, vol. 28, no. 35, pp. 5280–5290, 2007.

[112] H. Zhang, S.-J. Zhu, W. Wang, Y.-J. Wei, and S.-S. Hu, "Transplantation of microencapsulated genetically modified xenogeneic cells augments angiogenesis and improves heart function," *Gene Therapy*, vol. 15, no. 1, pp. 40–48, 2008.

[113] Y. Wang, G. Zhang, Y. Hou et al., "Transplantation of microencapsulated Schwann cells and mesenchymal stem cells augment angiogenesis and improve heart function," *Molecular and Cellular Biochemistry*, vol. 366, no. 1-2, pp. 139–147, 2012.

[114] J. M. Rosenstein, J. M. Krum, and C. Ruhrberg, "VEGF in the nervous system," *Organogenesis*, vol. 6, no. 2, pp. 107–114, 2010.

[115] J. H. Houtgraaf, R. de Jong, K. Monkhorst et al., "Feasibility of intracoronary GLP-1 eluting cellbead™ infusion in acute myocardial infarction," *Cell Transplantation*, vol. 22, no. 3, pp. 535–543, 2013.

[116] M. F. Berry and J. Friedberg, "Chest wall/diaphragmatic complications," *Thoracic Surgery Clinics*, vol. 16, no. 3, pp. 277–285, 2006.

[117] H.-J. Wei, C.-H. Chen, W.-Y. Lee et al., "Bioengineered cardiac patch constructed from multilayered mesenchymal stem cells for myocardial repair," *Biomaterials*, vol. 29, no. 26, pp. 3547–3556, 2008.

[118] H.-W. Kang, S. J. Lee, I. K. Ko, C. Kengla, J. J. Yoo, and A. Atala, "A 3D bioprinting system to produce human-scale tissue constructs with structural integrity," *Nature Biotechnology*, vol. 34, no. 3, pp. 312–319, 2016.

[119] D. B. Kolesky, K. A. Homan, M. A. Skylar-Scott, and J. A. Lewis, "Three-dimensional bioprinting of thick vascularized tissues," *Proceedings of the National Academy of Sciences of the United States of America*, vol. 113, no. 12, pp. 3179–3184, 2016.

Hindawi Publishing Corporation
Stem Cells International
Volume 2016, Article ID 4968724, 11 pages
http://dx.doi.org/10.1155/2016/4968724

Research Article

Adipose Derived-Mesenchymal Stem Cells Viability and Differentiating Features for Orthopaedic Reparative Applications: Banking of Adipose Tissue

Ilaria Roato,[1] Daniela Alotto,[2] Dimas Carolina Belisario,[1] Stefania Casarin,[2] Mara Fumagalli,[2] Irene Cambieri,[2] Raimondo Piana,[3] Maurizio Stella,[2] Riccardo Ferracini,[3] and Carlotta Castagnoli[2]

[1]*CeRMS, A.O.U. Città della Salute e della Scienza, Torino, Italy*
[2]*Skin Bank, Department of General and Specialized Surgery, A.O.U. Città della Salute e della Scienza, Torino, Italy*
[3]*Department of Orthopaedic Oncology, CTO Hospital, Torino, Italy*

Correspondence should be addressed to Ilaria Roato; roato78@libero.it

Received 1 September 2016; Revised 24 October 2016; Accepted 2 November 2016

Academic Editor: Giorgio Mori

Copyright © 2016 Ilaria Roato et al. This is an open access article distributed under the Creative Commons Attribution License, which permits unrestricted use, distribution, and reproduction in any medium, provided the original work is properly cited.

Osteoarthritis is characterized by loss of articular cartilage also due to reduced chondrogenic activity of mesenchymal stem cells (MSCs) from patients. Adipose tissue is an attractive source of MSCs (ATD-MSCs), representing an effective tool for reparative medicine, particularly for treatment of osteoarthritis, due to their chondrogenic and osteogenic differentiation capability. The treatment of symptomatic knee arthritis with ATD-MSCs proved effective with a single infusion, but multiple infusions could be also more efficacious. Here we studied some crucial aspects of adipose tissue banking procedures, evaluating ATD-MSCs viability, and differentiation capability after cryopreservation, to guarantee the quality of the tissue for multiple infusions. We reported that the presence of local anesthetic during lipoaspiration negatively affects cell viability of cryopreserved adipose tissue and cell growth of ATD-MSCs in culture. We observed that DMSO guarantees a faster growth of ATD-MSCs in culture than trehalose. At last, ATD-MSCs derived from fresh and cryopreserved samples at −80°C and −196°C showed viability and differentiation ability comparable to fresh samples. These data indicate that cryopreservation of adipose tissue at −80°C and −196°C is equivalent and preserves the content of ATD-MSCs in Stromal Vascular Fraction (SVF), guaranteeing the differentiation ability of ATD-MSCs.

1. Introduction

In the last years many studies have been focused on tissue regeneration and reparative medicine, particularly to cure osteoarthritis, characterized by loss of articular cartilage also due to a reduced chondrogenic activity of mesenchymal stem cells (MSCs) from patients [1]. Adult MSCs, originally retrieved from bone marrow [2], can also be isolated from adipose tissue with higher frequency than in bone marrow [3] and show a great seductive potential to the orthopaedic community for their reparative capabilities and differentiation ability towards adipogenic, osteogenic, and chondrogenic lineages [4, 5], to home in injured tissues, to release factors for wound healing, and to modulate the immune system [5–7]. Even though adipose tissue is mainly constituted by adipocytes, it also contains the Stromal Vascular Fraction (SVF) that comprehends adipose tissue-derived MSCs (ATD-MSCs), endothelial cells, pericytes, fibroblasts, and hematopoietic-lineage cells [4, 5, 8, 9]. ATD-MSCs express many markers common to bone marrow-derived stem cells [10, 11], such as CD90, CD44, CD73, CD105, and CD271 [5, 12]. In particular, CD271 has been proposed as marker of primary choice for tissue regeneration by ATD-MSCs in older subjects, since this subpopulation is maintained in elderly people [13], and CD271+ MSCs are associated with a high efficiency of proliferation and trilineage differentiation compared to CD271− MSCs [12, 14].

The treatment of symptomatic knee arthritis with ATD-MSCs proved effective with a single infusion [15–19]; the efficacy of multiple infusions of ATD-MSCs in the articular

joint is considered but still debated due to lack of data from clinical trials [19]. The availability of banking adipose tissue would allow treating with multiple infusions patients, avoiding repeated liposuction procedures for patients. Until now, many studies have been done to define protocols of banking able to guarantee effective quantity and quality of ATD-MSCs [20–24], without a conclusive statement. In the present work, we investigated banking procedures of adipose tissue, studying ATD-MSCs viability and differentiation capability after cryopreservation. In attempt to define the best condition for cryopreservation of adipose tissue, we analysed different parameters affecting it. In particular, confirming literature data [25], we reported that the presence of anesthetic during lipoaspiration negatively affects cell viability of cryopreserved adipose tissue and cell growth of ATD-MSCs in culture. Between the two cryoprotectant tested agents, we observed that DMSO guarantees a faster growth of MSCs in culture than trehalose. At last, ATD-MSCs derived from fresh and cryopreserved samples at −80°C and −196°C showed viability and differentiation ability comparable to fresh samples. These data indicate that cryopreservation of adipose tissue at −80°C and −196°C is equivalent and preserves the content of ATD-MSCs in SVF, guaranteeing the differentiation ability of ATD-MSCs.

2. Methods

2.1. Sample Collection. A total number of 80 lipoaspirate samples were collected after informed written consent of donors, according to the local ethic committee. Thirty-five patients were treated with Klein solution (lidocaine 1%, sodium bicarbonate 10 mEq, and adrenaline 1 mg/mL in 500 mL of solution of NaCl 0.9%) and 23 patients were treated with a solution without anesthetic (adrenaline 1 mg/mL in 500 mL of solution of NaCl 0.9%). Since the analysis between these two groups showed that the presence of anesthetic reduced MSC growth, the last 22 patients were collected without anesthetic.

Low-pressure liposuction with fenestrated blunt cannulae, according to Coleman procedure, was used to harvest adipose tissue [26, 27]. The lipoaspirates were centrifuged at 3000 rpm for 3 minutes to collect the fat phase and then washed twice with PBS by centrifugation at 1700 rpm for 10 minutes. The fat phase was processed either for the analysis of cell components or for cryopreservation.

2.2. Cryopreservation and Viability Assay of Adipose Tissue. Fat phase was frozen in 5 mL cryotubes with 2 different cryoprotective solutions: (i) fetal bovine serum (FBS: Fetal Bovine Serum, certificated-EDQ, Bio West SAS) + 10% dimethyl sulfoxide (DMSO-Cry-on, AL.CHI.MI.A.Srl), *n* 30 and (ii) FBS + 0,35 M trehalose (Sigma-Aldrich), *n* 34. Trehalose is a valid alternative to DMSO because it is not toxic for cells at normal body temperature. Samples were mixed with a cool cryopreservative solution and then transferred in freezing container, which guarantees a 1°C/min cooling rate, required for successful cryopreservation of cells and put at −80°C for 3 days, and then part of the sample was stored in liquid nitrogen (−196°C).

The frozen tissues were fast thawed in a water bath at 37°C; the cryopreservation solution was diluted with medium supplemented with 10% FBS and centrifuged to remove the CPA.

2.3. Isolation of SVF from Adipose Tissue. SVFs were isolated from fresh and thawed adipose tissue by enzymatic digestion with Collagenase NB4 (Serva Electrophoresis) 0,3 U/mL using a tube rotator for 40 minutes at 37°C. The activity of enzyme was neutralized by the addition of DMEM low glucose + 10% FBS, and then the samples were centrifuged at 1700 rpm for 10 minutes. The pellet was resuspended in medium, then passed through 100 μm and 70 μm cell strainers, washed by saline solution, collected, and counted. The phenotype of MSCs contained in the SVF was evaluated at T0, soon after SVF isolation. The SVF cells were seeded in T25 flasks and cultured in DMEM with 10% FBS, 2 mM glutamine, and 1% antibiotics (Gibco, Life Technologies) and the medium was replaced to eliminate nonadherent cells after 24 h. After 7 days of culture, the growth rate was calculated by counting the number of cells grown for mL of adipose tissue. Then MSCs were cultured for 2 passages; then their phenotype was analysed by flow cytometry.

2.4. Phenotype of ATD-MSCs. Cell surface markers of ATD-MSCs were analysed by flow cytometry on fresh SVF and on SVF derived after thawing of adipose tissue and its collagenase treatment. ATD-MSCs were identified as CD105, CD44, CD73, and CD271 positive cells and negative for CD45 expression. Standard labelling protocol was performed with the following antibodies fluorochrome-conjugated and isotypic controls: human CD105 PE (Invitrogen), CD73 FITC (kindly provided by Professor Malavasi, University of Turin), CD44 FITC, CD45 PerCP, CD3 PerCP, CD271 APC, IgG1 PE, IgG1 APC, and IgG2a PerCP (Miltenyi Biotec), and IgG1 FITC-conjugated (Immunostep). About 10^5 events/sample were used for capture with CellQuest software. All data were analysed with FlowJo software (Tree Star).

2.5. Tissue Biopsies and Staining Procedures. All fresh and preserved samples were processed for staining procedures. Adipose tissue samples were snap frozen in isopentane quenched in liquid nitrogen, mounted in OCT 4583 embedding compound (Sakura), and stored at −80°C. Ten-micron-thick cryostat sections were cut and transferred to polylysine-coated slides. The slides were air dried for two hours and then processed. For histological analysis a section from each biopsy was counterstained with Mayer's hematoxylin solution (DAKO) and mounted with an aqueous mounting medium (Kaiser's glycerol gelatin, from MERCK), to confirm the adequacy of the specimen. Slides were examined double blindly; microphotographs were taken using Leica DMLA microscope.

For immunohistochemical analysis (IHC) the sections were incubated with primary mouse monoclonal antibodies (MoAb) CD31 (Clone 10G9 ABCAM; 1 : 100), CD105 (Clone 266 BD PHARMINGEN; 1 : 50), and CD68 (Clone EBM11 DAKO; 1 : 500). They were titrated to yield maximal specific

staining and minimal nonspecific or background staining. The endogenous peroxidase activity was inhibited by the addition of methyl alcohol and 0.03% hydrogen peroxide. A second incubation with biotinylated secondary antibody and an avidin-biotin-horseradish peroxidase complex LSAB + (DAKO) were performed. Staining was developed with 3-amino-9-ethyl carbazole as a chromogen. All samples were counterstained with Mayer's hematoxylin solution (DAKO) and mounted with Kaiser's glycerol gelatin. Slides were examined double blindly and microphotographs were taken using a DMLA Leica microscope equipped with a digital camera (Leica DFC 425C). Images were acquired using LAS software (Leica Application Suite).

Immunofluorescence staining with (Moab) Aggrecan (Clone 969D4D11 Invitrogen; 1 : 25) was performed using appropriate Rhodamin (Chemicon 1 : 100) conjugated isotype-specific secondary antibodies. Slides were examined double blindly; microphotographs were taken using a DMLA Leica microscope equipped with a digital camera (Leica DFC 425C). Images were acquired using LAS software (Leica Application Suite).

2.6. MTT on Adipose Tissue Samples. Ten samples with similar weight, including 2 negative controls, were chosen and tested from each adipose tissue specimen. MTT salts solution (0.5 mg/mL) was added and the samples were then incubated at 37°C and 5% CO_2. After 3 hrs of incubation the precipitate salts were solubilized for 3 hrs with the use of 2-methoxyethanol (Sigma-Aldrich). The solution was then read on a spectrophotometer (570 nm). A negative control was always set up in double (a heat-denatured specimen for 20 minutes at maximum temperature) for each experimental condition. The negative control was then treated as other samples and optical density (OD) subtracted from each sample.

Adipose tissue viability of the adipose sample was expressed as viability index, deriving by the ratio between the samples' OD and their weight in grams. Noncryopreserved fresh tissue samples were used as control group. The formulas used in the determinations were Index of Viability (I.V.) = optical density (595 nm)/grams of tissue. Percent viability (% viability) = (I.V. of cryopreserved samples/I.V. of control fresh samples) × 100.

2.7. Evaluation of Chondrogenic and Osteogenic Potential of ATD-MSCs Derived from Fresh and Thawed Samples. We cultured SVF in DMEM low glucose supplemented with 10% FBS to obtain a population of ATD-MSCs, which were then cultured with StemPro Chondrogenesis Differentiation kit (Gibco, Life technologies) according to the manufacturers' instructions to induce chondrogenesis. After 21 days, cells were stained for immunofluorescence by Aggrecan. To study osteogenesis we plated ATD-MSCs in differentiating medium according to Brunetti et al. [28] for 14 days, and then we stained them for alkaline phosphatase according to kit produced by Sigma-Aldrich. The mineralization activity of osteoblasts was studied by culturing ATD-MSCs in alpha-MEM supplemented with 10% FBS, 50 μg/mL ascorbic acid, 10^{-8} M dexamethasone, and 10 mM beta-glycerophosphate (Sigma-Aldrich) for 8 weeks. The formation of mineralized nodules was accessed by von Kossa staining.

Table 1: Viability index with different cryoprotectants. Viability indexes (I.V.) was similar between the two CPAs.

	DMSO $N = 30$	Trehalose $N = 34$
Age	47 (37–54)	47 (42–57)
I.V. of fresh samples	12,3 (10,1–14,8)	14,7 (11,2–16,7)
I.V. after cryopreservation	6,48 (5,45–9,40)	6,59 (5,73–7,79)

2.8. Statistical Analysis. All statistical analysis was carried out using GraphPad Prism 7. Data were presented as mean with standard error and calculated by One-way Anova with multiple comparisons by Bonferroni test. Results were considered significant with $p < 0.05$. For evaluation of the growth rate we used Mann-Whitney test.

3. Results

3.1. Local Anesthetic Reduces ATD-MSC Growth. Adipose tissues harvested with (n 35)/without (n 23) local anesthetic maintained normal histological structure without evident differences between 2 groups. Both with and without anesthetic, the tissues were compact, with polygonal cells and good stroma, without any evidence of fatty tissue degeneration or necrosis (Figures 1(a) and 1(b)). These data were also confirmed by the IHC analysis, showing that the different cellular components of adipose tissue, stained with specific antibodies, resulted comparably in all analysed samples (Figures 1(c)–1(f)). Despite the absence of effects on cell morphology, the presence of the anesthetic significantly reduced the number of cells isolated from adipose tissues harvested with or without anesthetic (Figure 2(a)). Moreover, after 7 days of *in vitro* culture, we observed that cell growth was reduced when anesthetic was present in the infiltration solution, particularly in relation to the increase of the patients' age, $p < 0.001$ (Figure 2(b)).

3.2. DMSO Is Better Than Trehalose for Cryopreservation of Adipose Tissue. As cryoprotectant agents (CPA) for adipose tissue, we tested DMSO and trehalose, showing a comparable viability of samples with both CPA after thawing (Table 1). In contrast, cell cultures showed that ATD-MSCs isolated from lipoaspirates cryopreserved in DMSO had a more rapid growth and arrived at confluence in a few days with a better morphology as opposed to the cells with trehalose (Figures 3(a) and 3(b)). The morphological analysis and the staining for CD31 and CD105 showed that the cellular structures were better preserved in samples cryopreserved with DMSO than with trehalose (Figures 3(c) and 3(d)).

3.3. Cryopreservation of Lipoaspirates at Both −80°C and −196°C Guarantees Viability of Adipose Tissue and ATD-MSCs. In a first series of cases, to define the best temperature

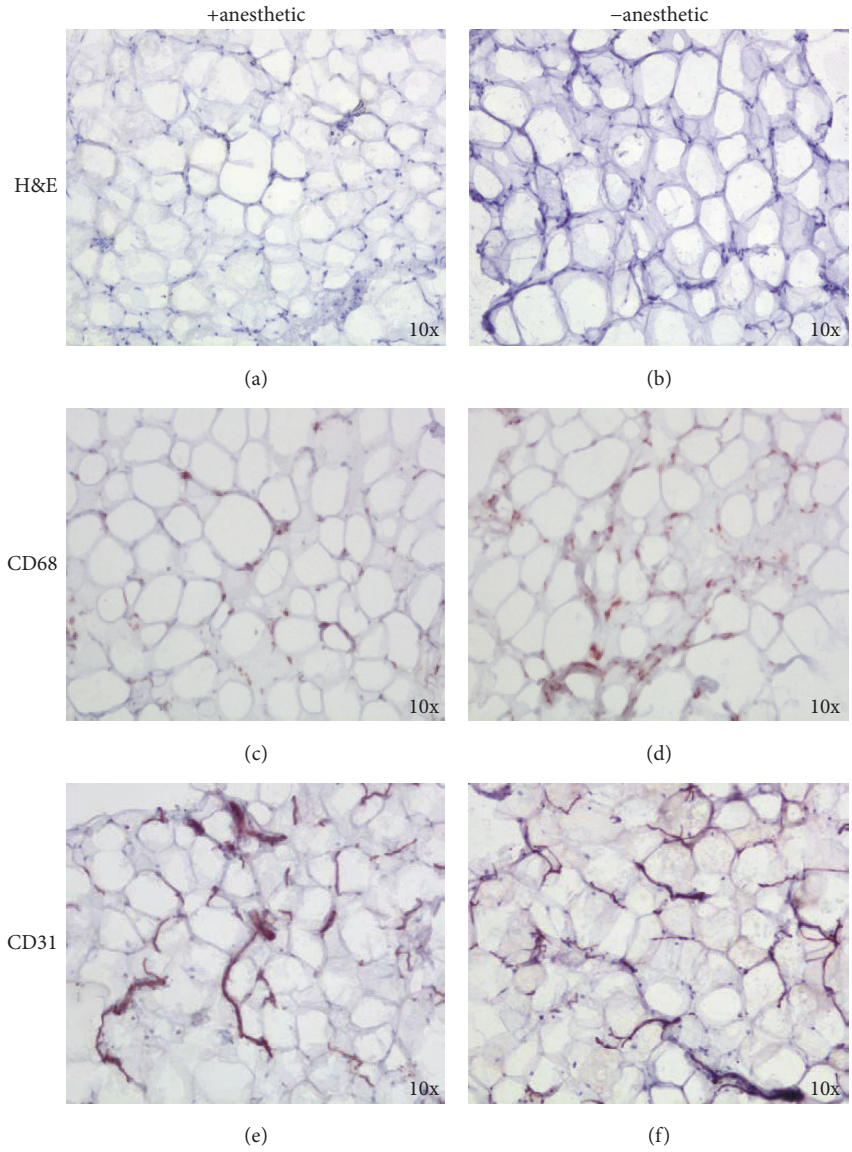

Figure 1: Local anesthetic did not interfere with adipose tissue morphology. H&E staining showed a similar morphology of adipose tissue harvested with or without local anesthetic. No evidence of adipose tissue degeneration or necrosis was evident (a, b). IHC analysis showed comparable staining for CD68 and CD31, in both samples harvested with or without anesthetic (c–f).

of cryopreservation for adipose tissue, we evaluated by MTT assay the viability of tissue derived from lipoaspirates after cryopreservation at −20°C and −80°C. Fat preserved at lower temperature showed a greater viability index (I.V.) than samples preserved at −20°C, Table 2. The samples preserved at −20°C showed a damaged structure and the tissue resulted in suffering compared to fresh and −80°C (Figure 4). Due to the low quality of preservation at−20°C, we then decided to compare −80°C and −196°C. The percentages of viability for adipose tissue after thawing were 77,6% and 91,6% for samples cryopreserved at −80°C and −196°C, respectively (Figure 5(a)). The mean I.V. values were reported in Table S1 (in Supplementary Material available online at http://dx.doi.org/10.1155/2016/4968724). The analysis of cell mortality in the SVF, derived after collagenase digestion of adipose tissue, showed a major number of dead cells in cryopreserved (17% of 7-AAD+ cells) compared to fresh samples (7% of 7-AAD+ cells), $p < 0.05$, but again there was not any difference between the two temperatures of cryopreservation (Figure 5(b)). To further confirm this result, the morphology of cryopreserved adipose tissue at −80°C and −196°C showed well-maintained structures, without evidence of tissue degeneration or necrosis, comparable to the fresh sample (Figures 6(a)–6(c)).

We analysed a panel of standard surface markers for MSCs to study the phenotype of SVF derived from fresh and thawed adipose tissue, showing that the percentage of CD105/CD44/CD73+/CD45− cells and the subpopulation also expressing CD271 were comparable between the two temperatures and with fresh sample (Figures 6(d) and 6(e)). Thus the

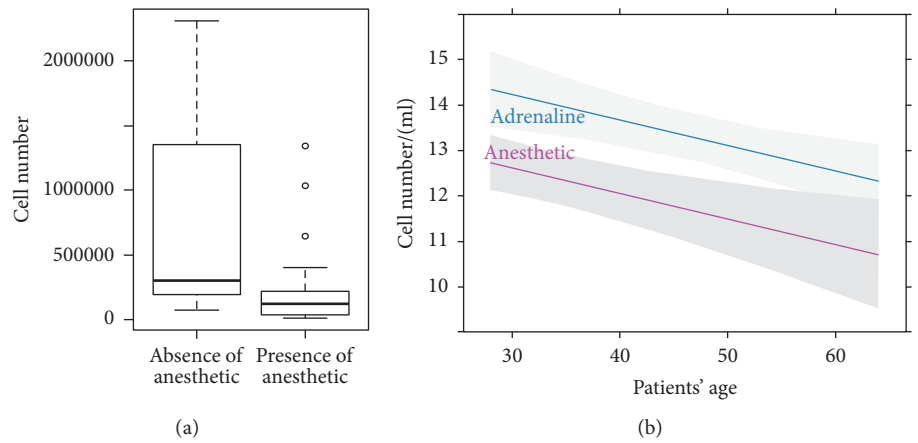

Figure 2: Local anesthetic reduced ATD-MSCs growth. (a) Box and whisker plot showed a significant difference in the number of cells isolated from adipose tissues harvested with or without anesthetic. (b) The regression analysis showed that, after 7 days, the number of cells grown in culture was reduced when the anesthetic was added to the solution of infiltration, particularly in relation to the increasing of the patients' age, $p < 0.001$.

Table 2: Viability index at different temperatures of cryopreservation. The viability index (I.V.) of cryopreserved samples was significantly higher at −80°C compared to −20°C, $p < 0.05$.

	−20°C $N = 25$	−80°C $N = 39$
Age	46 (36–53)	49 (42–57)
I.V. of fresh samples	12 (9,6–13,1)	15,8 (11,5–16,8)
I.V. after cryopreservation	5,6 (5,2–7,1)	7,2* (5,6–10,3)

The viability index (I.V.) of cryopreserved samples was significantly higher at −80°C compared to −20°C; ∗ refers to p value.

cryopreservation at both −80°C and −196°C did not interfere with the content of ATD-MSCs.

3.4. Cryopreservation of Lipoaspirates at Both −80°C and −196°C Preserves Differentiating Abilities of ATD-MSCs In Vitro. We cultured *in vitro* SVF cells derived from collagenase treatment of adipose tissue both fresh and thawed, showing the proliferation of cell with the typical fibroblast-like morphology (Figure 7(a)), that expressed mesenchymal markers such as CD105, CD44, CD73, and CD271 (Figures 7(b)–7(e)), whereas they were negative for hematopoietic markers (data not shown). In these cultures, we observed a selective growth of mesenchymal population expressing CD105/CD44/CD73 and of CD105/CD44/CD73/CD271+ subpopulation, comparable between the two temperatures of cryopreservation (Figures 7(f) and 7(g)). To test whether cryopreservation affects the chondrogenesis and osteogenesis capabilities of these ATD-MSCs, we cultured them in specific media, showing formation of chondrocytes and osteoblasts, both from adipose tissue cryopreserved at −80°C and −196°C (Figures 7(h)–7(k)). We also tested the activity of these osteoblasts, showing their ability to mineralize (Figures 7(l) and 7(m)).

4. Discussion

Regenerative and in particular reparative medicine represent the new frontier for orthopaedic diseases, such as osteoarthritis, that can benefit of treatments with ATD-MSCs. Indeed, to date, clinical studies suggest that SVF and ATD-MSCs are safe and capable of tissue repairing [15, 18, 19, 29, 30]. Various well-defined harvesting techniques are available for liposuction procedure [27, 31, 32], even though there is not one method providing the best results in terms of viability and volume of adipose tissue with its cellular components. Previously published data reported a marked influence of local anesthetics on the quantity and quality of viable preadipocytes [25, 33]. Our results showed that lidocaine seems not to affect morphology of adipose tissue, but the derived ATD-MSCs reduced their growth in cultures *in vitro*. These data were in accordance with the literature, which also showed a reduced ATD-MSC viability [34] and chondrocyte cytotoxicity due to local anesthetics [35], prompting us to suggest performing liposuction without local anesthesia.

Literature data reported different methods of cryopreservation for human adipose tissue, investigating both the use of different CPAs and temperatures [21, 36, 37]. Different CPAs alone or in combinations can improve the viability of this tissue during the procedure of freezing and thawing [38], since CPAs reduced the osmotic stress. Here we tested DMSO and trehalose, showing a viability of samples comparable to fresh ones, with both CPAs after thawing. Nonetheless, ATD-MSCs isolated from lipoaspirates cryopreserved in DMSO grew faster and with a better morphology than the cells derived from trehalose cryopreservation. Even though DMSO is known for its cytotoxicity and its clinical use is limited, it gave us the best results, and thus we are considering utilizing the GMP grade DMSO, which is available for clinical use.

The optimal temperature for cryopreservation of adipose tissue is still under investigation; indeed some works report that −20°C is comparable to liquid nitrogen for a short term storage of adipose tissue [36, 37]. The length of the

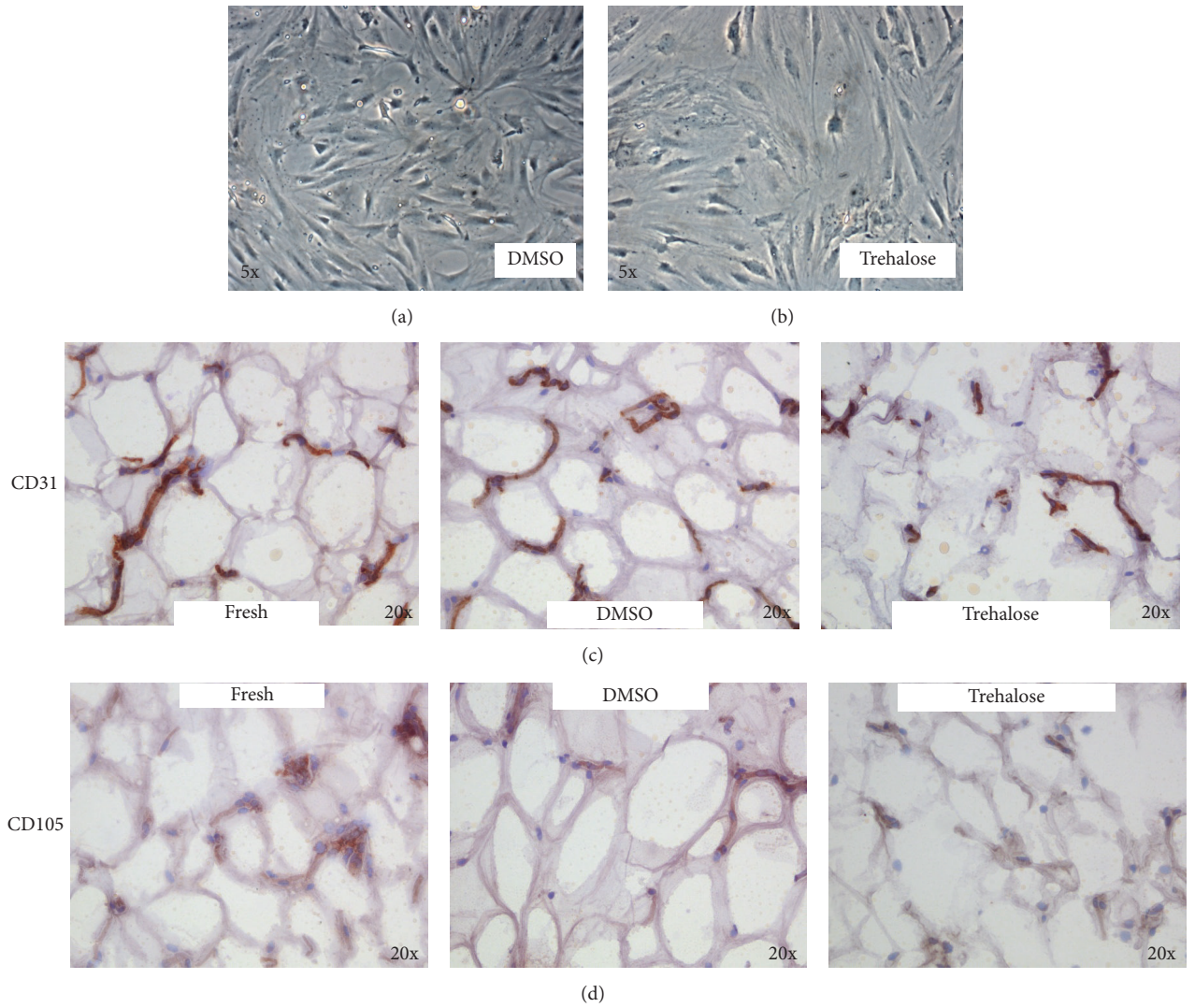

Figure 3: DMSO cryopreserved adipose tissue better than trehalose. ATD-MSCs isolated from DMSO cryopreserved lipoaspirates showed a better morphology compared with trehalose ((a) and (b)). The IHC staining for CD31 (line (c)) and CD105 (line (d)) showed that the different cellular structures were better preserved in samples cryopreserved with DMSO than with trehalose.

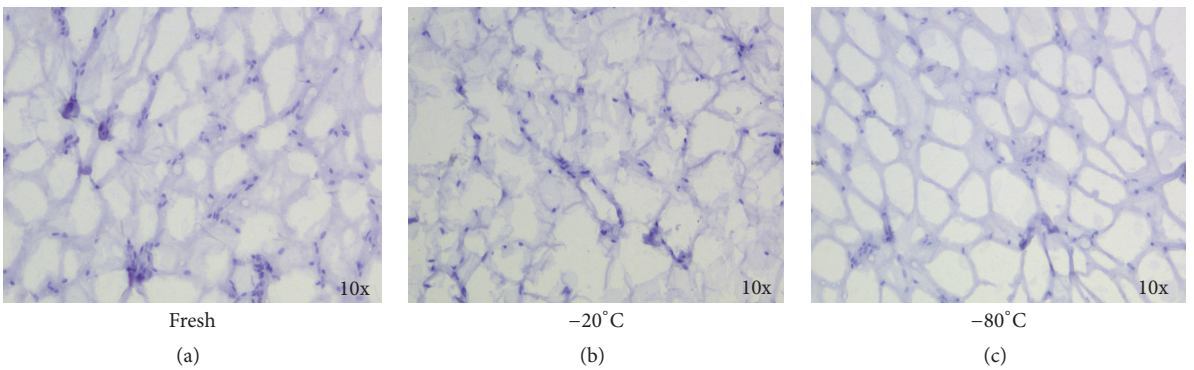

Figure 4: Adipose tissue is better preserved at −80°C than −20°C. The samples cryopreserved at −20°C (b) showed a damaged structure compared to fresh (a) and −80°C (c).

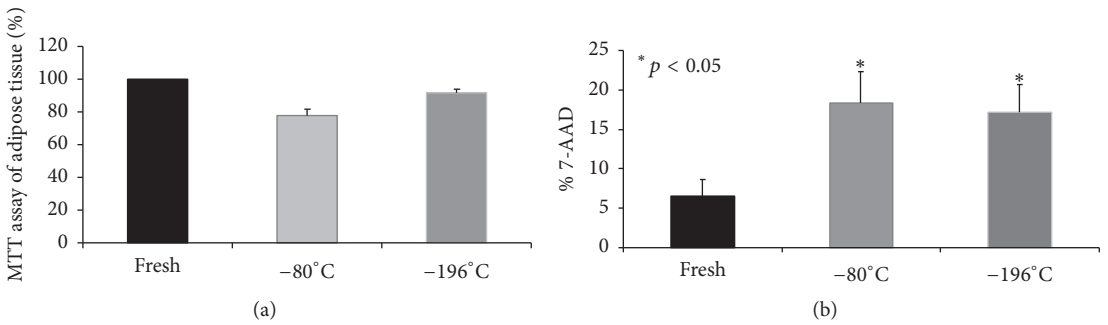

Figure 5: Cryopreservation at −80°C and −196°C guaranteed viability of adipose tissue and ATD-MSCs. The percentages of viability of adipose tissue normalized on fresh sample are reported (a). 7-AAD staining showed a significant increase of dead cells in cryopreserved compared to fresh samples, $p < 0.05$, but there was not any difference between the two temperatures of cryopreservation (b).

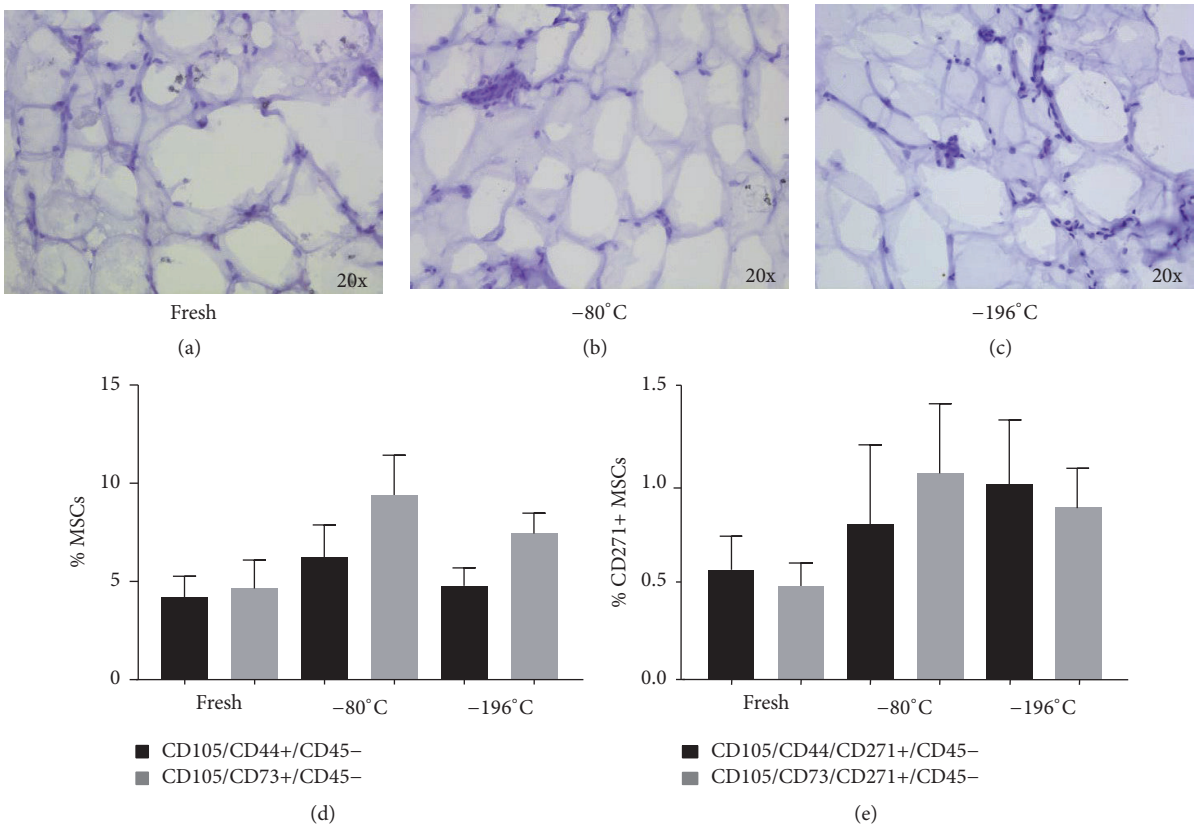

Figure 6: Cryopreservation at −80°C and −196°C maintained morphology of adipose tissue and the content of ATD-MSCs. The morphology of cryopreserved adipose tissue at −80°C and −196°C was maintained, without evidence of tissue degeneration or necrosis, comparable to the fresh sample (a–c). The percentage of CD105, CD44, and CD73+ ATD-MSCs and the CD271+ subpopulation was comparable to fresh samples and also between the two temperatures (d, e).

cryopreservation period is particularly relevant, since to allow multiple infusions it is necessary to store adipose tissue for long time, and thus it is mandatory to investigate both different CPAs and temperatures for longer times. We started to thaw one month after freezing, showing a significant reduced viability of lipoaspirates at −20°C compared to −80°C, according to Wolter et al. [39]. Since Moscatello et al. examined storage at −20°C and liquid nitrogen, suggesting that the last is better [40], we decided to compare −80°C and −196°C to evaluate viability of adipose tissue and above all the maintenance of ATD-MSC ability to differentiate into osteoblasts and chondrocytes. Literature reports only one study that contemporarily compared −20°C, −80°C, and liquid nitrogen temperatures, which did not show any differences in cell viability about the three temperatures. Nonetheless, in this work the period of storage was short and their aim was to examine the viability of adipose tissue and adipocytes for fat graft in plastic surgery [36]. Here, we report the results on adipose

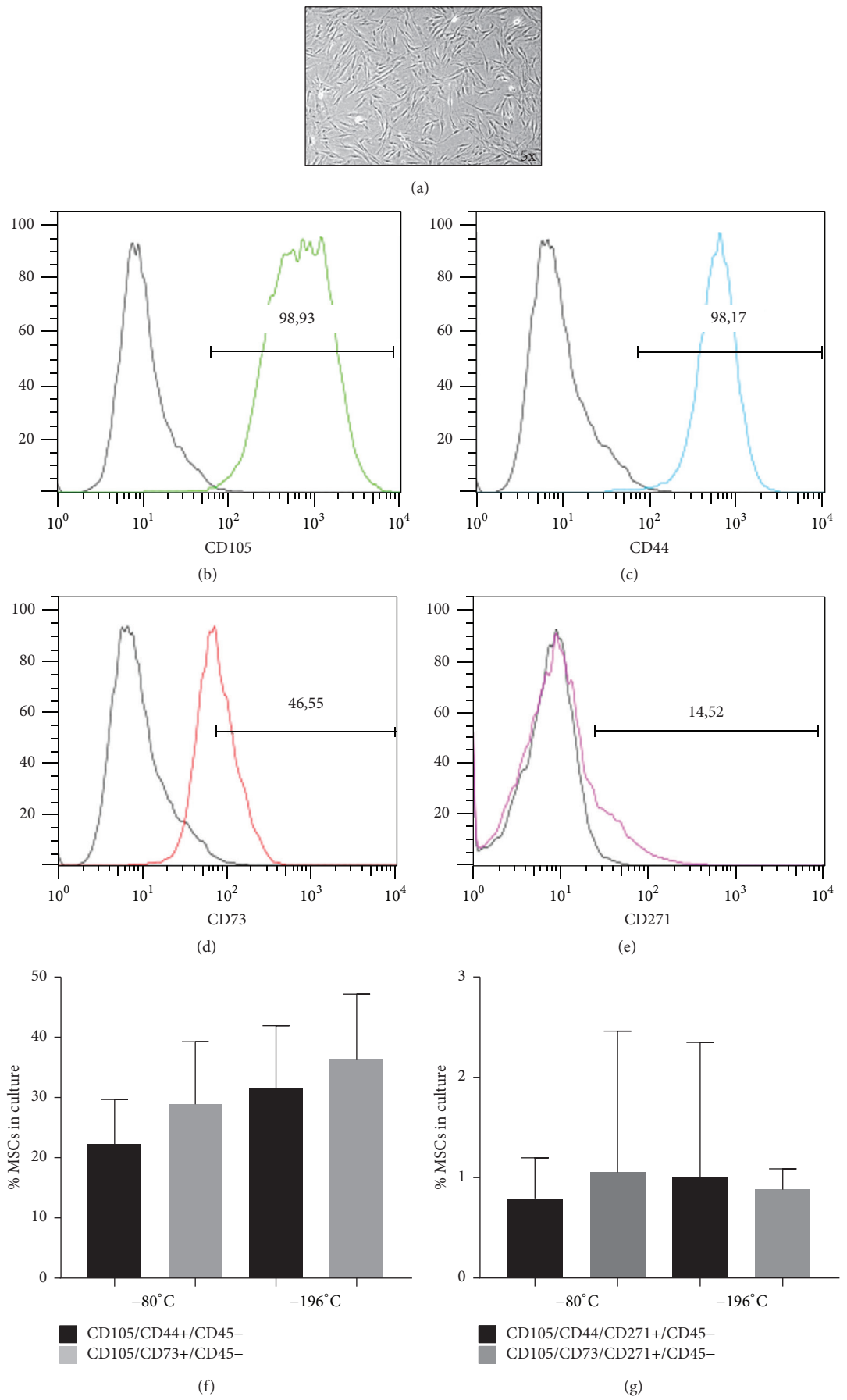

Figure 7: Continued.

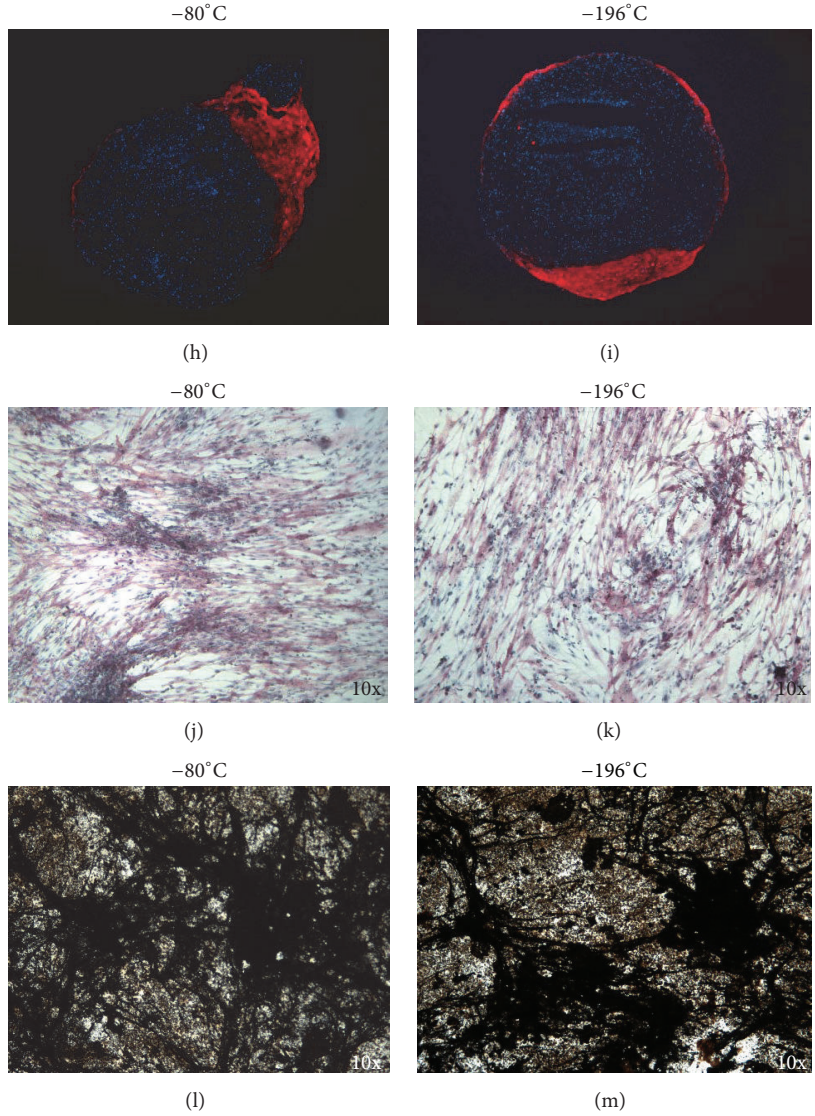

Figure 7: ATD-MSCs differentiating abilities *in vitro* were preserved at both temperatures of cryopreservation. After cell culture, ATD-MSCs assumed the typical fibroblast-like morphology (a) and expressed CD105, CD44, CD73, and CD271 (b–e). The immunophenotype of MSCs expressing CD105/CD44/CD73 and of the subpopulation CD105/CD44/CD73/CD271+ cells was comparable with both the temperatures of cryopreservation (f, g). Chondrocytes (h, i) and osteoblasts (j, k) formed from both adipose tissues cryopreserved at −80°C and −196°C. von Kossa staining showed that osteoblasts had comparable ability to mineralize at both temperatures (l, m).

tissue viability and differentiation capabilities of ATD-MSCs towards osteoblasts and chondrocytes, after one month of cryopreservation at −20°C, −80°C, and −196°C. We demonstrated that the I.V. of samples cryopreserved at −80°C and in liquid nitrogen was comparable to fresh samples, whereas at −20°C the viability was reduced. We also observed that no differences were present between samples cryopreserved at −80°C and −196°C, thawing after two months (data not shown).

Among the different markers available for the characterization of MSCs, described by the Mesenchymal and Tissue Stem Cell Committee of the International Society for Cellular Therapy [41], we tested positivity for CD105, CD44, CD73, and the contemporary negativity for CD45. We also studied the expression of CD271, since CD271+ ATD-MSCs are associated with a high efficiency of proliferation and trilineage differentiation compared to CD271− counterpart [12]. Moreover, even though a decrease in stem cell number is typical in elderly people, the subpopulation of MSCs expressing CD271 is also reduced during ageing [13, 42]; however, they are always present in all age groups according to Cuevas-Diaz Duran et al. [13], and thus CD271 has been proposed as marker of primary choice for tissue regeneration by ATD-MSCs in older subjects. We reported that cryopreservation did not alter the frequency of CD105/CD44/CD73+/CD45− cells and of the subpopulation expressing CD271, in SVFs derived from fresh and thawed samples. This result is relevant since even though the percentage of dead cells was slightly

increased in thawed samples compared to the fresh ones, the cryopreservation both at −80°C and at −196°C did not interfere with the content of ATD-MSCs, likely due to a protective action of adipose tissue on these cells.

ATD-MSCs derived from cryopreserved samples at both −80°C and −196°C differentiated into chondrocytes and osteoblasts, which showed also mineralization activity. Thus, according to literature [20], ATD-MSCs derived from cryopreserved adipose tissue were functionally equivalent to freshly isolated ones.

In conclusion, the creation of an Autologous Adipose Tissue Bank would avoid repeated lipoaspiration procedures for patients to guarantee the availability of SVF for multiple injections. The demonstration that cryopreservation of adipose tissue, for long time, allows maintaining the viability of SVF, particularly of ATD-MSCs, would allow testing the efficacy of multiple infusions of SVF in treatment of patients with osteoarthritis. This could be an alternative approach to the expansion *ex vivo* of ATD-MSCs, since a direct transfer of the cellular component from the donor to the acceptor site of the same patient is a simple and straightforward method, avoiding the complexity of constructs and *ex vivo* cell cultures performed in laboratory.

Competing Interests

The authors declare that there is no conflict of interests regarding the publication of this paper.

Acknowledgments

This work was supported by CRT and Compagnia di San Paolo Foundations and by Fondazione Ricerca Molinette ONLUS. The authors thank Professor Michele Zocchi for his magisterial lesson in adipose tissue harvesting. Special thanks are due to Dr. Paola Berchialla for statistical analysis and to Dr. Claudia Pizzo and Filippo Rivarossa for collecting patients' adipose tissue samples and clinical data.

References

[1] J. M. Murphy, K. Dixon, S. Beck, D. Fabian, A. Feldman, and F. Barry, "Reduced chondrogenic and adipogenic activity of mesenchymal stem cells from patients with advanced osteoarthritis," *Arthritis and Rheumatism*, vol. 46, no. 3, pp. 704–713, 2002.

[2] A. J. Friedenstein, R. K. Chailakhjan, and K. S. Lalykina, "The development of fibroblast colonies in monolayer cultures of guinea-pig bone marrow and spleen cells," *Cell and Tissue Kinetics*, vol. 3, no. 4, pp. 393–403, 1970.

[3] J. K. Fraser, I. Wulur, Z. Alfonso, and M. H. Hedrick, "Fat tissue: an underappreciated source of stem cells for biotechnology," *Trends in Biotechnology*, vol. 24, no. 4, pp. 150–154, 2006.

[4] A. Dicker, K. Le Blanc, G. Åström et al., "Functional studies of mesenchymal stem cells derived from adult human adipose tissue," *Experimental Cell Research*, vol. 308, no. 2, pp. 283–290, 2005.

[5] L. E. Kokai, K. Marra, and J. P. Rubin, "Adipose stem cells: biology and clinical applications for tissue repair and regeneration," *Translational Research*, vol. 163, no. 4, pp. 399–408, 2014.

[6] S. Wakitani, K. Imoto, T. Yamamoto, M. Saito, N. Murata, and M. Yoneda, "Human autologous culture expanded bone marrow mesenchymal cell transplantation for repair of cartilage defects in osteoarthritic knees," *Osteoarthritis and Cartilage*, vol. 10, no. 3, pp. 199–206, 2002.

[7] R. Kuroda, K. Ishida, T. Matsumoto et al., "Treatment of a full-thickness articular cartilage defect in the femoral condyle of an athlete with autologous bone-marrow stromal cells," *Osteoarthritis and Cartilage*, vol. 15, no. 2, pp. 226–231, 2007.

[8] P. A. Zuk, M. Zhu, P. Ashjian et al., "Human adipose tissue is a source of multipotent stem cells," *Molecular Biology of the Cell*, vol. 13, no. 12, pp. 4279–4295, 2002.

[9] J. M. Gimble, "Adipose tissue-derived therapeutics," *Expert Opinion on Biological Therapy*, vol. 3, no. 5, pp. 705–713, 2003.

[10] P. Bourin, B. A. Bunnell, L. Casteilla et al., "Stromal cells from the adipose tissue-derived stromal vascular fraction and culture expanded adipose tissue-derived stromal/stem cells: a joint statement of the International Federation for Adipose Therapeutics and Science (IFATS) and the International Society for Cellular Therapy (ISCT)," *Cytotherapy*, vol. 15, no. 6, pp. 641–648, 2013.

[11] C. Merceron, S. Portron, M. Masson et al., "The effect of two- and three-dimensional cell culture on the chondrogenic potential of human adipose-derived mesenchymal stem cells after subcutaneous transplantation with an injectable hydrogel," *Cell Transplantation*, vol. 20, no. 10, pp. 1575–1588, 2011.

[12] G. Calabrese, R. Giuffrida, D. Lo Furno et al., "Potential effect of CD271 on human mesenchymal stromal cell proliferation and differentiation," *International Journal of Molecular Sciences*, vol. 16, no. 7, pp. 15609–15624, 2015.

[13] R. Cuevas-Diaz Duran, M. T. González-Garza, A. Cardenas-Lopez, L. Chavez-Castilla, D. E. Cruz-Vega, and J. E. Moreno-Cuevas, "Age-related yield of adipose-derived stem cells bearing the low-affinity nerve growth factor receptor," *Stem Cells International*, vol. 2013, Article ID 372164, 9 pages, 2013.

[14] G. Cox, S. A. Boxall, P. V. Giannoudis et al., "High abundance of $CD271^+$ multipotential stromal cells (MSCs) in intramedullary cavities of long bones," *Bone*, vol. 50, no. 2, pp. 510–517, 2012.

[15] J. Michalek, R. Moster, L. Lukac et al., "Autologous adipose tissue-derived stromal vascular fraction cells application in patients with osteoarthritis," *Cell Transplant*, 2015.

[16] Y.-G. Koh, Y.-J. Choi, S.-K. Kwon, Y.-S. Kim, and J.-E. Yeo, "Clinical results and second-look arthroscopic findings after treatment with adipose-derived stem cells for knee osteoarthritis," *Knee Surgery, Sports Traumatology, Arthroscopy*, vol. 23, no. 5, pp. 1308–1316, 2015.

[17] Y. S. Kim, H. J. Lee, Y. J. Choi et al., "Does an injection of a stromal vascular fraction containing adipose-derived mesenchymal stem cells influence the outcomes of marrow stimulation in osteochondral lesions of the talus? A clinical and magnetic resonance imaging study," *The American Journal of Sports Medicine*, vol. 42, no. 10, pp. 2424–2434, 2014.

[18] J. Freitag, J. Ford, D. Bates et al., "Adipose derived mesenchymal stem cell therapy in the treatment of isolated knee chondral lesions: design of a randomised controlled pilot study comparing arthroscopic microfracture versus arthroscopic microfracture combined with postoperative mesenchymal stem cell injections," *BMJ Open*, vol. 5, no. 12, Article ID e009332, 2015.

[19] C. H. Jo, Y. G. Lee, W. H. Shin et al., "Intra-articular injection of mesenchymal stem cells for the treatment of osteoarthritis of the knee: a proof-of-concept clinical trial," *STEM CELLS*, vol. 32, no. 5, pp. 1254–1266, 2014.

[20] M. S. Choudhery, M. Badowski, A. Muise, J. Pierce, and D. T. Harris, "Cryopreservation of whole adipose tissue for future use in regenerative medicine," *Journal of Surgical Research*, vol. 187, no. 1, pp. 24–35, 2014.

[21] M. L. González-Fernández, S. Pérez-Castrillo, P. Ordás-Fernández, M. E. López-González, B. Colaço, and V. Villar-Suárez, "Study on viability and chondrogenic differentiation of cryopreserved adipose tissue-derived mesenchymal stromal cells for future use in regenerative medicine," *Cryobiology*, vol. 71, no. 2, pp. 256–263, 2015.

[22] T. Martinello, I. Bronzini, L. Maccatrozzo et al., "Canine adipose-derived-mesenchymal stem cells do not lose stem features after a long-term cryopreservation," *Research in Veterinary Science*, vol. 91, no. 1, pp. 18–24, 2011.

[23] G. Liu, H. Zhou, Y. Li et al., "Evaluation of the viability and osteogenic differentiation of cryopreserved human adipose-derived stem cells," *Cryobiology*, vol. 57, no. 1, pp. 18–24, 2008.

[24] Y. Liu, X. Xu, H. Ma, J. Liu, and Z. Cui, "Effect of various freezing solutions on cryopreservation of mesenchymal stem cells from different animal species," *Cryo-Letters*, vol. 32, no. 5, pp. 425–435, 2011.

[25] M. Keck, M. Zeyda, K. Gollinger et al., "Local anesthetics have a major impact on viability of preadipocytes and their differentiation into adipocytes," *Plastic and Reconstructive Surgery*, vol. 126, no. 5, pp. 1500–1505, 2010.

[26] S. R. Coleman and A. P. Saboeiro, "Fat grafting to the breast revisited: safety and efficacy," *Plastic and Reconstructive Surgery*, vol. 119, no. 3, pp. 775–787, 2007.

[27] L. L. Q. Pu, S. R. Coleman, X. Cui, R. E. H. Ferguson, and H. C. Vasconez, "Autologous fat grafts harvested and refined by the Coleman technique: a comparative study," *Plastic and Reconstructive Surgery*, vol. 122, no. 3, pp. 932–937, 2008.

[28] G. Brunetti, R. Rizzi, A. Oranger et al., "LIGHT/TNFSF14 increases osteoclastogenesis and decreases osteoblastogenesis in multiple myeloma-bone disease," *Oncotarget*, vol. 5, no. 24, pp. 12950–12967, 2014.

[29] F. Davatchi, B. S. Abdollahi, M. Mohyeddin, F. Shahram, and B. Nikbin, "Mesenchymal stem cell therapy for knee osteoarthritis. Preliminary report of four patients," *International Journal of Rheumatic Diseases*, vol. 14, no. 2, pp. 211–215, 2011.

[30] F. Perdisa, N. Gostyńska, A. Roffi, G. Filardo, M. Marcacci, and E. Kon, "Adipose-derived mesenchymal stem cells for the treatment of articular cartilage: a systematic review on preclinical and clinical evidence," *Stem Cells International*, vol. 2015, Article ID 597652, 13 pages, 2015.

[31] W. J. F. M. Jurgens, M. J. Oedayrajsingh-Varma, M. N. Helder et al., "Effect of tissue-harvesting site on yield of stem cells derived from adipose tissue: implications for cell-based therapies," *Cell and Tissue Research*, vol. 332, no. 3, pp. 415–426, 2008.

[32] M. Aguena, R. D. Fanganiello, L. A. L. Tissiani et al., "Optimization of parameters for a more efficient use of adipose-derived stem cells in regenerative medicine therapies," *Stem Cells International*, vol. 2012, Article ID 303610, 7 pages, 2012.

[33] M. Keck, J. Janke, and K. Ueberreiter, "Viability of preadipocytes in vitro: the influence of local anesthetics and pH," *Dermatologic Surgery*, vol. 35, no. 8, pp. 1251–1257, 2009.

[34] A.-C. Girard, M. Atlan, K. Bencharif et al., "New insights into lidocaine and adrenaline effects on human adipose stem cells," *Aesthetic Plastic Surgery*, vol. 37, no. 1, pp. 144–152, 2013.

[35] A. Breu, K. Rosenmeier, R. Kujat, P. Angele, and W. Zink, "The cytotoxicity of bupivacaine, ropivacaine, and mepivacaine on human chondrocytes and cartilage," *Anesthesia and Analgesia*, vol. 117, no. 2, pp. 514–522, 2013.

[36] B.-W. Li, W.-C. Liao, S.-H. Wu, and H. Ma, "Cryopreservation of fat tissue and application in autologous fat graft: in vitro and in vivo study," *Aesthetic Plastic Surgery*, vol. 36, no. 3, pp. 714–722, 2012.

[37] J. W. MacRae, S. S. Tholpady, R. C. Ogle, R. F. Morgan, J. H. Carraway, and H. C. Vasconez, "Ex vivo fat graft preservation: effects and implications of cryopreservation," *Annals of Plastic Surgery*, vol. 52, no. 3, pp. 281–283, 2004.

[38] X. D. Cui, D. Y. Gao, B. F. Fink, H. C. Vasconez, and L. L. Q. Pu, "Cryopreservation of human adipose tissues," *Cryobiology*, vol. 55, no. 3, pp. 269–278, 2007.

[39] T. P. Wolter, D. von Heimburg, I. Stoffels, A. Groeger, and N. Pallua, "Cryopreservation of mature human adipocytes: in vitro measurement of viability," *Annals of Plastic Surgery*, vol. 55, no. 4, pp. 408–413, 2005.

[40] D. K. Moscatello, M. Dougherty, R. S. Narins, and N. Lawrence, "Cryopreservation of human fat for soft tissue augmentation: viability requires use of cryoprotectant and controlled freezing and storage," *Dermatologic Surgery*, vol. 31, no. 11, part 2, pp. 1506–1510, 2005.

[41] M. Dominici, K. Le Blanc, I. Mueller et al., "Minimal criteria for defining multipotent mesenchymal stromal cells. The International Society for Cellular Therapy position statement," *Cytotherapy*, vol. 8, no. 4, pp. 315–317, 2006.

[42] T. Yamada, H. Akamatsu, S. Hasegawa et al., "Age-related changes of p75 neurotrophin receptor-positive adipose-derived stem cells," *Journal of Dermatological Science*, vol. 58, no. 1, pp. 36–42, 2010.

Hindawi Publishing Corporation
Stem Cells International
Volume 2016, Article ID 3595941, 9 pages
http://dx.doi.org/10.1155/2016/3595941

Research Article

In Vitro Characterization of Human Mesenchymal Stem Cells Isolated from Different Tissues with a Potential to Promote Complex Bone Regeneration

Áron Szepesi,[1,2] Zsolt Matula,[1] Anna Szigeti,[1,2] György Várady,[1] József Szalma,[3] Gyula Szabó,[3] Ferenc Uher,[4] Balázs Sarkadi,[1,5] and Katalin Német[2]

[1]*Research Centre for Natural Sciences, Hungarian Academy of Sciences, Budapest, Hungary*
[2]*Creative Cell Ltd., Budapest, Hungary*
[3]*Department of Dentistry, Oral and Maxillofacial Surgery, University of Pécs Medical School, Pécs, Hungary*
[4]*National Blood Service, Budapest, Hungary*
[5]*Molecular Biophysics Research Group of the Hungarian Academy of Sciences, Semmelweis University, Budapest, Hungary*

Correspondence should be addressed to Áron Szepesi; szepesi.aron@koki.mta.hu

Received 8 July 2016; Accepted 19 October 2016

Academic Editor: Filiberto Mastrangelo

Copyright © 2016 Áron Szepesi et al. This is an open access article distributed under the Creative Commons Attribution License, which permits unrestricted use, distribution, and reproduction in any medium, provided the original work is properly cited.

Bone tissue regeneration is a major, worldwide medical need, and several strategies have been developed to support the regeneration of extensive bone defects, including stem cell based bone grafts. In addition to the application of stem cells with high osteogenic potential, it is important to maintain proper blood flow in a bone graft to avoid inner graft necrosis. Mesenchymal stem cells (MSCs) may form both osteocytes and endothelial cells; therefore we examined the combined *in vitro* osteogenic and endothelial differentiation capacities of MSCs derived from adipose tissue, Wharton's jelly, and periodontal ligament. Based on a detailed characterization presented here, MSCs isolated from adipose tissue and periodontal ligament may be most appropriate for generating vascularized bone grafts.

1. Introduction

There is a great clinical demand for improved methods of bone tissue regeneration after trauma or medical bone resections, as spontaneous recovery is slow or in many cases nonexistent. This is well exemplified in critical-size bone defects [1], which may affect the oral cavity as a result of trauma, aggressive periodontitis, or tumor surgery [2]. Since the availability of donor-derived bone grafts is limited and the extraction of autologous bone grafts is often associated with considerable pain and donor-site morbidity, there is an increasing demand for *in vitro* engineered bone tissues [3].

In order to help the bone healing process, recent technologies promote the use of various tissue grafts, containing autologous or allogenic bone-forming cells. The cells used in such a bone tissue regeneration therapy should have high bone-forming potential for rapid and effective incorporation.

In addition to osteoblasts, cells promoting angiogenesis should be also important participants in bone graft formation and regeneration, especially in the case of large bone defects, in order to promote osseointegration and avoid inner graft necrosis. Clearly, to ensure the long-term function of the bone graft, cells capable of forming blood vessels within the bone tissue should also be present [4]. Stem or progenitor cells capable of differentiating into both osteoblast and blood vessel endothelial cell may provide a solution in this regard.

Mesenchymal stem cells (MSCs) are currently considered to be key sources in regenerative medicine. MSCs are multipotent with self-renewal ability and a capacity to differentiate into different mesenchymal lineages, including adipose tissue, bone, and cartilage [5, 6]. Tissue-derived MSCs do not raise major ethical concerns in medical applications [7]. In addition, due to their immunosuppressive characteristics even allogeneic MSCs can be used in various therapeutic approaches [8].

MSCs were initially described in the bone marrow stroma [9] and later found in numerous human tissues including fat and in different dental tissues [5, 10]. Bone marrow derived (BM) MSCs have been used for tissue engineering for several years. However, the invasive collection procedure of BM-MSCs possesses disadvantages, including pain and potential medical complications [5]. MSCs from adult adipose tissue (AD-MSCs) can be readily harvested in large numbers with very low donor-site morbidity. AD-MSCs therefore are broadly used in various regenerative therapeutic interventions and may also serve as cells for bone grafts [11]. In addition Wharton's jelly of the umbilical cord (WJ-MSC) and the tissues of the placenta also provide a rich source of MSCs for potential therapies [12].

The periodontal ligament is a soft connective tissue developed from the neural crest and has anchoring, homeostatic, and regenerative functions in the periodontium. Periodontal ligament contains stem cells (PDLSC) possessing MSC properties [10, 13]. The enhanced osseointegration effect of human PDLSCs was confirmed after transplantation of these cells with bone graft [14].

In the present work we have compared several properties of *in vitro* cultured and differentiated human AD-MSCs, WJ-MSCs, and PDLSCs. Under identical conditions we have examined their frequency of colonies, immunophenotype, trilineage differentiation capacity, and the expressed pluripotency and mesodermal markers. Furthermore, we have characterized in detail the endothelial differentiation capacity of these MSCs.

2. Materials and Methods

2.1. Isolation, Culturing, and Differentiation of Cells. All samples were obtained from healthy donors. Work with human tissues was performed with the permission of the Ethical Committee of the Hungarian Medical Research Council (ETT; ID: 24083-3/2013/HER). Most of the reagents below were purchased from Thermo Fisher Scientific (Waltham, USA), all others as indicated.

MSCs from liposuction derived adipose tissue ($n = 3$) and periodontal ligament ($n = 3$) were isolated as described previously [13, 15]. Wharton's jelly of the umbilical cord was collected from full-term births ($n = 3$). The anatomical localization of the periodontal ligament and Wharton's jelly is presented on Figure 1.

For isolation of Wharton's jelly derived MSC, the cord was cut into 1-2 cm segments and the vessels were removed. The outstretched tissue was treated with 2 mg/mL collagenase type IV and 100 IU/mL hyaluronidase (Sigma-Aldrich, St. Louis, USA). The cord pieces were washed with DMEM medium and Wharton's jelly was collected and passed through an 18 G needle. The cell suspension was then resuspended in high glucose DMEM medium supplemented with 20% fetal bovine serum (FBS) and 16 ng/mL fibroblast growth factor 2. Cells were plated with $2 \times 10^5/\text{cm}^2$ density. Growth medium (DMEM-F12 1 : 1 with 10% FBS, 2 mM L-glutamine, and 50 μg/mL gentamicin plus 1 ng/mL FGF-2) was used after third medium changes, and cells were subcultured once a week at a density of $4 \times 10^3/\text{cm}^2$.

To assess the differentiation potential of the MSC isolates, cells between passages 4 and 8 were differentiated into adipocyte, osteoblast, and chondrocyte phenotypes as documented [13].

Human umbilical vein endothelial cells (HUVEC) were kind gifts of Adrienn Németh. The isolation method and culture conditions were detailed by [16].

The human embryonic stem cell line 9 (HUES9) was a kind gift of Douglas Melton, Harvard University, USA. The HUES culture conditions were used as described in detail by Apáti et al. [17].

2.2. Flow Cytometry. The expression of cell surface immunomarkers was assessed by flow cytometry [13]. Cells were stained with the following mouse monoclonal antibodies: anti-human CD13, CD14, CD29, CD31, CD34, CD44, CD45, CD73, CD90, CD105, CD106, CD117, CD133, CD144, CD146, CD166, CD271, CD309, and HLA-DR or the corresponding isotype controls. For references of the antibodies see Supplementary Table 1 in Supplementary Material available online at http://dx.doi.org/10.1155/2016/3595941. Dead cells were identified by staining with propidium iodide. Measurements were carried out in a 4-color FACSCalibur flow cytometer (BD Biosciences). In the case of ABCG2, unconjugated 5D3 monoclonal antibody was used as described previously [13].

Data were expressed both as mean percentage of positive cells and as median fluorescence intensity (MFI) ratio determined using the median fluorescence value of the specific marker analyzed, divided by the median fluorescence value of the isotype control.

2.3. Colony Forming Unit-Fibroblast Assay (CFU-F). The CFU-F assay was performed at passages 3–6 as previously described [13].

2.4. Immunocytochemistry. Cells were fixed [15] and stained with unconjugated monoclonal anti-α-smooth muscle actin (α-SMA; Sigma-Aldrich; cat. number: A5228) or anti-GATA6 (R&D Systems Minneapolis, USA; cat. number: AF1700) primary antibody or the matched isotype control for 1 hour at room temperature in the dilution according to manufacturer's instructions. AlexaFluor488 (α-SMA) or AlexaFluor568 (GATA6) secondary antibodies were applied for fluorescent detection, and nuclei were counterstained with DAPI. The fluorescence membrane stain $\text{DiSC}_3(5)$ was used in final concentration of 5 μM.

2.5. Endothelial Differentiation and Matrigel Tube Formation Assay. Cells were stimulated with Endothelial Cell Growth Medium (EGM-2, Lonza, Basel, Switzerland) for 7 days in a humidified thermostat. Chilled Matrigel (Corning, New York, USA) was added to a 24-well plate and incubated at 37°C. 5×10^4 of the induced cells were suspended in EGM-2 medium and added to the solidified Matrigel. Morphological changes were observed under an inverted microscope during a 24-hour incubation period. Representative pictures were taken in every hour and analyzed using the TubeCount software [18] to determine the number and length of tubes. When a maximum level of tube forming was observed, three

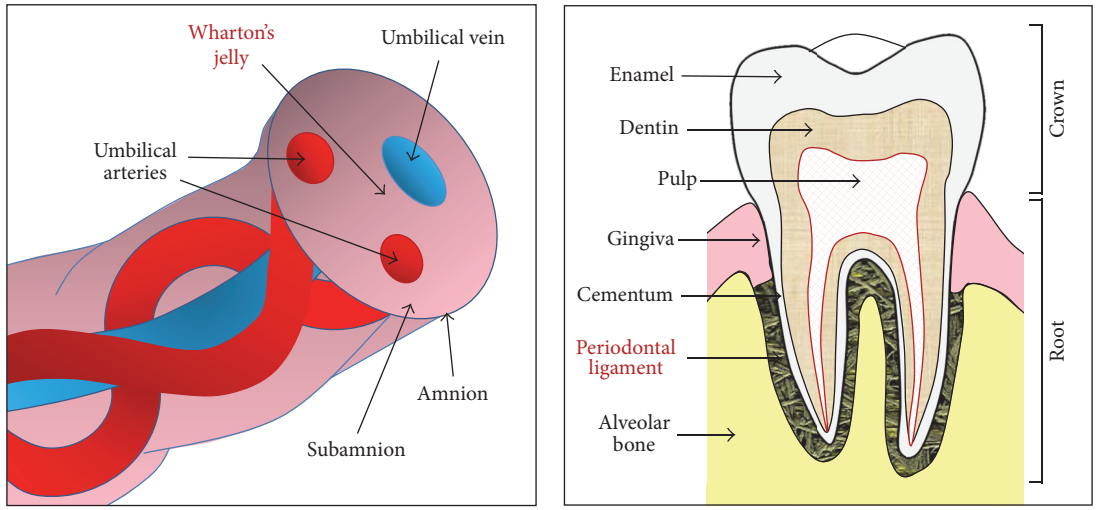

(a) (b)

Figure 1: Schematic cross-sectional diagram of human umbilical cord (a) and tooth (b) shows anatomical compartments, including Wharton's jelly (a) and periodontal ligament (b), as a source of stem cells.

pictures were taken from different fields of each well. The data were presented as averages of three different experiments.

2.6. Gene Expression Analysis. Total RNA was isolated from undifferentiated and differentiated cells and cDNA was synthesized [15]. The expression levels of OCT4, SOX2, NANOG, telomerase reverse transcriptase (TERT), tissue-nonspecific alkaline phosphatase (ALP), peroxisome proliferator-activated receptor gamma (PPARγ), and platelet endothelial cell adhesion molecule 1 (PECAM1) genes were measured using TaqMan reagents. The expression of runt-related transcription factor 2 (RUNX2) mRNA was determined by using Power SYBR Green reagents in StepOne Plus qPCR instruments (Thermo Fisher Scientific). Gene expression levels were calculated with $2^{(-\Delta Ct)}$ method relative to glyceraldehyde-3-phosphate dehydrogenase (GAPDH) as a reference. For references of the primers see Supplementary Table 2.

2.7. Statistical Analysis. The data are presented as the mean of three repeated experiments of the biological parallels ± SD. Statistical comparisons were performed using Student's *t-test*. *P* values <0.001 were considered significant.

3. Results

3.1. Colony Forming Unit-Fibroblast Assay. The efficiency by which MSCs can form colonies at low densities on the plastic surface still remains an important assay for the quality control of cell preparations. (The heterogeneity of the different MSC isolates is demonstrated in Figure 2(a).) PDLSCs produced 94.3 ± 27.0 colonies from 400 cells which is significantly higher than in the case of AD-MSC (46.3 ± 21.0) or WJ-MSC (24.2 ± 8.9) isolates (Figures 2(b) and 2(c)).

3.2. Cell Surface Markers. The immunophenotypic profile of adherent cells from each culture was determined by testing a panel of surface markers using flow cytometry. Essentially, 100% of all the different MSCs expressed the most commonly reported positive markers CD13, CD29, CD44, CD73, CD90, CD105, and CD166. Endothelial markers CD31, CD144, and CD309 and the markers involved in hematopoiesis like CD14, CD34, CD45, CD117, or CD133 and HLA-DR were absent or indeterminably low. It should be noted that CD90 expression decreased during passages in the case of a WJ-MSC isolate.

In agreement with the data in the literature, the vascular cell adhesion molecule 1 (VCAM-1, CD106) was present in a small subpopulation of the PDL (20.6 ± 4.5%) derived cells, while AD-MSCs and WJ-MSCs failed to express this marker. The melanoma cell adhesion molecule (MCAM, CD146), known as a pericyte marker, was present in 25–55% of the WJ-MSC and PDL cells, while AD-MSCs, in contrast to data in the literature, did not express CD146 (Figure 2(d)).

The common MSC markers were found to be present in all cell types examined, while marker density was variable in the MSCs from different tissue sources. The presence or the expression level of a marker in MSCs usually refers to a special property of the cell. For example, it has been described that CD29, CD44, CD73, CD90, CD105, and CD166 have roles in the multilineage differentiation processes [19–21]. Thus we tried to establish a correlation between the expression levels of these surface markers and the osteogenic, adipogenic, or angiogenic differentiation potential of the MSC isolates from different tissue sources. The expression intensity of the markers was determined by flow cytometry. In our experiments we found that Thy-1 (CD90) was present at high levels on the surface of AD-MSCs and PDLSCs, while this marker level was low in the case of WJ-MSCs. The ectonucleotidase CD73 was expressed at significantly higher levels in the PDL cells, as compared to other MSC isolates. Furthermore, the integrin family member CD29 was expressed only modestly in AD-MSCs (Figure 2(e)).

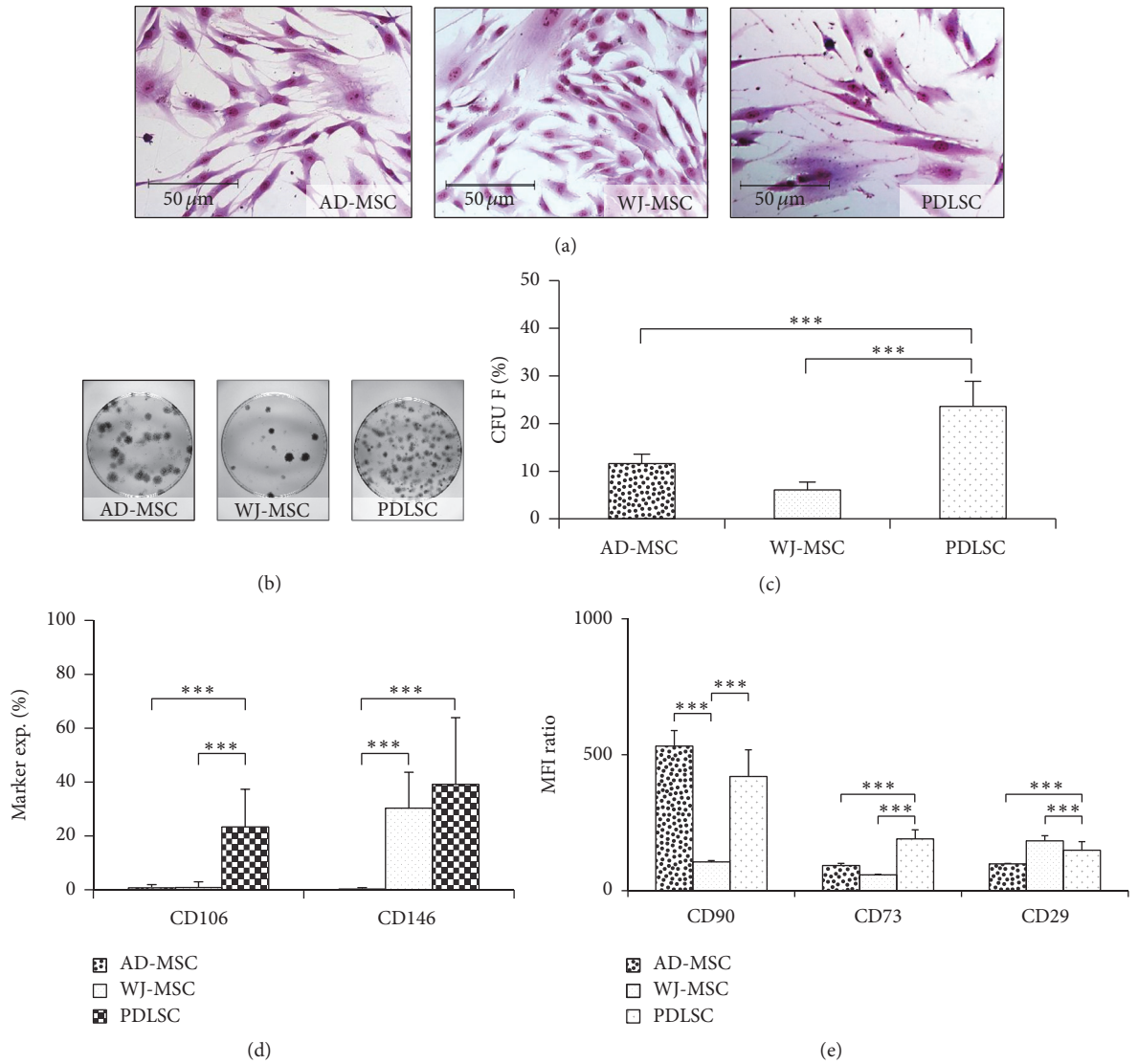

Figure 2: Heterogeneity of the different MSC samples. The morphology of the cells was demonstrated with Giemsa staining (a). The colony forming ability of MSCs was investigated on 10 cm petri dishes (b). Colony forming efficiency was calculated as the number of colonies divided by the total number of seeded cells (c). The CD106 and CD146 expression in different MSC isolates determined by flow cytometry (d). The expression levels of CD90, CD73, and CD29 markers of MSC samples were determined with flow cytometry and represented as median fluorescence intensities (MFI) (e). The photos demonstrate representative samples. $^{***}P$ value less than 0.001.

3.3. Osteogenic, Adipogenic, and Chondrogenic Differentiation. The trilineage differentiation capacity of MSCs was confirmed by standard induction protocols. The bone-forming ability of MSCs was followed by RT-qPCR analysis of RUNX2 and ALP mRNA expression after 7 days of differentiation in an osteogenic medium. RUNX2 is the master transcription factor in osteogenic development, while ALP is recognized as an early marker of osteoblastic differentiation and indispensable for extracellular matrix maturation. When induced, all cell types showed upregulated expression of RUNX2, and no significant differences were noticeable between MSC isolates in this expression (Figure 3(a)). After stimulation, the increased expression levels of ALP mRNA were found to be similar in AD-MSCs and PDLSCs, while significantly lower ALP gene expression was observed in the WJ-MSC samples (Figure 3(b)).

After 14 days of osteogenic MSC differentiation induction, alizarin red staining was performed to directly visualize the mineralization of the extracellular matrix in these cultures. The quantification of the staining showed the high calcium accumulation in AD-MSC and PDLSC isolates. The mineralization capability of WJ-MSCs lagged far behind those observed in MSCs from other tissues (Figures 3(c) and 3(d)). We observed significant correlation between the CD90 expression patterns and the levels of calcium deposition in the different MSC isolates (Figure 2(e)).

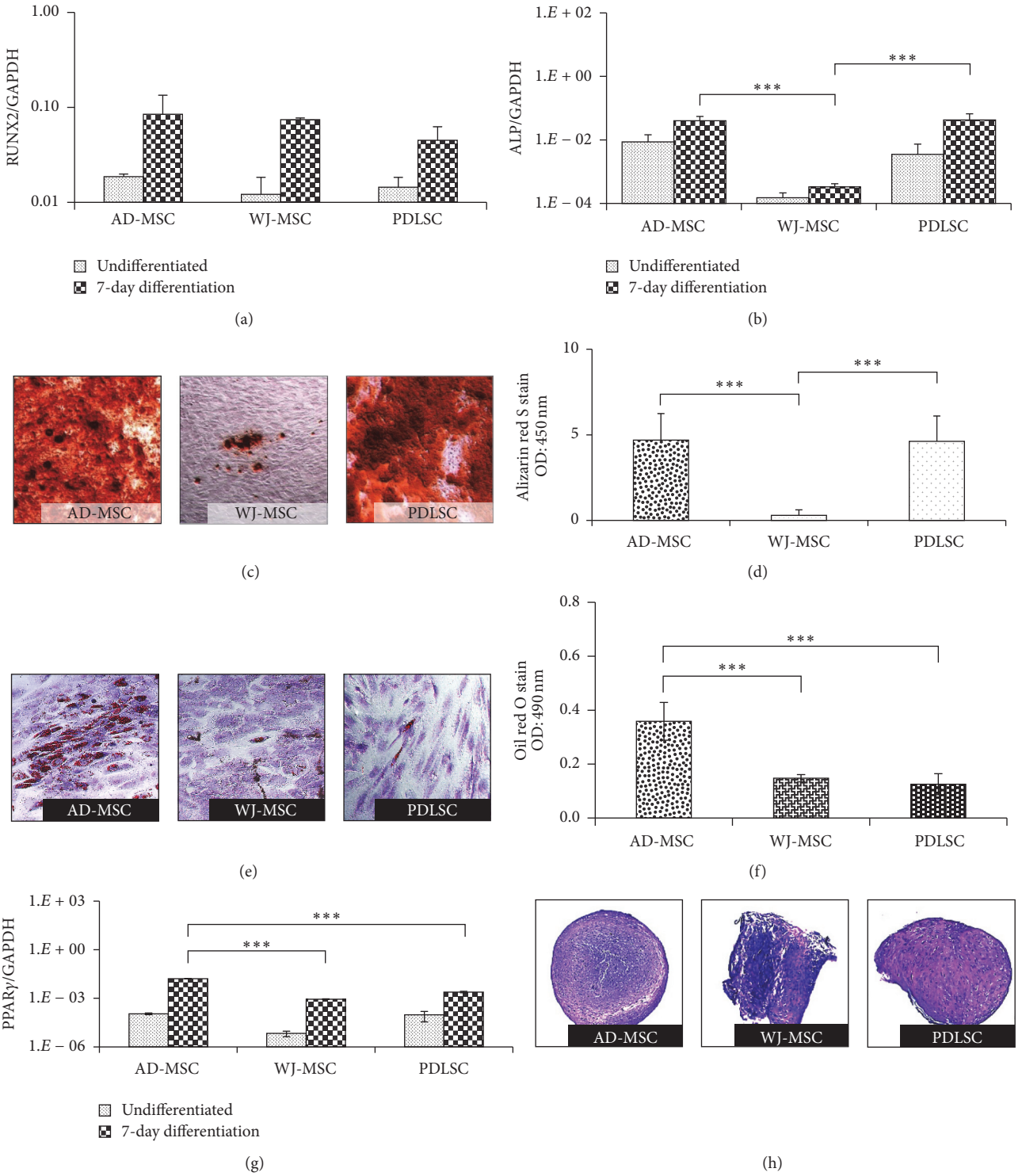

Figure 3: The trilineage differentiation ability of MSC isolates. The expression level of the RUNX2 (a) and ALP (b) genes in the undifferentiated and differentiated samples, determined with RT-qPCR measurements. Alizarin red staining was used to demonstrate the calcium deposition of the matured bone matrix after 14 days of osteogenic induction (c). The stain was dissolved and quantified colorimetrically (d). Lipid accumulation was confirmed by oil red O staining (red dots) after adipogenic induction; cells were counterstained with dimethyl methylene blue stain (e). The concentration of the red stain was determined colorimetrically (f). The adipogenesis was followed with RT-qPCR measurement of PPARγ gene (g). Chondrogenic differentiation was confirmed in all samples (h). The photos demonstrate representative samples. $^{***}P$ value less than 0.001.

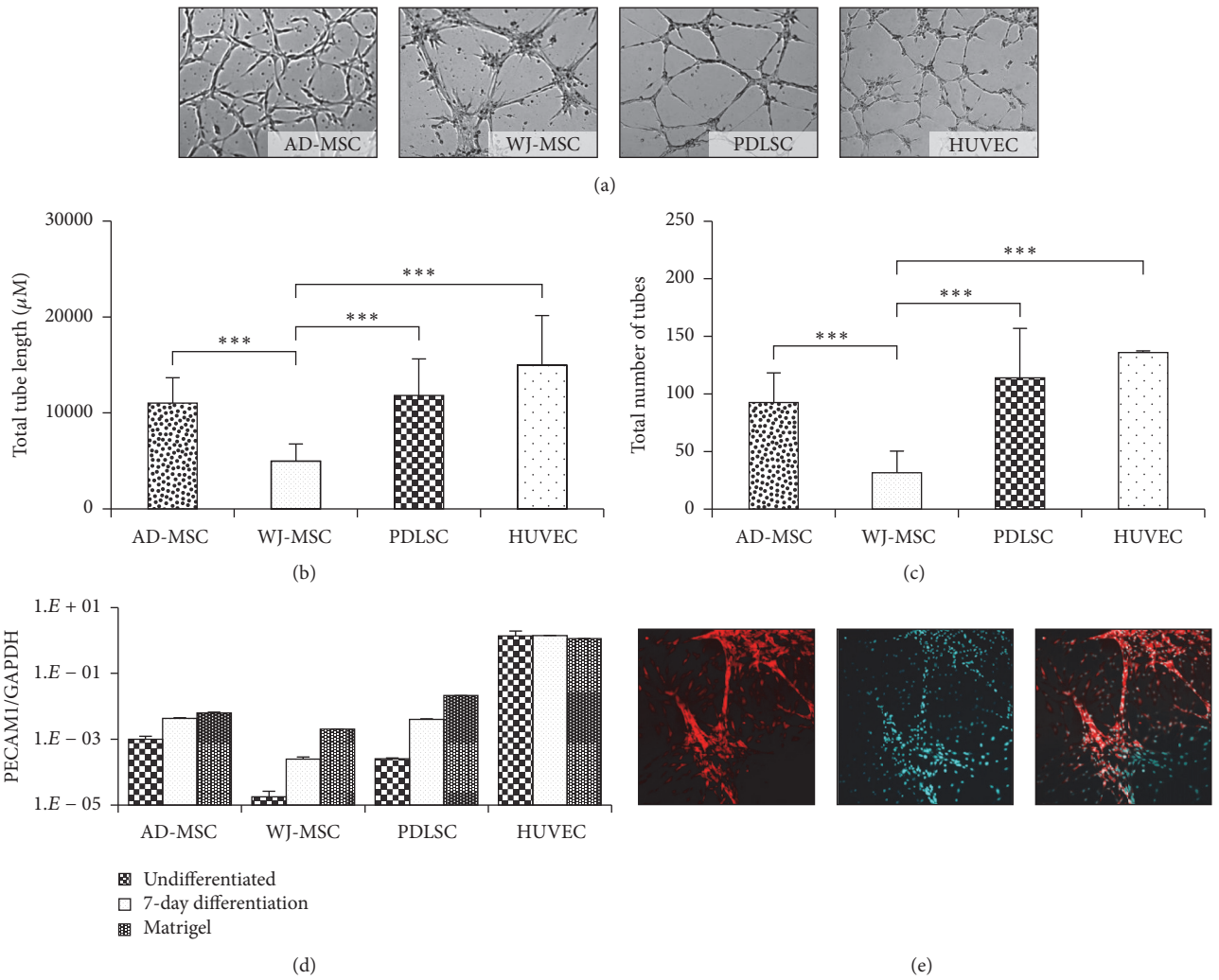

FIGURE 4: Endothelial differentiation potential of the MSCs was tested in Matrigel tube formation assay. Tubular-like structures were photographed (a) and analyzed with TubeCount software. Human umbilical vein endothelial cells (HUVEC) were used as controls. Total tube length (b) and numbers (c) were counted and presented in the diagrams. The changes in the expression of PECAM1 during endothelial differentiation were followed with RT-qPCR. Samples were collected from undifferentiated and predifferentiated states (7-day endothelial induction) and after angiogenesis in a Matrigel assay (d). The 3D network developed by a representative PDLSC sample was demonstrated with fluorescence staining of the cell membrane by $DiSC_3(5)$ (red) and the nucleus by DAPI (cyan) (e). The photos demonstrate representative samples. $^{***}P$ value less than 0.001.

In the adipogenic differentiation experiments AD-MSCs accumulated significantly higher amounts of lipids, as compared to the other MSC preparations (Figures 3(e) and 3(f)). The mRNA expression levels of PPARγ, a key factor in adipogenesis, were in close correlation with the amounts of lipid deposition, indicating that AD-MSCs can produce adipocytes most effectively (Figure 3(g)). We found that CD29 expression levels in AD-MSCs were the lowest (Figure 2(e)); thus CD29 expression may be inversely related to the adipogenic differentiation potential as in accordance with the findings of Rodeheffer et al. [22].

We have also performed chondrogenic differentiation of the various MSC preparations. We found that all MSC types were capable for this differentiation (Figure 3(h)).

3.4. Endothelial Differentiation. The endothelial forming potential of the MSCs was examined in an angiogenesis assay, wherein we found that AD-MSCs and WJ-MSCs reached a maximum tube-forming potential between 3 and 7 hours after seeding, while the PDLSCs needed 18–20 hours to form a well-developed capillary-like tubule network. The tube-forming potential of AD-MSCs and PDLSCs was similar to that observed in the HUVEC, while the tubular networks formed by WJ-MSCs were significantly less developed, as compared to other isolates (Figures 4(a), 4(b), and 4(c)). Moreover, the tubes generated by MSCs derived from different tissues showed significantly different phenotypes. AD-MSCs and WJ-MSCs formed relatively short tubes and the tubes of WJ-MSCs were much thicker than those formed

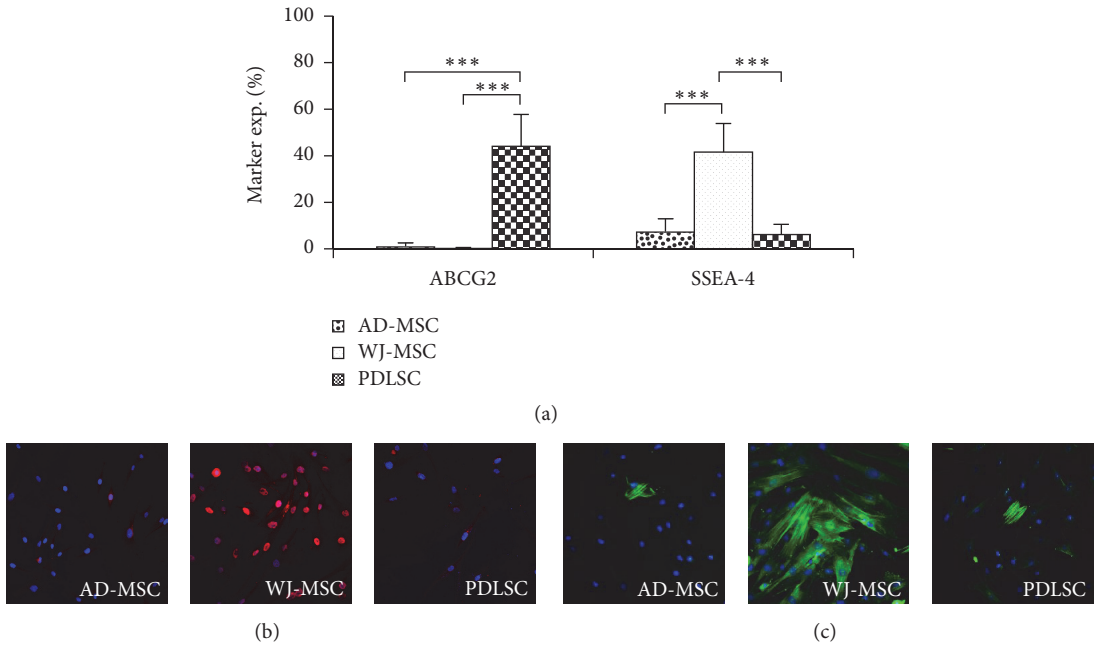

Figure 5: Pluripotency and mesodermal markers of MSCs. The embryonic stem cell marker ABCG2 was detectable uniquely in PDLSCs, while a remarkable SSEA4 expressing population was found in WJ-MSC isolates, as determined by flow cytometer (a). Immunohistochemical staining of GATA6 (red, DAPI-blue) (b) and α-SMA (green, DAPI-blue) (c) showed significant expression only in WJ-MSCs. The photos demonstrate representative samples. $^{***}P$ value less than 0.001.

by the other MSC isolates. The extensive tubular network formed by PDLSC mostly consisted of long and thin tubes, resembling capillaries. A characteristic sample of a tubular network formed by fluorescently stained PDL stem cells is demonstrated in Figure 4(e).

The messenger RNA expression of the endothelial specific marker PECAM1 was analyzed by real-time qPCR after prestimulation of the MSCs and after retrieval of the cells from the Matrigel (Figure 4(d)). An elevation in PECAM1 mRNA expression level was observed after the induction in all MSC preparations. Furthermore, an additional elevation was noticeable in the expression of PECAM1 when the cells formed endothelial structures. However, PECAM1 mRNA expression was still significantly smaller as compared to that found in the HUVEC, in which no further activation of this gene expression was observed either in an angiogenesis inducing medium or in the Matrigel environment.

All these results indicate a higher endothelial differentiation ability and vessel-forming potential of PDLSCs and AD-MSCs, as compared to the WJ-MSCs.

3.5. Expression of Pluripotency and Mesodermal Markers in the MSC Preparations. In these experiments we have examined whether WJ-MSCs, suggested to be in more early stages of stem cell development, express any special pluripotency markers. The expression of mRNA of transcription factors indicating a pluripotent stem cell state, including OCT4, SOX2, Nanog, or that of TERT, a major factor in maintaining self-renewal capacity, was not detectable in either of the MSC isolates examined here (data not shown). However, the stage-specific embryonic antigene-4 (SSEA-4), a marker of undifferentiated state in human embryonic stem cells, was present in a remarkable quantity on the surface of the WJ-MSCs (37–65%), in contrast to that found in AD-MSCs and PDLSCs (6–8%). The presence of the ABCG2 protein, another potential stem cell marker, was detectable with flow cytometry exclusively in the PDLSCs (Figure 5(a)).

In immunocytochemistry studies the mesodermal marker proteins, α-SMA, typically expressed in smooth muscle cells, and the transcription factor GATA6, were observable only in WJ-MSCs (Figures 5(b) and 5(c)).

4. Discussion

MSCs derived from diverse tissues share some common properties [6]; however, on closer examination, cells with very heterogeneous properties can be found within individual isolates in the expression of various markers. The colony forming capacity and the differentiation potential of these isolates can vary as well.

In this study we found that the expression levels of CD90, CD73, and CD29 were variable, but representative for the MSCs isolated from different tissue sources. Here we observed that AD-MSCs and PDLSCs expressed higher CD90 levels and showed greater bone and endothelial differentiation ability, as compared to WJ-MSCs. In the literature an enhanced bone regeneration potential of AD-MSCs with high level expression of Thy-1 has already been found [23].

These data suggest that MSCs with high CD90 expression may have the ability to differentiate into both bone and endothelial cells.

The use of MSCs for tissue engineering applications was found to be safe [24]. The most relevant question in bone graft tissue engineering is how efficiently a progenitor cell can form bone nodules. In our experiments the calcification potential of AD-MSCs was similar to PDLSCs. However, the osteogenic capacity of WJ-MSCs was significantly lower, as compared to MSCs from other tissue sources. This observation is in agreement with the results of Yu et al. [25], reporting that differentiated PDLSCs showed a better mineral deposition as compared to WJ-MSCs, although no significant differences were observed in the upregulation of RUNX2 gene expression in these MSCs. The elevation in RUNX2 mRNA expression indicates the beginning of the ossification process, while in this period no matured osteoblasts can be developed as yet, as suggested by a low level ALP expression, which is an important factor in matrix maturation [26]. The high RUNX2 and low ALP mRNA levels in the WJ-MSCs may explain the relatively low calcification potential of these cells.

Here we showed that none of the examined MSCs expressed the classical embryonic stem cell markers OCT4, SOX2, hTERT, or Nanog. ABCG2, a potential pluripotency marker, was uniquely detectable at a relative high level on the surface of PDLSCs. The findings that WJ-MSCs expressed the highest level of the pluripotency marker SSEA-4 and only WJ-MSCs expressed α-SMA and GATA6 protein altogether indicate that this cell type is at an earlier stage of stem cell development. It may also explain the need for a longer induction time in *in vitro* differentiation experiments [27]. It is in accordance with the findings of Kubo et al. [28], whereas the knockdown of GATA6 expression by siRNA suppressed the self-renewal capacity of human MSCs. The limited differentiation potential of α-SMA expressing MSCs has already been reported [29]; however the role of SSEA-4 in the maintenance of pluripotency is still controversial [30, 31].

It is important to find the most suitable cell types and techniques to maintain proper blood flow inside of large bone grafts [5]. MSC therapy has been considered as an alternative clinical intervention. On one hand MSCs help healing by support angiogenesis, mediated by paracrine factors (e.g., VEGF). On the other hand, the endothelial differentiation ability of the transplanted MSCs directly leads to vessel formation. It has been demonstrated in clinical studies that transplantation of allogenic MSCs to the affected area is a safe and efficient procedure to promote regenerative vascularization [32]. Furthermore, the angiogenic potential of dental pulp derived stem cells has already been observed [33], indicating that dental stem cells can be suitable candidates to achieve complex bone replacement. Here we show that PDLSCs can form endothelial structures as effectively as AD-MSCs and thus may generate proper vasculature in bone grafts.

The main therapeutic advantage of AD-MSCs, namely, their availability in large numbers, may be overcome by the faster proliferation rates of PDLSCs (data not shown), while a disadvantage of these latter MSCs is the need for their *ex vivo* culturing to reach the required cell number for therapeutic applications.

As a summary, AD-MSCs and PDLSCs seem to be both suitable for complex bone replacement applications, complemented with a vascular network formed by the same donor cell types. These detailed *in vitro* studies may significantly promote further use of MSCs in *in vivo* therapeutic approaches in bone regeneration.

Competing Interests

No competing financial interests exist.

Acknowledgments

This research has been supported by grants KTIA_AIK_12-1-2012-0025 (Hungary), KMOP-114-11/B-2011-0165 (Hungary), and OTKA 115375 (Hungary). The authors are grateful for the help of Margit Bakki. The HUES9 cell line was provided by Ágota Apáti and the HUVEC were provided by Adrienn Németh.

References

[1] M. A. König, D. D. Canepa, D. Cadosch et al., "Direct transplantation of native pericytes from adipose tissue: a new perspective to stimulate healing in critical size bone defects," *Cytotherapy*, vol. 18, no. 1, pp. 41–52, 2016.

[2] L. Larsson, A. M. Decker, L. Nibali, S. P. Pilipchuk, T. Berglundh, and W. V. Giannobile, "Regenerative medicine for periodontal and peri-implant diseases," *Journal of Dental Research*, vol. 95, no. 3, pp. 255–266, 2016.

[3] M. Fröhlich, W. L. Grayson, L. Q. Wan, D. Marolt, M. Drobnic, and G. Vunjak-Novakovic, "Tissue engineered bone grafts: biological requirements, tissue culture and clinical relevance," *Current Stem Cell Research and Therapy*, vol. 3, no. 4, pp. 254–264, 2008.

[4] Á. E. Mercado-Pagán, A. M. Stahl, Y. Shanjani, and Y. Yang, "Vascularization in bone tissue engineering constructs," *Annals of Biomedical Engineering*, vol. 43, no. 3, pp. 718–729, 2015.

[5] P. A. Zuk, M. Zhu, H. Mizuno et al., "Multilineage cells from human adipose tissue: implications for cell-based therapies," *Tissue Engineering*, vol. 7, no. 2, pp. 211–228, 2001.

[6] M. Dominici, K. Le Blanc, I. Mueller et al., "Minimal criteria for defining multipotent mesenchymal stromal cells. The International Society for Cellular Therapy position statement," *Cytotherapy*, vol. 8, no. 4, pp. 315–317, 2006.

[7] X. Wei, X. Yang, Z.-P. Han, F.-F. Qu, L. Shao, and Y.-F. Shi, "Mesenchymal stem cells: a new trend for cell therapy," *Acta Pharmacologica Sinica*, vol. 34, no. 6, pp. 747–754, 2013.

[8] M. L. Weiss, C. Anderson, S. Medicetty et al., "Immune properties of human umbilical cord Wharton's jelly-derived cells," *STEM CELLS*, vol. 26, no. 11, pp. 2865–2874, 2008.

[9] A. J. Friedenstein, K. V. Petrakova, A. I. Kurolesova, and G. P. Frolova, "Heterotopic transplants of bone marrow," *Transplantation*, vol. 6, no. 2, pp. 230–247, 1968.

[10] B. M. Seo, M. Miura, S. Gronthos et al., "Investigation of multipotent postnatal stem cells from human periodontal ligament," *The Lancet*, vol. 364, pp. 149–155, 2004.

[11] V. Feisst, S. Meidinger, and M. B. Locke, "From bench to bedside: use of human adipose-derived stem cells," *Stem Cells and Cloning: Advances and Applications*, vol. 8, pp. 149–162, 2015.

[12] V. N. Veryasov, A. M. Savilova, O. A. Buyanovskaya, M. M. Chulkina, S. V. Pavlovich, and G. T. Sukhikh, "Isolation of mesenchymal stromal cells from extraembryonic tissues and their characteristics," *Bulletin of Experimental Biology and Medicine*, vol. 157, no. 1, pp. 119–124, 2014.

[13] Á. Szepesi, Z. Matula, A. Szigeti et al., "ABCG2 is a selectable marker for enhanced multilineage differentiation potential in periodontal ligament stem cells," *Stem Cells and Development*, vol. 24, no. 2, pp. 244–252, 2015.

[14] A. Shirmohammadi, M. T. Chitsazi, and A. Lafzi, "A clinical comparison of autogenous bone graft with and without autogenous periodontal ligament graft in the treatment of periodontal intrabony defects," *Clinical Oral Investigations*, vol. 13, no. 3, pp. 279–286, 2009.

[15] P. Tátrai, Á. Szepesi, Z. Matula et al., "Combined introduction of Bmi-1 and hTERT immortalizes human adipose tissue-derived stromal cells with low risk of transformation," *Biochemical and Biophysical Research Communications*, vol. 422, no. 1, pp. 28–35, 2012.

[16] C. Bodor, J. P. Nagy, B. Végh et al., "Angiotensin II increases the permeability and PV-1 expression of endothelial cells," *American Journal of Physiology—Cell Physiology*, vol. 302, no. 1, pp. C267–C276, 2012.

[17] Á. Apáti, T. I. Orbán, N. Varga et al., "High level functional expression of the ABCG2 multidrug transporter in undifferentiated human embryonic stem cells," *Biochimica et Biophysica Acta (BBA)—Biomembranes*, vol. 1778, no. 12, pp. 2700–2709, 2008.

[18] K. Janeczek Portalska, A. Leferink, N. Groen et al., "Endothelial differentiation of mesenchymal stromal cells," *PLoS ONE*, vol. 7, no. 10, article e46842, 2012.

[19] M. Ciciarello, R. Zini, L. Rossi et al., "Extracellular purines promote the differentiation of human bone marrow-derived mesenchymal stem cells to the osteogenic and adipogenic lineages," *Stem Cells and Development*, vol. 22, no. 7, pp. 1097–1111, 2013.

[20] M. Maleki, F. Ghanbarvand, M. R. Behvarz, M. Ejtemaei, and E. Ghadirkhomi, "Comparison of mesenchymal stem cell markers in multiple human adult stem cells," *International Journal of Stem Cells*, vol. 7, no. 2, pp. 118–126, 2014.

[21] O. G. Davies, P. R. Cooper, R. M. Shelton et al., "Isolation of adipose and bone marrow mesenchymal stem cells using CD29 and CD90 modifies their capacity for osteogenic and adipogenic differentiation," *Journal of Tissue Engineering*, vol. 6, 2015.

[22] M. S. Rodeheffer, K. Birsoy, and J. M. Friedman, "Identification of white adipocyte progenitor cells in vivo," *Cell*, vol. 135, no. 2, pp. 240–249, 2008.

[23] M. T. Chung, C. Liu, J. S. Hyun et al., "CD90 (Thy-1)-positive selection enhances osteogenic capacity of human adipose-derived stromal cells," *Tissue Engineering—Part A*, vol. 19, no. 7-8, pp. 989–997, 2013.

[24] Z. Gamie, R. J. MacFarlane, A. Tomkinson et al., "Skeletal tissue engineering using mesenchymal or embryonic stem cells: clinical and experimental data," *Expert Opinion on Biological Therapy*, vol. 14, no. 11, pp. 1611–1639, 2014.

[25] S. Yu, J. Long, J. Yu et al., "Analysis of differentiation potentials and gene expression profiles of mesenchymal stem cells derived from periodontal ligament and wharton's jelly of the umbilical cord," *Cells Tissues Organs*, vol. 197, no. 3, pp. 209–223, 2013.

[26] E. Torreggiani, G. Lisignoli, C. Manferdini et al., "Role of slug transcription factor in human mesenchymal stem cells," *Journal of Cellular and Molecular Medicine*, vol. 16, no. 4, pp. 740–751, 2012.

[27] Z.-Y. Zhang, S.-H. Teoh, M. S. K. Chong et al., "Superior osteogenic capacity for bone tissue engineering of fetal compared with perinatal and adult mesenchymal stem cells," *Stem Cells*, vol. 27, no. 1, pp. 126–137, 2009.

[28] H. Kubo, M. Shimizu, Y. Taya et al., "Identification of mesenchymal stem cell (MSC)-transcription factors by microarray and knockdown analyses, and signature molecule-marked MSC in bone marrow by immunohistochemistry," *Genes to Cells*, vol. 14, no. 3, pp. 407–424, 2009.

[29] N. P. Talele, J. Fradette, J. E. Davies, A. Kapus, and B. Hinz, "Expression of α-smooth muscle actin determines the fate of mesenchymal stromal cells," *Stem Cell Reports*, vol. 4, no. 6, pp. 1016–1030, 2015.

[30] E. J. Gang, D. Bosnakovski, C. A. Figueiredo, J. W. Visser, and R. C. R. Perlingeiro, "SSEA-4 identifies mesenchymal stem cells from bone marrow," *Blood*, vol. 109, no. 4, pp. 1743–1751, 2007.

[31] H. He, T. Nagamura-Inoue, H. Tsunoda et al., "Stage-specific embryonic antigen 4 in Wharton's jelly-derived mesenchymal stem cells is not a marker for proliferation and multipotency," *Tissue Engineering Part A*, vol. 20, no. 7-8, pp. 1314–1324, 2014.

[32] S.-S. Yang, N.-R. Kim, K.-B. Park et al., "A phase I study of human cord blood-derived mesenchymal stem cell therapy in patients with peripheral arterial occlusive disease," *International Journal of Stem Cells*, vol. 6, no. 1, pp. 37–44, 2013.

[33] K. Iohara, L. Zheng, H. Wake et al., "A novel stem cell source for vasculogenesis in ischemia: subfraction of side population cells from dental pulp," *STEM CELLS*, vol. 26, no. 9, pp. 2408–2418, 2008.

Hindawi Publishing Corporation
Stem Cells International
Volume 2016, Article ID 7230987, 16 pages
http://dx.doi.org/10.1155/2016/7230987

Research Article

Highly Efficient *In Vitro* Reparative Behaviour of Dental Pulp Stem Cells Cultured with Standardised Platelet Lysate Supplementation

Pasquale Marrazzo,[1] Francesco Paduano,[1] Francesca Palmieri,[1] Massimo Marrelli,[1,2] and Marco Tatullo[1,2]

[1] *Tecnologica Research Institute, Biomedical Section, Crotone, Italy*
[2] *Unit of Experimental Surgery, Calabrodental, Crotone, Italy*

Correspondence should be addressed to Marco Tatullo; marco.tatullo@tecnologicasrl.com

Received 2 July 2016; Revised 4 August 2016; Accepted 7 August 2016

Academic Editor: Giorgio Mori

Copyright © 2016 Pasquale Marrazzo et al. This is an open access article distributed under the Creative Commons Attribution License, which permits unrestricted use, distribution, and reproduction in any medium, provided the original work is properly cited.

Dental pulp is an accessible source of multipotent mesenchymal stromal cells (MSCs). The perspective role of dental pulp stem cells (DPSCs) in regenerative medicine demands an *in vitro* expansion and *in vivo* delivery which must deal with the safety issues about animal serum, usually required in cell culture practice. Human platelet lysate (PL) contains autologous growth factors and has been considered as valuable alternative to fetal bovine serum (FBS) in cell cultures. The optimum concentration to be added of such supplement is highly dependent on its preparation whose variability limits comparability of results. By *in vitro* experiments, we aimed to evaluate a standardised formulation of pooled PL. A low selected concentration of PL (1%) was able to support the growth and maintain the viability of the DPSCs. The use of PL in cell cultures did not impair cell surface signature typically expressed by MSCs and even upregulated the transcription of Sox2. Interestingly, DPSCs cultured in presence of PL exhibited a higher healing rate after injury and are less susceptible to toxicity mediated by exogenous H_2O_2 than those cultured with FBS. Moreover, PL addition was shown as a suitable option for protocols promoting osteogenic and chondrogenic differentiation of DPSCs. Taken together, our results indicated that PL is a valid substitute of FBS to culture and differentiate DPSCs for clinical-grade use.

1. Introduction

Dental pulp stem cells (DPSCs) are multipotent stromal/mesenchymal stem cells (MSCs) representing a source, free of ethical issues, of replacement cells worthwhile in human therapies. From a clinical point of view, it is necessary to avoid any immunological reaction to the xenogenic material; then the investigation on xeno-free *ex vivo* expansion of MSCs is highly encouraged. Many platelet derivates were tested so far in different forms for cell culture to replace animal serum supplementation. Currently, the use of human platelet lysate (PL) in clinical settings led to many therapeutic successes including orthopaedic, periodontal, oral, and maxillofacial surgeries [1]. PL is biocompatible and has no risk of transmissible viral disease or prionic contamination. Platelet concentrates can be prepared by buffy coat or platelet-rich plasma (PRP) method [2], even from expired blood derivates. Freeze-and-thaw cycles, sonication, and thrombin/$CaCl_2$ activation have been used to obtain PL [2]. The variability in PL manufacturing influences the content of main growth factors (GFs) that will be available in cell culture, such as PDGF isoforms, TGF-β1, and also VEGF, HGF, and bFGF. The inconsistency of the results makes PL functionality *in vitro* still not exhaustively explored. Furthermore, specific and optimal culture conditions will be searched [3, 4] especially for MSCs [5].

DPSCs received great attention for their osteogenic potential; besides they demonstrated an angiogenic potential [6], a commitment to melanogenesis [7], differentiation in neurons [8], and islet-like aggregates formation [9]. The transcriptomes and cytogenetical stability of DPSCs expanded under PL and FBS were previously compared and revealed

similar profiles [10]. Also CFU-potential, the immunophenotype, and trilineage differentiation according to MSC requisites were comparable [10]. 5% PL was defined as the concentration for increased cellular proliferation and for good mineralisation *in vitro* for DPSCs [10–12]. In addition, the same concentration was used to seed DPSCs on biomaterials, showing positive effects on regeneration *in vivo* [11]. Often 10% PL inhibited the proliferation of DPSCs. Interestingly, DPSC cultures in PL had a higher ALP activity compared to FBS [11, 12]. We initially combined different assays to select an optimal PL concentration for DPSCs growth, by evaluating different cell health indicators, such as membrane permeability, cell division, and metabolic activity. The comparison between FBS and the selected PL concentration for mesenchymal stem cell capacity was evaluated by surface marker expression and gene expression of relevant transcriptional factors.

We focused on PL effects on repairing properties of DPSCs by performing *in vitro* migration and survival assay. Finally, we introduced PL in osteogenic and chondrogenic inducer media in order to evaluate its effect on DPSCs differentiation.

We characterised a standardised commercially available human allogenic platelet lysate as an attractive candidate for *in vitro* culture of DPSCs [10]. The use of this safe, quality-controlled, and potentially advantageous supplement could establish a preparatory study for regenerative medicine applications.

2. Materials and Methods

2.1. DPSCs Source and Cell Culture. Human-impacted third molars were extracted from 20-year-old healthy patients from Calabrodental Clinic (Crotone). All donors signed a written informed consent according to the Ethical Committee policy. To isolate DPSCs, the obtained normal teeth were washed in saline solution containing antibiotic solutions and immediately transferred to the cell culture laboratory. Mesenchymal stem cells were isolated under sterile conditions according to a previously published method [13, 14]. Briefly, pulp tissues were isolated and washed several times with PBS and further cut with a scalpel into small pieces. Subsequently, the whole small pieces were dissociated to have single cell suspension by enzymatic digestion, using 3 mg/mL type I collagenase and 4 mg/mL dispase (Sigma-Aldrich, Saint Louis) in Hank's Balanced Salt Solution (Invitrogen, Carlsbad). Then, samples were incubated for 1 h at 37°C in agitation and the digest was diluted in alpha-minimal essential medium (α-MEM, Gibco, Grand Island) supplemented with 10% FBS (Gibco, Grand Island) and centrifuged at 300 ×g for 5 min. The pellet was finally resuspended in fresh medium, seeded in culture dishes, and incubated at 37°C 5% CO_2. DPSCs were routinely expanded in growth medium consisting of α-MEM supplemented at 10% FBS. Trilineage differentiation of DPSCs was early assessed and cell stocks were cryopreserved. Two donors were used for the study. PL was purchased from Sclavo Diagnostics (Sovicille).

2.2. Viability Assays. For live/dead imaging, DPSCs were grown on sterile cover slides 24 × 24 mm and cultured for 5 days in FBS or PL media. After formalin fixation, the cells were stained with a solution of Calcein AM-EthD-III (Biotium, Hayward) according to the kit indications. Epifluorescent signal was detected and relative images were acquired through SP5 microscope (Leica, Wetzlar). Metabolic activity of DPSCs was assessed by PrestoBlue (Molecular Probes, Eugene) assay. Briefly, cryopreserved DPSCs were thawed and resuspended in α-MEM containing FBS at 10% or PL at 5%, 2%, and 1%. Cells were seeded at 2500 cell/well in one 96-well plate for each analysed time point; more than 6 wells were replicated for each condition. An aliquot of fresh medium was provided to the plates that were cultured for more than 4 days. The PrestoBlue reagent was incubated as supplier instruction to a final volume of 100 μL; after 2 hours the collected supernatant was measured for absorbance with Multiskan GO (Thermo Fisher, Waltham) spectrophotometer (570–600 nm). An additional control was set using human serum (HS) 10%. For viable cell counts, the samples were trypsinized after 3 days or 3 weeks and measured by ADAM-MC (AlphaMetrix, Rödermark) system to evaluate cell membrane permeability by dye exclusion.

2.3. Flow Cytometry. To investigate cellular proliferation, DPSCs were labelled with 5 μM of 5-chloromethylfluorescein diacetate (CMFDA) in α-MEM for 45 min at 37°C CO_2. Cells were washed in medium and seeded at 10^5/well in a 12 well-plate, in duplicate, for different time points (2, 3, and 4 days). Cytoplasmic amount reduction of the dye was measured using NAVIOS flow cytometer (Beckman Coulter, Brea). The data were analysed with FlowJo software. For immunophenotype analysis, cells cultured for 1 week with 10% FBS or 1% PL were trypsinized and aliquoted in FACS tube. Cells were washed twice with PBS 0,1% BSA. To limit unspecific binding, a blocking step is performed by resuspension of the pellets with PBS 1% BSA for 15 min. Cells were stained on ice for 1 h with saturating concentrations of primary conjugated antibodies diluted 1 : 50 in PBS 0,1% BSA. CD13-PE (mouse IgG1), CD29-APC (mouse BALB/c IgG1), CD44-FITC (mouse IgG2b), CD45-APC-H7 (mouse IgG1), CD73-FITC (mouse IgG1), CD90-PE (mouse BALB/c IgG1), and CD105-APC (Mouse BALB/c IgG1) monoclonal antibodies purchased from BD (Franklin Lakes) and CD146-PE (mouse IgG1), CD34-FITC (mouse IgG2a), and HLA-DR-PE (recombinant human IgG1) monoclonal antibodies purchased from Miltenyi Biotec (Bergisch Gladbach) were used to define the MSC panel as previously described [15]. At least 10000 events were counted for each sample.

2.4. Real-Time PCR. To analyse cell differentiation state, gene expression was analysed as previously described [15, 16]. Briefly, RNA samples were obtained after extraction with PureLink RNA mini kit (Thermo Fisher, Waltham) following the manufacturer's instruction. Total RNA was quantified through spectrophotometry and 500 ng of RNA was subjected to reverse-transcription reaction using the High Capacity RNA-to-cDNA Kit (Applied Biosystem, Foster City). One microliter of cDNA was amplified by

real-time PCR with the Power SYBR green PCR Master Mix (Applied Biosystem, Foster City). Real-time PCR reactions were carried out in a PikoReal 96 (Thermo Fisher, Waltham) apparatus with the following conditions: initial denaturation step at 95°C for 10 min, followed by 40 cycles of 10 s at 95°C and 1 min at 60°C. The specificity of PCR products was checked by analysis of melting curves. The expression of each gene was determined from the Ct value, and relative expression levels were calculated using the ΔΔCt method after normalisation to the expression of the HRPT housekeeping gene. All primer pairs sequences are listed in Table S1 in Supplementary Material available online at http://dx.doi.org/10.1155/2016/7230987.

2.5. Wound Scratch Assay. For scratch assay, DPSCs were seeded and grown until confluence in 35 mm dishes. An *in vitro* wound (600 μm average size) was created in the monolayer by scraping it over the total diameter with a sterile 10 μL pipette tip. Dishes were washed twice in α-MEM to smooth the scratch edges and remove any suspended cells. Cultures were refed with fresh complete medium containing 10% FBS or 1% PL. Reference markings were made on the external surface of the dishes to identify scraped zones to be photographed 2 hours and 24 hours after scratch. To quantify the wound healing capacity, images were manually analysed. A digital rectangle zone free of cells and centred on the wound breadth was set on 2-hour controls and thus was superimposed on the corresponding 24-hour images. Cell dense regions were drawn trough polygonal selection tool and measured by ImageJ software. Multiple selections were summed and healing was determined as percentage of the open (wound) area at 24 hours.

2.6. Chemotaxis Assay. An under-agarose method was adapted from Vogel et al. [17] Briefly, sterile melt 1% agarose in α-MEM was poured in 60 mm dishes. Three equally distant wells (≈5 mm) were made by pressing a sterile tip on the agarose gel surface. The gel was equilibrated overnight in α-MEM. DPSCs were harvested at exponential phase, washed in α-MEM, and seeded in the central well at concentration of 3.5×10^4 cells/70 μL. A volume of 70 μL medium containing 10% FBS or 1% PL was added to the right well in order to create a chemoattractant gradient in culture, while a same volume of α-MEM was added to the left well as negative control of chemotaxis. After 24 hours of incubation at 37°C 5% CO_2, both left and right wells were refilled of their content. At 48 hours, the dishes were gently washed and fixed in formalin 5% overnight at 4°C. Four pictures (10x zoom) were taken at 24 hours for quantitative analysis at each interwell's zone. The images were tiled and cell number was manually counted in ImageJ software. Only cells completely outside the well and under the agarose were considered. The counted number of migrated cells is corrected subtracting the number of cells which moved towards the negative control well.

2.7. Cell Survival Assay. The damaging effect of millimolar concentrations of H_2O_2 on DPSCs was tested in dose-dependent manner after 1-hour exposition in basal medium (BM) which consisted of α-MEM. PrestoBlue assay was performed after 48 hours to detect the challenge on viability [18, 19]; therefore an EC_{50} of 500 μM was established for following experiments (Fig. S3). For cell survival test, DPSCs were seeded as 3.5×10^4 DPSCs/well of a 96-well plate and left to adhere in complete media, 10% FBS or 1% PL. On the next day, all the wells were washed with PBS and 500 μM H_2O_2 was added in basal medium (BM) or complete medium (CM) containing 10% FBS or 1% PL. Subsequently, cells were treated for 1 h in incubator. At the end of the treatment, H_2O_2 dilution was replaced with new complete medium. After 6 hours, at 37°C 5% CO_2, PrestoBlue was incubated for 2 hours and its absorbance read. Alternatively, DPSCs were seeded in 12-well plates, treated as above, and trypsinized 6 hours later to perform viable counting by ADAM-MC.

2.8. In Vitro Osteogenic Differentiation. For osteogenic differentiation, growing cells were detached and seeded subconfluently in 60 mm Petri dishes. At 85–90% of confluence, cell medium was changed to osteogenic medium composed of α-MEM with glutamine (Gibco, Grand Island), 1% PL, 0,2 mM L-ascorbic acid-2-phosphate (Sigma-Aldrich, Saint Louis), 100 nM dexamethasone (Sigma-Aldrich, Saint Louis), 10 mM β-glycerophosphate (Sigma-Aldrich, Saint Louis), penicillin-streptomycin solution (Sigma-Aldrich, Saint Louis), and 0.25 mg/mL amphotericin B (Sigma-Aldrich, Saint Louis). The positive control group medium included 20% FBS in place of PL. Osteogenic induction was performed for 4 weeks, replacing media twice a week.

The differentiation was assessed by Alizarin red, quantified via spectrophotometry (405 nm) after dissolution in 10% acetic acid, and analysed by real-time PCR (primer listed in Table S1) for gene expression levels of osteogenic markers.

2.9. In Vitro Chondrogenic Differentiation. For chondrogenesis differentiation, DPSCs were initially detached and seeded subconfluently in 60 mm dishes. At 85–90% of confluence, growth medium was changed to chondrogenic medium composed of DMEM High Glucose (Gibco, Grand Island), 1% PL, ITS + 1 Supplement (Sigma-Aldrich, Saint Louis), 100 nM dexamethasone (Sigma-Aldrich, Saint Louis), 50 mg/mL L-ascorbic acid-2-phosphate (Sigma-Aldrich, Saint Louis), and freshly added 10 ng TGF-β1 (Miltenyi Biotec, Bergisch Gladbach). The positive control groups' medium did not include PL in the formula. Chondrogenic induction was performed for 3 weeks, replacing the media twice a week. Alcian blue staining was extracted in acetic acid and its relative quantification was performed by spectrophotometry (620 nm). For micromass culture 5×10^5 cells were pelleted at 300 g and washed in 1 mL of medium free of TGF-β1 and then left to aggregate in incubator in 1 mL of chondrogenic medium (with TGF-β1). Chondrogenic induction was performed for 3 weeks, replacing the media twice a week.

2.10. Histology. In several wound scratch assays, the scraped dishes were fixed and stained with eosin for qualitative late time points (3 days and 7 days) analysis and storage of samples. For osteogenesis confirmation, the dishes were fixed in 10% formalin for 15 min, washed in distilled water,

and stained with Alizarin red (5 mg/mL) for 30 min. The samples were then washed several times with distilled water until clarity. For chondrogenesis confirmation, wells were fixed in 10% formalin for 15 min, washed in distilled water, and stained with Alcian blue pH 2.5 (Bio-Optica, Milan) following the supplier's indications. Finally, the samples were washed twice in abundant distilled water. Chondrogenic micromasses were formalin-fixed overnight, embedded into agarose block, and processed for classical histology. Sections of 3,5 μm thickness were prepared using microtome (Leica). The slides were finally stained with Alcian blue and counterstained in Azocarmine Red (Bio-Optica, Milan). All histological samples were photographed for qualitative analysis using optical microscopes and color cameras (Leica suite).

2.11. Statistics. All the plots were edited in GraphPad Prism software. The specific statistical method to interpret the graphs is described within the individual captions. Differences were considered statistically significant when $P < 0.05$. $^{*}P < 0.05$; $^{**}P < 0.01$; $^{***}P < 0.001$; $^{****}P < 0.0001$.

3. Results

3.1. Viability and Proliferation. The effect of different concentrations of PL ranging from 5% (high) to 1% (low) was initially compared to 10% FBS by observing viability parameters. The imaging of DPSCs, grown at high density for 5 days and marked with fluorescent live/dead staining, reported a high viability rate in all compared conditions, with only rare detection of dead cells across the whole sample (Figure 1(a)). Slightly morphological changes appeared in 2% (mid) and 5% (high) concentrations of PL, where long intercellular processes and circular association were visible at minor density. After 3 days of culture, no statistically significant difference among the conditions was shown, despite the fact that the average number of cells grown with 5% PL seemed to be lower (Figure 1(b)). Through relative viability quantification of the counted samples, we confirmed the live/dead staining qualitative results (Figure 1(c)). Viable counts of long-term cultures showed that 1% PL is still competitive in viability with respect to 10% FBS (Figure 1(d)). Different trends of metabolic activity were emphasised instead by PrestoBlue assay (Figure 1(e)). In particular, compared to FBS, both 1% and 2% PL showed a higher metabolic rate during the first days of culture, while the 5% PL never outdid FBS. Despite the fact that 1% PL and 2% PL showed a similar trend, 1% concentration brought fewer changes during the last days and presented more similarity to FBS controls until the plateau growth phase (10 days). To further assess if this low PL concentration was sufficient to promote DPSCs proliferation, cells within first days of culture were analysed by flow cytometry for the CMFDA tracer (Figure 1(f)). CMFDA labelling of DPSCs highlighted a significant higher rate of proliferation in 1% PL compared to 10% FBS during 48 hours from seeding (Figure 1(g)).

3.2. Stem Cell Properties. To verify the identity of MSCs after the switch to 1% PL as supplement in cell medium, the DPSCs were analysed for MSCs surface markers by flow cytometry. The immunophenotype of DPSCs cultured in 1% PL resulted in coexpression of the obligatory ISCT markers [20] CD73, CD90, and CD105 and also the positive signal by CD13, CD29, CD44, and CD146 (Figure 2(a)), while it did not express negative markers such as CD34, CD45, and HLA-DR (Fig. S1). Intriguingly, the half population of DPSCs increased their CD146 expression when cultured in 1% PL. Compared to their controls, fluorescence geometric mean of PL is higher for CD13 and CD73 (data not shown). OCT4, Nanog, and Sox2 pluripotency markers were evaluated by quantitative PCR (Figure 2(b)). Samples cultured with PL until 6 days maintained the level of transcription of OCT4 compared to those cultured with FBS. On the other hand, PL supplementation timely increased Sox2 transcripts levels, while Nanog levels were significantly higher only at the last time point.

3.3. Migration Capacity. Platelet-derived GFs are involved in wound healing process [4]; thus we performed a scratch assay. Capturing images of different time points, we highlighted a greater level of wound closure for DPSCs scraped and then maintained in low-PL medium rather than in FBS medium. The enhanced cell migration in PL cultures from the wound edges is clearly evident 24 hours later (Figure 3(a)). Moreover, DPSCs cultured in low-PL medium continued to reduce the gap space after 3 and 7 days with a faster rate in comparison to FBS cultures (Figure 3(b)). One week after scratch, DPSCs in 1% PL were able to fully close the open wound area (Figure 3(c)). We also microscopically detected cell division in the wound space (Fig. S2), thus not restricting the repairing stimulation of PL to the migration of cells that were already present before the injury. Moreover, we counted the number of cells migrated at 24 h to have a quantitative result (Figure 3(d)). To address the question if this migrating ability can be associated with the soluble GFs contained in PL, we performed an under-agarose chemotaxis assay. After 24 hours, a conspicuous number of DPSCs positively responded to chemoattraction by PL, while very few cells migrated under the agarose gel to FBS containing compartment (Figure 3(e)).

3.4. Resistance to Cellular Damage Induced by H_2O_2. The early effect on survival/recovery of cells treated with 500 μM of H_2O_2 was analysed either by PrestoBlue assay (Figure 4(a)) or viable counting (Figure 4(b)) after 6 hours from the treatment. The presence in medium of PL before, during, and after treatment (complete media, CM) marked a non-significant difference output between untreated and treated samples, thus neutralising or rescuing the cells from the reactive oxygen species (ROS) action. On the contrary, the continuative presence of FBS in the wells (CM) was not sufficient to avoid cytotoxic effects of H_2O_2. Indeed, DPSCs conditioned in FBS or PL media but then exposed to H_2O_2 in basal media (BM) incubation reduced their vital activity measured by PrestoBlue reagent and were affected in own membrane integrity noticeable by dye exclusion cell counts.

3.5. Bony and Cartilaginous Differentiation. To test the suitability of PL for *in vitro* differentiation protocols, we basically

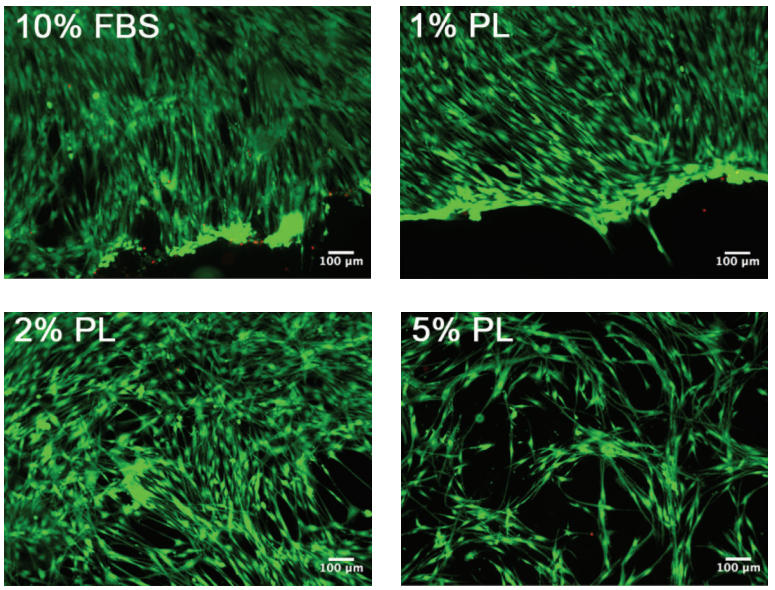

(a)

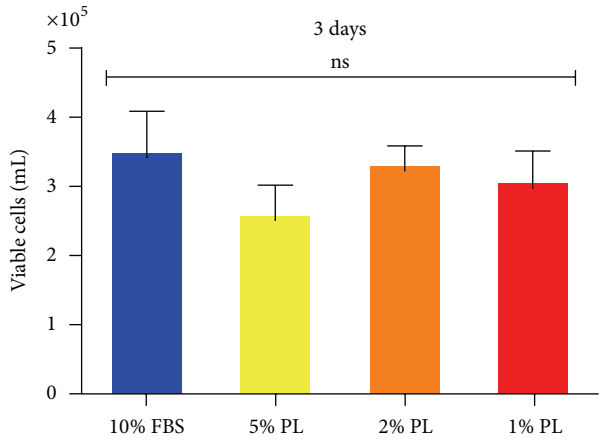

(b)

	10% FBS	5% PL	2% PL	1% PL
Mean	94.33	93.33	93.67	92.67
Std. deviation	3.215	3.786	4.509	0.5774

(c)

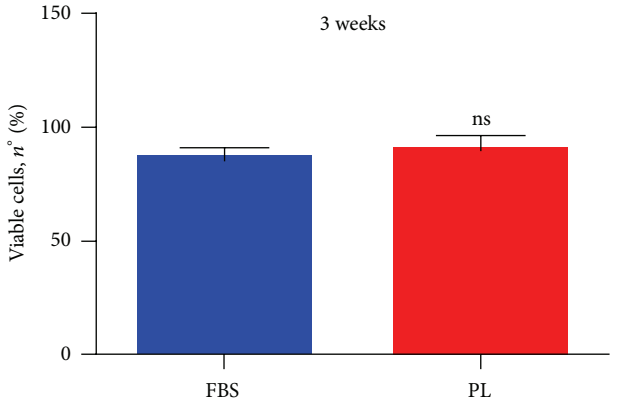

(d)

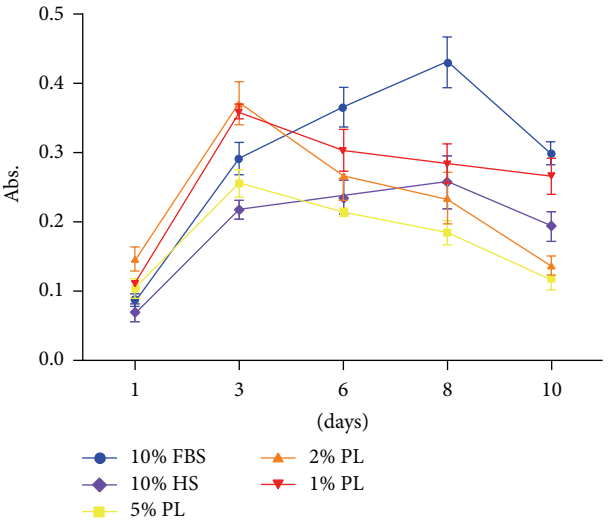

(e)

Figure 1: Continued.

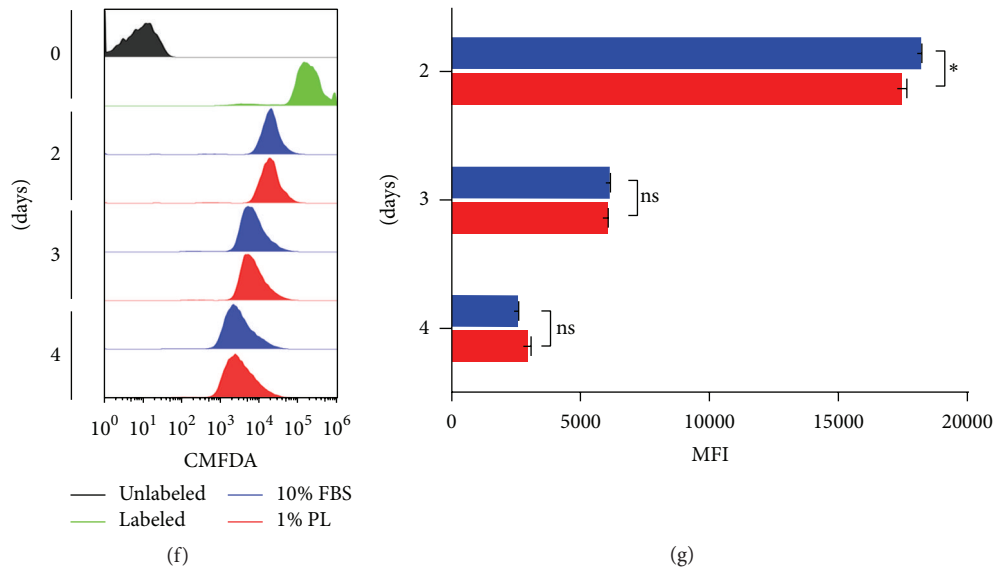

Figure 1: Effect of PL on the growth of DPSCs. (a) Representative images from live/dead fluorescence assay after 5 days of culture in different culture conditions. Green = live; red = dead. (b) Viable counts quantified by ADAM system after 3 days of culture. Data shown as mean + SD, $n = 3$, statistical significance according to 2-way ANOVA method ($P < 0.05$); ns: not significant. (c) Statistic values (average viability percentages) derived from samples in (b). (d) Viability after long-term culture of 3 weeks. Data shown as mean + SD, $n = 2$. ns: not significant according to unpaired t-test. (e) Cell growth activity measured by PrestoBlue assay. Data shown as mean + SD, $n = 2$. (f) CMFDA proliferation assay. Time-course comparing FBS and PL-selected condition. (g) Quantification of MFI derived from samples in (f). Statistics based on 2-way ANOVA method ($^*P < 0.05$). ns: not significant.

substituted 20% FBS to 1% PL for osteogenesis of DPSCs; otherwise we added 1% PL to the serum-free formula for chondrogenesis. Results from Alcian blue staining showed the deposition of proteoglycans in both 2D (monolayers, Figures 5(a)–5(d)) and 3D conditions (micromasses, Figures 5(g) and 5(h)), confirming that PL did not impair chondrogenic differentiation of DPSCs. These results were confirmed by spectrophotometric measurement of Alcian blue complex formation (Figures 5(e) and 5(f)). Besides, FBS replacement with PL did not modify the formation of calcium deposits stainable by Alizarin red (Figures 6(a)–6(e)). Again, the differentiating condition in PL was statistically different compared to its respective undifferentiated control, as well as FBS condition (Figures 6(c) and 6(f)). Regarding genes analysis, PL samples showed at the end of differentiation a higher ALP expression compared to the respective basal state, a situation that did not correspond in FBS controls (Figure 6(g)). While FBS seemed to upregulate OSC and DMP-1 osteoblastic markers in 4 weeks in differentiating samples, we cannot affirm the same for PL differentiated cultures, in fact, showing lower relative levels at the same time of analysis (Figure 6(g)). RUNX2 transcription factor had a comparable fold increase in FBS samples as well as in PL samples (Figure 6(g)).

4. Discussion

So far, it has been observed that the proliferation rate of MSCs cultured in PL-supplemented medium was higher than that of those cultured in FBS-supplemented medium [21, 22]. The used concentrations of PL usually ranged from 10% to lesser than 1%, but the great heterogeneity of the results, mostly due to the preparation of PL, still delays the finding of the best concentrations to be used for specific cell type and application. The highest percentages, for example, 10% PL, often were not suitable to culture or expand the cells [11, 12], while 5% PL was the most tested and promising concentration for MSCs [23–26]. Here, we observed a good viability for 5% PL cultures but at the same time we noted resistance to trypsinization at this concentration. Partially, in accordance with other reports [27, 28], the DPSCs had easier and faster detaching from the plate compared to FBS when the concentrations were lower than 5% PL. At 1% PL, we could see that DPSCs attached quicker than FBS after cell seeding. Using the same low-PL concentration, DPSCs displayed a good viability and proliferation profile. Already Lee et al. showed the feasibility of low-percentage supplementation of PL for DPSCs growing and osteogenic differentiation [29]. On the base of our results, we choose 1% PL as selected concentration to adopt in culture for characterising DPSCs stemness, multipotency, and role in repair.

The immunophenotype of DPSCs cultured in PL was completely faithful to MSCs markers panel, confirming previous studies by colleagues [10]. Many stem cell lines express CD13; among the MSCs sources it is particularly present in oral tissues, while it is absent in bone marrow compartment [30]. The lack of this receptor was shown to impair *in vitro* adhesion to several ECM proteins, migration, and invasion [31]. Our PL cultures of DPSCs consistently expressed CD13. CD13 together with CD29 and CD73 [32] and CD44 [33] were associated with enhanced migrating phenotype of MSCs. CD146 is an endothelial and pericyte marker [34]. It is known

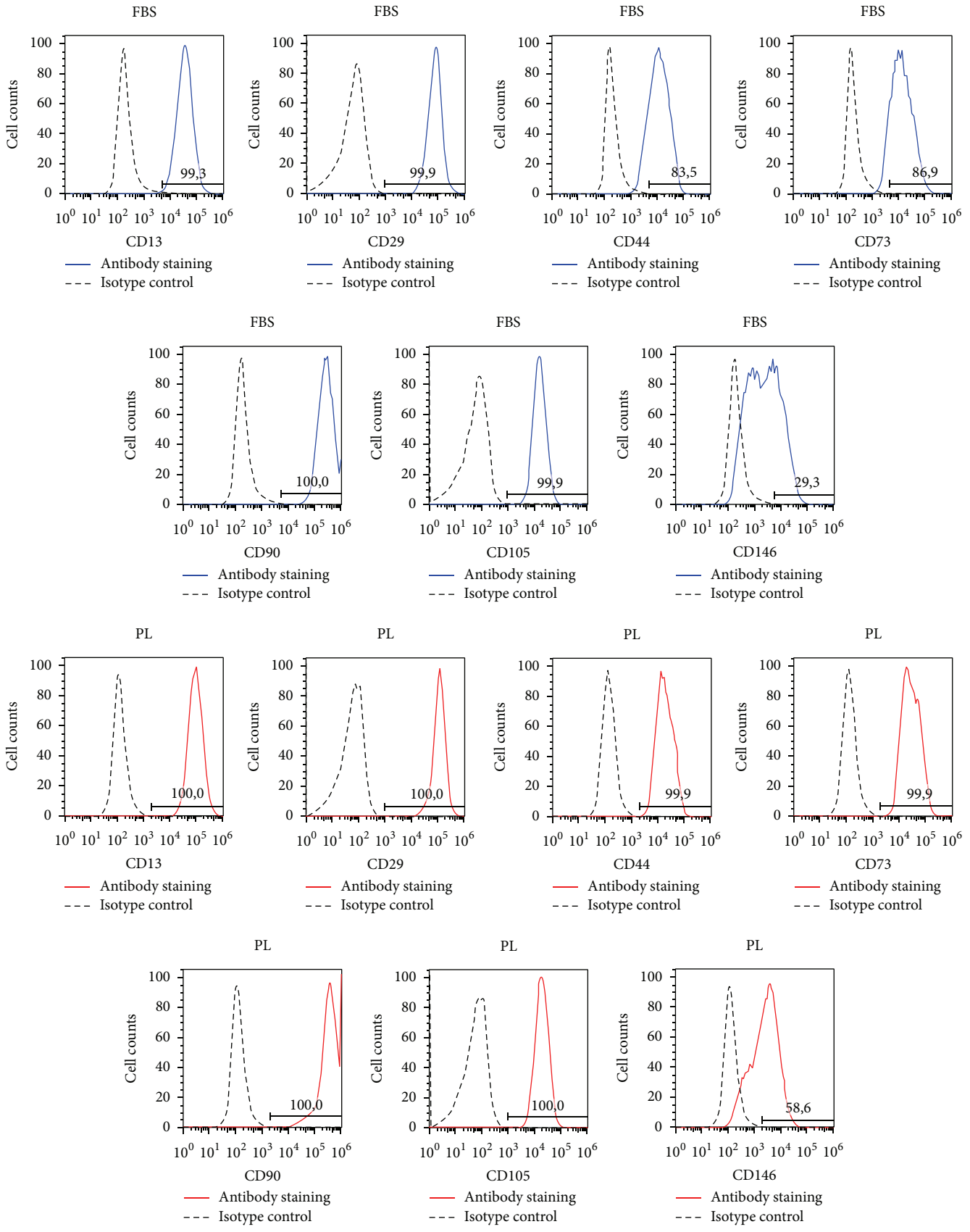

(a)

Figure 2: Continued.

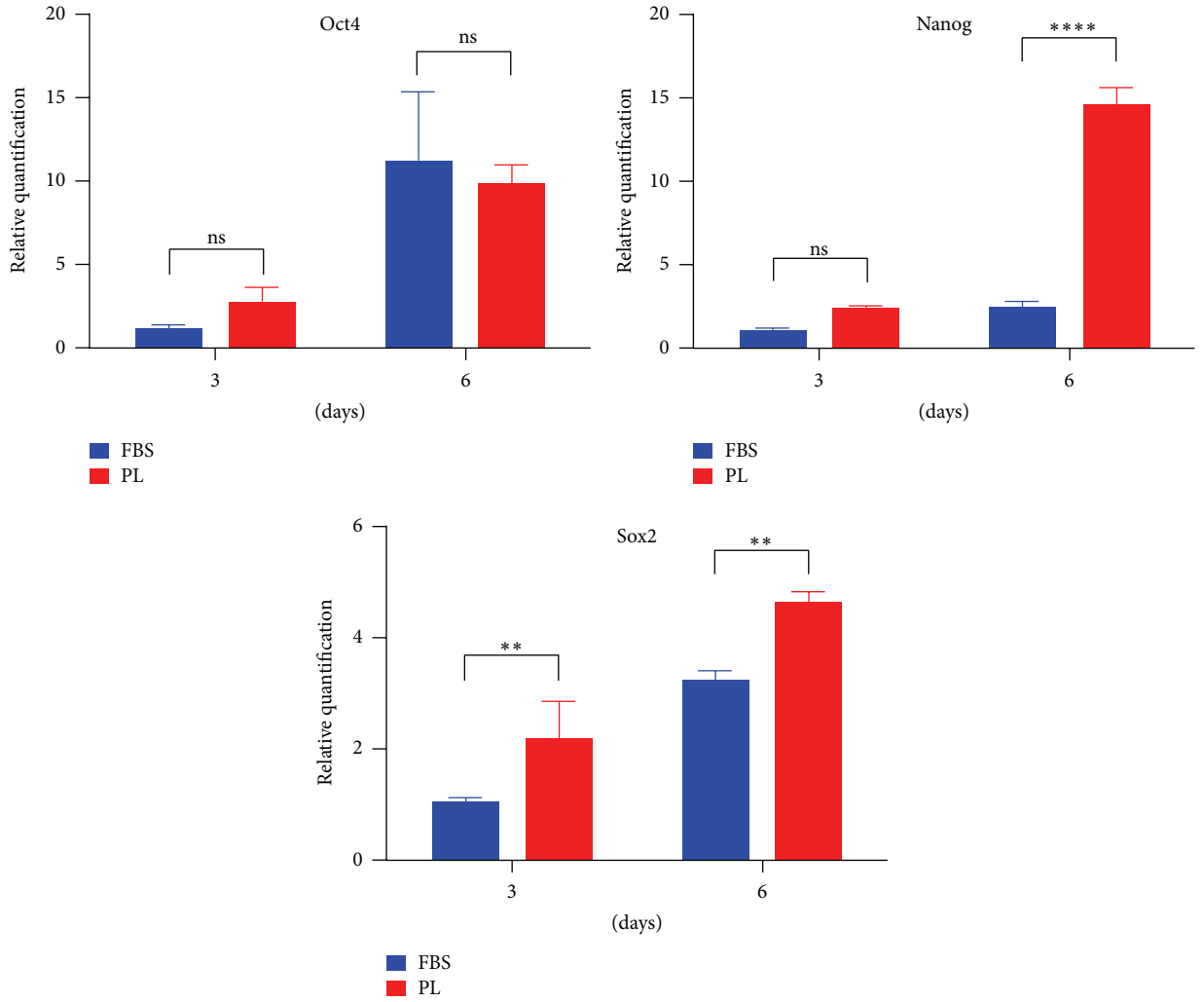

(b)

FIGURE 2: Stem cell markers comparison between FBS and PL cultures of DPSCs. (a) Immunophenotype for expressed MSC surface markers by flow cytometric analysis. The number specifies the percentage of gated cells positive for the indicated protein. Data representative of two experiments. (b) Relative levels of transcripts (fold change) for stemness markers derived from real-time PCR analysis. Statistical significance determined by 2-way ANOVA ($^{*}P < 0.05$; $^{**}P < 0.01$; $^{***}P < 0.001$; $^{****}P < 0.0001$), mean + SD, $n = 3$.

to be downregulated in culture with FBS [35]. Moreover, our DPSCs expressed the CD146 receptor on their membrane when cultured in PL in comparison to FBS. This agrees with recent data about CD146 increased expression by BM-MSC in PL medium [24]. Both CD13 and CD146 are angiogenic markers; thus our study generated preliminary data to further include DPSCs angiogenesis protocols. Embryonic stem cell markers, in particular transcription factors such as Oct4, Nanog, and Sox2, were usually thought to have a similar role in maintenance of stemness also in DPSCs [36–38]. In general, they are indicative of a more immature phenotype for MSCs [39]. Nonetheless, it is very hard to understand the impact of their transcripts levels in DPSCs; an increase of their expression sustains a proliferating condition by cells. Our DPSCs cultures in PL sustained a higher gene expression of Sox2 [40], which also plays a role in migration of DPSCs [41].

MSCs can be exposed to various chemical or physical stresses, which may induce a cellular decay. MSCs [42] and HSCs [43] share with leucocytes the capacity of homing to damaged sites in several tissues. It is essential that DPSCs will move to the site of new skeletogenesis or during MSC-mediated tissue repair. Many migration assays are available tools for oral regeneration studies [44]. PL was also already described as efficient in promoting *in vitro* wound healing of dermal fibroblast [45], C2C12 mouse myoblasts [46], keratinocytes [47], and other human cells [48]. So far, an indirect enhanced migration and chemotaxis by BM-MSCs were induced by coating of platelet lysate on HA/b-TCP scaffolds [49]. In response to the injury, the DPSCs cultured in PL improved their ability to fix an induced mechanical damage such as a wound. In addition, we demonstrated that PL had a superior chemotactic activity than FBS, a reason which is likely correlated to the better migration of DPSCs towards

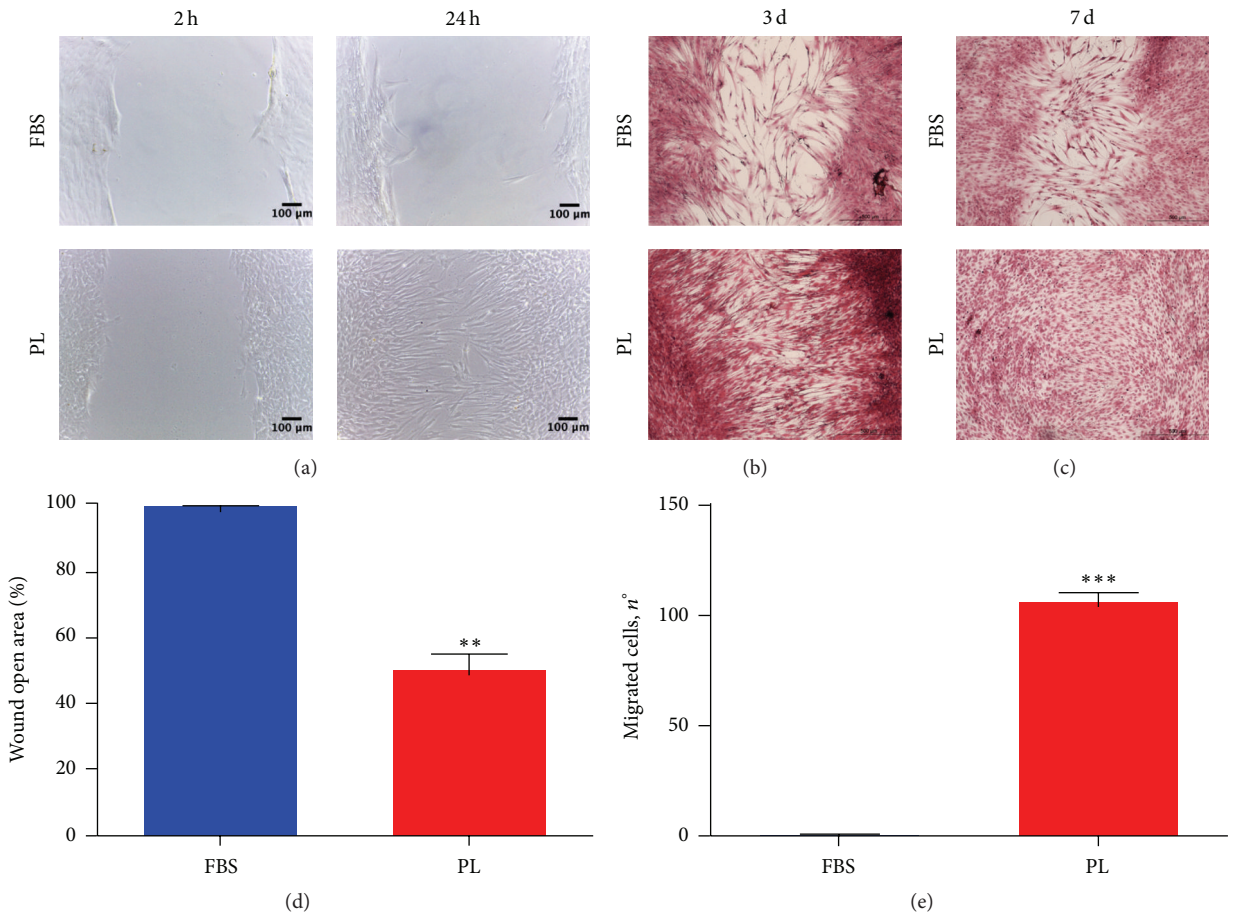

Figure 3: *In vitro* migration capacity of DPSCs is enhanced by PL. (a) Representative images of early time points during the scratch assay. Images were taken 2 hrs and 24 hrs after the initial scratch and are representative of 3 independent experiments. The cells were fixed and stained at different endpoints as shown in (b) for 3 days and (c) 7 days. (d) Quantitative analysis of wound healing at 24 hrs after scratch. 100% is set as open area 2 h time points. Data shown as mean + SD, $n = 3$. Statistical significance determined using unpaired t-test ($^{**}P < 0, 1$). (e) Quantification of chemotaxis derived from under-agarose assay. Data were collected using 24 h time points light microscope images. Data shown as mean + SD, $n = 3$. Statistical significance determined using unpaired t-test ($^{***}P < 0.001$).

the wounded region. Even though our experimental setting aimed to show how the healing of a scratched monolayer of DPSCs involved just the migration mechanism, surprisingly also cell genesis was active during the reparative process. Oxidative stress can lead to a wide range of cellular damage, such as damage to membrane lipids, proteins, and DNA. It is widely accepted that increasing concentration of free radicals augmented premature senescence even *in vitro* [50] or associated with bone disorders [51]. The platelets are very reactive *in vivo* against H_2O_2 which is a modulator and an efficient inducer of their aggregation [52]. SOD enzyme, also derived from the platelets, inhibited neutrophils excessive production in reactive oxygen species (ROS). Despite the role of platelets in releasing free radicals, their granules contained also the enzyme catalase. Our experiments supposed the rescue of DPSCs treated with H_2O_2, implying a neutralization action (supported by cell membrane permeability data) or high-level metabolic recovery (mostly mitochondrial). We speculate that the quite antioxidant activity detected with PL could mainly derive from catalase residues in the preparation and may be a beneficial protecting feature for MSCs, if this supplement is used. However, it is not possible to exclude that the less susceptibility to H_2O_2 is an intrinsic capacity that the cells acquire for the adding of PL. Nonetheless, a deeper comprehension would be desirable; this effect of PL we showed was not observable at the same level for FBS.

Moreover, PL is highly requested for cell-based therapies such as tissue engineering and bone and cartilage regenerative approaches [53]. Chondrogenic and osteogenic potentials were broadly studied and they were retained and influenced by PL added in cultures of MSCs [21, 54, 55]. MSCs cultured in 5% PL were seen to spontaneously activate osteoblastic gene expression [56]. Many authors documented that appropriate concentrations (i.e., 5% PL) enhanced, in particular, DPSCs mineralised differentiation and showed odontogenic potency [11, 12, 24]. The generation of protocols aimed at chondrogenesis taking advantage of PL is an expanding field [10, 21, 25, 57, 58], because PL is a rich source of natural TGF-β and the regenerative potential of primary chondroblasts is more restricted. PL was recently

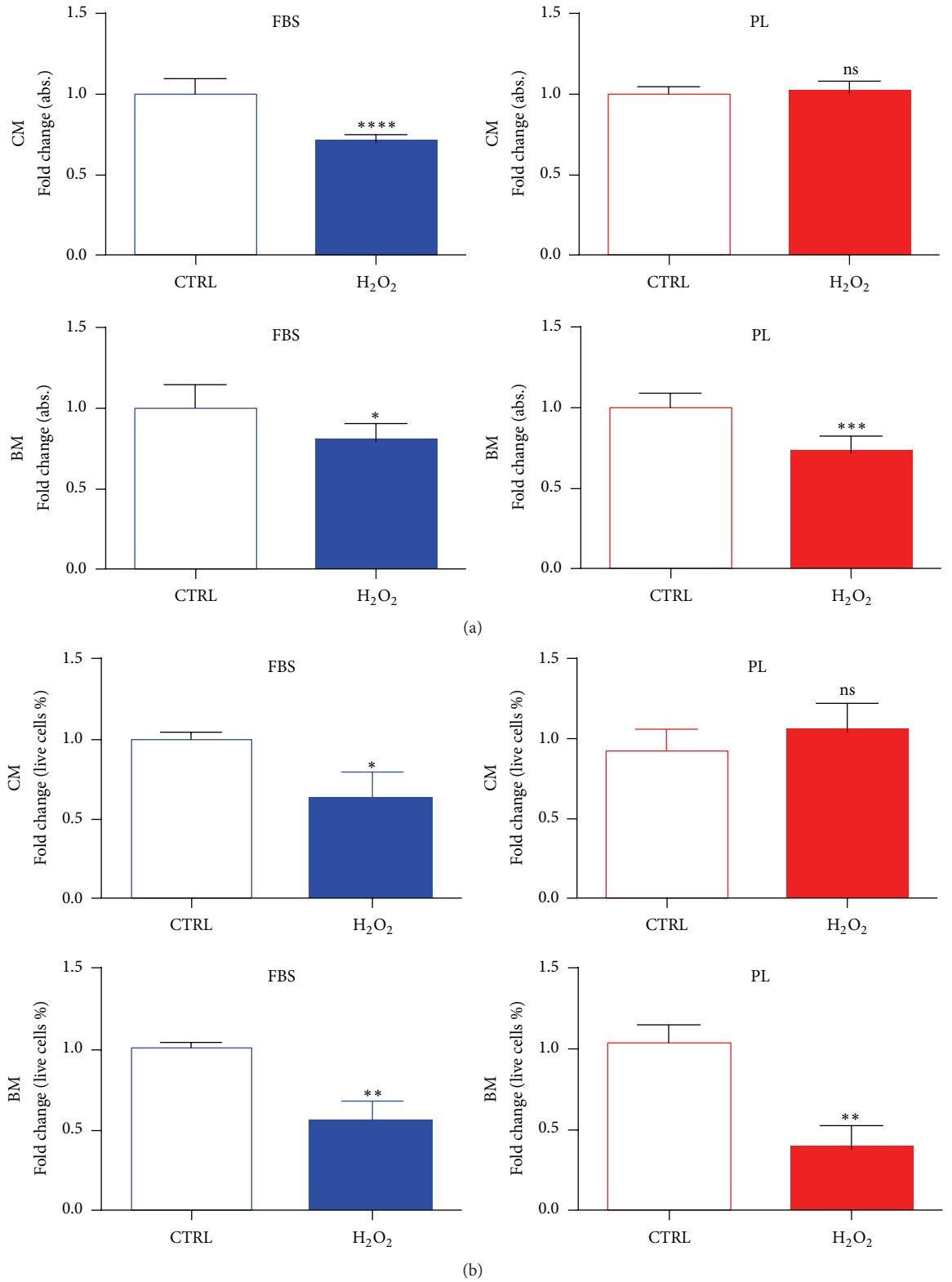

Figure 4: Impact of H_2O_2 on cellular viability is influenced by PL in culture. (a) Metabolic activity of cultures measured by PrestoBlue conversion 6 hrs after the treatment with H_2O_2. Data are expressed as mean + SD, $n = 3$, derived from 2 experiments. (b) Automatic viable cell counts after 6 hrs of treatment. Data were normalised to median value of control samples and shown as mean + SD, $n = 3$. To determine significant results, the unpaired t-test was performed ($^{*}P < 0.05$; $^{**}P < 0.01$; $^{***}P < 0.001$; $^{****}P < 0.0001$). CM, treatment performed in complete medium; BM, treatment performed in basal medium.

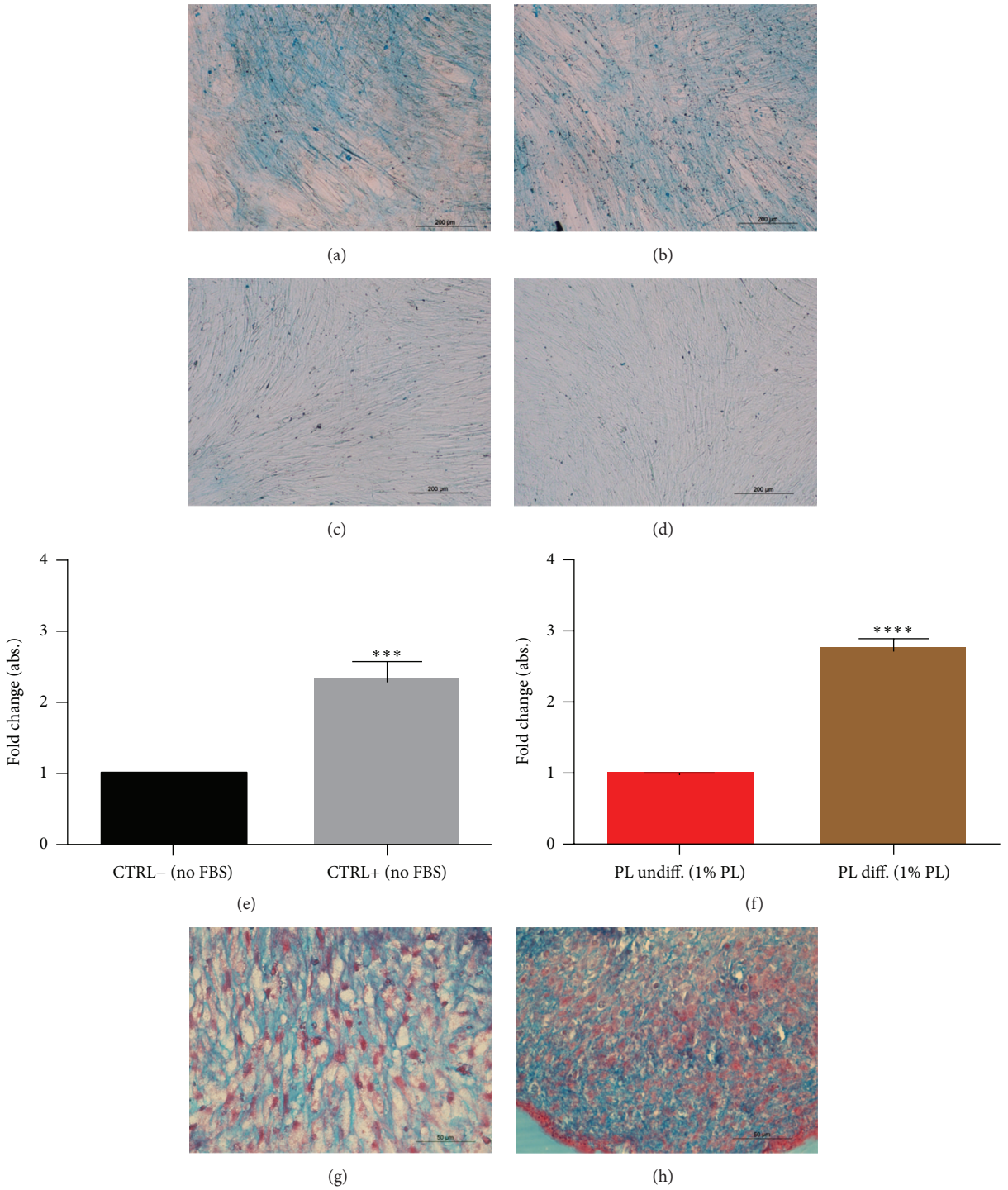

FIGURE 5: Effect of PL on chondrogenic differentiation of DPSCs. (a–d) Representative images of DPSC cultured for 21 days in chondrogenic medium without (a) or with (b) PL. They were positively stained by Alcian blue, while cells maintained in 10% FBS (c) or 1% PL (d) growth media were not. (e, f) Quantification of Alcian blue by spectrophotometry for assay controls (e) and samples containing PL (f). Significant levels according to unpaired t-test ($^{***}P < 0.001$ and $^{****}P < 0.0001$). Data shown as mean + SD, obtained from three experiments. (g, h) Micromass culture of DPSCs showing positive histological staining for chondrogenesis for control (g) as well as the micromasses cultured with differentiating medium with 1% PL (h).

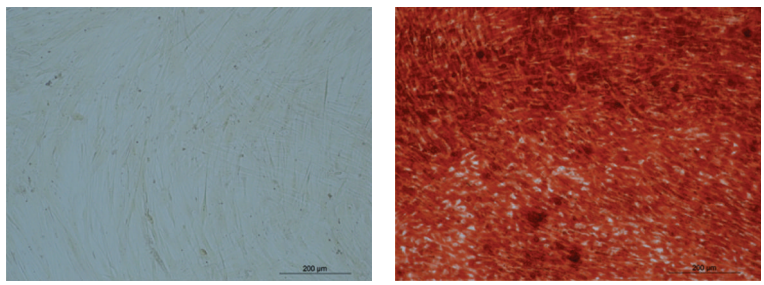

(a) (b)

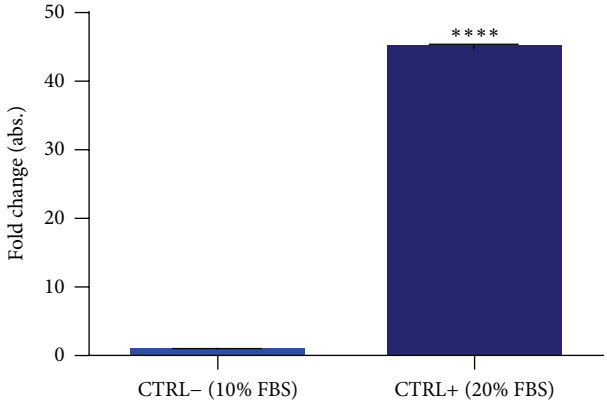

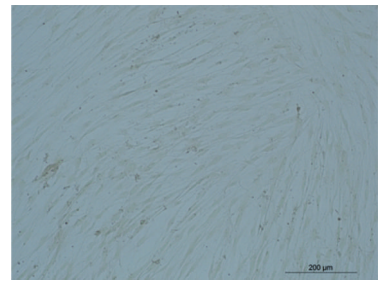

(c) (d)

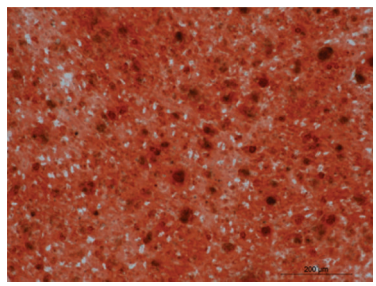

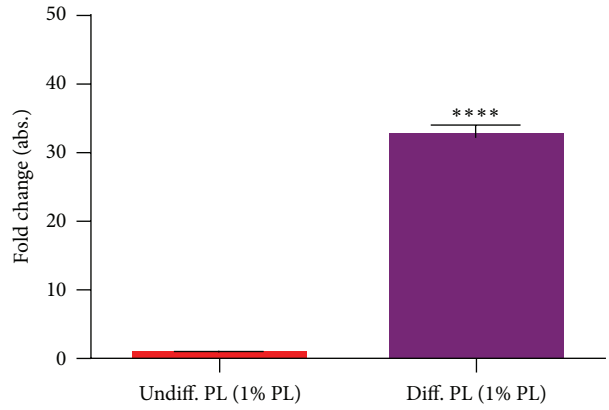

(e) (f)

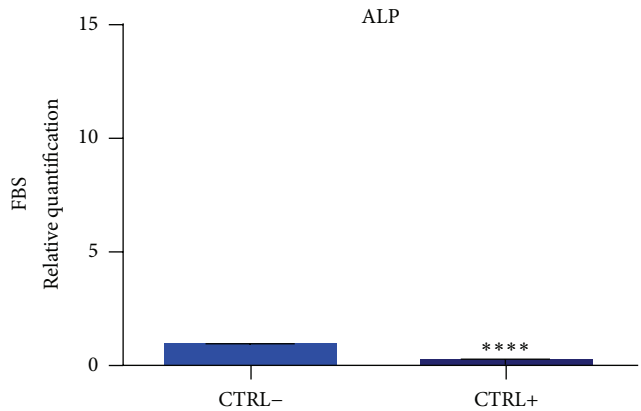

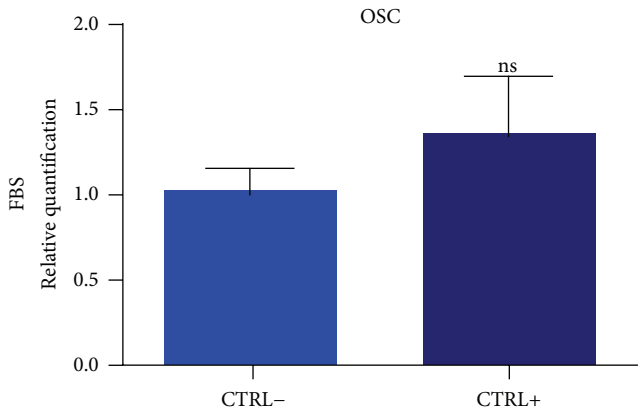

Figure 6: Continued.

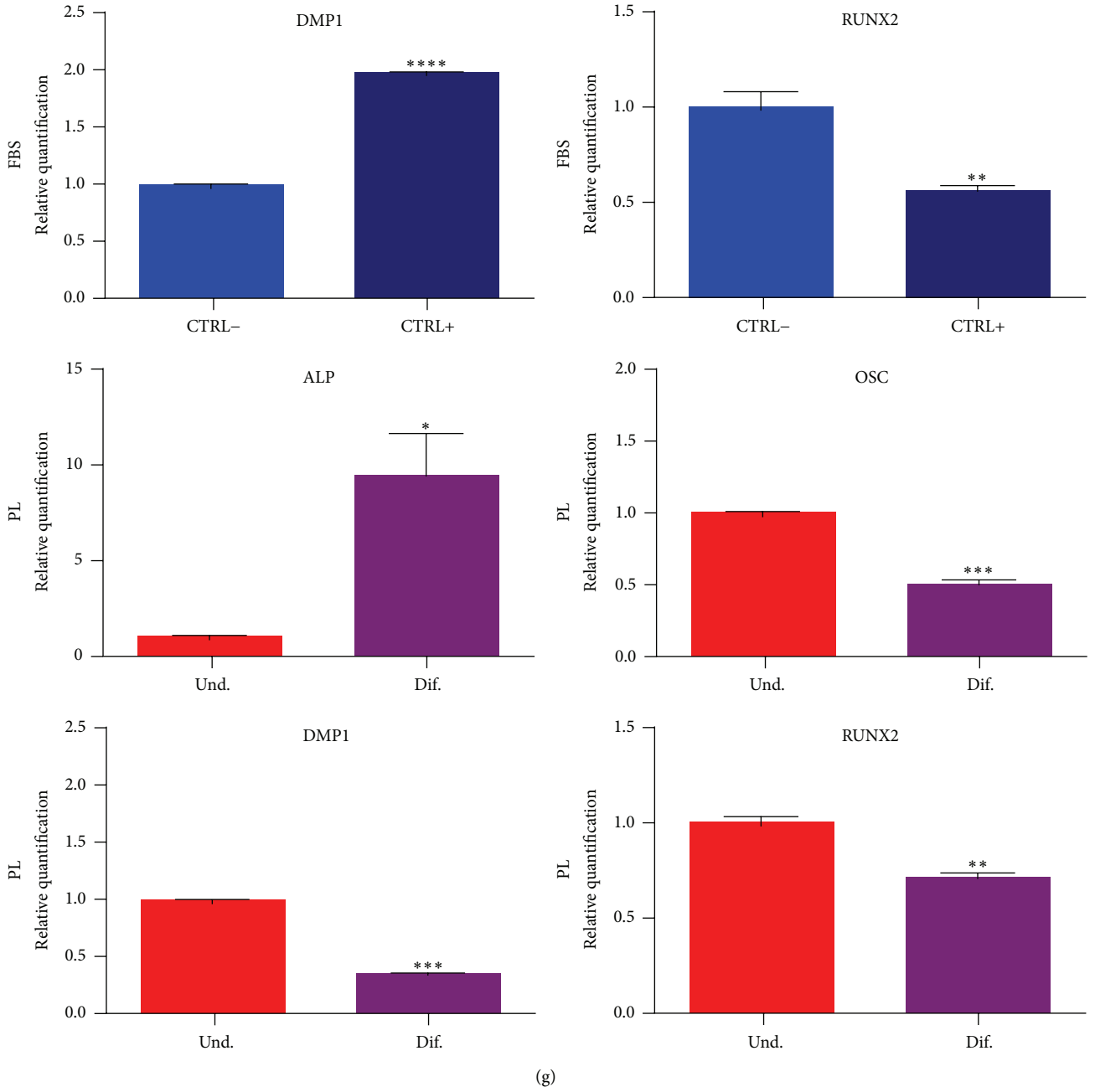

(g)

FIGURE 6: Effect of PL on osteogenic differentiation of DPSCs. Alizarin red staining on undifferentiated sample cultured in growth medium with 10% FBS (a) or 1% PL (d) and on samples differentiated with osteogenic medium containing 20% FBS (b) or 1% PL (e). Relative quantification of the same staining by spectrophotometry. Data shown as mean + SD, $n = 3$ samples. Two different experiments were performed. Significant levels according to unpaired t-test ($^{*}P < 0.05$; $^{**}P < 0.01$; $^{***}P < 0.001$; $^{****}P < 0.0001$). (g) Relative quantification of osteogenic markers by real-time PCR on samples derived from the end (28 days) of the differentiating protocol. Data shown as mean + SD, $n = 3$. Significant levels according to unpaired t-test ($^{*}P < 0.05$; $^{**}P < 0.01$; $^{***}P < 0.001$; $^{****}P < 0.0001$).

implemented in scaffolds construction [59] and scaffolds functionalization procedures [49]. We assessed the compatibility for the low-percentage concentration of commercial PL to be introduced in osteogenic and chondrogenic traditional protocols for DPSCs. Indeed successful colorimetric detection was measured either for calcium deposits by Alizarin or for proteoglycans by Alcian blue. We found an active gene transcription of the two osteoprogenitor markers ALP and RUNX2. Even if a total improvement in osteogenesis after the supplement comparison cannot be assumed at the selected concentration, the objective advantage of a xeno-free condition outlines an optimal reason to switch for our research-grade protocols in which GFs are delivered from PL. Actually, the positive controls conditions for differentiation were considerably different from testing conditions. Indeed, a 20% FBS and 1% PL, for the osteogenesis, were compared.

Respectively, the presence of PL during chondrocytic development was used instead of absence of serum, suggested from the historical protocol [60].

Further studies will helpfully evaluate the feasibility of the use of PL in DPSCs isolation as already described for BM-MSC [23, 54, 61]. Other elucidations are required for the immunomodulation function in the presence of standardised PL preparations, like the one tested in this work. So far, the dual combination of PL with platelet-poor plasma (PPP) was shown to be particularly efficient to boost the number of clonogenic precursors from tissue biopsies, that is, primary cultures of MSCs from bone marrow, umbilical cord, and adipose tissue [62, 63].

5. Conclusion

Taken together, our results suggest that human allogenic PL is a suitable alternative to FBS for expansion and differentiation of DPSCs *in vitro*. Furthermore, up to our knowledge, this is the first study reporting the influence of PL on DPSCs migration and antioxidant effect during *ex vivo* maintenance.

Competing Interests

The authors declare that they have no competing interests.

Acknowledgments

The present study was supported by ICARE Project-Infrastruttura Calabrese per la medicina Rigenerativa: "generazione di biobanche per la criopreservazione di cellule staminali umane e di tessuto osseo per uso clinico e design e sviluppo di bioscaffold innovativi" (PON03PE_00009_2.2).

References

[1] M. Tatullo, M. Marrelli, and F. Paduano, "The regenerative medicine in oral and maxillofacial surgery: the most important innovations in the clinical application of mesenchymal stem cells," *International Journal of Medical Sciences*, vol. 12, no. 1, pp. 72–77, 2015.

[2] D. T.-B. Shih and T. Burnouf, "Preparation, quality criteria, and properties of human blood platelet lysate supplements for *ex vivo* stem cell expansion," *New Biotechnology*, vol. 32, no. 1, pp. 199–211, 2015.

[3] C. Rauch, E. Feifel, E.-M. Amann et al., "Alternatives to the use of fetal bovine serum: human platelet lysates as a serum substitute in cell culture media," *ALTEX*, vol. 28, no. 4, pp. 305–316, 2011.

[4] T. Burnouf, D. Strunk, M. B. C. Koh, and K. Schallmoser, "Human platelet lysate: replacing fetal bovine serum as a gold standard for human cell propagation?" *Biomaterials*, vol. 76, pp. 371–387, 2016.

[5] H. Hemeda, B. Giebel, and W. Wagner, "Evaluation of human platelet lysate versus fetal bovine serum for culture of mesenchymal stromal cells," *Cytotherapy*, vol. 16, no. 2, pp. 170–180, 2014.

[6] C. Marchionni, L. Bonsi, F. Alviano et al., "Angiogenic potential of human dental pulp stromal (stem) cells," *International Journal of Immunopathology and Pharmacology*, vol. 22, no. 3, pp. 699–706, 2009.

[7] F. Paino, G. Ricci, A. De Rosa et al., "Ecto-mesenchymal stem cells from dental pulp are committed to differentiate into active melanocytes," *European Cells and Materials*, vol. 20, pp. 295–305, 2010.

[8] A. Arthur, G. Rychkov, S. Shi, S. A. Koblar, and S. Gronthose, "Adult human dental pulp stem cells differentiate toward functionally active neurons under appropriate environmental cues," *Stem Cells*, vol. 26, no. 7, pp. 1787–1795, 2008.

[9] V. Govindasamy, V. S. Ronald, A. N. Abdullah et al., "Differentiation of dental pulp stem cells into islet-like aggregates," *Journal of Dental Research*, vol. 90, no. 5, pp. 646–652, 2011.

[10] V. Govindasamy, V. S. Ronald, A. N. B. Abdullah et al., "Human platelet lysate permits scale-up of dental pulp stromal cells for clinical applications," *Cytotherapy*, vol. 13, no. 10, pp. 1221–1233, 2011.

[11] B. Chen, H.-H. Sun, H.-G. Wang, H. Kong, F.-M. Chen, and Q. Yu, "The effects of human platelet lysate on dental pulp stem cells derived from impacted human third molars," *Biomaterials*, vol. 33, no. 20, pp. 5023–5035, 2012.

[12] D. Abuarqoub, A. Awidi, and N. Abuharfeil, "Comparison of osteo/odontogenic differentiation of human adult dental pulp stem cells and stem cells from apical papilla in the presence of platelet lysate," *Archives of Oral Biology*, vol. 60, no. 10, pp. 1545–1553, 2015.

[13] S. Gronthos, M. Mankani, J. Brahim, P. G. Robey, and S. Shi, "Postnatal human dental pulp stem cells (DPSCs) in vitro and in vivo," *Proceedings of the National Academy of Sciences of the United States of America*, vol. 97, no. 25, pp. 13625–13630, 2000.

[14] M. Marrelli, F. Paduano, and M. Tatullo, "Human periapical cyst-mesenchymal stem cells differentiate into neuronal cells," *Journal of Dental Research*, vol. 94, no. 6, pp. 843–852, 2015.

[15] F. Paduano, M. Marrelli, L. J. White, K. M. Shakesheff, M. Tatullo, and X. Liu, "Odontogenic differentiation of human dental pulp stem cells on hydrogel scaffolds derived from decellularized bone extracellular matrix and collagen type I," *PLoS ONE*, vol. 11, no. 2, Article ID e0148225, 2016.

[16] M. Marrelli, F. Paduano, and M. Tatullo, "Cells isolated from human periapical cysts express mesenchymal stem cell-like properties," *International Journal of Biological Sciences*, vol. 9, no. 10, pp. 1070–1078, 2013.

[17] S. Vogel, T. Trapp, V. Börger et al., "Hepatocyte growth factor-mediated attraction of mesenchymal stem cells for apoptotic neuronal and cardiomyocytic cells," *Cellular and Molecular Life Sciences*, vol. 67, no. 2, pp. 295–303, 2010.

[18] O. Baud, A. E. Greene, J. Li, H. Wang, J. J. Volpe, and P. A. Rosenberg, "Glutathione peroxidase-catalase cooperativity is required for resistance to hydrogen peroxide by mature rat oligodendrocytes," *Journal of Neuroscience*, vol. 24, no. 7, pp. 1531–1540, 2004.

[19] Y. Ido, A. Duranton, F. Lan et al., "Acute activation of AMP-activated protein kinase prevents H_2O_2-induced premature senescence in primary human keratinocytes," *PLoS ONE*, vol. 7, no. 4, Article ID e35092, 2012.

[20] M. Dominici, K. Le Blanc, I. Mueller et al., "Minimal criteria for defining multipotent mesenchymal stromal cells. The International Society for Cellular Therapy position statement," *Cytotherapy*, vol. 8, no. 4, pp. 315–317, 2006.

[21] C. Doucet, I. Ernou, Y. Zhang et al., "Platelet lysates promote mesenchymal stem cell expansion: a safety substitute for animal serum in cell-based therapy applications," *Journal of Cellular Physiology*, vol. 205, no. 2, pp. 228–236, 2005.

[22] K. Bieback, A. Hecker, A. Kocaömer et al., "Human alternatives to fetal bovine serum for the expansion of mesenchymal stromal cells from bone marrow," *STEM CELLS*, vol. 27, no. 9, pp. 2331–2341, 2009.

[23] C. Capelli, M. Domenghini, G. Borleri et al., "Human platelet lysate allows expansion and clinical grade production of mesenchymal stromal cells from small samples of bone marrow aspirates or marrow filter washouts," *Bone Marrow Transplantation*, vol. 40, no. 8, pp. 785–791, 2007.

[24] J. Brun, T. Abruzzese, B. Rolauffs, W. K. Aicher, and M. L. Hart, "Choice of xenogenic-free expansion media significantly influences the myogenic differentiation potential of human bone marrow-derived mesenchymal stromal cells," *Cytotherapy*, vol. 18, no. 3, pp. 344–359, 2016.

[25] H.-J. Prins, H. Rozemuller, S. Vonk-Griffioen et al., "Bone-forming capacity of mesenchymal stromal cells when cultured in the presence of human platelet lysate as substitute for fetal bovine serum," *Tissue Engineering—Part A*, vol. 15, no. 12, pp. 3741–3751, 2009.

[26] K. Schallmoser, E. Rohde, A. Reinisch et al., "Rapid large-scale expansion of functional mesenchymal stem cells from unmanipulated bone marrow without animal serum," *Tissue Engineering—Part C: Methods*, vol. 14, no. 3, pp. 185–196, 2008.

[27] S. H. Zaky, A. Ottonello, P. Strada, R. Cancedda, and M. Mastrogiacomo, "Platelet lysate favours in vitro expansion of human bone marrow stromal cells for bone and cartilage engineering," *Journal of Tissue Engineering and Regenerative Medicine*, vol. 2, no. 8, pp. 472–481, 2008.

[28] A. Kocaoemer, S. Kern, H. Klüter, and K. Bieback, "Human AB serum and thrombin-activated platelet-rich plasma are suitable alternatives to fetal calf serum for the expansion of mesenchymal stem cells from adipose tissue," *STEM CELLS*, vol. 25, no. 5, pp. 1270–1278, 2007.

[29] U.-L. Lee, S. H. Jeon, J.-Y. Park, and P.-H. Choung, "Effect of platelet-rich plasma on dental stem cells derived from human impacted third molars," *Regenerative Medicine*, vol. 6, no. 1, pp. 67–79, 2011.

[30] R. Calloni, E. A. A. Cordero, J. A. P. Henriques, and D. Bonatto, "Reviewing and updating the major molecular markers for stem cells," *Stem Cells and Development*, vol. 22, no. 9, pp. 1455–1476, 2013.

[31] M. M. Rahman, J. Subramani, M. Ghosh et al., "CD13 promotes mesenchymal stem cell-mediated regeneration of ischemic muscle," *Frontiers in Physiology*, vol. 4, article 402, 2014.

[32] A. Ode, J. Kopf, A. Kurtz et al., "CD73 and CD29 concurrently mediate the mechanically induced decrease of migratory capacity of mesenchymal stromal cells," *European Cells & Materials Journal*, vol. 22, pp. 26–42, 2011.

[33] H. Zhu, N. Mitsuhashi, A. Klein et al., "The role of the hyaluronan receptor CD44 in mesenchymal stem cell migration in the extracellular matrix," *Stem Cells*, vol. 24, no. 4, pp. 928–935, 2006.

[34] F. Paduano, M. Marrelli, F. Palmieri, and M. Tatullo, "CD146 expression influences periapical cyst mesenchymal stem cell properties," *Stem Cell Reviews*, In press.

[35] I. Müller, S. Kordowich, C. Holzwarth et al., "Animal serum-free culture conditions for isolation and expansion of multipotent mesenchymal stromal cells from human BM," *Cytotherapy*, vol. 8, no. 5, pp. 437–444, 2006.

[36] C.-E. Huang, F.-W. Hu, C.-H. Yu et al., "Concurrent expression of Oct4 and Nanog maintains mesenchymal stem-like property of human dental pulp cells," *International Journal of Molecular Sciences*, vol. 15, no. 10, pp. 18623–18639, 2014.

[37] M. La Noce, F. Paino, A. Spina et al., "Dental pulp stem cells: state of the art and suggestions for a true translation of research into therapy," *Journal of Dentistry*, vol. 42, no. 7, pp. 761–768, 2014.

[38] M. Atari, M. Barajas, F. Hernández-Alfaro et al., "Isolation of pluripotent stem cells from human third molar dental pulp," *Histology and Histopathology*, vol. 26, no. 8, pp. 1057–1070, 2011.

[39] W. Zhao, X. Ji, F. Zhang, L. Li, and L. Ma, "Embryonic stem cell markers," *Molecules*, vol. 17, no. 6, pp. 6196–6236, 2012.

[40] D. S. Yoon, Y. H. Kim, H. S. Jung, S. Paik, and J. W. Lee, "Importance of Sox2 in maintenance of cell proliferation and multipotency of mesenchymal stem cells in low-density culture," *Cell Proliferation*, vol. 44, no. 5, pp. 428–440, 2011.

[41] P. Liu, J. Cai, D. Dong et al., "Effects of SOX2 on proliferation, migration and adhesion of human dental pulp stem cells," *PLoS ONE*, vol. 10, no. 10, Article ID e0141346, 2015.

[42] M. W. Maijenburg, C. E. van der Schoot, and C. Voermans, "Mesenchymal stromal cell migration: possibilities to improve cellular therapy," *Stem Cells and Development*, vol. 21, no. 1, pp. 19–29, 2012.

[43] T. Trotta, S. Di Gioia, D. Piro et al., "Effect of acute lung injury on VLA-4 and CXCR4 expression in resident and circulating hematopoietic stem/progenitor cells," *Respiration*, vol. 85, no. 3, pp. 252–264, 2013.

[44] M. Weinreb and C. E. Nemcovsky, "In vitro models for evaluation of periodontal wound healing/regeneration," *Periodontology 2000*, vol. 68, no. 1, pp. 41–54, 2015.

[45] E. Ranzato, L. Mazzucco, M. Patrone, and B. Burlando, "Platelet lysate promotes in vitro wound scratch closure of human dermal fibroblasts: different roles of cell calcium, P38, ERK and PI3K/AKT," *Journal of Cellular and Molecular Medicine*, vol. 13, no. 8, pp. 2030–2038, 2009.

[46] E. Ranzato, V. Balbo, F. Boccafoschi, L. Mazzucco, and B. Burlando, "Scratch wound closure of C2C12 mouse myoblasts is enhanced by human platelet lysate," *Cell Biology International*, vol. 33, no. 9, pp. 911–917, 2009.

[47] R. E. Backly, V. Ulivi, L. Tonachini, R. Cancedda, F. Descalzi, and M. Mastrogiacomo, "Platelet lysate induces in vitro wound healing of human keratinocytes associated with a strong proinflammatory response," *Tissue Engineering—Part A*, vol. 17, no. 13-14, pp. 1787–1800, 2011.

[48] M. C. Barsotti, P. Losi, E. Briganti et al., "Effect of platelet lysate on human cells involved in different phases of wound healing," *PLoS ONE*, vol. 8, no. 12, Article ID e84753, pp. 1–11, 2013.

[49] J. Leotot, L. Coquelin, G. Bodivit et al., "Platelet lysate coating on scaffolds directly and indirectly enhances cell migration, improving bone and blood vessel formation," *Acta Biomaterialia*, vol. 9, no. 5, pp. 6630–6640, 2013.

[50] J. Duan, J. Duan, Z. Zhang, and T. Tong, "Irreversible cellular senescence induced by prolonged exposure to H_2O_2 involves DNA-damage-and-repair genes and telomere shortening," *The International Journal of Biochemistry & Cell Biology*, vol. 37, no. 7, pp. 1407–1420, 2005.

[51] M. Li, L. Zhao, J. Liu et al., "Hydrogen peroxide induces G2 cell cycle arrest and inhibits cell proliferation in osteoblasts," *Anatomical Record*, vol. 292, no. 8, pp. 1107–1113, 2009.

[52] H. Ikeda, Y. Koga, T. Oda et al., "Free oxygen radicals contribute to platelet aggregation and cyclic flow variations in stenosed and endothelium-injured canine coronary arteries," *Journal of*

the American College of Cardiology, vol. 24, no. 7, pp. 1749–1756, 1994.

[53] Y. Yamada, S. Nakamura, K. Ito et al., "A feasibility of useful cell-based therapy by bone regeneration with deciduous tooth stem cells, dental pulp stem cells, or bone-marrow-derived mesenchymal stem cells for clinical study using tissue engineering technology," *Tissue Engineering—Part A*, vol. 16, no. 6, pp. 1891–1900, 2010.

[54] E. Lucarelli, A. Beccheroni, D. Donati et al., "Platelet-derived growth factors enhance proliferation of human stromal stem cells," *Biomaterials*, vol. 24, no. 18, pp. 3095–3100, 2003.

[55] C. Lange, F. Cakiroglu, A.-N. Spiess, H. Cappallo-Obermann, J. Dierlamm, and A. R. Zander, "Accelerated and safe expansion of human mesenchymal stromal cells in animal serum-free medium for transplantation and regenerative medicine," *Journal of Cellular Physiology*, vol. 213, no. 1, pp. 18–26, 2007.

[56] N. Chevallier, F. Anagnostou, S. Zilber et al., "Osteoblastic differentiation of human mesenchymal stem cells with platelet lysate," *Biomaterials*, vol. 31, no. 2, pp. 270–278, 2010.

[57] S. M. Jonsdottir-Buch, R. Lieder, and O. E. Sigurjonsson, "Platelet lysates produced from expired platelet concentrates support growth and osteogenic differentiation of mesenchymal stem cells," *PLoS ONE*, vol. 8, no. 7, article e68984, 2013.

[58] F. Hildner, M. J. Eder, K. Hofer et al., "Human platelet lysate successfully promotes proliferation and subsequent chondrogenic differentiation of adipose-derived stem cells: a comparison with articular chondrocytes," *Journal of Tissue Engineering and Regenerative Medicine*, vol. 9, no. 7, pp. 808–818, 2015.

[59] A. Moroz, R. A. C. Bittencourt, R. P. Almeida, S. L. Felisbino, and E. Deffune, "Platelet lysate 3D scaffold supports mesenchymal stem cell chondrogenesis: an improved approach in cartilage tissue engineering," *Platelets*, vol. 24, no. 3, pp. 219–225, 2013.

[60] B. Johnstone, T. M. Hering, A. I. Caplan, V. M. Goldberg, and J. U. Yoo, "*In vitro* chondrogenesis of bone marrow-derived mesenchymal progenitor cells," *Experimental Cell Research*, vol. 238, no. 1, pp. 265–272, 1998.

[61] N. Fekete, M. Gadelorge, D. Fürst et al., "Platelet lysate from whole blood-derived pooled platelet concentrates and apheresis-derived platelet concentrates for the isolation and expansion of human bone marrow mesenchymal stromal cells: production process, content and identification of active components," *Cytotherapy*, vol. 14, no. 5, pp. 540–554, 2012.

[62] A. Muraglia, M. R. Todeschi, A. Papait et al., "Combined platelet and plasma derivatives enhance proliferation of stem/progenitor cells maintaining their differentiation potential," *Cytotherapy*, vol. 17, no. 12, pp. 1793–1806, 2015.

[63] G. Mori, G. Brunetti, S. Collucci et al., "Osteoblast apoptosis in periodontal disease: role of TNF-related apoptosis-inducing ligand," *International Journal of Immunopathology and Pharmacology*, vol. 22, no. 1, pp. 95–103, 2009.

Hindawi Publishing Corporation
Stem Cells International
Volume 2016, Article ID 2545214, 13 pages
http://dx.doi.org/10.1155/2016/2545214

Research Article

Semaphorin 3A Shifts Adipose Mesenchymal Stem Cells towards Osteogenic Phenotype and Promotes Bone Regeneration In Vivo

Xiangwei Liu,[1] Naiwen Tan,[1] Yuchao Zhou,[1] Xueying Zhou,[2] Hui Chen,[3] Hongbo Wei,[1] Ji Chen,[1] Xiaoru Xu,[1] Sijia Zhang,[1] Guodong Yang,[4] and Yingliang Song[1]

[1] *State Key Laboratory of Military Stomatology and National Clinical Research Center for Oral Diseases and Shaanxi Engineering Research Center for Dental Materials and Advanced Manufacture, Department of Implant Dentistry, School of Stomatology, Fourth Military Medical University, Xi'an 710032, China*
[2] *Department of Ultrasound Diagnostics, Tangdu Hospital, Fourth Military Medical University, Xi'an, China*
[3] *Department of Plastic Surgery, Tangdu Hospital, Fourth Military Medical University, Xi'an, China*
[4] *Department of Biochemistry and Molecular Biology, Fourth Military Medical University, Xi'an, China*

Correspondence should be addressed to Guodong Yang; yanggd@fmmu.edu.cn and Yingliang Song; yingliangsong@163.com

Received 18 June 2016; Revised 17 August 2016; Accepted 18 August 2016

Academic Editor: Giacomina Brunetti

Copyright © 2016 Xiangwei Liu et al. This is an open access article distributed under the Creative Commons Attribution License, which permits unrestricted use, distribution, and reproduction in any medium, provided the original work is properly cited.

Adipose mesenchymal stem cells (ASCs) are considered as the promising seed cells for bone regeneration. However, the lower osteogenic differentiation capacity limits its therapeutic efficacy. Identification of the key molecules governing the differences between ASCs and BMSCs would shed light on manipulation of ASCs towards osteogenic phenotype. In this study, we screened semaphorin family members in ASCs and BMSCs and identified Sema3A as an osteogenic semaphorin that was significantly and predominantly expressed in BMSCs. The analyses in vitro showed that the overexpression of Sema3A in ASCs significantly enhanced the expression of bone-related genes and extracellular matrix calcium deposition, while decreasing the expression of adipose-related genes and thus lipid droplet formation, resembling a BMSCs phenotype. Furthermore, Sema3A modified ASCs were then engrafted into poly(lactic-co-glycolic acid) (PLGA) scaffolds to repair the critical-sized calvarial defects in rat model. As expected, Sema3A modified ASCs encapsulation significantly promoted new bone formation with higher bone volume fraction and bone mineral density. Additionally, Sema3A was found to simultaneously increase multiple Wnt related genes and thus activating Wnt pathway. Taken together, our study here identifies Sema3A as a critical gene for osteogenic phenotype and reveals that Sema3A-modified ASCs would serve as a promising candidate for bettering bone defect repair.

1. Introduction

Bone defects are common in trauma, tumor resection, or congenital local bone absence, among which approximately 5–10% could not heal spontaneously due to excessive bone loss or abnormal bone metabolism [1]. Autogenous bone graft or bone graft substitutes are needed in this situation [2, 3]; however, sometimes autografting is insufficient or problematic in certain conditions of great bone trauma or systemic diseases [2, 3]. Therefore, bone graft substitute is a promising alternative [2, 3]; in particular, tissue engineering derived bone consisting of seed cells, scaffolds, and growth factors is becoming a new trend in the field. As to the seed cells, bone marrow mesenchymal stem cells (BMSCs) are the first rational seed cells for bone defect repair and regeneration, while the sources of BMSCs are limited [4, 5]. In 2002, Zuk et al. [6] found a new source of seed cells, adipose-derived stem cells (ASCs), which are readily available, able to differentiate into osteocytes, and potent in replication [7–9]. Compared with the BMSCs, ASCs have a poor performance in osteogenesis due to their origin, with the detailed mechanism unknown [10–13]. Approaches to increase the osteogenic capacity of ASCs would possibly facilitate the utility of ASCs in bone repair and regeneration.

Previously, a number of approaches aiming at increasing the osteogenic capacity of ASCs were tried. ASCs are heterogeneous cells populations, with the osteogenic and self-renewal capacities being different [14–16]. To this end,

the ASCs subpopulations with strong osteogenesis potential were sorted via flow cytometry [17] and utilized for bone engineering. Besides, osteogenic stimuli are added to promote or activate the bone forming capacity of ASCs before transplantation. For example, short-time exposure to osteogenic medium of ASCs would upgrade the role in bone defect healing, and this pretreatment would also prevent tumor formation theoretically [18]. Besides, many other biological factors, such as osteoprotegerin, platelet-derived growth factor BB and bone morphogenetic protein, loaded directly or on various vehicles for control release, have also been tried, with different beneficial outcomes [19, 20]. Clarification of the mechanisms underlying the osteogenic differences between BMSC and ASCs would provide clues for improving the osteogenesis of ASCs, shedding light on the bone regeneration.

Semaphorin family, composed of more than twenty secreted and membrane-associated proteins, plays a critical role in development and wound repair, such as neural axonal guidance, angiogenesis, and bone formation [21]. Accumulating studies indicate that some semaphorin family members are involved in bone remodeling by promoting osteogenesis [22–28], further suggesting the potent role of semaphorin in bone development and regeneration. Up to now, whether semaphorin is responsible for the difference between ASC and BMSC in osteogenesis is totally unknown.

In this study, we compared the expression of semaphorin members in mesenchymal stem cells with varied osteogenic capacities, namely, young BMSCs, aged BMSCs, and ASCs. Semaphorin 3A was identified as a gene highly expressed in the mesenchymal stem cells with strong osteogenic capacity. In vitro studies further confirmed the osteogenic role of Sema3A by both Sema3A knockdown and overexpression. Transplantation of Sema3A infected ASCs greatly improves the bone repair and regeneration capacities in the calvarial critical size bone defect model. Our study has revealed that manipulating ASCs with Sema3A holds as a promising approach for bone repair and regeneration in the future.

2. Materials and Methods

2.1. Cell Isolation and Culture. Sprague Dawley (SD) rats (4 weeks or 12 months old), obtained from the animal center of Fourth Military Medical University (FMMU), were grown and processed in accordance with Institutional Animal Care and Use Committee (IACUC) approval of FMMU. For ASCs isolation, the rats were sacrificed by euthanization followed by cervical dissection. The bilateral inguinal adipose tissues were harvested under sterile conditions and then digested with 0.2% collagenase I for 40 mins and filtered with 100 μm strainer mesh. The obtained filtrate was centrifuged (5 min, 1000 r/min) and resuspended in DMEM medium (GIBCO, USA) containing 10% fetal bovine serum (GIBCO, USA) and 1% antibiotics (200 mg/mL penicillin and 200 mg/mL streptomycin,) and cultured in an humidified atmosphere of 5% CO_2 at 37°C. ASCs were passaged upon reaching 80% confluency. For BMSCs isolation, bone marrows of the femur and tibia were harvested by syringe flushing, and then the pelleted cells were resuspended and cultured in the same way above. Passage 3 cultures were applied for both in vivo and in vitro experiments in this study.

2.2. Lentivirus Packaging and Infection of ASCs. The lentivirus plasmid expressing Sema3A gene was constructed by cloning the Sema3A CDS into pWPI vector, designated as pWPI-Sema3A. Lentivirus expressing Sema3A was packaged by transfecting 293T cells with pWPI (or pWPI-Sema3A), psPAX2, and pMD2G plasmids at the mass ratio of 10 : 5 : 1. The obtained lentivirus expresses Sema3A and green fluorescent protein (GFP) in pWPI-Sema3A or in control pWPI. For lentivirus infection, the obtained lentivirus was incubated with polybrene (8 μg/mL) before being added into the ASCs. To define the MOI, ASCs were seeded at a density of 4×10^5/well into a six-well plate in average DMEM medium and infection efficiency was determined by flow cytometric detection of GFP expression.

2.3. Flow Cytometric Analysis. The infection efficiency was analyzed by flow cytometry. Forty-eight hours after infection, approximately 3×10^5 ASCs either without infection or infected with control pWPI lentivirus or Sema3A expressing lentivirus were digested with trypsin/EDTA and resuspended in 500 μL PBS. The expression of GFP in the above three groups was analyzed by flow cytometry (BD, FACSAria).

2.4. Western Blot. Whole-cell protein was isolated from ASCs using the Total Extraction Sample Kit (Sigma) according to the instruction. For western blot analysis, equal proteins were loaded on 12% SDS-PAGE gels and then separated completely using vertical electrophoresis at 120 V. After transferring onto a 0.5 μm pore size nitrocellulose membrane at 200 mA, the separated proteins were blocked with 5% bovine serum albumin and incubated with rabbit polyclonal anti-Sema3A(Abcam, ab23393) and mouse polyclonal anti-GAPDH primary antibodies diluted in 5% TBST for 8 hours at 4°C. The protein bands were visualized using the Odyssey Infrared Imager system (LI-COR) after incubation with corresponding fluorescent secondary antibody for 1 hour at room temperature.

2.5. Cell Proliferation and Migration Assay. For cell proliferation analysis, two thousand cells with indicated treatments in 150 μL medium were seeded per well in 96-well plate. Ten μL cck-8 reagents were gently added and mixed evenly into each well at indicated time. After 2 hours of incubation at 37°C, the absorbance value was read at 490 nm. For cell migration assay, about 20,000 mesenchymal stem cells were seeded on the Transwell insert with 8 μm pore size followed by surface wetting utilizing serum-free medium for 1 hours, with the bottom chamber containing 500 μL Sema3A ASC conditioned or control medium. Forty-eight hours later, migrated cells were fixed and stained with crystal violet. The migrated cells were visualized and counted under inverted microscope.

2.6. Adipogenic and Osteogenic Differentiation Induction. ASCs were maintained in the growth medium till confluence. One day after confluence, ASCs were converted into

adipogenic induction medium (50 μM 3-isobutyl-1-methylxanthine (Sigma-Aldrich), 10 μM dexamethasone (Sigma-Aldrich), 10 μM rosiglitazone (Sigma-Aldrich), and 10 μg/mL insulin). The medium was changed every 3 days. The differentiated cells were fixed in 4% formaldehyde for 15 minutes at room temperature and lipid droplets were identified by Oil red O (Sigma-Aldrich) staining. For osteogenic differentiation, 70% confluent cells were induced by osteogenic induction medium containing 10 mM disodium β-glycerophosphate (Sigma-Aldrich), 0.1 μM dexamethasone (Sigma-Aldrich), and 50 mg/mL l-ascorbic acid (Sigma-Aldrich). The medium was also changed every 3 days and full osteogenic differentiation was achieved by 3-week induction, during which time we measured alkaline phosphatase (ALP) activity of ASCs and performed ALP staining after a 7-day osteogenic differentiation induction, using ALP assay kit and ALP color development kit. Osteogenic differentiation was examined by Alizarin Red (Sigma-Aldrich) staining of mineralized matrix. The CPC (cetylpyridinium chloride, Sigma-Aldrich) method was used to quantify the mineralized matrix as described elsewhere [29]. Briefly, after staining with Alizarin Red, CPC (10%, w/v, in distilled water) solution was added to each sample (800 μL per well in 24-well plate) and incubated for 1 h at 37°C. After incubation, the CPC solution was transferred to a 96-well plate (80 μL per well) for absorbance reading at 570 nm.

2.7. Real-Time Quantitative PCR Analysis. Total RNA was isolated using the Trizol (Invitrogen) before being subjected to reverse transcription using PrimeScript RT Reagent kit (Takara). Real-time PCR analysis (qPCR) was conducted with SYBR Premix Ex Taq II (Takara) using a CFX96 Real-Time System (Bio-Rad). GAPDH or β-actin was selected as the internal control. The referred primer sequences are listed in Supplementary Table 1 in Supplementary Material available online at http://dx.doi.org/10.1155/2016/2545214.

2.8. Topflash Luciferase Reporter Assay. Wnt activity was analyzed by Topflash analysis. Briefly, $ASCs^{-control}$ and $ASCs^{-Sema3A}$ were, respectively, plated in 24-well plates at a density of 1×10^5 cells per well and cultured for 24 hours. Then, the 200 ng Topflash or Fopflash plasmid together with 10 ng pGL4.75 plasmid was transfected using Lipofectamine 2000 Transfection Reagent. Forty-eight hours after transfection, the cells were lysed and the relative luciferase activities were measured using Dual Luciferase Reporter Assay System according to the protocol.

2.9. Immunofluorescence. Immunofluorescence was included for probing the subcellular location of β-catenin in $ASC^{-Sema3A}$ and control ASCs. Briefly, the cells were fixed for 15 minutes in 4% formaldehyde and blocked with PBS containing 3% BSA and 0.3% tween for 1 h. After that, cells were incubated with primary anti-β-catenin antibody (ab32572, 1 : 200, Abcam) overnight at 4°C. The secondary antibody Alexa Fluor 555 goat anti-rabbit IgG antibody was added for 1 hour to visualize primary antibody at room temperature. Nuclei were counterstained in blue with Hoechst (1/1000). Images were visualized with confocal microscope (Nikon, Japan).

2.10. Construction of PLGA Scaffold-ASCs Implant. Poly(lactic-co-glycolic acid) copolymer-collagen scaffolds were fabricated as described before [16], with minor modification. Briefly, ten-gram NaCl particles varying from 125 μm to 300 μm in diameter were seeded evenly in an 8 cm glass dish. And one gram 65 : 35 PLGA (Sigma-Aldrich) was dissolved entirely in 9 mL dichloromethane (DCM). Then, the PLGA solution was poured into the glass dish, and another ten-gram NaCl particles were added into the glass as soon as the liquid level sank down to NaCl particles. All the procedure was done in the chemical hood and the DCM was removed by evaporation. NaCl was removed by flushing with large amounts of water. Five mm diameter PLGA discs were obtained utilizing electric trephine. The obtained discs were sterilized by Co60 irradiation and further immersed into 50 mg/mL collagen I solution for one hour to increase the compatibility with cells. The ASCs-scaffold complex was manipulated by dropping 50 μL ASCs solution (2 million cells) onto the scaffold. The surface morphology of empty scaffold and ASCs encapsulated scaffold were analyzed by scanning electron microscopy. The acquired implants were cocultured in the osteogenic medium for 48 hours before being transplanted in vivo.

2.11. Creation of the Critical Size Calvarial Defect Model and Transplantation of ASCs-Scaffold Implant. Adult male SD rats, weighing 250–300 g, were intraperitoneally injected with pentobarbital (1%, 0.4 mL/100 g) and then subjected to local anesthesia with primacaine. The surgical field was shaved and sterilized; 2 cm long incisions were made approximately from the occipital middle region to the nose. Using a trephine with saline irrigation cooling, 5 mm full-thickness bone defects were created. The rats were randomly divided into four groups according to the differences of implants: (1) control group, (2) PLGA scaffold only, (3) PLGA scaffold with $ASCs^{-control}$, and (4) PLGA scaffold with $ASCs^{-Sema3A}$. Following suture and postoperative anti-inflammation treatment with gentamycin, animals were kept for 4- and 16-week recovery before microCT and histology study.

2.12. Histology and Immunohistochemistry. To analyze the cell survival and cell migration on the scaffolds, PLGA scaffold with different fabrications was taken out from the defects five days after implantation. Then, the complexes were embedded in paraffin and cut into 5 μm sections. Immunohistochemistry was carried out as reported by Zavatti et al. and so forth [30]. Briefly, the sections were treated with boiling EDTA buffer to expose the antigens. Then the sections blocked with 3% BSA were further incubated with the rabbit anti-collagen I antibody for 1 hour at RT. After 3 times washing, the samples were incubated for 1 hour at RT with the secondary antibody diluted 1 : 200 before DAB staining. After washing again, the sections were counter stained with hematoxylin.

For histological analysis after 4- or 12-week recovery, the decalcified specimens were embedded in paraffin and then cut into 5 μm sections. The sections were stained with

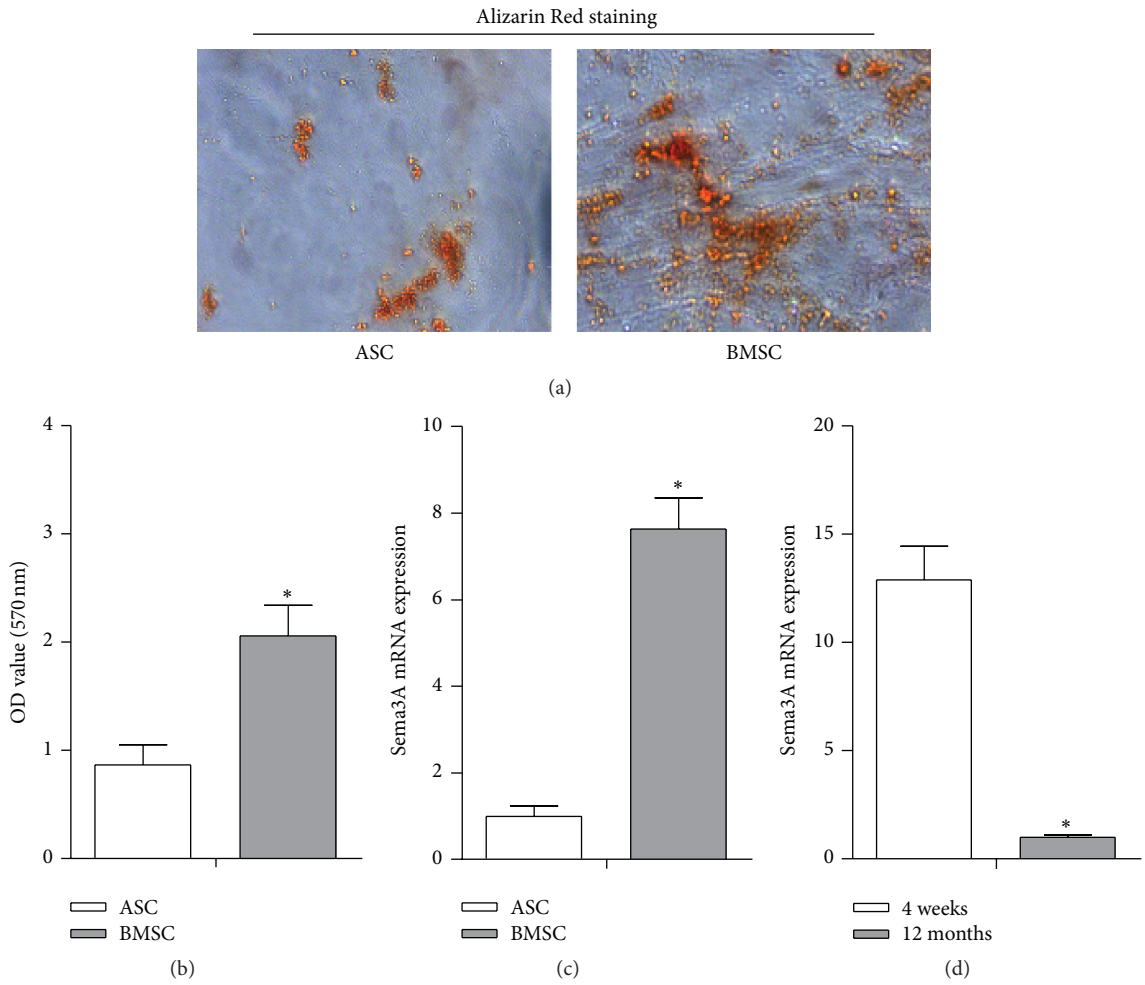

FIGURE 1: High expression of Sema3A correlates with the potent osteogenic capacity in BMSCs. (a) ASCs and BMSCs from the same rat were cultured in the osteogenic medium and significantly less mineralization nodules were found in ASCs than that in BMSCs after 21 days of osteogenic induction. (b) Quantification data of ECM mineralization in Figure 1(a). (c) Sema3A expression was significantly less in ASCs than that in BMSCs, as detected by qPCR. (d) Lower Sema3A expression was also found in 12-month rat derived BMSCs, compared with that from 4-week rat derived BMSCs. Mean ± SD, $n = 3$, and $^{*}p < 0.05$. Sema3A, semaphorin 3A; ECM, extracellular matrix.

hematoxylin and eosin (H&E) to highlight the different tissues. The digital sections images were captured with the aid of light microscope.

2.13. Micro-CT Scanning. After being intraperitoneally injected with excessive pentobarbital, rats were sacrificed and the calvariae around the bone defect were excised and placed in 10% neutral buffered formaldehyde for 12 hours. For further imaging examination, a high-resolution micro-CT scanner was employed. Samples were scanned with a resolution of 20 μm; afterwards, whole cranium was reconstructed using data analysis software. Five mm in diameter along the edge of defect was set as the region of interest. The bone volume fraction (BVF) and the trabecular thickness were calculated.

2.14. Statistical Analysis. All data were expressed as mean ± SD. Statistical significance was determined with Student's t-test or ANOVA using SPSS software. Statistical significance was accepted for $p < 0.05$.

3. Results

3.1. Specific High Expression of Sema3A in Young BMSCs Correlates with the Potent Osteogenic Capacity. Consistent with previous findings that BMSCs have stronger osteogenic capacity than ASCs, Alizarin Red staining confirmed that the BMSCs were more likely differentiated into osteoblasts (Figures 1(a) and 1(b)). To reveal the molecular determinants for the phenotype differences, we mainly focus on the semaphorin family, which has been reported to play important roles in cell fate commitment [31, 32]. We screened the expression of semaphorin family members (semaphorins 3A, 3B, 3C, 3D, 3E, 3F, 4A, 4B, 4C, 4D, 4F, 4G, 5A, 5B, 6A, 6B, 6C, 6D, and 7A) in ASCs and BMSCs and found strikingly higher expression of Sema3A and Sema3D in

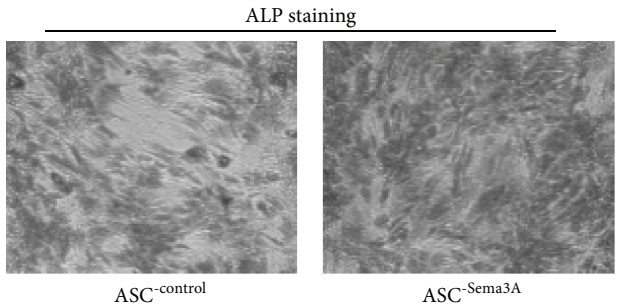

(a)

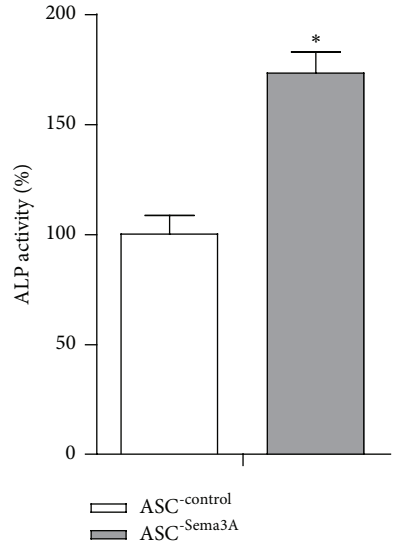

(b)

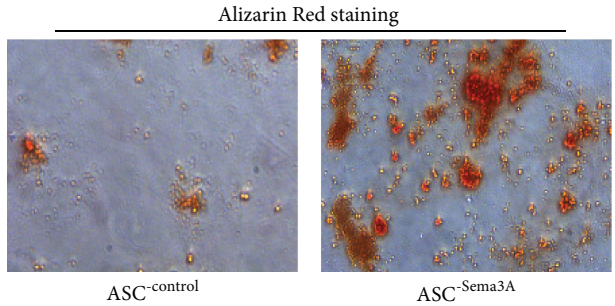

(c)

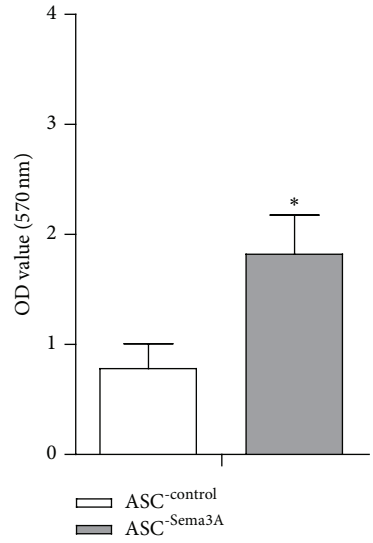

(d)

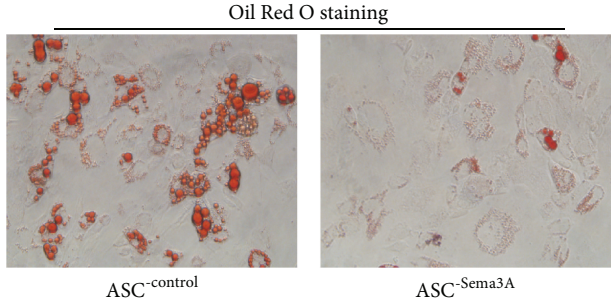

(e)

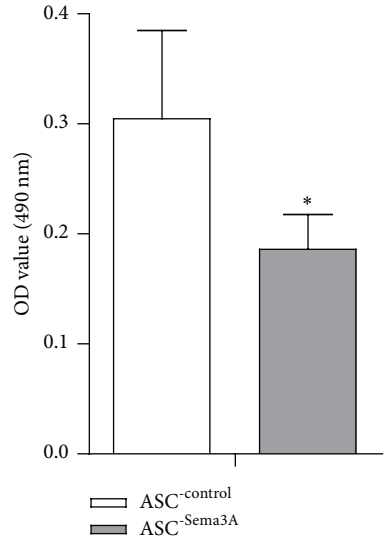

(f)

Figure 2: Continued.

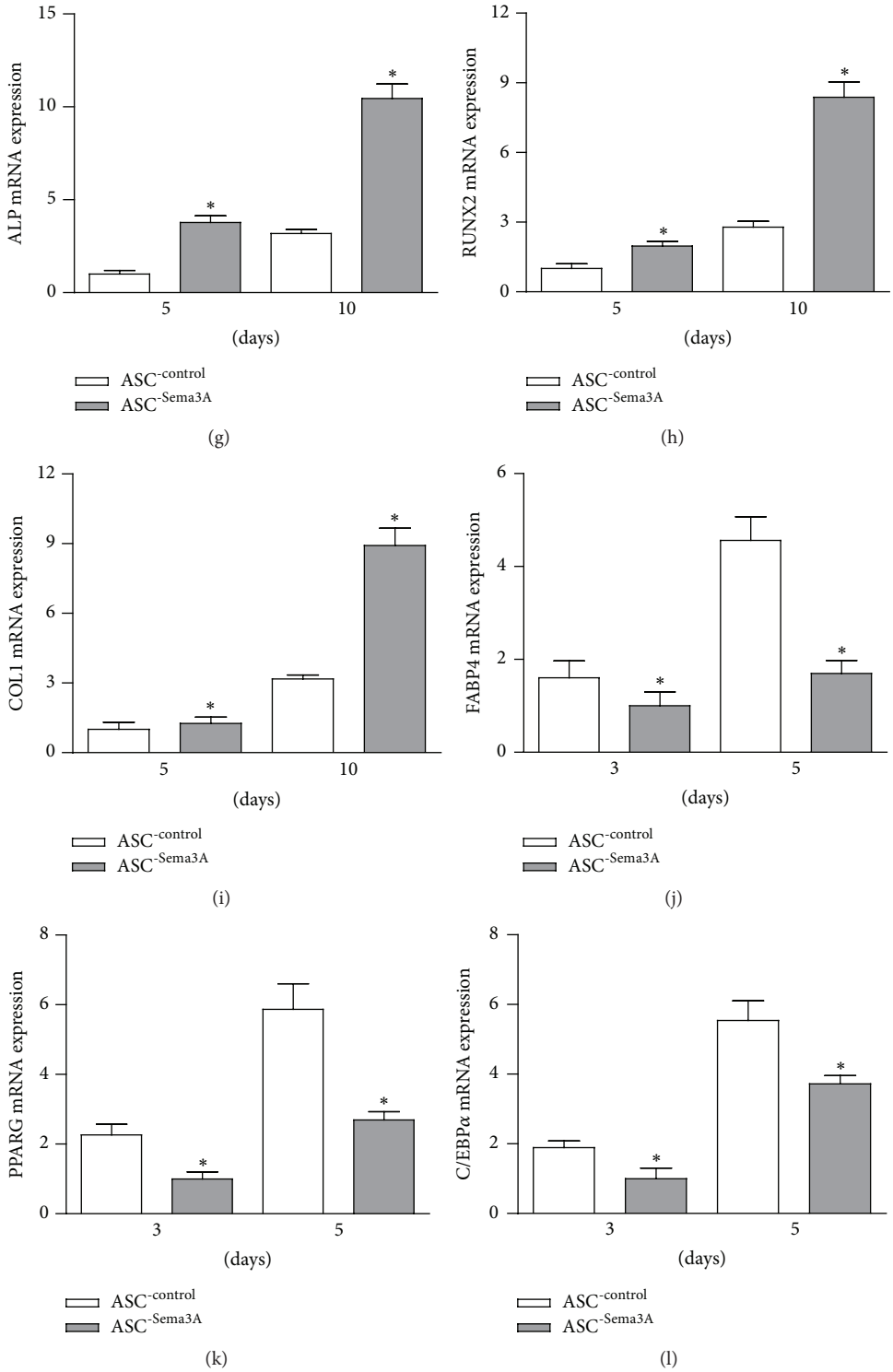

Figure 2: Sema3A promotes osteogenic differentiation while inhibiting adipogenic differentiation in ASCs. (a) ASCs were infected with either empty pWPI or Sema3A overexpression lentivirus, respectively. $ASC^{-Sema3A}$ showed higher ALP activity than $ASC^{-control}$ after 7-day osteogenic induction. (b) Quantification data of ALP activity. (c) Significantly more mineralization nodules were found in $ASC^{-Sema3A}$ group than that in $ASC^{-control}$ group after 21 days of osteogenic induction. (d) Quantification data of ECM mineralization in Figure 2(c). (e) Sema3A significantly reduced lipid droplet formation in ASCs after 9 days of adipogenic induction. (f) Quantification data of lipid droplets in Figure 2(e). (g, h, and i) Expression of the osteogenesis related genes including ALP, RUNX2, and COL-1 after 5 and 10 days of osteogenic induction. (j, k, and l) Expression of the adipogenesis related genes including FABP4, PPARG, and C/EBPA after 3 and 5 days of adipogenic induction. Mean ± SD, $n = 3$, and $^{*}p < 0.05$.

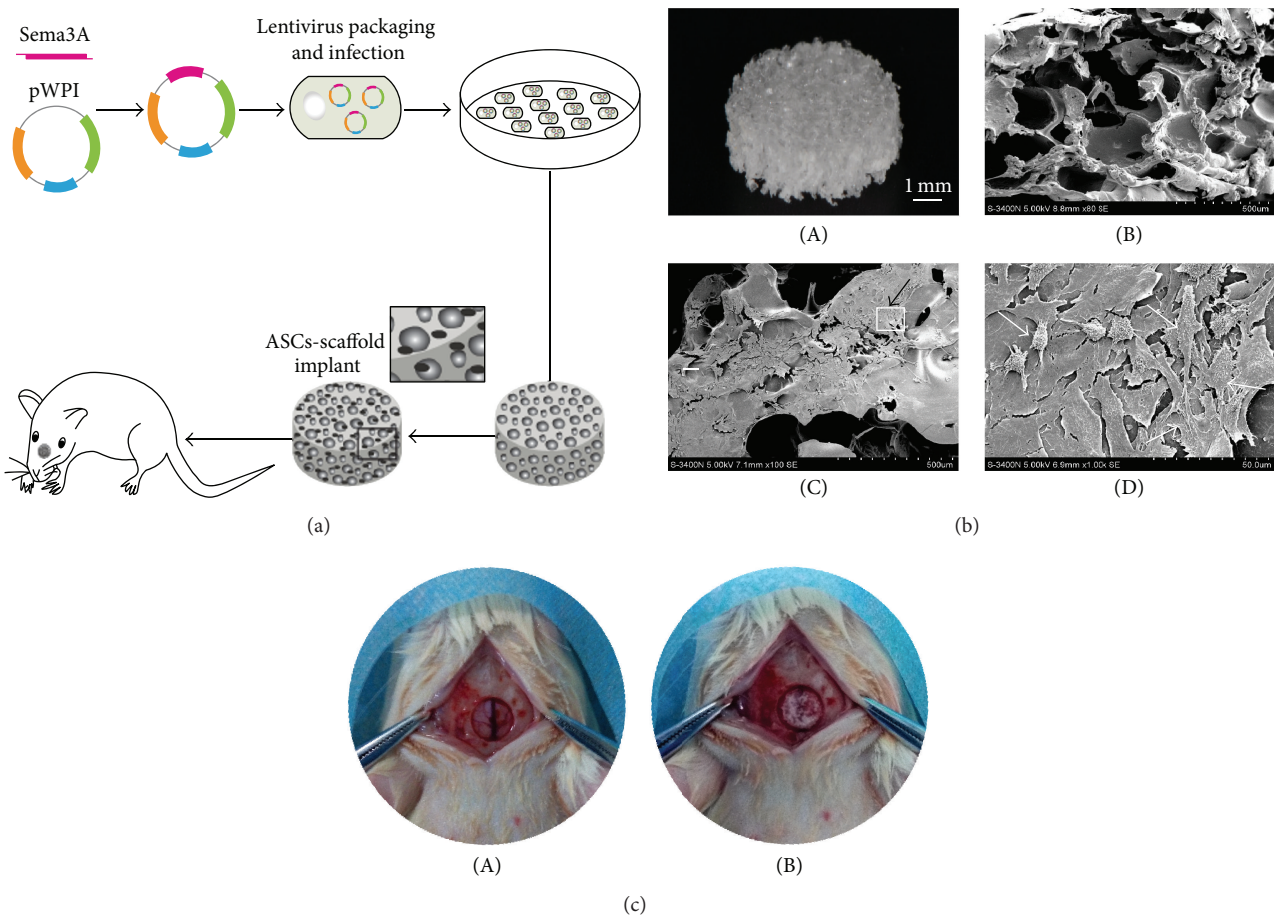

Figure 3: The fabrication of PLGA scaffolds engrafted with ASCs. (a) Schematic diagram of experiment procedure. (b) The morphology of PLGA scaffold-ASCs implants: (A) gross observation, (B) the lateral view of the scaffold without cells observed by SEM, (C) the surface view of the scaffold-ASCs implants under SEM, and (D) magnification to the inset in Figure 3(b)(C) and the cells were indicated by white arrow. (c) The critical size bone defect before (A) and after the transplantation of scaffold- ASCs implants (B).

BMSCs (Figures 1(c) and 1(d), Supplementary Figures 1A-B). Sema3A decreased with aging, while Sema3D did not change significantly in the aging process (Figures 1(c) and 1(d), Supplementary Figures 1A-B). In addition, the absolute abundance of Sema3D in BMSCs was much smaller than Sema3A in BMSCs (data not shown). Taken together, we proposed that Sema3A might be an important molecular determinant for the osteogenic differences between ASCs and BMSCs.

3.2. Overexpression of Sema3A Shifts the Cells towards Osteogenic Phenotype. In view of the above-mentioned data, we next explored the possible role of Sema3A in osteogenesis and adipogenesis. Control and Sema3A expressing lentivirus were packaged using the pWPI lentivirus system. ASCs were infected with the lentivirus at MOI = 100, and the infection efficiency was confirmed by the simultaneous expression of EGFP as detected by flow cytometry (Supplementary Figure 2A). Q-PCR and western blot analysis further confirmed the overexpression efficiency (Supplementary Figures 2B-C).

With the increase of Sema3A in ASCs, both ALP activity and deposition of calcified extracellular matrix were increased, as detected by ALP assay and Alizarin Red staining results (Figures 2(a)-2(d)). In contrast, Oil Red O staining revealed that Sema3A overexpression reduced the adipogenesis of ASCs (Figures 2(e) and 2(f)). The Sema3A induced osteogenesis shift was further confirmed by qPCR analysis of the osteogenic and adipogenic marker genes.

As expected, osteogenic markers, including ALP, Runx2, and Col1a1, were significantly higher in Sema3A overexpressing ASCs, after both 5-day and 10-day osteogenic inductions (Figures 2(g)–2(i)). In contrast, the adipogenic marker genes, including FABP4, PPARG, and C/EBPA, were significantly suppressed by Sema3A expression after both 3-day and 5-day adipogenic inductions (Figures 2(j)–2(l)). Consistent with the osteogenesis promoting role of Sema3A, knockdown of Sema3A in BMSCs by siRNA significantly decreased the osteogenic capacity of BMSCs, as revealed by the Alizarin Red staining (Supplementary Figures 3A–C).

3.3. PLGA Scaffold Encapsulated with Sema3A Modified ASCs Promotes Bone Regeneration In Vivo. We next explored

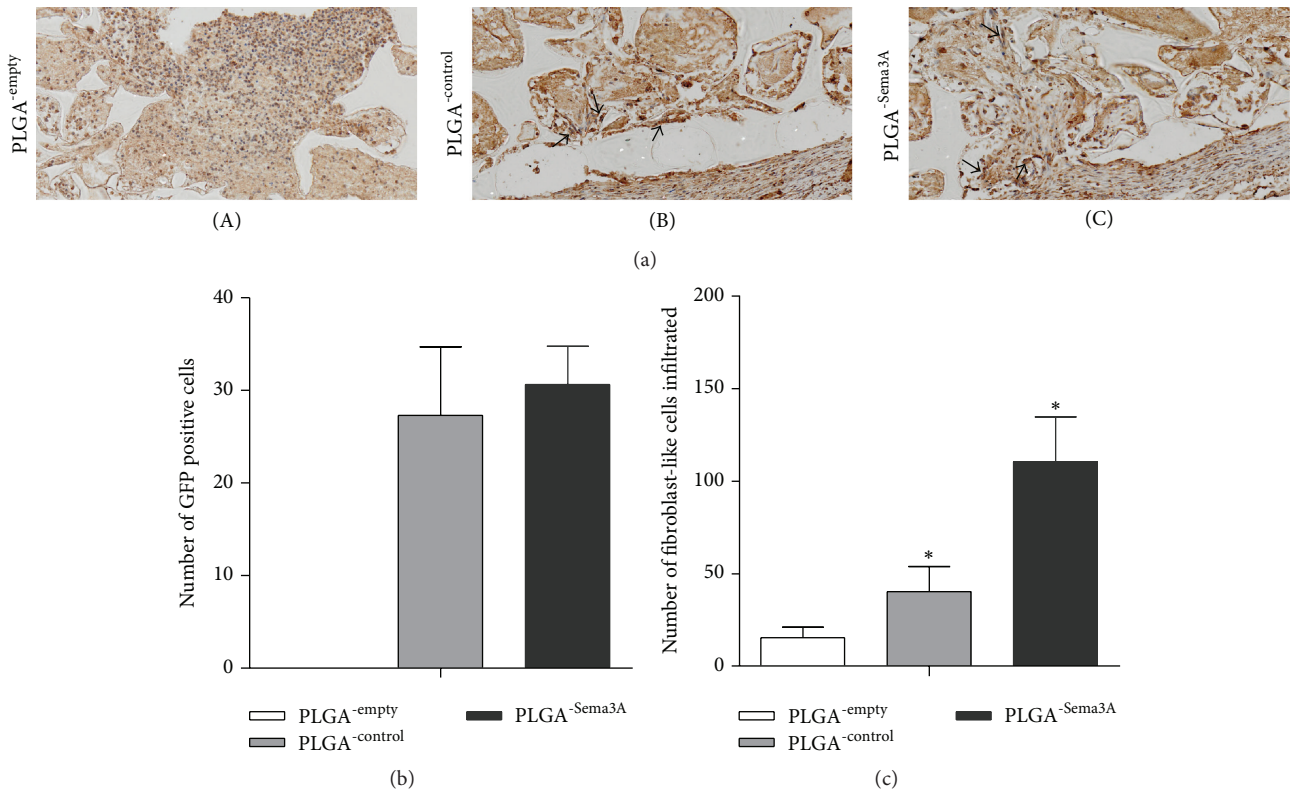

Figure 4: Sema3A infected ASCs decrease the immune cell infiltration while increasing fibroblast-like cells migrated to the implants. (a) The scaffolds were harvested 5 days after transplantation and immune-stained with collagen. (A) No GFP^+ fibroblast-like cells were found in the empty implants and multiple inflammatory cells were shown, (B) a small fraction of fibroblast-like cells were found in implants seeded with $ASC^{-control}$, and (C) Multiple fibroblast-like cells were found migrated and migrating towards the scaffold in implants seeded with $ASC^{-Sema3A}$. (b) Quantification data of survival GFP^+ ASCs in the scaffold. (c) Quantification data of migrated fibroblast-like cells. Mean ± SD, $n = 3$, and $^* p < 0.05$.

whether Sema3A modified ASCs could promote bone regeneration in vivo in the calvarial bone defect model, with the detailed procedure summarized in Figure 3(a). PLGA scaffold was fabricated in a round mold, with the diameter of 5 mm and thickness of 1 mm, and the porous structure of the scaffold was achieved by soaking the sodium particles into the PLGA solution. SEM analysis confirmed the porous structure (Figure 3(b)). After culture of the ASCs on the scaffold for about 24 hours, abundant ASCs attached and spread out onto the porous surface of the scaffold, as observed under SEM (Figure 3(b)). Then, the scaffolds were transplanted into the bone defect region, which fitted well with the critical size bone defect (Figure 3(c)).

Five days after transplantation, the scaffolds were harvested for analyzing the cell survival and infiltration. As seen in the histology and collagen staining of the scaffold sections, there were abundant immune cells infiltrated in the PLGA scaffolds without ASCs. In contrast, there are few immune cells infiltrated in the PLGA scaffolds encapsulated with control or Sema3A modified ASCs (Figure 4(a)). Additionally, Sema3A modified ASCs recruited abundant collagen positive cells towards the scaffold (Figures 4(a) and 4(c)). Notably, Sema3A did not alter the survival of encapsulated ASCs in the scaffold, as no significant differences in the number of fluorescent positive cells were observed between the implants loaded with $ASCs^{-Sema3A}$ or $ASCs^{-control}$ (Figure 4(b)).

Furthermore, we analyzed the bone repair efficacy in vivo at both 4 weeks and 12 weeks after transplantation by histology and microCT. MicroCT reconstruction images indicated that the PLGA scaffolds encapsulated with $ASCs^{-Sema3A}$ induced the largest new bone formation at both 4 weeks and 12 weeks, with minimal defects left at 12 weeks after transplantation (Figure 5(a)). Different from the Sema3A group, PLGA only and PLGA with control ASCs only had marginal bone repair promoting effects (Figure 5(a)). Quantitative analysis further revealed that PLGA scaffolds encapsulated with $ASCs^{-Sema3A}$ increased the bone volume fraction but may not by changing trabecular thickness (Figures 5(b) and 5(c)).

Consistent with the microCT findings, histology analysis revealed that PLGA scaffold degraded significantly at 4 weeks after transplantation, and meanwhile new bone formation began (Figure 6). Although no significant differences were found in the matrix deposited at 4 weeks after transplantation, there was a trend that there were more cell components and matrix in the PLGA scaffolds encapsulated with $ASCs^{-Sema3A}$. Twelve weeks after transplantation, the

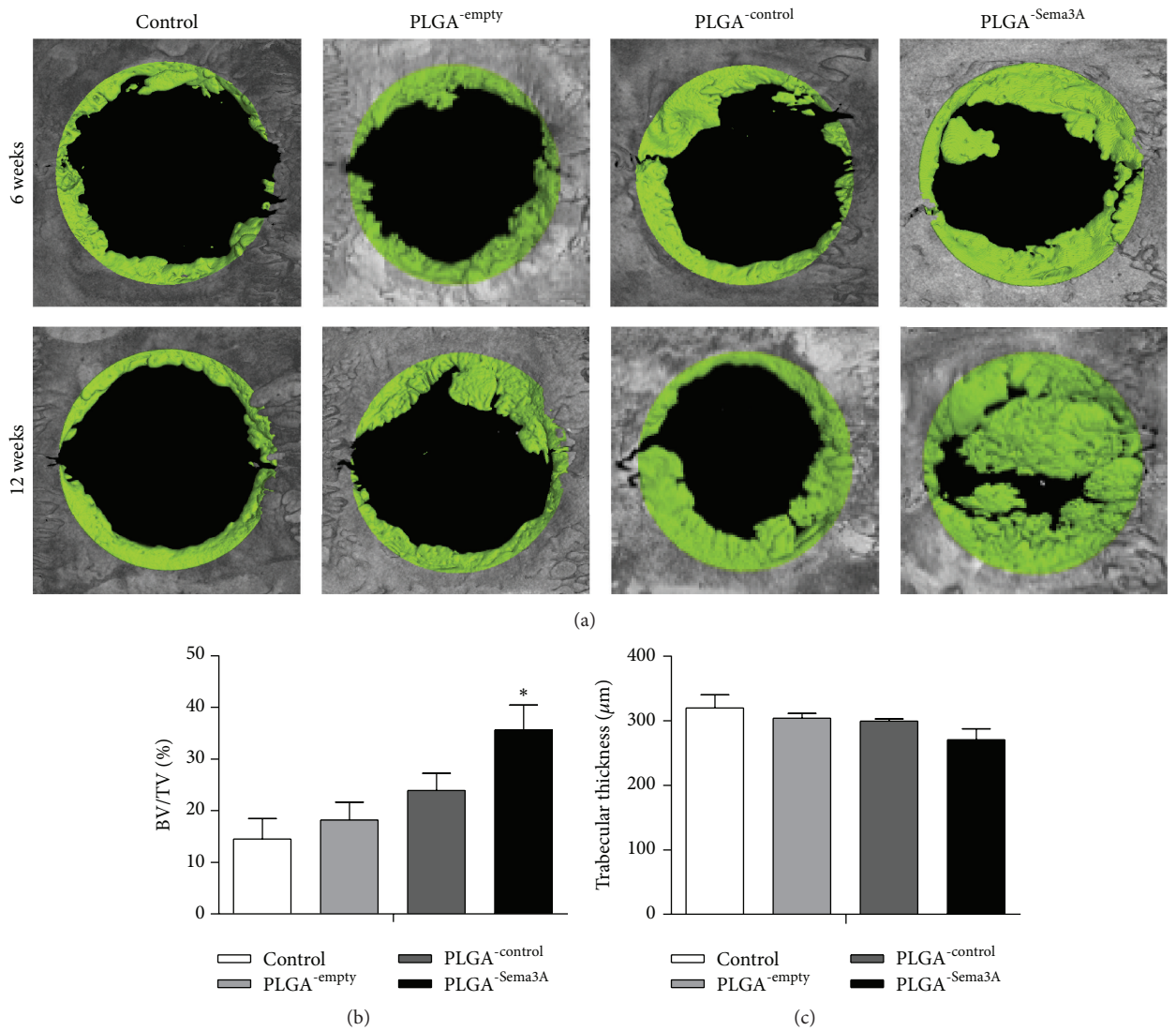

FIGURE 5: ASC$^{-Sema3A}$ engrafted PLGA scaffold increases bone repair in the calvarial defect model. (a) Representative images showing bone defect healing after 4 or 16 weeks of treatments. Control indicates that defects received nothing; PLGA^{-empty}, PLGA$^{-control}$, and PLGA$^{-Sema3A}$ indicate that defects implanted with ASC, ASC$^{-control}$, and ASC$^{-Sema3A}$, respectively. BV/TV (b) and trabecular thickness (c) of the regenerated bone 16 weeks after transplantation. Mean ± SD, $n = 5$, and $^{*}p < 0.05$. BV, bone volume; TV, total volume.

ASCs$^{-Sema3A}$ scaffold group showed the most abundant regenerated bone, which almost filled up the cranium defect. In contrast, the newly formed bones were much less in other groups, although ASCs$^{-control}$ scaffold group also had robust bone repair when compared with the control and PLGA only group (Figure 6).

3.4. Sema3A Reprograms the ASCs towards BMSCs at Least Partially via Wnt Activation. From the above PLGA scaffold mediated bone regeneration data, we could see that Sema3A promotes bone regeneration in vivo via shifting ASCs towards BMSCs. Besides cell fate shift, Sema3A seems inducing cell recruitment while not changing the ASCs numbers in vivo. To further explore the underlying mechanisms, we then tested the effects of Sema3A on proliferation and migration. Consistent with in vivo data, no significant difference on proliferation was observed upon Sema3A overexpression (Figure 7(a)). Furthermore, the conditioned medium from Sema3A infected ASCs induced a significant increase of mesenchymal stem cell migration (Figures 7(b) and 7(c)). Taken together, we could draw the conclusions that Sema3A promotes bone regeneration in vivo via simultaneously shifting ASCs towards BMSCs and inducing robust mesenchymal stem cell recruitment.

Previously, Wnt pathway was found to be essential in tipping the balance towards osteogenesis in mesenchymal stem cells [33]. We thus tested whether Wnt pathway was involved in the function of Sema3A. Topflash/Fopflash plasmids, a reporter system for Wnt activity, were included. As shown from the TOP/FOP ratio, Sema3A significantly increased the Wnt activity (Figure 7(d)). Consistent with the reporter

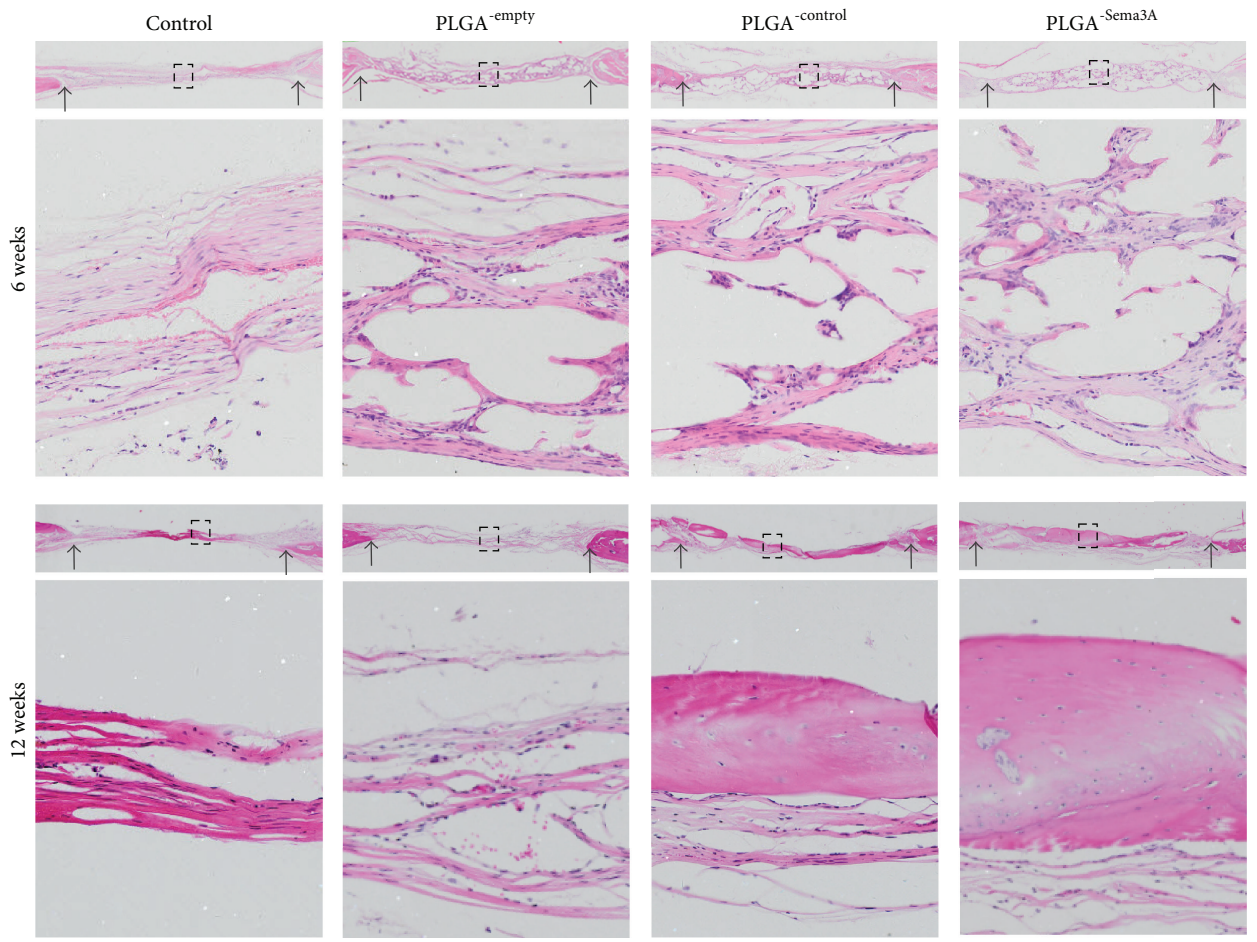

Figure 6: ASC$^{-Sema3A}$ engrafted PLGA scaffold increases bone repair in the calvarial defect model. Bone regeneration of calvarial defects evaluated by HE staining. Control indicates that defects received nothing; PLGA^{-empty}, PLGA$^{-control}$, and PLGA$^{-Sema3A}$ indicate that defects implanted with ASC, ASC$^{-control}$, and ASC$^{-Sema3A}$, respectively. Data presented are representative HE staining images from 5 different experiments. Black arrows point to the defect margins, and the lower panels are the magnifications of the insets in each group.

assay, nuclei β-catenin staining was significantly increased in the Sema3A infected ASCs (Figure 7(e)). In addition, a few upstream and downstream Wnt pathway genes, like Wnt3a, Wnt10a, and Axin2, were found to be increased in Sema3A infected cells (Figures 7(f)–7(h)). All of these data sets suggest that Sema3A activates Wnt pathway through coordinately regulating multiple Wnt pathway genes.

4. Discussion

Our study here for the first time indicates that the implants combining the Sema3A modified ASCs with osteoinductive PLGA scaffolds successfully promote bone defect repair in a critical size cranium defect model, as revealed by both micro-CT and histological evidence. Mechanistically, Sema3A acts as a potent osteogenesis inducer via reprogramming ASCs towards osteogenesis in a Wnt dependent manner.

Bone defect repair capacity is affected by various factors including the age, metabolic status of the subjects, and the site, size, and shape of the injury [34–36]. Critical size bone defect could not be repaired without medical intervention. Current therapeutic approaches include autogenous or allogeneic bone graft and bone substitutes [2, 3]. In the bone substitutes field, tissue engineering bone has become the focus, and PLGA is an excellent osteoinductive scaffold candidate with porous structure, excellent compatibility property, and some plasticity. Accordingly, our in vivo and vitro studies here further confirmed the applicability of PLGA scaffold in bone repair and regeneration.

Besides the scaffold, the seeding cell is another essential component of the tissue engineered bone substitute. The origin and identity of the seeded cells directly influence the output of tissue engineered bone [37]. Seed cell usually refers to stem cells in tissue engineering, which contains various types, among which BMSCs and ASCs are the common ones2. Both BMSCs and ASCs are thought mainly of pericyte origin [38, 39] and consist of an heterogeneous cell populations without specific cell markers [40–42]. These two cell types also display distinct biological features. Previous researches have shown that the differentiation tendency of mesenchymal stem cell is related to its tissue origin, with

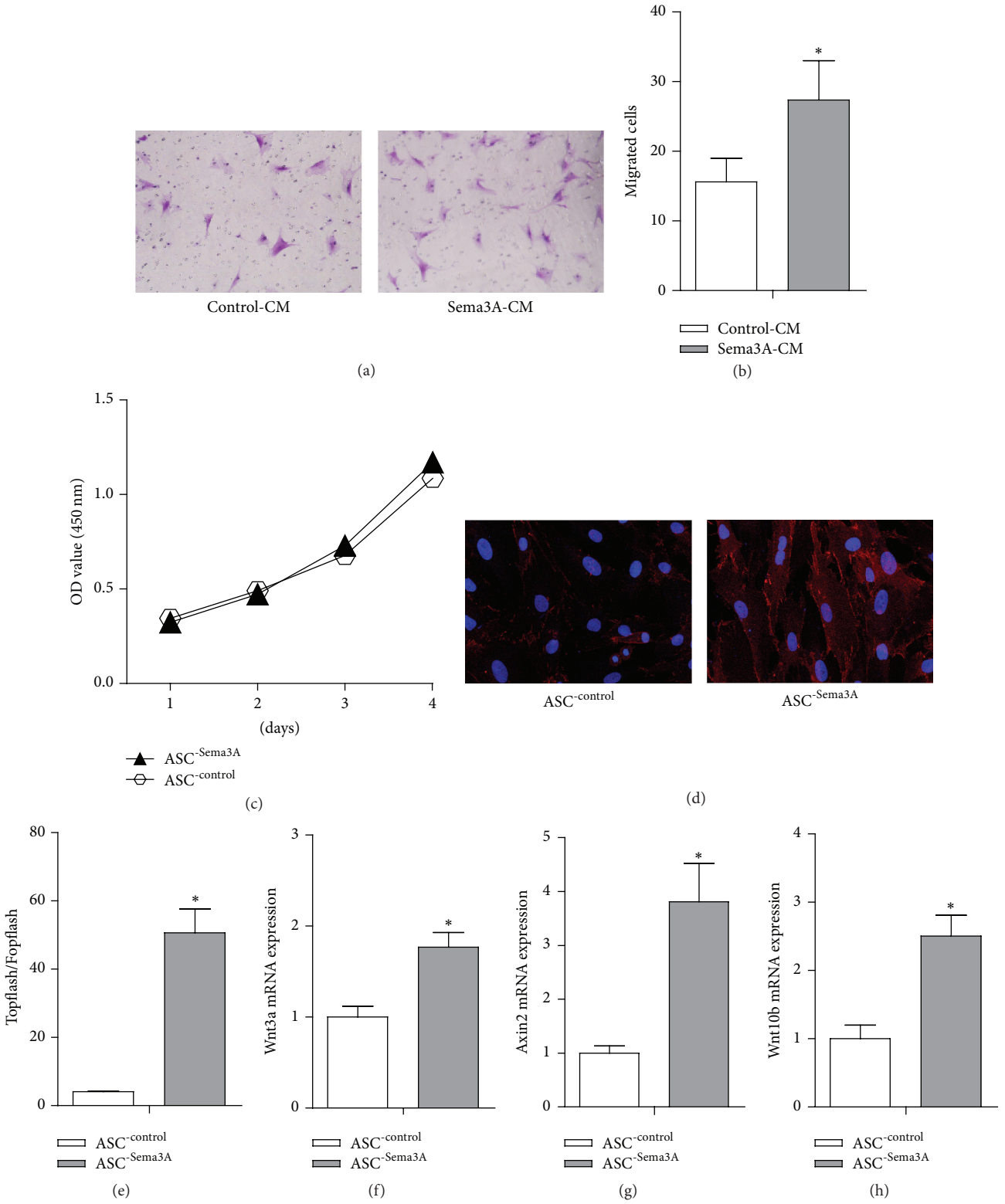

FIGURE 7: Sema3A significantly activates Wnt/β-catenin pathway in ASCs. (a) Conditioned medium from the Sema3A infected cells increased the migrated cells number. (b) Quantitative analysis of migrated cells in Figure 7(a). (c) No significant differences were found in the proliferation rate between $ASC^{-control}$ and $ASC^{-Sema3A}$. (d) Immunofluorescence staining of β-catenin in control and Sema3A overexpressed ASCs, and Sema3A induced nuclear translocation of β-catenin. (e) Sema3A overexpression significantly increased the Topflash/Fopflash ratio, indicating activation of Wnt pathway. (f, g, and h) The mRNA expression analysis of the Wnt pathway related genes and downstream transcriptional targets of β-catenin in control and Sema3A overexpressed ASCs. Mean ± SD, $n = 3$, and $^{*}p < 0.05$. CM, conditioned medium.

BMSCs tending to differentiate into osteoblasts, while ASCs are sensitive to adipogenic differentiation [11, 13]. BMSCs work efficiently in bone repair as observed in animal experiments and clinical studies [43]; however, the limited resources restrict its clinical application. Different from BMSCs, ASCs are readily available and closely related to BMSCs. Identification of the molecules responsible for the differences would certainly shed light on fine-tuning the cell identity towards the destination beneficial for bone regeneration. We here screened the semaphorin family members in BMSCs and ASCs. Among the semaphorins 3A, 3B, 3C, 3D, 3E, 3F, 4A, 4B, 4C, 4D, 4F, 4G, 5A, 5B, 6A, 6B, 6C, 6D, and 7A, Sema3A was identified as the key differential expression molecule. Consistent with previous concept that Sema3A promotes osteogenesis [24], we also found that restoration of Sema3A in ASCs promotes ASC osteogenic differentiation. Moreover, we found that expression of Sema3A in ASCs from 12-month old rats was further decreased, when compared with that in ASCs from 4-week old rats. All of these data sets confirm that Sema3A acts as a key determining factor for the different osteogenic capacity between BMSCs and ASCs. Accordingly, we transfected ASCs with Sema3A and explored its capacity in bone defect repair. In vitro analysis revealed that ASCs$^{\text{-Sema3A}}$ increased the osteogenesis, migration, concomitant with decreased adipogenic potential. ASCs$^{\text{-Sema3A}}$ grafted PLGA scaffold exhibits distinctly enhanced bone matrix secretion in the cranial bone defect model. These functional changes initiated by Sema3A transfection indicate that Sema3A could induce a BMSCs phenotype in ASCs.

To further clarify the detailed molecular mechanism of how Sema3A reprograms ASCs to BMSCs like phenotype, we here focused on the role of Wnt/β-catenin signaling pathway which is closely relevant to both osteogenic differentiation and adipogenic differentiation [33, 44]. Our data revealed that Wnt/β-catenin activation was at least partially involved in the function of Sema3A. The findings here are consistent with the accumulating evidence revealing that Wnt is essential for promoting osteogenesis and inhibiting adipogenesis [33, 44]. However, we cannot exclude other possible signal molecules involved. In fact, Sema3A itself is an endocrine factor and could function as a chemotaxis inducer in different systems [44]. It is thus reasonable to hypothesize that increasing cell recruitment of endogenous MSCs might be another function of Sema3A modified ASCs in our system. Systemic analysis of the gene expression of ASCs, Sema3A modified ASCs, and BMSCs would further solidify our conclusion. In addition, encapsulation of Sema3A factor in the PLGA scaffold in cranial bone defect model would further pave the way for Sema3A application in bone repair.

5. Conclusion

Our study here has identified that high expression of Sema3A in BMSCs is essential for its potent osteogenic capacity, which functions as a determinant of the BMSC phenotype. Transferring Sema3A into ASCs at least partially reprograms the cells towards BMSCs and thus increases the osteogenic capacity via Wnt activation and possibly other mechanisms. Encapsulation of Sema3A modified ASCs in the PLGA scaffold significantly increased the bone defect repairing efficacy, which provides a promising strategy to overcome the limit resource of BMSCs in bone regeneration and repair.

Competing Interests

The authors declare no competing interests.

Acknowledgments

This study was funded by the Nature Science Foundation of China ((NSFC) Nos. 81470775, 81170984, 81271579, and 81300918).

References

[1] C.-H. Lu, Y.-H. Chang, S.-Y. Lin, K.-C. Li, and Y.-C. Hu, "Recent progresses in gene delivery-based bone tissue engineering," *Biotechnology Advances*, vol. 31, no. 8, pp. 1695–1706, 2013.

[2] T. Uemura, J. Dong, Y. Wang et al., "Transplantation of cultured bone cells using combinations of scaffolds and culture techniques," *Biomaterials*, vol. 24, no. 13, pp. 2277–2286, 2003.

[3] R. Cancedda, P. Giannoni, and M. Mastrogiacomo, "A tissue engineering approach to bone repair in large animal models and in clinical practice," *Biomaterials*, vol. 28, no. 29, pp. 4240–4250, 2007.

[4] L. Watson, S. J. Elliman, and C. M. Coleman, "From isolation to implantation: a concise review of mesenchymal stem cell therapy in bone fracture repair," *Stem Cell Research and Therapy*, vol. 5, article 51, 2014.

[5] G. Asatrian, D. Pham, W. R. Hardy, A. W. James, and B. Peault, "Stem cell technology for bone regeneration: current status and potential applications," *Stem Cells and Cloning: Advances and Applications*, vol. 8, pp. 39–48, 2015.

[6] P. A. Zuk, M. Zhu, P. Ashjian et al., "Human adipose tissue is a source of multipotent stem cells," *Molecular Biology of the Cell*, vol. 13, no. 12, pp. 4279–4295, 2002.

[7] P. A. Zuk, "The adipose-derived stem cell: looking back and looking ahead," *Molecular Biology of the Cell*, vol. 21, no. 11, pp. 1783–1787, 2010.

[8] C.-Y. Li, X.-Y. Wu, J.-B. Tong et al., "Comparative analysis of human mesenchymal stem cells from bone marrow and adipose tissue under xeno-free conditions for cell therapy," *Stem Cell Research and Therapy*, vol. 6, no. 1, article 55, 2015.

[9] H. H. Ahn, K. S. Kim, J. H. Lee et al., "In vivo osteogenic differentiation of human adipose-derived stem cells in an injectable in situ-forming gel scaffold," *Tissue Engineering—Part A*, vol. 15, no. 7, pp. 1821–1832, 2009.

[10] A. H. Kisiel, L. A. McDuffee, E. Masaoud, T. R. Bailey, B. P. Esparza Gonzalez, and R. Nino-Fong, "Isolation, characterization, and in vitro proliferation of canine mesenchymal stem cells derived from bone marrow, adipose tissue, muscle, and periosteum," *American Journal of Veterinary Research*, vol. 73, no. 8, pp. 1305–1317, 2012.

[11] P. Niemeyer, K. Fechner, S. Milz et al., "Comparison of mesenchymal stem cells from bone marrow and adipose tissue for bone regeneration in a critical size defect of the sheep tibia and the influence of platelet-rich plasma," *Biomaterials*, vol. 31, no. 13, pp. 3572–3579, 2010.

[12] B.-J. Kang, H.-H. Ryu, S. S. Park et al., "Comparing the osteogenic potential of canine mesenchymal stem cells derived from adipose tissues, bone marrow, umbilical cord blood, and Wharton's jelly for treating bone defects," *Journal of Veterinary Science*, vol. 13, no. 3, pp. 299–310, 2012.

[13] A. Lotfy, M. Salama, F. Zahran, E. Jones, A. Badawy, and M. Sobh, "Characterization of mesenchymal stem cells derived from rat bone marrow and adipose tissue: a comparative study," *International Journal of Stem Cells*, vol. 7, no. 2, pp. 135–142, 2014.

[14] S. Gronthos, D. M. Franklin, H. A. Leddy, P. G. Robey, R. W. Storms, and J. M. Gimble, "Surface protein characterization of human adipose tissue-derived stromal cells," *Journal of Cellular Physiology*, vol. 189, no. 1, pp. 54–63, 2001.

[15] F. Guilak, K. E. Lott, H. A. Awad et al., "Clonal analysis of the differentiation potential of human adipose-derived adult stem cells," *Journal of Cellular Physiology*, vol. 206, no. 1, pp. 229–237, 2006.

[16] L. Hu, G. Yang, D. Hägg et al., "IGF1 promotes adipogenesis by a lineage bias of endogenous adipose stem/progenitor cells," *Stem Cells*, vol. 33, no. 8, pp. 2483–2495, 2015.

[17] M. Yamamoto, H. Nakata, J. Hao, J. Chou, S. Kasugai, and S. Kuroda, "Osteogenic potential of mouse adipose-derived stem cells sorted for CD90 and CD105 in Vitro," *Stem Cells International*, vol. 2014, Article ID 576358, 17 pages, 2014.

[18] T. Reya, S. J. Morrison, M. F. Clarke, and I. L. Weissman, "Stem cells, cancer, and cancer stem cells," *Nature*, vol. 414, no. 6859, pp. 105–111, 2001.

[19] B. P. Hung, D. L. Hutton, K. L. Kozielski et al., "Platelet-derived growth factor BB enhances osteogenesis of adipose-derived but not bone marrow-derived mesenchymal stromal/stem cells," *STEM CELLS*, vol. 33, no. 9, pp. 2773–2784, 2015.

[20] X. Zhang, J. Guo, G. Wu, and Y. Zhou, "Effects of heterodimeric bone morphogenetic protein-2/7 on osteogenesis of human adipose-derived stem cells," *Cell Proliferation*, vol. 48, no. 6, pp. 650–660, 2016.

[21] B. C. Jongbloets and R. Jeroen Pasterkamp, "Semaphorin signalling during development," *Development*, vol. 141, no. 17, pp. 3292–3297, 2014.

[22] G. Delorme, F. Saltel, E. Bonnelye, P. Jurdic, and I. Machuca-Gayet, "Expression and function of semaphorin 7A in bone cells," *Biology of the Cell*, vol. 97, no. 7, pp. 589–597, 2005.

[23] T. Negishi-Koga, M. Shinohara, N. Komatsu et al., "Suppression of bone formation by osteoclastic expression of semaphorin 4D," *Nature Medicine*, vol. 17, no. 11, pp. 1473–1480, 2011.

[24] M. Hayashi, T. Nakashima, M. Taniguchi, T. Kodama, A. Kumanogoh, and H. Takayanagi, "Osteoprotection by semaphorin 3A," *Nature*, vol. 485, no. 7396, pp. 69–74, 2012.

[25] T. Fukuda, S. Takeda, R. Xu et al., "Sema3A regulates bone-mass accrual through sensory innervations," *Nature*, vol. 497, no. 7450, pp. 490–493, 2013.

[26] R. Xu, "Semaphorin 3A a new player in bone remodeling," *Cell Adhesion & Migration*, vol. 8, no. 1, pp. 5–10, 2014.

[27] S. Saad, A. A. S. S. K. Dharmapatni, T. N. Crotti et al., "Semaphorin-3a, neuropilin-1 and plexin-A1 in prosthetic-particle induced bone loss," *Acta Biomaterialia*, vol. 30, pp. 311–318, 2016.

[28] S. Khosla, J. J. Westendorf, and U. I. Mödder, "Concise review: insights from normal bone remodeling and stem cell-based therapies for bone repair," *Stem Cells*, vol. 28, no. 12, pp. 2124–2128, 2010.

[29] J. Tang and T. Saito, "Effect of dentine phosphophoryn-derived RGD peptides on odontoblast-like cells," *International Endodontic Journal*, vol. 49, no. 7, pp. 670–683, 2016.

[30] M. Zavatti, L. Bertoni, T. Maraldi et al., "Critical-size bone defect repair using amniotic fluid stem cell/collagen constructs: effect of oral ferutinin treatment in rats," *Life Sciences*, vol. 121, pp. 174–183, 2015.

[31] J. Kim, W.-J. Oh, N. Gaiano, Y. Yoshida, and C. Gu, "Semaphorin 3E-plexin-d1 signaling regulates VEGF function in developmental angiogenesis via a feedback mechanism," *Genes and Development*, vol. 25, no. 13, pp. 1399–1411, 2011.

[32] W. Joo, L. Sweeney, L. Liang, and L. Luo, "Linking cell fate, trajectory choice, and target selection: genetic analysis of sema-2b in olfactory axon targeting," *Neuron*, vol. 78, no. 4, pp. 673–686, 2013.

[33] R. Baron and M. Kneissel, "WNT signaling in bone homeostasis and disease: from human mutations to treatments," *Nature Medicine*, vol. 19, no. 2, pp. 179–192, 2013.

[34] J. O. Hollinger and J. C. Kleinschmidt, "The critical size defect as an experimental model to test bone repair materials," *The Journal of Craniofacial Surgery*, vol. 1, no. 1, pp. 60–68, 1990.

[35] E. Gibon, L. Lu, and S. B. Goodman, "Aging, inflammation, stem cells, and bone healing," *Stem Cell Research & Therapy*, vol. 7, article 44, 2016.

[36] K. F. Moseley, "Type 2 diabetes and bone fractures," *Current Opinion in Endocrinology, Diabetes and Obesity*, vol. 19, no. 2, pp. 128–135, 2012.

[37] Y. J. Jeon, J. Kim, J. H. Cho, H. M. Chung, and J. I. Chae, "Comparative analysis of human mesenchymal stem cells derived from bone marrow, placenta, and adipose tissue as sources of cell therapy," *Journal of Cellular Biochemistry*, vol. 117, no. 5, pp. 1112–1125, 2016.

[38] A. I. Caplan, "All MSCs are pericytes?" *Cell Stem Cell*, vol. 3, no. 3, pp. 229–230, 2008.

[39] A. Armulik, G. Genové, and C. Betsholtz, "Pericytes: developmental, physiological, and pathological perspectives, problems, and promises," *Developmental Cell*, vol. 21, no. 2, pp. 193–215, 2011.

[40] S. Sauerzweig, T. Munsch, V. Leßmann, K. G. Reymann, and H. Braun, "A population of serumdeprivation-induced bone marrow stem cells (SD-BMSC) expresses marker typical for embryonic and neural stem cells," *Experimental Cell Research*, vol. 315, no. 1, pp. 50–66, 2009.

[41] R. D. González-Cruz and E. M. Darling, "Adipose-derived stem cell fate is predicted by cellular mechanical properties," *Adipocyte*, vol. 2, no. 2, pp. 87–91, 2014.

[42] D. C. de Almeida, M. R. P. Ferreira, J. Franzen et al., "Epigenetic classification of human mesenchymal stromal cells," *Stem Cell Reports*, vol. 6, no. 2, pp. 168–175, 2016.

[43] L.-H. Chiu, W.-F. T. Lai, S.-F. Chang et al., "The effect of type II collagen on MSC osteogenic differentiation and bone defect repair," *Biomaterials*, vol. 35, no. 9, pp. 2680–2691, 2014.

[44] G. Chen, J. Sima, M. Jin et al., "Semaphorin-3A guides radial migration of cortical neurons during development," *Nature Neuroscience*, vol. 11, no. 1, pp. 36–44, 2008.

Hindawi Publishing Corporation
Stem Cells International
Volume 2016, Article ID 9378081, 18 pages
http://dx.doi.org/10.1155/2016/9378081

Research Article

Characterization of Cellular and Molecular Heterogeneity of Bone Marrow Stromal Cells

Mona Elsafadi,[1,2] Muthurangan Manikandan,[1] Muhammad Atteya,[1,3] Jamil Amjad Hashmi,[4] Zafar Iqbal,[5] Abdullah Aldahmash,[1,6] Musaad Alfayez,[1] Moustapha Kassem,[1,2] and Amer Mahmood[1,2]

[1]*Stem Cell Unit, Department of Anatomy, College of Medicine, King Saud University, Riyadh, Saudi Arabia*
[2]*Molecular Endocrinology Laboratory (KMEB), Department of Endocrinology, University of Southern Denmark, Odense, Denmark*
[3]*Department of Histology, Faculty of Medicine, Cairo University, Egypt*
[4]*Center for Genetics and Inherited Diseases, Taibah University, Al-Madina Al-Munawara, Saudi Arabia*
[5]*College of Applied Medical Sciences, King Saud Bin Abdulaziz University for Health Sciences (KSAU-HS), National Guards Health Affairs, Riyadh, Saudi Arabia*
[6]*Prince Naïf Health and Research Center, College of Medicine, King Saud University, Riyadh, Saudi Arabia*

Correspondence should be addressed to Amer Mahmood; ammahmood@ksu.edu.sa

Received 14 April 2016; Accepted 26 May 2016

Academic Editor: Giorgio Mori

Copyright © 2016 Mona Elsafadi et al. This is an open access article distributed under the Creative Commons Attribution License, which permits unrestricted use, distribution, and reproduction in any medium, provided the original work is properly cited.

Human bone marrow-derived stromal stem cells (hBMSC) exhibit multiple functions, including differentiation into skeletal cells (progenitor function), hematopoiesis support, and immune regulation (nonprogenitor function). We have previously demonstrated the presence of morphological and functional heterogeneity of hBMSC cultures. In the present study, we characterized in detail two hTERT-BMSC clonal cell populations termed here CL1 and CL2 that represent an opposing phenotype with respect to morphology, markers expression: alkaline phosphatase (ALP) and CD146, and *ex vivo* differentiation potential. CL1 differentiated readily to osteoblasts, adipocytes, and chondrocytes as shown by expression of lineage specific genes and proteins. Whole genome transcriptome profiling of CL1 versus CL2 revealed enrichment in CL1 of bone-, mineralization-, and skeletal muscle-related genes, for example, *ALP*, *POSTN*, *IGFBP5 BMP4*, and *CXCL12*. On the other hand, CL2 transcriptome was enriched in immune modulatory genes, for example, *CD14, CD99, NOTCH3, CXCL6, CFB*, and *CFI*. Furthermore, gene expression microarray analysis of osteoblast differentiated CL1 versus CL2 showed significant upregulation in CL1 of bone development and osteoblast differentiation genes which included several homeobox genes: *TBX15, HOXA2* and *HOXA10*, and *IGF1, FGFR3, BMP6, MCAM, ITGA10, IGFBP5*, and *ALP*. siRNA-based downregulation of the *ALP* gene in CL1 impaired osteoblastic and adipocytic differentiation. Our studies demonstrate the existence of molecular and functional heterogeneity in cultured hBMSC. ALP can be employed to identify osteoblastic and adipocytic progenitor cells in the heterogeneous hBMSC cultures.

1. Introduction

Human bone marrow stromal (also known as skeletal or mesenchymal) stem cells (hBMSC) are increasingly employed in clinical trials for enhancing tissue regeneration following injury [1]. Typically, hBMSC are isolated by their ability to adhere to the plastic surfaces of *in vitro* culture plates. However, the cultured hBMSC exhibit morphological heterogeneity suggesting the presence of functional heterogeneity [2, 3]. It has also been suggested that the use of heterogeneous cell populations in clinical trials of hBMSC-based therapies caused variability in the observed treatment effects [4]. Thus, for the efficient use of hBMSC in therapy, better cellular and molecular characterization of hBMSC is required [1, 4].

There exist no specific markers that define the hBMSC phenotype. The plastic-adherent hBMSC are defined by the presence of surface expression of some CD surface markers with variable sensitivity and specificity [1]. Single cell clonal analysis revealed that only 25% of the cells are true stem cells based on their ability to differentiate into osteoblasts,

adipocytes, and chondrocytes (trilineage differentiation) and to form heterotopic bone and bone marrow organ when implanted *in vivo* subcutaneously in immune deficient mice [5]. The identity of the remaining cells is not clarified, but they may represent lineage-committed cells [3]. Therefore, it is plausible that functional heterogeneity exists in cultured hBMSC, reflecting the *in vivo* functional and developmental heterogeneity of hBMSC [6].

In addition to their ability to differentiate into skeletal tissue cells (known as progenitor function), hBMSC possess immunomodulatory characteristics (known as nonprogenitor functions) [7]. It is not clear whether these different functions are mediated by a number of independent subpopulations within the hBMSC [2]. Only a few studies have tried to identify the subpopulation within cultured hBMSC based on surface markers, for example, STRO1 and alkaline phosphatase (ALP), but limited molecular phenotyping has been conducted [8].

We have previously demonstrated the presence of morphological and functional heterogeneity of clones isolated from telomerized hMSC (hMSC-TERT) cell line [3]. The aim of the present study was therefore to further study in detail the heterogeneity of cultured hBMSC as demonstrated by two clonal cell lines with opposite cellular and functional phenotype. We also employed the DNA microarrays to define their molecular signature and signaling pathways associated with their functional phenotype.

2. Experimental Procedures

2.1. Cell Culture. As a model for hBMSC, we employed immortalized hBMSC-TERT cell line that is created from normal human BMSC by overexpression of human telomerase reverse transcriptase gene (hTERT) [9]. The hBMSC-TERT cells have been extensively characterized, and they exhibit similar cellular and molecular phenotype to primary MSC [10]. CL1 and CL2 cells are clonal cell populations of hBMSC-TERT identified in long term culture (passage numbers 15–25) of hBMSC-TERT and were chosen based on their distinct and different morphologies. Cells were cultured in Dulbecco's Modified Eagle Medium (DMEM) supplemented with D-glucose 4500 mg/L, 4 mM L-glutamine and 110 mg/L sodium pyruvate, 10% Fetal Bovine Serum (FBS), 1x penicillin-streptomycin (Pen-strep), and nonessential amino acids (all purchased from Gibco-Invitrogen, USA). For some control experiments, primary bone marrow derived MSC (phBMSC) were employed. Sixty milliliters of bone marrow was aspirated from the iliac crest bone of consenting healthy donors. This procedure was approved by the King Khalid University Hospital-King Saud University ethics committee. phBMSC were isolated from bone marrow mononuclear cells by plastic adherence as described previously [9].

2.2. Cell Proliferation. Cell proliferation rate was determined by counting cell number and calculating population doubling (PD) rate. The cells were cultured in 25 cm^2 tissue culture Petri dish at cell density 0.5×10^6 cells (28000 cells/cm^2). At confluence, the cells were trypsinized and counted manually by hemocytometer. At each passage, population doubling was determined by the following formula: $\log N / \log 2$, where N is the number of cells at confluence divided by the initial cell number. Cumulative PD level is the sum of population doublings, and PD rate is PD/time in culture.

2.3. Flow Cytometry. Cells were trypsinized to a single cell suspension, were recovered by centrifugation at 200 g for 5 min, washed twice in ice-cold PBS supplemented with 2% BSA, and resuspended at a concentration of 10^5 cells/antibody. After incubation with the preconjugated antibodies, or matched isotype controls, for 30 min on ice in the dark, cells were washed with PBS, resuspended in 500 μL of PBS, and analyzed in the BD FACSCalibur flow cytometer (BD Biosciences). Living cells were gated in a dot plot of forward versus side scatter signals acquired on a linear scale. At least 10,000 gated events were acquired on a log fluorescence scale. Positive staining was distinct as the emission of a fluorescence signal that surpassed levels achieved by >99% of control cell population stained with corresponding isotype antibodies. The ratios of fluorescence signals versus scatter signals were calculated, and histograms were generated using the software Cell Quest Pro Software Version 3.3 (BD Biosciences). The following antibodies were used all from BD Biosciences: FITC-PE-APC-Mouse IgG1k isotype control, APC-Mouse Anti-Human CD44 (#559942), FITC-Mouse Anti-Human CD63 (#557305), PE-Mouse Anti-Human CD73 (#550257), PE-Mouse Anti-Human CD105 (#560839), PE-Mouse Anti-Human CD146 (#550315), PE-Mouse Anti-Human CD166 (#560903), and Alexa Fluor® 488 Mouse Anti-Human Alkaline Phosphatase (#561495).

2.4. Electron Microscopy. After trypsinizing the hBMSC cells from the flasks or 6-well plates were collected, the samples were washed with PBS, and the pellets were resuspended directly in 2.5% glutaraldehyde in 0.1 M phosphate buffer (pH 7.2), and kept at 4°C for 4 hr. First, the cells were washed with 0.1 M phosphate buffer (pH 7.2) and transferred to 1% osmium tetroxide (OsO4) solution in 0.1 M phosphate buffer (pH 7.2) for two hr. The cells were dehydrated in ascending grades of ethanol. The cells were then resuspended in acetone and were aliquoted into BEEM embedding capsules and infiltrated with acetone: resin mixture followed by embedding in a pure resin mixture for two hr. Semithin sections (0.5 μm thickness) and ultrathin sections (70 nm thickness) were prepared, examined, and photographed under a transmission electron microscope (TEM) (Jeol 1010, Jeol, Tokyo, Japan).

2.5. In Vitro Osteoblast Differentiation. Cells were grown in standard DMEM growth medium in 6-well plates at 20,000 cell/cm^2. When 70–80% confluence was achieved, test cells were cultured in DMEM supplemented with osteoblastic induction mixture (referred to as OS) containing 10% FBS, 1% Pen-strep, 50 μg/mL L-ascorbic acid (Wako Chemicals, Neuss, Germany), 10 mM β-glycerophosphate (Sigma) and 10 nM calcitriol (1α,25-dihydroxyvitamin D3; Sigma), and 10 nM dexamethasone (Sigma); noninduced cells (referred to as Cont) were cultured in normal growth media for the same duration as induced. The media were replaced three times per week. Cells cultured in standard culture medium were considered as control. At day 14 of differentiation,

mineralized nodules became apparent and were stained with Alizarin Red S and ALP.

2.6. In Vitro Adipocyte Differentiation. Cells were grown in standard DMEM growth medium in 6-well plates at 0.3 $\times 10^6$ cells/mL. At 90–100% confluence, cells were cultured in DMEM supplemented with adipogenic (Adip) induction mixture containing 10% FBS, 10% Horse Serum (Sigma), 1% Pen-strep, 100 nM dexamethasone, 0.45 mM isobutyl methylxanthine (Sigma), 3 μg/mL insulin (Sigma), and 1 μM Rosiglitazone (Novo Nordisk, Bagsvaerd, Denmark). The media were replaced three times per week. Cells cultured in standard culture medium were considered as control. From day 3 of differentiation, small lipid droplets became visible and at day 7 they were stained with Oil Red-O and Nile red.

2.7. In Vitro Chondrogenic Differentiation. Both CL1 and CL2 cells were trypsinized and counted, around 1×10^6 cells taken in each 15 mL conical tube centrifuged at 400 ×g for 5 minutes. For chondrocyte differentiation pellet culture system used, chondrocyte induction was done in media containing advanced DMEM/F12 supplemented with 1% ITS Premix Tissue Culture Supplement, 100 nM dexamethasone, Glutamax, and 10 ng/mL transforming growth factor-beta-3 (TGFβ-3). Cells were maintained in chondrocyte differentiation media for 21 days and changed every two days.

2.8. Cytochemical Staining

2.8.1. Alkaline Phosphatase (ALP) Staining. CL1 and CL2 cells were stained before OS differentiation for the basal ALP expression and after OB differentiation at day 7 of induction. Cells cultured in 6-well plates were washed in PBS −/− (-Ca, -Mg) and fixed in acetone/citrate buffer 10 mM at pH 4.2 for 5 min at room temperature. The Naphthol/Fast Red stain [0.2 mg/mL Naphthol AS-TR phosphate substrate (Sigma)] [0.417 mg/mL of Fast Red (Sigma)] was added for one hour at room temperature.

Histological tissue blocks were sectioned at 4 microns. Immunohistochemical staining was performed on CL1 and CL2 chondrocyte 3D pellets using DAKO EnVision and PowerVision according to the manufacturer's instructions (DAKO, Glostrup, Denmark). Briefly, paraffin sections were incubated for 1 hour at room temperature with primary antibodies diluted in ChemMate (DAKO) (Human Anti-Col-10 and Human Anti-Col-2 ABI). Sections were washed subsequently in Tris-buffered saline (TBS, 0.05 M, pH 7.4), incubated for 30 minutes with secondary anti-mouse Ig/HRP-conjugated polymers (K4001, En Visionþ, DAKO), and visualized with 3,30-diaminobenzidine tetrahydrochloride (DAB, S3000, DAKO) or with 3-amino-9-ethylcarbazole (AEC, DAKO) according to manufacturer's instruction. Controls were performed with nonimmune immunoglobulins of the same isotype as the primary antibodies (negative controls) and processed under identical conditions. Alcian blue staining was used to detect chondrocytes. Sections of paraffin-embedded implants were stained with Alcian blue (Sigma) solution, pH 2.5; at this pH all the glycoproteins (neutral and acidic) will be stained blue.

2.9. Alizarin Red S Staining for Mineralized Matrix. Seven-day-old OS differentiated cells in 6-well plates were used for Alizarin Red S staining. The cell layer was washed with PBS and then fixed with 70% ice-cold ethanol for 1 hr at −20°C. After removing the ethanol, the cell layer was rinsed with distilled water and stained with 40 nM AR-S (Sigma) pH 4.2 for 10 minutes at room temperature. Excess dye was washed off with water followed by a wash with PBS for few minutes to minimize nonspecific AR-S stain.

For quantifying the Alizarin Red S staining, the air-dried plates, the Alizarin Red S dye was eluted in 800 μL of acetic acid incubated in each well for 30 minutes at room temperature as described [11] and measured in spectrophotometer (BioTek, Epoch) at 405 nm.

2.10. Quantitative ALP Activity. To quantify ALP activity in CL1 and CL2 hBMSC before and after OS differentiation, we used the BioVision ALP activity colorimetric assay kit (BioVision, Inc, CA, USA) with some modifications. Cells were cultured in 96-well plates under normal conditions; then on day of analysis, wells were rinsed once with PBS and were fixed using 3.7% formaldehyde in 90% ethanol for 30 seconds at room temperature. Subsequently, fixative was removed, and 50 μL of pNPP solution was added to each well and incubated for 1 hour in the dark at room temperature. The reaction was subsequently stopped by adding 20 μL stop solution and gently shaking the plate. OD was then measured at 405 nm.

2.11. Oil Red-O Staining for Lipid Droplets. CL1 and CL2 cells differentiated to adipocytes with Adip induction media at day 7 were used. Accumulated cytoplasmic lipid droplets were visualized by staining with Oil Red-O. After washing cells grown in 6-well plates with PBS, the cells were fixed in 4% formaldehyde for 10 min at room temperature and then rinsed once with 3% isopropanol and stained for 1 hr at room temperature with filtered Oil Red-O staining solution (prepared by dissolving 0.5 g Oil Red-O powder in 60% isopropanol). To quantify staining of fat droplets, Oil Red-O was used as a stain. Oil Red-O was eluted by adding 100% isopropanol to each well, and color changes were measured by spectrophotometer at 510 nm (BioTek Spectrophotometer, Epoch).

2.12. Nile Red Fluorescence Determination and Quantification of Adipogenesis. A stock solution of Nile red (1 mg/mL) in DMSO was prepared and stored at −20°C protected from light. Staining was performed on unfixed cells. Cultured undifferentiated and day 7 adipocyte differentiated cells were grown in Corning polystyrene; flat bottom 96-well TC-treated black microplates (Corning, NY, USA) were washed once with PBS. The dye was then added directly to the cells (5 μg/mL in PBS), and the preparation was incubated for 10 min at room temperature and then washed twice with PBS. Fluorescent signal was measured using SpectraMax/M5 fluorescence spectrophotometer plate reader (Molecular Devices Co, Sunnyvale, CA, USA) using bottom well-scan mode where nine readings were taken per well using Ex (485 nm) and Em (572 nm) spectra.

2.13. Quantitative Real-Time PCR (qRT-PCR) Analysis. Total RNA was extracted using MagNA pure compact RNA isolation kit (Roche Applied Science, Germany, Cat number 04802993001) in an automated MagNA pure compact system (Roche, Germany) as recommended by the manufacturer. The total RNA was quantified by Nanodrop spectrophotometer (Nanodrop 2000, Thermo Scientific, USA). Complementary DNA (cDNA) was synthesized from 1 μg of the RNA samples using High Capacity cDNA Reverse Transcription kit (Applied Biosystems, USA) using Labnet, Multigene thermocycler according to the manufacturer's instructions. Relative levels of mRNA were determined from cDNA by real-time PCR (Applied Biosystems-Real-Time PCR Detection System) with Power SYBR Green PCR kit (Applied Biosystems, UK) according to the manufacturer's instructions. Following normalization to the reference gene GAPDH, quantification of gene expression was carried out using a comparative Ct method, where ΔCt is the difference between the CT values of the target and the reference gene, and fold induction was performed from the control (Cont) for the same time point. Primers (Supplementary Table 1 in Supplementary Material available online at http://dx.doi.org/10.1155/2016/9378081) were obtained from Applied Biosystems (USA) as TAQMAN primers, or previously published primers were used (see Supplementary Table 1).

2.14. DNA Microarray Global Gene Expression Analysis. Four hundred ng of total RNA was used as input for generating biotin-labeled cRNA (Ambion, Austin, TX, United States). cRNA samples were then hybridized onto Illumina® human-8 BeadChips version 3. Hybridization, washing, Cy3-streptavidin staining, and scanning were performed on the Illumina BeadStation 500 platform (Illumina, San Diego, CA, USA), according to the manufacturer's instructions, and everything was done in triplicate. Expression data analysis was carried out using the Partek® genomic suite software. Raw data were background-subtracted, normalized using the "rank invariant" algorithm, and filtered for significant expression on the basis of negative control beads. Genes were considered significantly expressed with detection p values ≤ 0.01. Differential expression analysis was performed with the Illumina custom method using freshly isolated primary hBMSC (used at passage 3) as a reference control. The following parameters were set to identify statistical significance: differential p values ≤ 0.01; fold change ratio > 1.5. Pathway analysis was performed using DAVID Bioinformatics Resources 6.7 (http://david.abcc.ncifcrf.gov/) and GeneSpring GX software (Agilent Technologies). Pathway analysis for CL1 OS D14 versus CL2 OS D14 was conducted using the Single Experiment Pathway analysis feature in GeneSpring 12.0 (Agilent Technologies).

2.15. Small Interfering (si)RNA Transfection. For transfection, hBMSC in logarithmic growth phase were transfected with Silencer Select Predesigned ALP siRNA (25 nM) (Assay ID; s1298 and Cat number 4390824) (Ambion, The RNA Company, USA) using Lipofectamine RNAiMAX Reagent (Invitrogen, CA, USA) plus serum-free Opti-MEM®I medium under the conditions described by the manufacturer. At day 3 of transfection, the cells were induced for osteogenic differentiation for an additional 7 days. ALP staining was used as a control for the siRNA transfection efficiency and timeline.

2.16. Statistical Analysis. All of the results were presented as the mean and standard deviation (SD) of at least 3 independent experiments, with 3–5 technical repeats in each experiment. Student's t-test (two-tailed) was used for testing differences between groups. p value <0.05 was considered statistically significant.

3. Results

3.1. Comparison between CL1 and CL2: Differences in Morphology, Proliferation, and Marker Expression Profile. We isolated two distinct clonal cell populations of hBMSC-TERT: hBMSC-CL1 and hBMSC-CL2 (for easiness will be termed hereafter CL1 and CL2) based on differences in cell morphology (Figure 1(a)). CL1 cells had cuboidal morphology whereas CL2 cells have spindle-shaped fibroblast-like morphology. CL1 cells had higher proliferation rate compared to CL2 (Figure 1(b)): mean PD rates of CL1 and CL2 were 0.714 and 0.429 PD/day, respectively (Figure 1(b)). Both CL1 and CL2 expressed surface marker profiles characteristics of hBMSC (>90%): CD44+, CD63+, CD73+, CD105+, and CD166+ (Figure 1(c)). However CL1 cells showed higher expression of CD146 (92.7% versus 12%) and ALP (98% versus 0%) compared to CL2 (Figure 1(d)). TEM revealed the presence of abundant pseudopodia in CL1 indicating high motility (Figure 1(e)(A)) as well as well-developed mitochondria and rough endoplasmic reticulum (rER) suggesting high metabolic activity. CL2 cells contained abundant phagocytic vacuole (pv), microvilli (mi), and lysosomes (ly) (Figure 1(e)).

We performed quantitative real-time PCR (RT-PCR) for genes expressed in mesodermal progenitor cells [12]. CL1 expressed higher levels of BMP4, MIXL1, WNT3a, and TWIST compared to CL2 (Figure 1(f), $p < 0.01$). In contrast, CL2 expressed higher levels of Kinase Insert Domain Receptor (Type III Receptor Tyrosine Kinase) (KDR) expressed in endothelial cells and smooth muscle myosin heavy chain gene (smMHC) expressed in smooth muscle cells (Figure 1(f)).

3.2. CL1 Cells Exhibit Enhanced Osteoblast Differentiation. Following osteoblast (OB) differentiation induction, ALP staining and ALP enzymatic activity were significantly higher in CL1 compared to CL2 cells (Figure 2(a), $p < 0.01$). Similarly, Alizarin Red staining and quantitation of formed mineralized matrix were more pronounced in CL1 cells (Figure 2(b), $p < 0.01$). In addition, CL1 cells expressed higher levels of osteoblastic genes, ALP, RUNX2, and osteopontin (OPN) (Figure 2(c) upper panel) compared to CL2 cells.

Global gene expression microarray analysis of OB differentiated cells at day 14 showed around 1060 genes significantly upregulated more than 2-fold ($p < 0.01$) in CL1. Among the upregulated genes, 80 genes were annotated to bone development and osteoblast differentiation (Table 1). The highest upregulated genes included paired-like homeodomain 2 (PITX2), Insulin-like growth factor 1 (IGF1) and

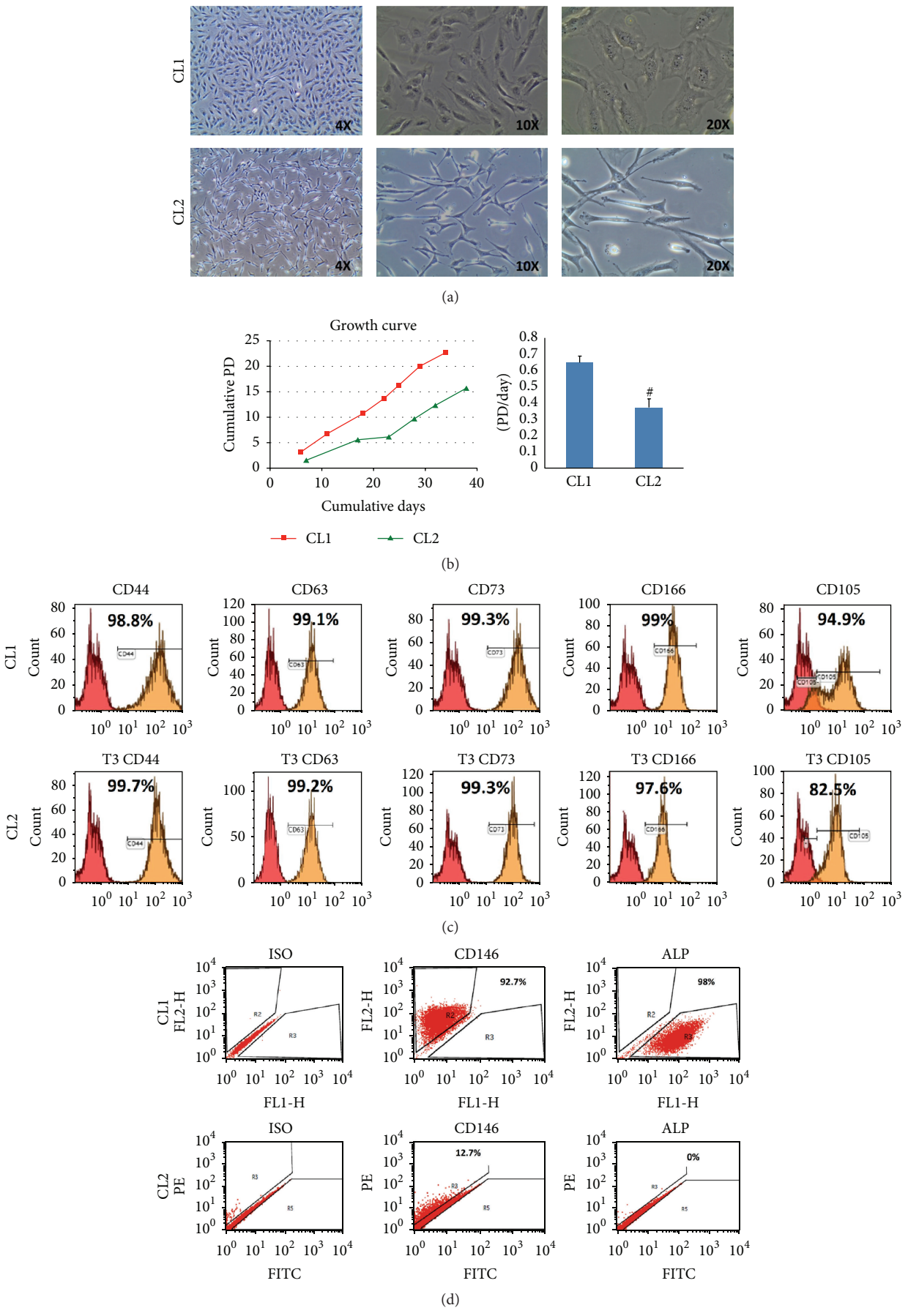

Figure 1: Continued.

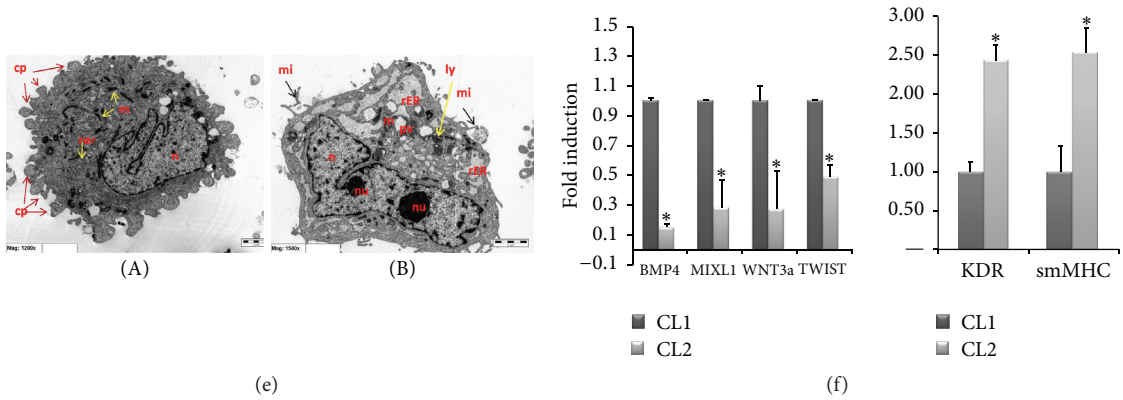

Figure 1: Cellular phenotype of two clonal populations of human bone marrow stromal stem cells: CL1 and CL2. (a) Cell morphology. CL1 cells showed large cuboidal morphology while CL2 cells had spindle-shaped fibroblast-like morphology. (b) Growth curves showing population doubling (PD) rate during long term culture. (c) Flow cytometry analysis (FACS) shows expression of CD44, CD63, CD73, CD105, and CD166 in CL1 and CL2 cells. Matched isotype control was used for gating. (d) Flow cytometry analysis presented as dot blot of CD146 and alkaline phosphatase (ALP) cell surface proteins. (e) Transmission electron microscope (TEM). (A): CL1 (1200x); (B): CL2 (1500x). n: nucleus, nu: nucleolus, rER: rough endoplasmic reticulum, ly: lysosomes, pv: phagocytic vacuole, and rer: reticular stalk of rER. (f) Gene expression analysis using RT-PCR for a group of mesodermal and stromal genes. Gene expression was normalized to GAPDH and presented as fold change. Data is shown as mean ± SD of three independent experiments. $^{*}p < 0.05$; $^{\#}p < 0.001$.

collagen, type V, alpha 3 (COL5A3), osteomodulin (OMD), and T-box 15 (TBX15) (Table 1). Furthermore, several known osteoblast-related genes were upregulated in CL1 cells such as bone morphogenetic protein 6 (BMP6), fibroblast growth factor receptor 3 (FGFR3), insulin-like growth factor binding protein 5 (IGFBP5), and vitamin D (1,25-dihydroxyvitamin D3) receptor (VDR) (Table 1). On the other hand, 1200 genes were upregulated in CL2 cells: 255 genes were annotated to immunity and immune response and defense. This category included genes from, complement system, chemokine (C-C motif) ligands, interferon family, chemokine (C-X-C motif) ligands, and receptor, major histocompatibility complex class II molecules, interleukins, and tumor necrosis factor receptor superfamily (Table 2 and Supplementary Table 3).

3.3. CL1 Cells Exhibit Enhanced Adipocyte Differentiation. We observed significant differences between CL1 and CL2 in their response to adipocytic differentiation induction. CL1 differentiated readily to adipocytes compared to CL2 (Figure 2(d), lower panel) evidenced by higher levels of adipocytic markers gene expression, LPL (lipoprotein lipase), and adiponectin, as well as formation of mature lipid filled adipocytes visualized by Oil Red-O staining and quantitative Nile red staining (Figure 2(d)).

3.4. CL1 Cells Differentiate to Chondrocytic Lineage. In pellet cultures, CL1 cells formed 3D pellets containing proteoglycan-secreting chondrocytes, which stained positive with Alcian blue. Limited chondrocyte differentiation was visible in cell pellets of CL2 cells. The differentiated chondrocytes in CL1 pellets expressed higher levels of collagen X and collagen II, which was overlapping the Alcian blue stain (Figure 2(e)).

3.5. Molecular Signature of CL1 and CL2 Cells. To define the molecular signature and molecular differences between CL1 and CL2, we compared the basal gene expression pattern of CL1 and CL2 cells using DNA microarrays. The PCA analysis showed a clear separation between CL1 and CL2 (Supplementary Figure 1). Comparison between CL1 with CL2 showed that 915 genes were differentially expressed in the two cell lines (>2-fold, $p < 0.01$): 462 genes were upregulated, and 452 were downregulated in CL1 versus CL2. The most relevant genes that were upregulated in CL1 are listed in Table 3(a). Among these 35 highly expressed genes in CL1, the following 11 genes were present in skeletal and muscular system development and function: FOLR3, CCL3L1, SERPINB2, POSTN, IGFBP5, CCL3, NOV, ALP, TNFRSF11B, ACTG2, and CDH11 (Table 3(a)). Functional annotation of the upregulated genes in CL1 using the Ingenuity Pathway Analysis (IPA) revealed enrichment in the following categories: "tissue development," "skeletal and muscular system development and function," and "organismal development" (Table 3(b)). Furthermore, the DAVID annotation tool was employed to assess the functional relationships of the upregulated genes in CL1 showing enrichment in ontologies: "skeletal and muscular system development and function" that included bone size, osteoblast differentiation, bone mineralization, and bone mineral density (Table 3(c)). CL1 exhibited upregulation of WNT pathway ligands: WNT5B (2-fold) and LRP5 (2-fold) (Table 1). Also, ALP was among the highly expressed genes together with POSTN, IGFBP5, SPP1, IL-6, and DKK1 (Tables 3(a) and 1). These genes are known to play an important role in osteoblast differentiation and bone formation. For CL2, inhibitors of WNT pathway were upregulated and included SFRP1 (11-fold), DKK2 (3.2-fold), FGF2 (3.1-fold), and GBP2 (2.4-fold). Functional annotation of the upregulated genes in CL2 revealed enrichment in the following categories: "developmental process," "multicellular organismal process," "biological adhesion," and "immune system process" (Supplementary Table 2A). In-depth analysis

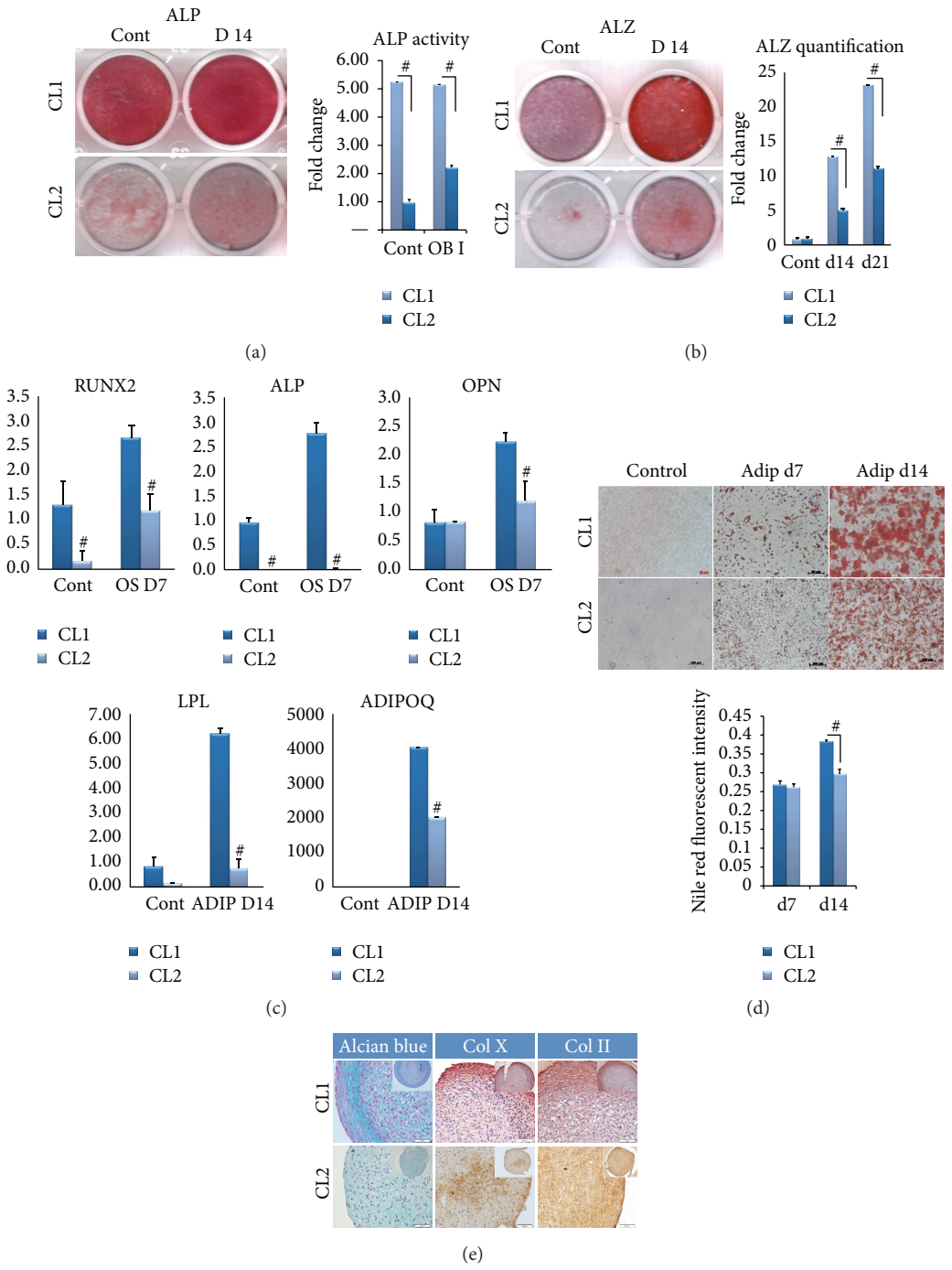

FIGURE 2: *In vitro* osteoblastic and adipocytic differentiation of two clonal populations of human bone marrow stromal stem cells: CL1 and CL2 cells. Both cell lines were induced for osteoblast differentiation using standard protocol described in the Methods. (a) ALP staining at day 14 in control noninduced (Cont) and osteoblast induced cells (D14). Right panel shows ALP activity ($n = 3$ independent experiments, $^{\#}p < 0.001$). (b) Mineralized matrix formation visualized by Alizarin Red S staining. Right panel shows Alizarin Red quantification at day 14 and 21 after osteoblast differentiation ($n = 3$ independent experiments, $^{\#}p < 0.001$). (c) Quantitative RT-PCR of osteoblastic and adipocyte gene markers in CL1 and CL2 during osteoblast (upper panel) and adipocyte (lower panel) differentiation. ALP = alkaline phosphatase, OPN = osteopontin, LPL = lipoprotein lipase, and ADIPOQ = adiponectin. Data are presented as fold change in expression of each target gene normalized to GAPDH ($n = 3$ independent experiments, $p < 0.05$; $^{\#}p < 0.001$). (d) CL1 and CL2 lines were induced for adipocyte differentiation using standard protocol described in the Methods. Adipocyte formation was visualized at day 7 (Adip d7) and day 14 (Adip d14) by Oil Red-O staining. Lower panel presents quantification of Nile red staining ($n = 3$ independent experiments, $^{\#}p < 0.001$). (e) CL1 and CL2 lines were induced for chondrocyte differentiation using 21-day pellet culture method as described in the Methods. The pellets were stained with Alcian blue, collagen 10 (Col X), and collagen 2 (Col II) (original magnification 5x).

Table 1: Microarray data analysis showing genes related to bone development and osteoblast differentiation upregulated in CL1 versus CL2 cells.

Probe ID	Genbank accession	Gene name	Gene symbol	FC
A_23_P167367	NM_153426	Paired-like homeodomain 2	PITX2	308.84
A_23_P13907	NM_000618	Insulin-like growth factor 1 (somatomedin C)	IGF1	118.00
A_23_P55749	NM_015719	Collagen, type V, alpha 3	COL5A3	75.11
A_23_P94397	NM_005014	Osteomodulin	OMD	56.07
A_24_P128442	NM_152380	T-box 15	TBX15	54.38
A_33_P3708413	NM_003480	Microfibrillar associated protein 5	MFAP5	53.73
A_24_P72064	NM_000163	Growth hormone receptor	GHR	51.47
A_23_P215454	NM_001278939	Elastin	ELN	50.15
A_24_P200854	NM_006735	Homeobox A2	HOXA2	44.99
A_23_P19624	NM_001718	Bone morphogenetic protein 6	BMP6	41.43
A_23_P500501	NM_000142	Fibroblast growth factor receptor 3	FGFR3	33.95
A_23_P154605	NM_018837	Sulfatase 2	SULF2	29.57
A_23_P28815	NM_000782	Cytochrome P450, family 24, subfamily A, polypeptide 1	CYP24A1	22.47
A_23_P210109	NM_019885	Cytochrome P450, family 26, subfamily B, polypeptide 1	CYP26B1	22.42
A_23_P323180	NM_006898	Homeobox D3	HOXD3	21.08
A_32_P405759	NM_152888	Collagen, type XXII, alpha 1	COL22A1	20.36
A_33_P3363799	NM_001242607	Neural cell adhesion molecule 1	NCAM1	17.33
A_33_P3381378	NM_001257096	Paired box 1	PAX1	17.12
A_23_P383009	NM_000599	Insulin-like growth factor binding protein 5	IGFBP5	14.67
A_33_P3382856	NM_133507	Decorin	DCN	14.38
A_23_P10206	NM_005328	Hyaluronan synthase 2	HAS2	14.33
A_24_P77904	NM_018951	Homeobox A10	HOXA10	13.64
A_23_P2814	NM_005905	SMAD family member 9	SMAD9	12.45
A_23_P88404	NM_003239	Transforming growth factor, beta 3	TGFB3	12.11
A_32_P4595	NM_000337	Sarcoglycan, delta (35 kDa dystrophin-associated glycoprotein)	SGCD	8.95
A_23_P162171	NM_006500	Melanoma cell adhesion molecule	MCAM	8.60
A_24_P38276	NM_003505	Frizzled class receptor 1	FZD1	7.81
A_23_P24129	NM_012242	Dickkopf WNT signaling pathway inhibitor 1	DKK1	7.04
A_33_P3264528	NM_005523	Homeobox A11	HOXA11	6.64
A_33_P3220470	NM_005585	SMAD family member 6	SMAD6	6.47
A_23_P23783	NM_000261	Myocilin, trabecular meshwork inducible glucocorticoid response	MYOC	6.41
A_33_P3263432	NM_003637	Integrin, alpha 10	ITGA10	6.35
A_23_P383009	NM_000599	Insulin-like growth factor binding protein 5	IGFBP5	6.18
A_33_P3219090	NM_005542	Insulin induced gene 1	INSIG1	5.78
A_23_P162589	NM_001017535	Vitamin D (1,25-dihydroxyvitamin D3) receptor	VDR	5.68
A_23_P374695	NM_000459	TEK tyrosine kinase, endothelial	TEK	5.65
A_24_P261169	NM_006378	Sema domain, immunoglobulin domain (Ig), transmembrane domain (TM), and short cytoplasmic domain, (semaphorin) 4D	SEMA4D	5.41
A_33_P3297930	NM_005202	Collagen, type VIII, alpha 2	COL8A2	5.138
A_23_P206359	NM_004360	Cadherin 1, type 1, E-cadherin (epithelial)	CDH1	5.12
A_24_P264943	NM_000095	Cartilage oligomeric matrix protein	COMP	5.07
A_33_P3214948	NM_014767	Sparc/osteonectin, cwcv, and kazal-like domains proteoglycan (testican) 2	SPOCK2	4.54

Table 1: Continued.

Probe ID	Genbank accession	Gene name	Gene symbol	FC
A_24_P55496	NM_053001	Odd-skipped related transcription factor 2	OSR2	4.38
A_24_P354689	NM_004598	Sparc/osteonectin, cwcv, and kazal-like domains proteoglycan (testican) 1	SPOCK1	4.23
A_23_P69030	NM_001850	Collagen, type VIII, alpha 1	COL8A1	3.93
A_23_P128084	NM_002206	Integrin, alpha 7	ITGA7	3.91
A_24_P3249	NM_000965	Retinoic acid receptor, beta	RARB	3.91
A_24_P168574	AJ224867	GNAS complex locus	GNAS	3.83
A_23_P320739	NM_002397	Myocyte enhancer factor 2C	MEF2C	3.74
A_23_P429383	NM_014213	Homeobox D9	HOXD9	3.54
A_23_P42322	NM_080680	Collagen, type XI, alpha 2	COL11A2	3.42
A_23_P160318	NM_001856	Collagen, type XVI, alpha 1	COL16A1	3.36
A_33_P3407013	NM_000600	Interleukin 6	IL6	3.30
A_23_P315364	NM_002089	Chemokine (C-X-C motif) ligand 2	CXCL2	3.29
A_33_P3413168	BC007696	Collagen, type XXVII, alpha 1	COL27A1	3.08
A_23_P43164	NM_015170	Sulfatase 1	SULF1	3.05
A_23_P58676	NM_001204375	Natriuretic peptide receptor 3	NPR3	3.04
A_33_P3290562	NM_000168	GLI family zinc finger 3	GLI3	3.00
A_23_P69497	NM_003278	C-type lectin domain family 3, member B	CLEC3B	2.99
A_24_P353619	NM_000478	Alkaline phosphatase, liver/bone/kidney	ALPL	2.99
A_33_P3305749	NM_000965	Retinoic acid receptor, beta	RARB	2.89
A_23_P307328	NM_007331	Wolf-Hirschhorn syndrome candidate 1	WHSC1	2.77
A_23_P152305	NM_001797	Cadherin 11, type 2, OB-cadherin (osteoblast)	CDH11	2.77
A_23_P216361	NM_021110	Collagen, type XIV, alpha 1	COL14A1	2.62
A_23_P7313	NM_001040058	Secreted phosphoprotein 1	SPP1	2.60
A_24_P267592	NM_015474	SAM domain and HD domain 1	SAMHD1	2.54
A_23_P210482	NM_000022	Adenosine deaminase	ADA	2.52
A_23_P148047	NM_000958	Prostaglandin E receptor 4 (subtype EP4)	PTGER4	2.51
A_23_P345725	NM_014621	Homeobox D4	HOXD4	2.47
A_24_P125283	NM_001015053	Histone deacetylase 5	HDAC5	2.37
A_33_P3231953	NM_004370	Collagen, type XII, alpha 1	COL12A1	2.34
A_24_P298027	NM_004655	Axin 2	AXIN2	2.31
A_24_P336551	NM_199173	Bone gamma-carboxyglutamate (gla) protein	BGLAP	2.29
A_33_P3313825	XM_006713316	Transforming growth factor, beta receptor II (70/80 kDa)	TGFBR2	2.23
A_23_P82990	NM_033014	Osteoglycin	OGN	2.20
A_32_P24585	NM_001017995	SH3 and PX domains 2B	SH3PXD2B	2.20
A_24_P944458	NM_016133	Insulin induced gene 2	INSIG2	2.14
A_23_P99063	NM_002345	Lumican	LUM	2.12
A_32_P5251	NM_001024809	Retinoic acid receptor, alpha	RARA	2.11
A_24_P935491	NM_000090	Collagen, type III, alpha 1	COL3A1	2.10
A_33_P3312104	NM_025099	CTS telomere maintenance complex component 1	CTC1	2.06
A_33_P3321342	NM_016133	Insulin induced gene 2	INSIG2	2.04
A_23_P100486	NM_206824	Vitamin K epoxide reductase complex, subunit 1	VKORC1	2.02
A_23_P53588	NM_030775	Wingless-type MMTV integration site family, member 5B	WNT5B	2.00
A_23_P616356	NM_001291902	Low density lipoprotein receptor-related protein 5	LRP5	2.00

Table 2: Microarray data analysis showing genes related immune modulation and immune defense genes upregulated in CL2 versus CL1 cells.

ID	Gene name	Gene symbol	Fold change
A_23_P128094	ATP-binding cassette, subfamily B (MDR/TAP), member 9	ABCB9	2.1
A_32_P156963	Actin, gamma 1	ACTG1	3.0
A_23_P28279	ARP1 actin related protein 1 homolog B, centractin beta (yeast)	ACTR1B	2.0
A_23_P211207	Adenosine deaminase, RNA-specific, B1	ADARB1	3.5
A_23_P381261	Adenylate cyclase 4	ADCY4	5.0
A_23_P169993	Adenylate cyclase 8 (brain)	ADCY8	3.2
A_23_P76823	Adenylosuccinate synthase-like 1	ADSSL1	7.0
A_23_P135486	Alpha hemoglobin stabilizing protein	AHSP	2.6
A_23_P216023	Angiopoietin 1	ANGPT1	7.6
A_23_P94501	Annexin A1	ANXA1	2.6
A_23_P121716	Annexin A3	ANXA3	346.8
A_23_P6398	Adaptor-related protein complex 1, beta 1 subunit	AP1B1	2.2
A_23_P120931	Apolipoprotein B mRNA editing enzyme, catalytic polypeptide-like 3C	APOBEC3C	2.2
A_23_P132316	Apolipoprotein B mRNA editing enzyme, catalytic polypeptide-like 3D	APOBEC3D	2.4
A_23_P357101	Apolipoprotein B mRNA editing enzyme, catalytic polypeptide-like 3F	APOBEC3F	2.3
A_23_P143713	Apolipoprotein B mRNA editing enzyme, catalytic polypeptide-like 3G	APOBEC3G	9.6
A_23_P93988	Rho guanine nucleotide exchange factor (GEF) 5	ARHGEF5	8.7
A_24_P20383	Actin related protein 2/3 complex, subunit 4, 20 kDa	ARPC4	2.2
A_23_P208389	AXL receptor tyrosine kinase	AXL	2.0
A_33_P3279353	Azurocidin 1	AZU1	4.8
A_33_P3262043	BCL2-associated agonist of cell death	BAD	2.3
A_24_P159648	BAI1-associated protein 2	BAIAP2	2.2
A_23_P370682	Basic leucine zipper transcription factor, ATF-like 2	BATF2	22.2
A_23_P160720	Basic leucine zipper transcription factor, ATF-like 3	BATF3	3.0
A_33_P3229272	Breast cancer antiestrogen resistance 1	BCAR1	3.3
A_23_P210886	BCL2-like 1	BCL2L1	3.4
A_23_P98350	Baculoviral IAP repeat containing 3	BIRC3	25.0
A_23_P31725	B lymphoid tyrosine kinase	BLK	7.3
A_33_P3419785	BCL2/adenovirus E1B 19 kDa interacting protein 3	BNIP3	7.3
A_19_P00802936	BRICK1, SCAR/WAVE actin-nucleating complex subunit	BRK1	2.2
A_23_P2431	Complement component 3a receptor 1	C3AR1	2.6
A_23_P97541	Complement component 4 binding protein, alpha	C4BPA	2.6
A_23_P92928	Complement component 6	C6	4.0
A_23_P213857	Complement component 7	C7	2.2
A_33_P3745146	Cell adhesion molecule 1	CADM1	34.3
A_23_P250347	Calcium/calmodulin-dependent protein kinase IV	CAMK4	3.4
A_23_P253791	Cathelicidin antimicrobial peptide	CAMP	3.3
A_23_P82324	Caspase recruitment domain family, member 11	CARD11	7.9
A_23_P500433	Caspase recruitment domain family, member 9	CARD9	2.4
A_23_P202978	Caspase 1, apoptosis-related cysteine peptidase	CASP1	2.4
A_23_P123853	Chemokine (C-C motif) ligand 19	CCL19	2.0
A_23_P17065	Chemokine (C-C motif) ligand 20	CCL20	14.6
A_23_P215484	Chemokine (C-C motif) ligand 26	CCL26	2.8
A_23_P503072	Chemokine (C-C motif) ligand 28	CCL28	4.3
A_33_P3316273	Chemokine (C-C motif) ligand 3	CCL3	2.3

Table 2: Continued.

ID	Gene name	Gene symbol	Fold change
A_23_P152838	Chemokine (C-C motif) ligand 5	CCL5	2.7
A_23_P78037	Chemokine (C-C motif) ligand 7	CCL7	16.0
A_23_P207456	Chemokine (C-C motif) ligand 8	CCL8	2.8
A_23_P361773	Cyclin D3	CCND3	2.3
A_33_P3284508	CD14 molecule	CD14	4.2
A_23_P259863	CD177 molecule	CD177	2.7
A_33_P3381513	CD274 molecule	CD274	10.8
A_23_P15369	CD300 molecule-like family member b	CD300LB	2.0
A_23_P416747	CD3e molecule, epsilon (CD3-TCR complex)	CD3E	2.7
A_24_P188377	CD55 molecule, decay accelerating factor for complement (Cromer blood group)	CD55	5.9
A_23_P300056	Cell division cycle 42	CDC42	4.5
A_32_P148710	Cofilin 1 (nonmuscle)	CFL1	2.8
A_33_P3217584	Cholinergic receptor, nicotinic, alpha 4 (neuronal)	CHRNA4	2.9
A_33_P3415300	Complexin 2	CPLX2	2.7
A_23_P133408	Colony stimulating factor 2 (granulocyte-macrophage)	CSF2	16.5
A_33_P3396139	Cytotoxic T-lymphocyte-associated protein 4	CTLA4	3.0
A_33_P3287631	Cathepsin B	CTSB	2.3
A_33_P3283480	Cathepsin C	CTSC	8.2
A_23_P7144	Chemokine (C-X-C motif) ligand 1 (melanoma growth stimulating activity, alpha)	CXCL1	6.5
A_33_P3712341	Chemokine (C-X-C motif) ligand 12	CXCL12	4.8
A_33_P3351249	Chemokine (C-X-C motif) ligand 16	CXCL16	11.6
A_23_P315364	Chemokine (C-X-C motif) ligand 2	CXCL2	3.3
A_24_P183150	Chemokine (C-X-C motif) ligand 3	CXCL3	2.9
A_23_P155755	Chemokine (C-X-C motif) ligand 6	CXCL6	5.0
A_33_P3214550	Chemokine (C-X-C motif) receptor 2	CXCR2	2.0
A_33_P3389230	Chemokine (C-X-C motif) receptor 3	CXCR3	2.3

of the biological processes revealed several immune-related pathways: "MAPKKK cascade," "immunity and defense," "signal transduction," "extracellular matrix protein-mediated signaling," and "interferon-mediated immunity," among others that were upregulated (Supplementary Table 2B). Also, 40 genes related to immune system related factors were identified as significantly enriched in CL2 compared to CL1 cells (Supplementary Table 2C). We chose the following genes for validation of the microarray results: NOV, IGFBP5, ALP, TAGLN, and CDH11 as they were highly expressed in CL1. RT-PCR analysis confirmed the microarray results (Figure 3).

Furthermore, we compared the molecular phenotype of CL1 and CL2 cells with that of phBMSC. We found that more than 80% of the genes expressed in CL1 and 90% in CL2 cells were common with primary phBMSC (Supplementary Figure 2), suggesting that CL1 and CL2 molecular phenotype exist within the heterogeneous population of phBMSC cultures.

3.6. ALP Knockdown Impairs Differentiation of CL1 Cells. Since ALP has been suggested as a marker for hBMSC progenitor cell lineage commitment [13] and was highly upregulated in CL1 cells, we tested its biological role in CL1 cells. ALP siRNA transfection decreased ALP protein level, ALP activity, and mRNA gene expression compared to control cells transfected with control siRNA ($p < 0.01$) and this inhibition was detectable up to day 7 days after osteoblast differentiation induction (Figures 4(A) and 4(B)). At day 14 of differentiation, mineralization ability of CL1 was significantly impaired (Figure 4(C)). In addition, we found that the number of mature adipocyte formations was significantly reduced to more than 75% ($p < 0.01$) (Figure 4(D)).

To identify relevant adipocyte differentiation associated genes that were targeted by ALP deficiency, we compared the downregulated genes of ALP deficient CL1 with the upregulated genes identified during adipocytic differentiation of CL1. We identified 62 genes that were common (Figure 5(a), Table 4) and among these genes were genes related to metabolism (primarily lipid and carbohydrate) and transport including CYB5B, CHST1, TAP1, ATP8A1, LRP8, PLCD1, and FABP5 (Table 4). We further performed quantitative real-time PCR of ALP deficient CL1 cells during adipocyte differentiation. The following adipocyte-associated genes were downregulated: PPARγ2, LPL, and aP2 (Figure 5(b)),

Table 3: Whole genome microarray analysis of two clonal populations of human bone marrow stromal stem cells: CL1 and CL2 cells. (a) Top 35 highly upregulated genes in CL1 cells versus CL2 cells. (b) Ingenuity® Pathway Analysis (IPA®) showing the different *physiological system development and function* genes found in each category and the corresponding p value. (c) Upper part IPA analysis showing the categories for *skeletal and muscular system development and function* upregulated in CL1 cells and lower part showing genes upregulated in CL2 cells. NOV = nephroblastoma overexpressed, IGFBP5 = insulin-like growth factor binding protein 5, ALP, TAGLN = transgelin, and CDH11 = OB-cadherin (osteoblast).

(a)

Gene ID	Fold change CL1 versus CL2
FOLR3	28.4721
CCL3L3	17.936
POSTN	15.5924
SERPINB2	−17.2599
IGFBP5	14.6708
CCL3	13.1203
NOV	11.2921
ACTG2	10.4493
CRYAB	10.0678
PSG4	9.68913
RAB3IL1	9.16897
SCIN	9.13702
MYL9	9.12814
TNFRSF11B	8.86049
TAGLN	8.75581
CDH12	8.06682
SHISA2	8.0291
THBS1	7.86854
SPP1	7.64205
LCE2A	7.41042
TMEM98	7.38011
PSG7	7.12183
MYPN	7.01837
FNDC1	6.88102
TNS3	6.72083
ABI3BP	6.67822
LRP3	6.64307
MMP3	6.34715
FAM167A	6.02684
HSPB2	6.01063
ALPL	6.01022
CTSK	5.87356
CXCL12	5.68572
THY1	4.89445
CDH10	4.86105

(b)

Name	p value	# molecules
Physiological system development and function		
Organismal development	$7.05E-10$–$1.43E-03$	181
Embryonic development	$1.00E-09$–$1.43E-03$	154
Organ development	$1.00E-09$–$1.43E-03$	145
Skeletal and muscular system development and function	$1.00E-09$–$1.02E-03$	123
Tissue development	$1.00E-09$–$1.43E-03$	236

(b) Continued.

Name	p value	# molecules
Skeletal and muscular system development and function	$1.00E-09$–$1.02E-03$	123
Tissue development	$1.00E-09$–$1.43E-03$	236

(c)

Functions annotation	p value	# molecules
Skeletal and muscular system development and function upregulated in CL1 cells		
Size of bone	$1.43E-06$	24
Differentiation of osteoblasts	$3.84E-06$	25
Mineralization of bone	$4.93E-06$	19
Bone mineral density	$3.65E-05$	19
Skeletal and muscular system development and function upregulated in CL2 cells		
Development of muscle	$1.00E-09$	44
Proliferation of muscle cells	$2.29E-06$	35
Remodeling of bone	$3.63E-06$	21
Resorption of bone	$3.94E-06$	19

confirming impairment of adipocytic differentiation of ALP deficient CL1 cells.

4. Discussion

We extensively studied two cell populations within cultured hBMSC that were identified based on differences in morphology. Cellular and molecular studies revealed differences in growth, differentiation capacity, and molecular signature. Our data support the notion of the presence of cellular and functional heterogeneity among cultured hBMSC.

Cellular heterogeneity of cultured hBMSC is recognized in an increasing number of reports. Several extrinsic and intrinsic factors may contribute to the observed hBMSC heterogeneity. Extrinsic factors include donor-to-donor variations in the number and quantity of initiating cells, which result in differences in cell growth rate and differentiation capacity [14, 15]. Intrinsic factors have been examined employing single cell clonal analysis and revealed variations in differentiation potential among individual colonies within hBMSC cultures ranging from the presence of cells with trilineage (osteoblast, adipocytes, and chondrocyte) potency to cells with null potency [16]. Also, variations in the ability of clonal cells to form heterotopic bone when implanted *in vivo* have been reported [5]. Our study corroborates these findings and provides more detailed cellular and molecular phenotyping of two examples of cell populations that exist within the heterogeneous hBMSC cultures [17].

Determining the molecular signature of CL1 and CL2 using whole genome microarray analysis showed enrichment of lineage-commitment associated genes in CL1. For example, insulin-like growth factor 5 (IGFBP5) and interleukin 6 (IL6)

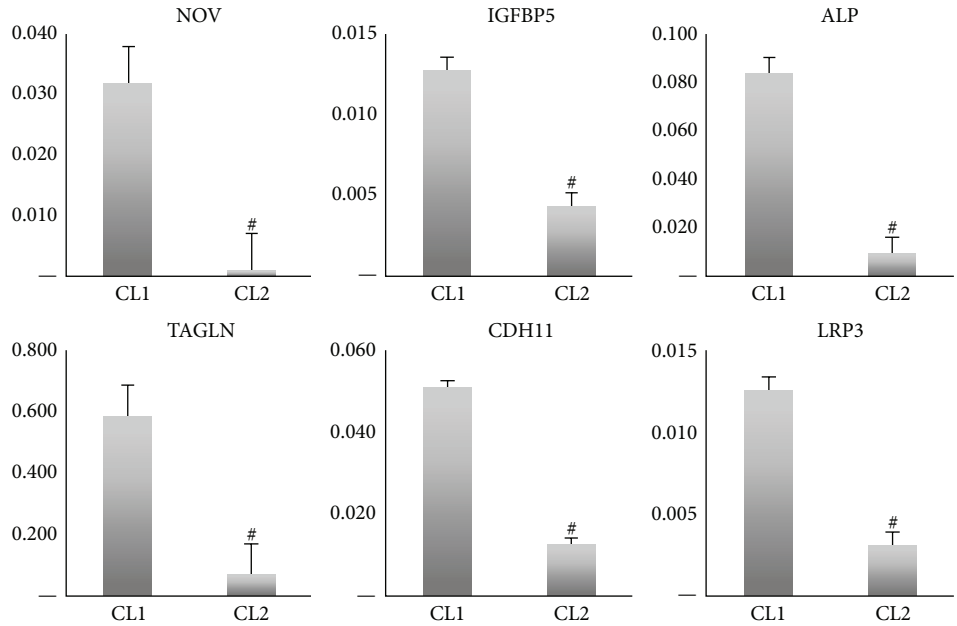

Figure 3: Validation of whole genome microarray analysis of two clonal populations of human bone marrow stromal stem cells: CL1 and CL2 cells. Quantitative real-time PCR for highly expressed genes in CL1 cells. NOV = nephroblastoma overexpressed, IGFBP5 = insulin-like growth factor binding protein 5, ALP, TAGLN = transgelin, and CDH11 = OB-cadherin (osteoblast). Data are presented as fold change in expression of each target gene normalized to GAPDH (n = three independent experiments, $^{\#}p < 0.001$) (see also Table 3).

were 14.7- and 3.3-fold upregulated in CL1 cells, respectively. Both factors are expressed in osteoprogenitor cells and important for osteoblast maturation [18]. We also observed that periostin (POSTN) gene was highly upregulated in CL1 cells (15.6-fold); POSTN is a 90 kDa secreted protein, originally identified in murine osteoblast-like cells and is upregulated by PTH [19]. Several studies employing murine and human cells have revealed important role of POSTN in osteoblast differentiation and during development in intramembranous ossification [20–23]. Another factor identified in CL1 cells is nephroblastoma overexpression (NOV) which is a member of the Cyr 61, connective tissue growth factor (CNN) family. The CCN family of proteins promotes osteoblast differentiation through interaction with integrins, WNT, BMP, and NOTCH signaling pathways [24–26]. In addition, a large number of signaling molecules known to be regulators of hBMSC lineage specific differentiation, for example, insulin-like growth factors [27–29], WNT [30–32], and MAPK [33–35], were enriched in CL1 cells. In contrast, CL2 expressed high levels of immune-related genes which may explain the poor differentiation response to osteoblast or adipocyte lineage. In a recent study the authors used telomerized hBMSC and showed clearly a clonal population that had very low *in vitro* and *in vivo* differentiation ability; however they had enhanced immune-related features including high IL7 expression. These nullipotent cells expressed CD317 which was associated with remarkably high basal level expression of factors with a proinflammatory and antiviral function [17]. We observed that this molecular phenotype was associated with distinct ultrastructural characteristics of the cells. In particular, CL2 had abundant phagocytic vacuole, microvilli, and lysosomes, features reminiscent of ultrastructure of immune-regulatory cells. Our data thus support the increasingly recognized feature that hBMSC exhibit immune modulatory functions and a part of the innate immune response [17].

We observed that ALP protein expression and enzymatic activity were significantly different between CL1 and CL2 cell lines and were thus a potential marker that distinguishes different cell populations with progenitor functions (CL1) from cells with nonprogenitor functions (CL2). ALP is expressed in a wide variety of tissues, including kidneys, bone, and liver [36, 37], but tissue-nonspecific ALP (ALPL) is considered a commitment marker for osteoblastic lineage [13, 38]. However, in a recent study the authors examined the differentiation potential of a number of hMSC clones *in vitro* and *in vivo* and reported that the hMSC clones with high levels of ALP expression were committed to trilineage differentiation [13]. Our data corroborate and extend these findings by reporting the effects of siRNA-mediated inhibition of ALP that resulted in an impaired hBMSC differentiation not only to osteoblasts, but also to adipocytes. Also, our results corroborate earlier studies that demonstrated in human bone biopsies the presence of ALP expression in bone marrow adipocytic cells [13, 17]. All these data suggest that ALP is a "stemness" marker of hBMSC and not just an indicator of osteoblastic lineage commitment.

While CL1 and CL2 were isolated from telomerized hMSC cell line, they are relevant to normal human physiology. We observed that the molecular phenotypes of CL1 and CL2 were contained within the molecular signature of primary hBMSC suggesting that CL1 and CL2 represent cell populations within the heterogeneous cultures of hBMSC. We have also previously reported that the molecular

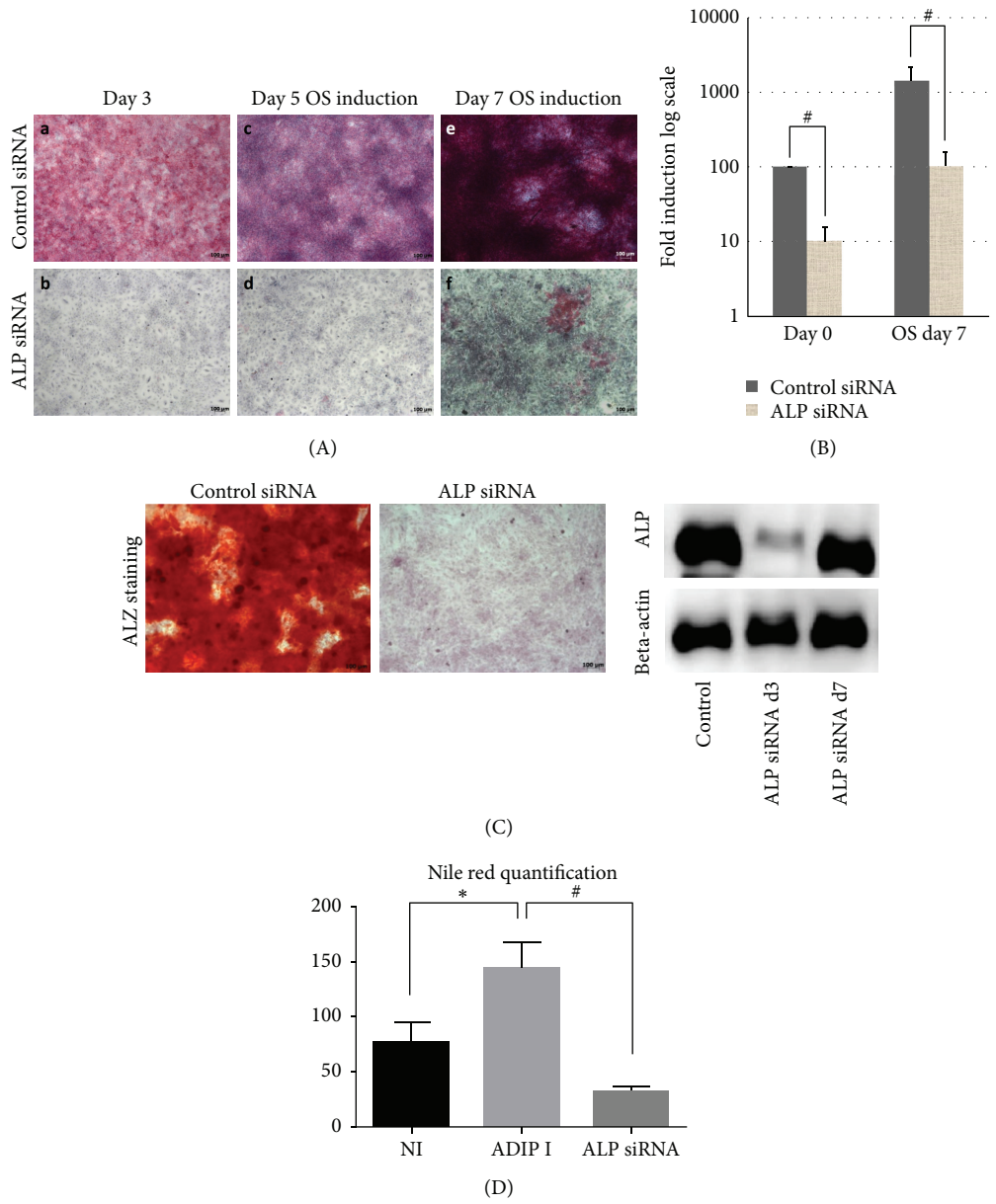

FIGURE 4: Effect of alkaline phosphatase (ALP) gene silencing by small interfering RNA (siRNA) on a clonal population of human bone marrow stromal stem cell CL1. (A) ALP staining at day 3, day 5, or day 7 days of osteoblast differentiation (OB induction). (B) Quantitative real-time PCR for ALP gene following ALP siRNA transfection at day 0 OB and day 7 of OB. Data are presented as fold change in expression of each target gene normalized to GAPDH (n = three independent experiments, $^{\#}p < 0.01$). Western blotting analysis of day 3 and day 7 after siRNA ALP transfection of CL1 cells, ALPL specific antibody, and B-actin was used. (C) Mineralized matrix formation as visualized by Alizarin Red S staining in siRNA transfected CL1 cells after 14 days of OB induction. (D) Nile red quantification of mature lipid filled adipocyte in control noninduced (Cont), adipocyte induced (Adip I), and ALP siRNA transfected cells that are adipocyte induced (ALP siRNA). Adipocyte induction was carried out for 7 days. $^{*}p < 0.05$.

phenotype and cellular responses of hMSC-TERT are similar to those of primary hMSC [10]. While we have identified ALP as a marker that can be used for a prospective identification of differentiation committed population of hBMSC, we identified additional distinctive molecular markers of the cells. For example, IGF-1, IGF-2, and IGF binding protein 5 were enriched in CL1 compared to CL2. IGFs and their binding proteins are very well-studied factors that play a role in hBMSC proliferation and osteoblast differentiation [18]. On the other hand, annexin A3 as well as several immune-related genes was highly enriched in CL2 compared to CL1. Future studies are needed to determine the functional significance of these molecules in relation to the functional identity of various cell populations within the hBMSC cultures and their usefulness as biomarkers to dissect the heterogeneous population of cultured hBMSC.

Our finding of the presence of functional diversity within hBMSC cultures that contain progenitor and nonprogenitor

Table 4: Microarray data analysis showing genes found to be upregulated during adipogenic differentiation and downregulated after ALP KO.

62 common elements in "AD up" and "ALP down"	Gene name	FC (ALP siRNA versus control siRNA)
APOBEC3G	Apolipoprotein B mRNA editing enzyme, catalytic polypeptide-like 3G	−15.938025
IFI44L	Interferon-induced protein 44-like	−11.520283
PAQR5	Progestin and adipoQ receptor family member V	−6.868241
PNMA2	Paraneoplastic antigen MA2	−5.9695344
DUSP23	Dual specificity phosphatase 23	−5.4786854
CLDN23	Claudin 23	−5.1885047
ANKDD1A	Ankyrin repeat and death domain containing 1A	−5.1646647
IL8	Interleukin 8	−4.887188
LRRC23	Leucine rich repeat containing 23	−4.7611775
IL6	Interleukin 6 (interferon, beta 2)	−4.693139
LIFR	Leukemia inhibitory factor receptor alpha	−4.6540866
PTGFR	Prostaglandin F receptor (FP)	−4.457529
FAM134B	Family with sequence similarity 134, member B	−4.403495
CYFIP2	Cytoplasmic FMR1 interacting protein 2	−4.260462
METTL7A	Methyltransferase-like 7A	−4.0480843
APOBEC3F	Apolipoprotein B mRNA editing enzyme, catalytic polypeptide-like 3F	−3.9502614
CA5B	Carbonic anhydrase VB, mitochondrial	−3.93889
ITGA10	Integrin, alpha 10	−3.9143775
FMO3	Flavin containing monooxygenase 3	−3.852087
IMPA2	Inositol monophosphatase 2 (human)	−3.8374884
CDO1	Cysteine dioxygenase, type I	−3.8181455
CCDC68	Coiled-coil domain containing 68	−3.7292893
CXCL1	Chemokine (C-X-C motif) ligand 1 (melanoma growth stimulating activity, alpha)	−3.5942702
IDO1	Indoleamine 2,3-dioxygenase 1	−3.5803545
KCNIP3	Kv channel interacting protein 3, calsenilin	−3.5442894
FADS1	Fatty acid desaturase 1	−3.2951858
LSR	Lipolysis stimulated lipoprotein receptor	−3.2215986
ITGA7	Integrin, alpha 7	−3.1355932
HLA-DMA	Major histocompatibility complex, class II, DM alpha	−3.1347752
APOBEC3B	Apolipoprotein B mRNA editing enzyme, catalytic polypeptide-like 3B	−3.1074922
BMP4	Bone morphogenetic protein 4	−3.0809238
DMBT1	Deleted in malignant brain tumors 1	−3.0760298
RDH5	Retinol dehydrogenase 5 (11-cis/9-cis)	−3.066812
EPAS1	Endothelial PAS domain protein 1	−3.0615559
CDKN3	Cyclin-dependent kinase inhibitor 3	−3.052319
GPC6	Glypican 6	−3.0460389
CDK4	Cyclin-dependent kinase 4	−2.9808035
FKBP5	FK506 binding protein 5	−2.9360793
PDE1B	Phosphodiesterase 1B, calmodulin-dependent	−2.8863106
JAM2	Junctional adhesion molecule 2	−2.884354
TFPI	Tissue factor pathway inhibitor (lipoprotein-associated coagulation inhibitor)	−2.8578906
NT5M	5′,3′-Nucleotidase, mitochondrial	−2.7555947
NFIA	Nuclear factor I/A	−2.7176137
TSPAN31	Tetraspanin 31	−2.627556
ZNF25	Zinc finger protein 25	−2.6183622
SULF2	Sulfatase 2	−2.5464642
MESP1	Mesoderm posterior 1 homolog (mouse)	−2.525513

Table 4: Continued.

62 common elements in "AD up" and "ALP down"	Gene name	FC (ALP siRNA versus control siRNA)
BCL2L1	BCL2-like 1	−2.5119667
PLTP	Phospholipid transfer protein	−2.4767148
TIMP4	TIMP metallopeptidase inhibitor 4	−2.465897
CYP27A1	Cytochrome P450, family 27, subfamily A, polypeptide 1	−2.4572072
TTC39B	Tetratricopeptide repeat domain 39B	−2.4439611
IL1R2	Interleukin 1 receptor, type II	−2.427431
FMOD	Fibromodulin	−2.4185398
LDLRAD3	Low density lipoprotein receptor class A domain containing 3	−2.4032724
PISD	Phosphatidylserine decarboxylase	−2.3884957
TMEM100	Transmembrane protein 100	−2.384632
CHST2	Carbohydrate (N-acetylglucosamine-6-O) sulfotransferase 2	−2.3805838
APOBEC3F	Apolipoprotein B mRNA editing enzyme, catalytic polypeptide-like 3F	−2.3759322
SCD	Stearoyl-CoA desaturase (delta-9-desaturase)	−2.3524246
SPAG4	Sperm associated antigen 4	−2.280867
MMD	Monocyte to macrophage differentiation associated human	−2.2055967
ASS1	Argininosuccinate synthase 1	−2.1725202
GK5	Glycerol kinase 5 (putative)	−2.1667244
PDE7B	Phosphodiesterase 7B	−2.166515
MT1X	Metallothionein 1X	−2.161843
ACACB	Acetyl-CoA carboxylase beta	−2.1512873
LEPR	Leptin receptor	−2.148686
HIF1A	Hypoxia inducible factor 1, alpha subunit (basic helix-loop-helix transcription factor)	−2.0954225
HEXDC	Hexosaminidase (glycosyl hydrolase family 20, catalytic domain) containing	−2.094836
SARM1	Sterile alpha and TIR motif containing 1	−2.0797038
BBS1	Bardet-Biedl syndrome 1	−2.0146718
SERPING1	Serpin peptidase inhibitor, clade G (C1 inhibitor), member 1	−2.0102212
FAM162A	Family with sequence similarity 162, member A	−2.005807
TCTN1	Tectonic family member 1	−2.0033443

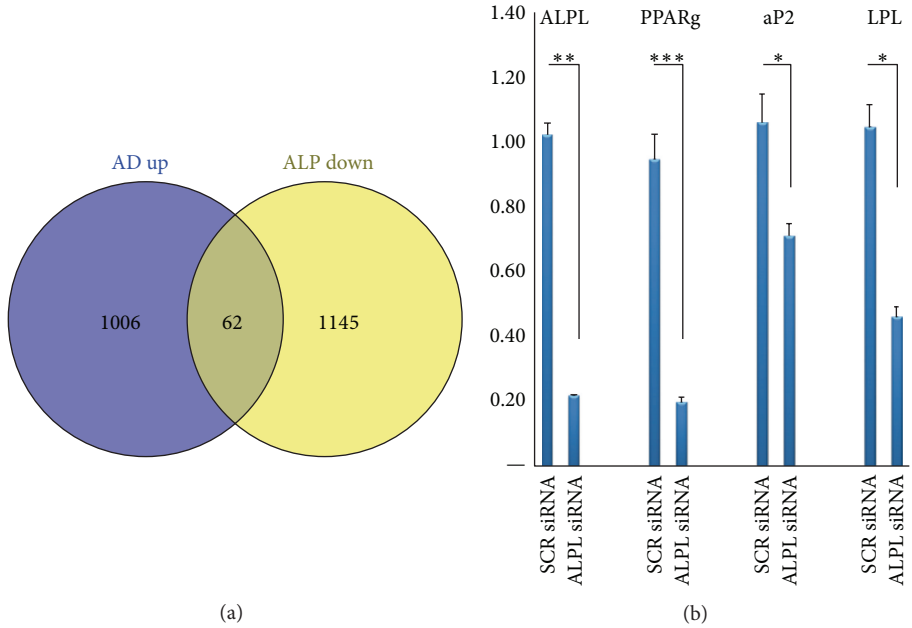

Figure 5: Adipocyte related genes downregulated in ALP knockdown CL1 cells. (a) Venn diagram of whole gene expression analysis of AD upregulated genes compared with ALP KD downregulated genes. (b) Quantitative real-time PCR of four selected common genes from Venn diagram including ALPL, PPARg2, aP2, and LPL. Data are presented as fold change in expression of each target gene normalized to GAPDH (n = three independent experiments, $^{*}p < 0.05$, $^{**}p < 0.01$, and $^{***}p < 0.001$).

cell populations has a clinical relevance. It demonstrates that the progenitor function and the immune modulatory roles of hBMSC [39] are mediated by specific and distinguishable populations of hBMSC. Thus, future clinical studies employing hBMSC should attempt to administer the relevant subpopulation of hBMSC dependent on the experimental aim, as a novel approach to improving the clinical efficiency, instead of the current use of heterogeneous hBMSC populations.

Competing Interests

The authors declare that they have no competing interests.

Authors' Contributions

Mona Elsafadi and Amer Mahmood contributed equally to this work.

Acknowledgments

These studies are supported by a grant from the College of Medicine Research Centre (CMRC), Deanship of Scientific Research, King Saud University, Riyadh, Saudi Arabia. The authors would like to thank Mr. Ali Al-Roalle for all his technical help. They thank Natalie Twine for advice on DNA microarray analysis.

References

[1] W. Zaher, L. Harkness, A. Jafari, and M. Kassem, "An update of human mesenchymal stem cell biology and their clinical uses," *Archives of Toxicology*, vol. 88, no. 5, pp. 1069–1082, 2014.

[2] S. Post, B. M. Abdallah, J. F. Bentzon, and M. Kassem, "Demonstration of the presence of independent pre-osteoblastic and pre-adipocytic cell populations in bone marrow-derived mesenchymal stem cells," *Bone*, vol. 43, no. 1, pp. 32–39, 2008.

[3] K. H. Larsen, C. M. Frederiksen, J. S. Burns, B. M. Abdallah, and M. Kassem, "Identifying a molecular phenotype for bone marrow stromal cells with in vivo bone-forming capacity," *Journal of Bone and Mineral Research*, vol. 25, no. 4, pp. 796–808, 2010.

[4] A. Rosenzweig, "Cardiac cell therapy—mixed results from mixed cells," *The New England Journal of Medicine*, vol. 355, no. 12, pp. 1274–1277, 2006.

[5] S. A. Kuznetsov, P. H. Krebsbach, K. Satomura et al., "Single-colony derived strains of human marrow stromal fibroblasts form bone after transplantation in vivo," *Journal of Bone and Mineral Research*, vol. 12, no. 9, pp. 1335–1347, 1997.

[6] M. Kassem and P. Bianco, "Skeletal stem cells in space and time," *Cell*, vol. 160, no. 1-2, pp. 17–19, 2015.

[7] A. I. Caplan and D. Correa, "PDGF in bone formation and regeneration: new insights into a novel mechanism involving MSCs," *Journal of Orthopaedic Research*, vol. 29, no. 12, pp. 1795–1803, 2011.

[8] K. Stewart, S. Walsh, J. Screen et al., "Further characterization of cells expressing STRO-1 in cultures of adult human bone marrow stromal cells," *Journal of Bone and Mineral Research*, vol. 14, no. 8, pp. 1345–1356, 1999.

[9] J. L. Simonsen, C. Rosada, N. Serakinci et al., "Telomerase expression extends the proliferative life-span and maintains the osteogenic potential of human bone marrow stromal cells," *Nature Biotechnology*, vol. 20, no. 6, pp. 592–596, 2002.

[10] M. Al-Nbaheen, R. Vishnubalaji, D. Ali et al., "Human stromal (mesenchymal) stem cells from bone marrow, adipose tissue and skin exhibit differences in molecular phenotype and differentiation potential," *Stem Cell Reviews and Reports*, vol. 9, no. 1, pp. 32–43, 2013.

[11] C. A. Gregory, W. G. Gunn, A. Peister, and D. J. Prockop, "An Alizarin red-based assay of mineralization by adherent cells in culture: comparison with cetylpyridinium chloride extraction," *Analytical Biochemistry*, vol. 329, no. 1, pp. 77–84, 2004.

[12] A. Mahmood, L. Harkness, H. D. Schrøder, B. M. Abdallah, and M. Kassem, "Enhanced differentiation of human embryonic stem cells to mesenchymal progenitors by inhibition of TGF-β/activin/nodal signaling using SB-431542," *Journal of Bone and Mineral Research*, vol. 25, no. 6, pp. 1216–1233, 2010.

[13] H.-J. Prins, A. K. Braat, D. Gawlitta et al., "In vitro induction of alkaline phosphatase levels predicts in vivo bone forming capacity of human bone marrow stromal cells," *Stem Cell Research*, vol. 12, no. 2, pp. 428–440, 2014.

[14] K. Stenderup, J. Justesen, C. Clausen, and M. Kassem, "Aging is associated with decreased maximal life span and accelerated senescence of bone marrow stromal cells," *Bone*, vol. 33, no. 6, pp. 919–926, 2003.

[15] D. G. Phinney, G. Kopen, W. Righter, S. Webster, N. Tremain, and D. J. Prockop, "Donor variation in the growth properties and osteogenic potential of human marrow stromal cells," *Journal of Cellular Biochemistry*, vol. 75, no. 3, pp. 424–436, 1999.

[16] C. M. Digirolamo, D. Stokes, D. Colter, D. G. Phinney, R. Class, and D. J. Prockop, "Propagation and senescence of human marrow stromal cells in culture: a simple colony-forming assay identifies samples with the greatest potential to propagate and differentiate," *British Journal of Haematology*, vol. 107, no. 2, pp. 275–281, 1999.

[17] S. James, J. Fox, F. Afsari et al., "Multiparameter analysis of human bone marrow stromal cells identifies distinct immunomodulatory and differentiation-competent subtypes," *Stem Cell Reports*, vol. 4, no. 6, pp. 1004–1015, 2015.

[18] B. Peruzzi, A. Cappariello, A. Del Fattore, N. Rucci, F. De Benedetti, and A. Teti, "c-Src and IL-6 inhibit osteoblast differentiation and integrate IGFBP5 signalling," *Nature Communications*, vol. 3, article 630, 2012.

[19] D. Fortunati, S. Reppe, Å.-K. Fjeldheim, M. Nielsen, V. T. Gautvik, and K. M. Gautvik, "Periostin is a collagen associated bone matrix protein regulated by parathyroid hormone," *Matrix Biology*, vol. 29, no. 7, pp. 594–601, 2010.

[20] A. Oshima, H. Tanabe, T. Yan, G. N. Lowe, C. A. Glackin, and A. Kudo, "A novel mechanism for the regulation of osteoblast differentiation: transcription of periostin, a member of the fasciclin I family, is regulated by the bHLH transcription factor, Twist," *Journal of Cellular Biochemistry*, vol. 86, no. 4, pp. 792–804, 2002.

[21] T. G. Kashima, T. Nishiyama, K. Shimazu et al., "Periostin, a novel marker of intramembranous ossification, is expressed in fibrous dysplasia and in c-Fos-overexpressing bone lesions," *Human Pathology*, vol. 40, no. 2, pp. 226–237, 2009.

[22] C. Galli, M. Piergianni, M. Piemontese et al., "Periostin improves cell adhesion to implantable biomaterials and osteoblastic differentiation on implant titanium surfaces in a topography-dependent fashion," *Journal of Biomedical Materials Research - Part A*, vol. 102, no. 11, pp. 3855–3861, 2014.

[23] D. L. Coutu, H. W. Jian, A. Monette, G.-É. Rivard, M. D. Blostein, and J. Galipeau, "Periostin, a member of a novel family of vitamin K-dependent proteins, is expressed by mesenchymal stromal cells," *The Journal of Biological Chemistry*, vol. 283, no. 26, pp. 17991–18001, 2008.

[24] T. Minamizato, K. Sakamoto, T. Liu et al., "CCN3/NOV inhibits BMP-2-induced osteoblast differentiation by interacting with BMP and Notch signaling pathways," *Biochemical and Biophysical Research Communications*, vol. 354, no. 2, pp. 567–573, 2007.

[25] W. Si, Q. Kang, H. H. Luu et al., "CCN1/Cyr61 is regulated by the canonical Wnt signal and plays an important role in Wnt3A-induced osteoblast differentiation of mesenchymal stem cells," *Molecular and Cellular Biology*, vol. 26, no. 8, pp. 2955–2964, 2006.

[26] Q. Luo, Q. Kang, W. Si et al., "Connective tissue growth factor (CTGF) is regulated by Wnt and bone morphogenetic proteins signaling in osteoblast differentiation of mesenchymal stem cells," *The Journal of Biological Chemistry*, vol. 279, no. 53, pp. 55958–55968, 2004.

[27] Y.-S. Yoon, N. Lee, and H. Scadova, "Myocardial regeneration with bone-marrow-derived stem cells," *Biology of the Cell*, vol. 97, no. 4, pp. 253–263, 2005.

[28] Y. S. Yoon, "Cardiac regeneration with novel bone marrow-derived multipotent stem cells," *Discovery Medicine*, vol. 5, pp. 204–208, 2005.

[29] Y.-S. Yoon, A. Wecker, L. Heyd et al., "Clonally expanded novel multipotent stem cells from human bone marrow regenerate myocardium after myocardial infarction," *Journal of Clinical Investigation*, vol. 115, no. 2, pp. 326–338, 2005.

[30] G. M. Boland, G. Perkins, D. J. Hall, and R. S. Tuan, "Wnt 3a promotes proliferation and suppresses osteogenic differentiation of adult human mesenchymal stem cells," *Journal of Cellular Biochemistry*, vol. 93, no. 6, pp. 1210–1230, 2004.

[31] D. A. Cook, S. W. Fellgett, M. E. Pownall, P. J. O'Shea, and P. G. Genever, "Wnt-dependent osteogenic commitment of bone marrow stromal cells using a novel GSK3β inhibitor," *Stem Cell Research*, vol. 12, no. 2, pp. 415–427, 2014.

[32] J. De Boer, R. Siddappa, C. Gaspar, A. Van Apeldoorn, R. Fodde, and C. Van Blitterswijk, "Wnt signaling inhibits osteogenic differentiation of human mesenchymal stem cells," *Bone*, vol. 34, no. 5, pp. 818–826, 2004.

[33] M. Al-Toub, A. Almusa, M. Almajed et al., "Pleiotropic effects of cancer cells' secreted factors on human stromal (mesenchymal) stem cells," *Stem Cell Research and Therapy*, vol. 4, article 114, 2013.

[34] L. Chen, D. Qanie, A. Jafari et al., "Delta-like 1/fetal antigen-1 (Dlk1/FA1) is a novel regulator of chondrogenic cell differentiation via inhibition of the Akt kinase-dependent pathway," *The Journal of Biological Chemistry*, vol. 286, no. 37, pp. 32140–32149, 2011.

[35] T. Matsunobu, K. Torigoe, M. Ishikawa et al., "Critical roles of the TGF-β type I receptor ALK5 in perichondrial formation and function, cartilage integrity, and osteoblast differentiation during growth plate development," *Developmental Biology*, vol. 332, no. 2, pp. 325–338, 2009.

[36] B. C. Nair, D. E. Johnson, R. J. Majeska, J. A. Rodkey, C. D. Bennett, and G. A. Rodan, "Rat alkaline phosphatase. II. Structural similarities between the osteosarcoma, bone, kidney, and placenta isoenzymes," *Archives of Biochemistry and Biophysics*, vol. 254, no. 1, pp. 28–34, 1987.

[37] P. J. Butterworth, "Alkaline phosphatase. Biochemistry of mammalian alkaline phosphatases," *Cell Biochemistry and Function*, vol. 1, no. 2, pp. 66–70, 1983.

[38] A. T. Ali, C. B. Penny, J. E. Paiker et al., "Alkaline phosphatase is involved in the control of adipogenesis in the murine preadipocyte cell line, 3T3-L1," *Clinica Chimica Acta*, vol. 354, no. 1-2, pp. 101–109, 2005.

[39] G. M. Spaggiari and L. Moretta, "Cellular and molecular interactions of mesenchymal stem cells in innate immunity," *Immunology and Cell Biology*, vol. 91, no. 1, pp. 27–31, 2012.

Hindawi Publishing Corporation
Stem Cells International
Volume 2016, Article ID 8281235, 7 pages
http://dx.doi.org/10.1155/2016/8281235

Research Article

Hair Follicle Morphogenesis in the Treatment of Mouse Full-Thickness Skin Defects Using Composite Human Acellular Amniotic Membrane and Adipose Derived Mesenchymal Stem Cells

Wu Minjuan, Xiong Jun, Shao Shiyun, Xu Sha, Ni Haitao, Wang Yue, and Ji Kaihong

Department of Histology and Embryology, Second Military Medical University, Shanghai 200433, China

Correspondence should be addressed to Wang Yue; wangyuesmmu@163.com and Ji Kaihong; jkhsmmu@163.com

Received 21 April 2016; Revised 24 June 2016; Accepted 3 July 2016

Academic Editor: Giorgio Mori

Copyright © 2016 Wu Minjuan et al. This is an open access article distributed under the Creative Commons Attribution License, which permits unrestricted use, distribution, and reproduction in any medium, provided the original work is properly cited.

Early repair of skin injury and maximal restoration of the function and appearance have become important targets of clinical treatment. In the present study, we observed the healing process of skin defects in nude mice and structural characteristics of the new skin after transplantation of isolated and cultured adipose derived mesenchymal stem cells (ADMSCs) onto the human acellular amniotic membrane (AAM). The result showed that ADMSCs were closely attached to the surface of AAM and grew well 24 h after seeding. Comparison of the wound healing rate at days 7, 14, and 28 after transplantation showed that ADMSCs seeded on AAM facilitated the healing of full-thickness skin wounds more effectively as compared with either hAM or AAM alone, indicating that ADMSCs participated in skin regeneration. More importantly, we noticed a phenomenon of hair follicle development during the process of skin repair. Composite ADMSCs and AAM not only promoted the healing of the mouse full-thickness defects but also facilitated generation of the appendages of the affected skin, thus promoting restoration of the skin function. Our results provide a new possible therapy idea for the treatment of skin wounds with respect to both anatomical regeneration and functional restoration.

1. Introduction

Local or systemic cutaneous lesions arising from skin injury are often related to the loss of barrier function. Early repair of skin injury and maximal restoration of the function and appearance have become important targets of clinical treatment. Autologous free skin grafting, skin flap transplantation, and allogenous or xenogeneic skin transplantation remain the first consideration in conventional clinical treatment of skin injury [1, 2]. Although these techniques are usually effective in most cases, how to solve the problem of covering large wound areas and reduce wound retraction and scar formation in patients with large and life-threatening wounds or those with beauty demands remains a clinical challenge. Construction of an ideal skin substitute has become an inevitable trend in burn and plastic surgery. In 1975, Rheinwald and Green [3] first reported successful treatment of wounds with transplantation of cultured human epidermal cells, which symbolizes a milestone in wound treatment. With the development of modern molecular and cellular biology and tissue engineering, advances in skin substitute research and application have gradually rendered it possible to reduce secondary injury from autologous skin transplantation [4]. Subsequently, researchers have created techniques of autologous epidermal cell culture and transplantation for the treatment of burn and various other acute/chronic wounds, thus providing permanent coverage for large-area wounds. However, the anti-infection ability of these skin substitutes is relatively low, and their functional and appearance degradation is also an unavoidable problem.

Epidermal substitutes are mainly used for superficial wounds [5]. The epidermis alone cannot survive long for large, deep, and extensive wounds because it cannot receive nutritional support from the dermis and therefore needs

mechanical protection of a dermal substitute. The dermal composition in the skin substitute can prevent the wound from retracting and increase mechanical stability. Knowing that the dermis plays an important role in the regulation of epidermal renewal and reconstruction, accelerating the construction of the dermis is an extremely important link in skin tissue engineering [6].

The human amniotic membrane (hAM) is a natural high-molecular biological material and can express multiple growth factors and mRNA-related proteins including collagen, glycoprotein, protein polysaccharide, integrin, and lamellar body, which are beneficial to cell growth and reproduction. For this reason, hAM is often used as a vector for cell growth and proliferation [7, 8]. Acellular amniotic membrane (AAM) is a natural biologic scaffold and can be used as an extracellular matrix to load cells for the construction of engineered tissues and organs [9]. There have been many reports about the use of AAM for wound coverage [10, 11]. But few studies have reported the use of composite AAM and stem cells for the treatment of skin defects and functional repair. In the present study, we intended to observe the healing of skin defects and histological and structural characteristics of the newborn skin after transplantation of isolated and cultured adipose derived mesenchymal stem cells (ADMSCs) onto AAM and using them to cover the skin defects in nude mice, in an attempt to explore the possibility of seeding ADMSCs on AAM to repair skin defects.

2. Materials and Methods

2.1. Characterization of ADMSCs. Fourth-passage ADMSCs stored in our laboratory were characterized for the expression pattern of mesenchymal and pluripotent markers by immunohistochemistry and flow cytometry. P4 ADMSCs were fixed with 4% paraformaldehyde in phosphate buffer for 4 min at room temperature. After being blocked with PBS containing 2% BSA, cells were permeabilized with 0.1% Triton-X 100 for 10 min. Slides were incubated sequentially overnight at 4°C with the following primary antibodies: Oct-4 (goat polyclonal, 1 : 50, Santa Cruz Biotechnology Inc.) and SH-2 (1 : 50, mouse polyclonal, Santa Cruz Biotechnology Inc.). The slides were washed with PBS ± 1% BSA after each step. Finally, cells were incubated for 40 min at room temperature with FITC or Cy3-coupled anti-goat or anti-mouse IgG secondary antibody (1 : 500, Jackson) and observed under a fluorescence microscope (BX41TB, Olympus, Tokyo, Japan).

For FACS analysis, cells were trypsinized and spun down by centrifugation for 5 min at 1000 rpm. The cell pellet was resuspended in 100 μL PBS and incubated on ice for 30 min with FITC or PE-conjugated monoclonal antibodies against CD29, CD44, CD105, CD90, CD34, and CD45 (Becton-Dickinson, San Jose, CA). After two washes with cold PBS, the labeled cells were analyzed with a FACStar flow cytometer (Becton-Dickinson, San Jose, CA, USA).

2.2. Preparation and Evaluation of AAM. hAM was decellularized using 0.03% (w/v) sodium dodecyl sulfate (SDS), with hypotonic tris buffer and protease inhibitors and nuclease treatment. Both intact hAM and AAM were fixed in 4% paraformaldehyde before HE staining to observe whether the epidermal layer of AAM had been removed completely.

2.2.1. Seeding of ADMSCs on AAM. P4 adipose stem cells were seeded on the surface of AAM at a density of 2×10^5 cells/cm^2, with the KC-SFM medium replaced on alternative days. After 7-day loading, cell adhesion and growth were observed under an optical microscope by HE staining.

2.3. Preparation of Full-Thickness Skin Defects in Nude Mice and Repair of the Skin Defects in Different Groups. After intraperitoneal anesthesia, full-thickness skin defects were made by cutting a 0.8 cm × 0.8 cm wound on the back deep to the fascia in 6-week-old healthy BALB/C-nu mice of either sex weighing 20~30 g. According to the different methods used for wound treatment, the 30 BALB/C-nu mice were equally randomized to three groups: hAM group, where the wounds were treated by native hAM; AAM group, where the wounds were treated with AAM alone; and ADMSCs seeded on AAM group, where the wounds were treated by transplanting composite ADMSCs and AAM to the wounds. Before treatment, the wounds were gently rinsed with gentamycin normal saline (NS). AAM was fixed on the surrounding skin with 1.0-gauge suture and dressed with NS gauze.

2.4. Observation and Measurement. Wound contraction: the wound area was measured 7, 14, and 28 days after transplantation in all groups, and the wound healing rate was calculated using the following equation: would healing rate = (original wound area − current wound area)/original wound area × 100%.

2.5. Immunohistofluorescence Analysis and HE Staining Observation. Immunohistofluorescence staining was used to examine the expression of cytokeratin 19 (CK19) and human derived mitochondria in the new skin tissue. At day 28 after treatment, OCT-embedded specimens were made into 10 μm thick continuous frozen sections. After being fixed with cold acetone, the slides were preincubated in the working normal goat serum concentration for 10 min and then incubated with a mouse polyclonal anti-CK19-specific antibody (1 : 50, Dako) or human derived mitochondria (1 : 200, Neomarks) at 4°C for 16 h. Then, the slides were incubated for 40 min at room temperature with FITC or Cy3-coupled IgG secondary antibody (1 : 500, Jackson), counterstained with DAPI (Sigma-Aldrich), and observed under a fluorescence microscope (BX41TB, Olympus, Japan). Additionally, part of the skin from the same site was fixed in 4% paraformaldehyde, HE stained, and observed for the skin structure and growth of the skin appendages under the optical microscope.

2.6. Statistical Treatment. Statistical analyses were performed using SPSS15.0. Measurement data were expressed as $X \pm S$. Intergroup comparison was performed using t-test. $P < 0.05$ was considered statistically significant.

Table 1: Comparison of the wound healing rate between different groups.

Groups	Day 7	Day 14	Day 28
hAM	33.39 ± 4.7	43.01 ± 2.8	85.42 ± 1.9
AAM	52.68 ± 3.5**	68.43 ± 2.4**	79.48 ± 1.6**
ADMSCs seeded on AAM	64.38 ± 3.9**	79.75 ± 3.8**	92.02 ± 4.2**

** $P < 0.05$.

3. Results

3.1. Evaluation of Cultured ADMSCs In Vitro. Primarily cultured ADMSCs were spindle-shaped, with a relatively large nucleus-cytoplasm ratio. Confluent cells began forming clones at day 4 after seeding. The size of the clonal cells was relatively small, with a large nucleus-cytoplasm ratio, where split kernels were visible. About 80% of the ADMSCs became confluent 12 days after seeding (Figure 1(a) P1). P4 ADMSCs were morphologically uniform (Figure 1(a) P4). Immunofluorescence staining of the fourth-passage adipose stem cells showed strong positive expression for Oct-4 and SH-2, with a positive rate of more than 90% (Figure 1(b)). Flow cytometry showed that P4 ADMSCs were positive for CD29, CD44, CD105, and CD90 and did not express CD45 or CD34 (markers for hematopoietic stem cells) (Figure 1(c)).

3.2. Evaluation of hAM and ADMSCs Seeded on AAM. Optical microscopic observation by HE staining: The epidermal layer of the cryopreserved intact hAM was complete and continuous with the nucleus clearly seen (Figure 2(a)) and disappeared after trypsin treatment but the basement membrane kept intact (Figure 2(b)). At day 3 of loading ADMSCs onto AAM, HE staining of optical microscopy showed that cells grew well with large cell bodies protuberating like spindles. At day 7, cells fused into patches covering the surface of AAM cells and turned from a single layer to multiple layers (Figure 2(c)).

3.3. Wound Healing in Different Groups. The healed skin was lower than the normal skin in all groups. At day 7 after seeding, AAM was attached onto the wound surface securely, and the wound surface began shrinking; at day 14 after seeding, AAM fell off from the wound surface and the sound surface further shrank and healed; and at day 28, the wound surface was stabilized. Comparison of the wound healing rate at days 7, 14, and 28 after transplantation showed that the wound healing rate in ADMSC-AAM seeding group was significantly higher than that in hAM and AAM groups, and the wound healing rate in AAM group was significantly higher than that in hAM group (Table 1).

3.4. Characteristics of the New Skin Tissue Structure. HE staining showed that, at day 28, the hair follicle-like structure appeared in ADMSC-AAM seeding group; the number of epidermal layers in ADMSC-AAM seeding group was greater than that in hAM and AAM groups, and all wounds in ADMSC-AAM seeding group healed completely (Figure 3). The typical hair follicle structure was observed at day 28 day after transplantation, when immunohistochemistry showed that some cells of new hair follicles in the healed epidermis were positive for both keratin 19 and human derived mitochondria. Keratin 19 is a marker when mesenchymal cells are transcribed to epithelial cells, and anti-human-derived mitochondria are often used as a tracing agent to demonstrate cells derived from human ADSCs. Image pro plus showed that the number of hair follicles in ADMSC-AAM seeding group was significantly higher than that in hAM and AAM groups. The process of hair follicle development showed that composite AAM and ADMSCs not only promoted the healing of the full-thickness defects in the mice but also facilitated generation of the appendages of the affected skin, thus promoting restoration of the skin function (Figure 4). HE staining showed that regeneration of skin appendages, especially regeneration of the hair follicle, is very similar to hair follicle formation in the process of normal skin development.

4. Discussion

The skin is known as the largest organ of the human integumentary system and is composed of complex tissue structures including hair follicles, sweat glands, sebaceous glands, and other appendages [6]. It plays important roles in barrier protection, thermoregulation, hair generation, and other physiological functions. The skin covers the body externally, making it vulnerable to injuries from various external factors such as burn, trauma, and chronic ulceration. There are about one million burn patients in China who need skin transplantation annually. However, as dermagrafts currently used in clinical practice contain the epidermis alone or epidermis with dermis but without hair follicles, sweat glands, melanin cells, capillaries, fat layers, and other appendages, they lack many physiological functions of the normal skin, thus seriously affecting the patient's quality of life.

Since the successful isolation of ADMSCs in vitro, they have become the most extensively used adult stem cells in tissue engineering and regenerative medicine [12–14]. ADMSCs express the mesenchymal and pluripotent markers [15, 16] as we examined, and compared with stem cells derived from other sources, ADMSCs have unique advantages of abundant sources, easy obtainment, high proliferative activity, and multidirectional differentiation potentiality and therefore have become common seed cells in tissue engineering [17, 18].

The use of ADMSCs with an AAM coculture system has been reposted as a stem cell therapy and scaffold transplantation for the treatment and functional repair of skin [16, 19]. Sánchez-Sánchez et al. [19] reported that the radiosterilized hAM and pig skin may prove to be suitable scaffolds for delivery of hADMSCs to promote tissue regeneration in skin injuries. Our present study also demonstrated the feasibility of seeding ADMSC onto AAM for the clinical treatment of skin defects. Both ADMSCs and AAM are easily accessible.

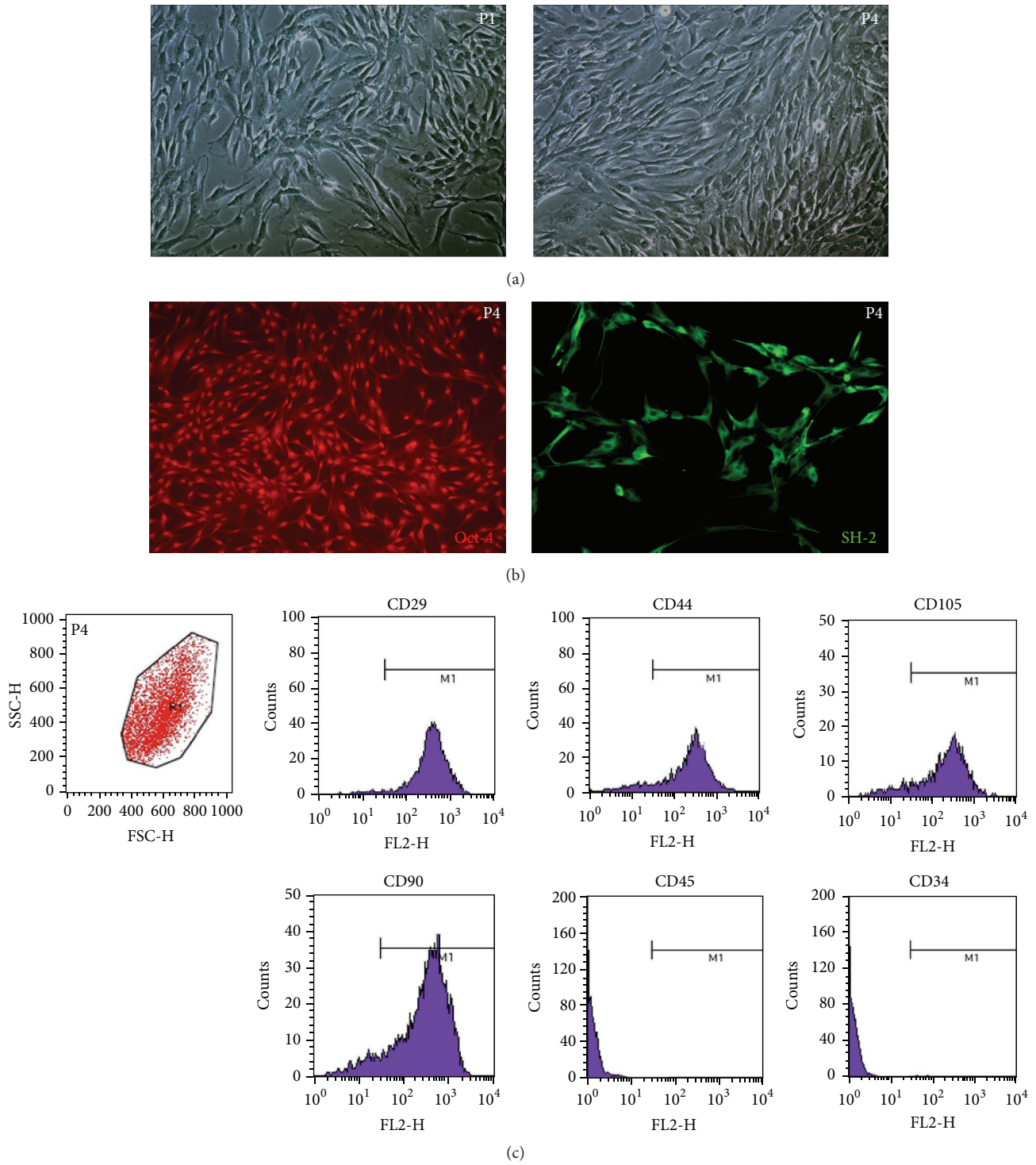

Figure 1: Morphology and molecular marker detection of isolated ADMSCs. (a) Phase-contrast micrographs of ADMSCs at P1 and P4. Most ADMSCs were spindle-shaped with scant cytoplasm and with granules around the nuclei (original magnification 100x). (b) Immunofluorescence detection: P4 ADMSCs were positive for Oct-4 and SH-2 (original magnification 100x). (c) FACS analysis: P4 ADMSCs were positive for CD29, CD44, CD105, and CD90 and negative for CD45 and CD34.

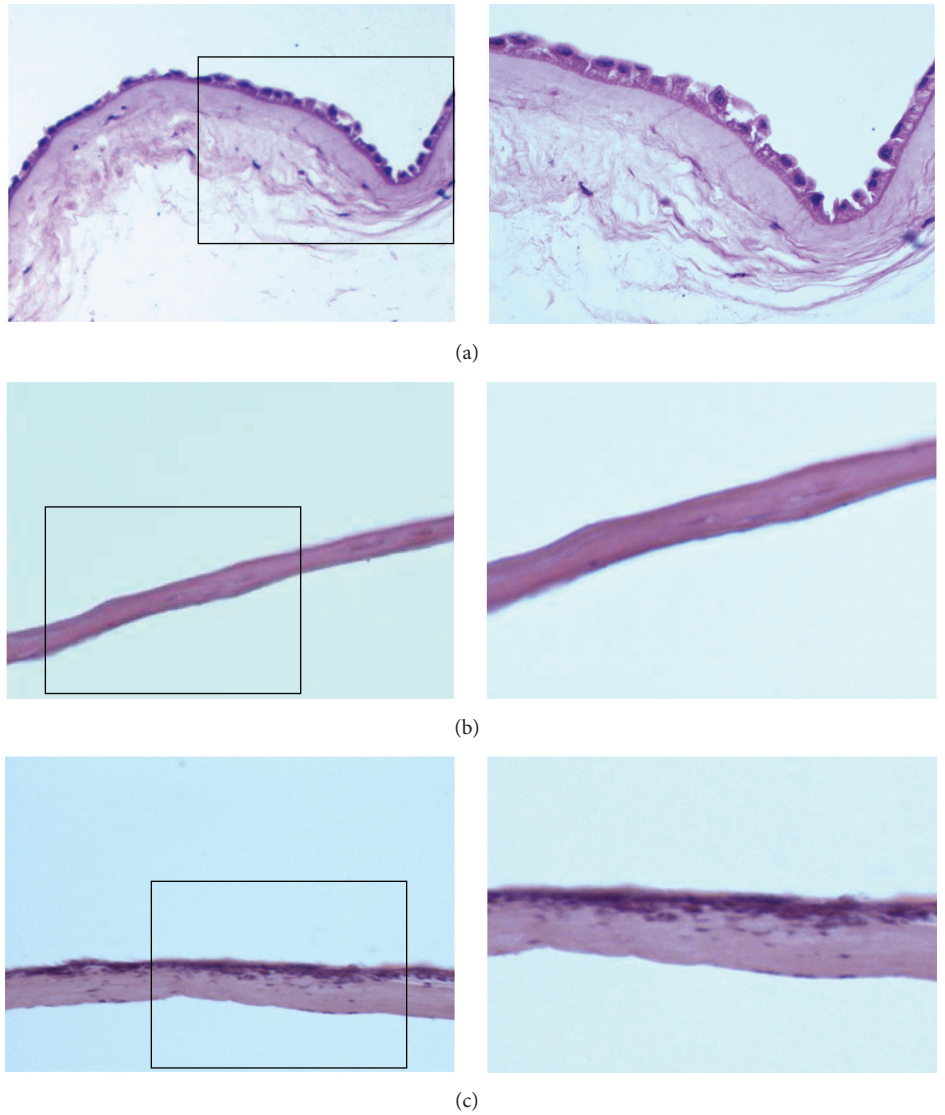

Figure 2: Morphology of hAM (a), AAM (b), and AAM loaded with ADMSCs (c). The right is the magnification of the left. HE staining showed that the epidermal layer of the intact AM was complete and continuous with the nucleus clearly seen and disappeared in AAM. After loading ADMSCs onto AAM, cells covered the surface of AAM and fused into patches.

Unlike fresh hAM, AAM can be preserved for a relatively long time as a safe and effective scaffold material [20]. Composite culture and transplantation of AAM are relatively easy without special technical requirements. The proliferation and differentiation abilities of hAM epithelial cells are not as good as those of ADMSCs. In addition, ADMSCs can differentiate to skin-related tissues [21]. It was found in the present study that the adipose stem cells were able to closely attach to the surface of AAM and grew well 24 h after seeding. At day 7 after seeding, cells fused to patches and covered the surface of the AAM. But as AAM is easily dried, contraction was observed in 50% of the wound area at day 7 after seeding and also in more than one-third of the wound area in ADMSC-AAM seeding group at day 28 after treatment. If this problem could be solved successfully, AAM's clinical value in skin tissue engineering would be further upgraded.

More importantly, we noticed a phenomenon of hair follicle development during the process of using composite ADMSCs and AAM to repair the full-thickness skin defects. Generally, only simple wound coverage is implemented in the process of repairing full-thickness skin defects or deep second-degree burns, without realizing the regeneration of skin appendages and functional recovery. In the present study, we rehearsed the process of skin appendage development and achieved functional recovery of the wounded skin. This result may prove to be clinically significant in the treatment of full-thickness skin defects using skin tissue engineering.

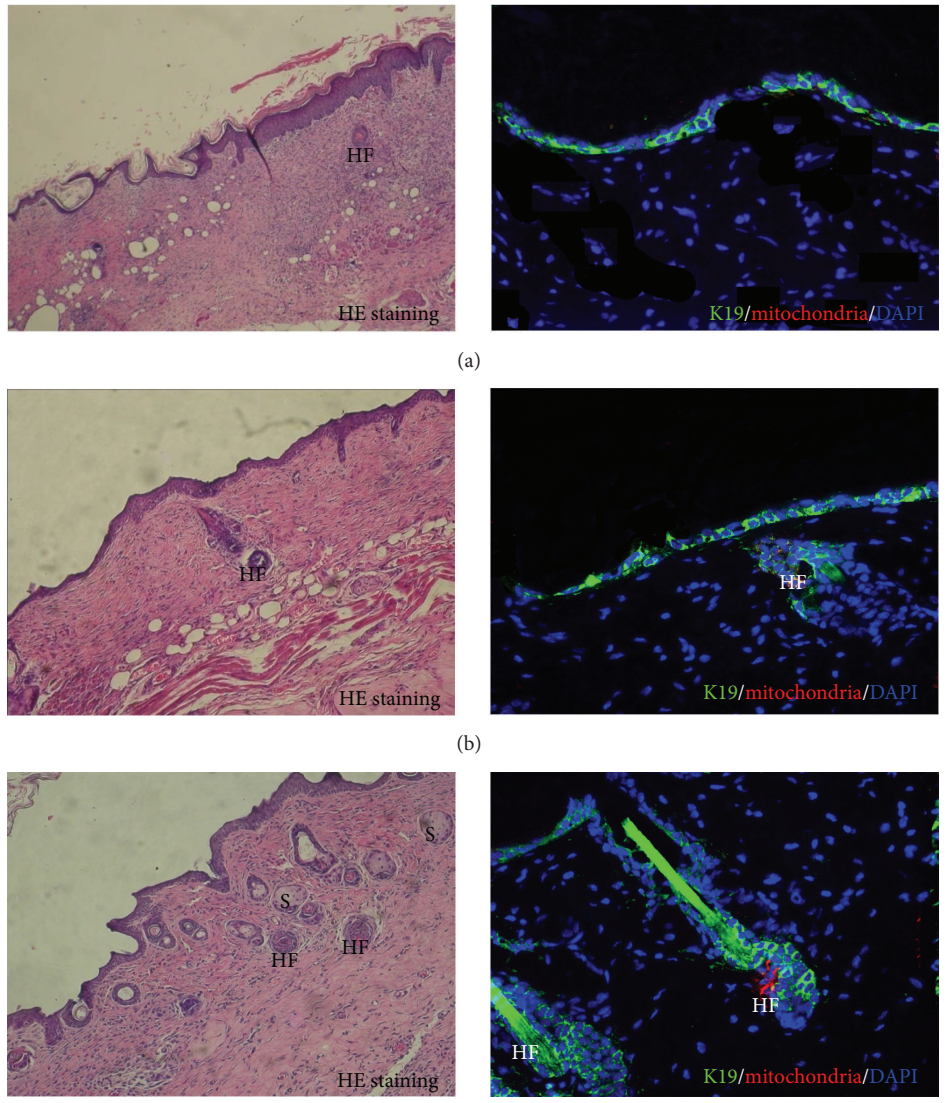

Figure 3: HE staining showed that, at day 28, a lot of typical hair follicle-like structures appeared in ADMSC-AAM seeding group (c) compared with hAM group (a) and AAM group (b). Immunohistochemistry showed that the healed epidermis was positive for cytokeratin 19. Some cells of new hair follicles were positive for both keratin 19 (green) and human derived mitochondria (red). S: sebaceous; HF: hair follicle.

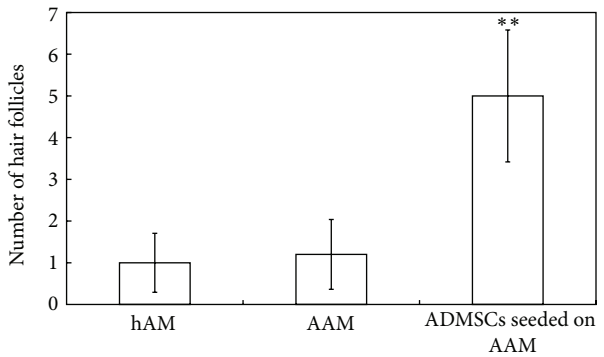

Figure 4: Comparison of hair follicles in different groups, $^{**}P < 0.05$. Image pro plus showed that the number of hair follicles in ADMSC-AAM seeding group was significantly higher than that in hAM and AAM groups.

Competing Interests

The authors declare that they have no competing interests.

Authors' Contributions

Wu Minjuan, Xiong Jun, and Shao Shiyun contributed equally to this work. Ji Kaihong is the corresponding author and Wang Yue is the co-corresponding author.

Acknowledgments

The present study was financed by the National Natural Science Foundation of China (81301649, 31101008) and the National Natural Science Foundation of Shanghai (14ZR1449400).

References

[1] D. Markeson, J. M. Pleat, J. R. Sharpe, A. L. Harris, A. M. Seifalian, and S. M. Watt, "Scarring, stem cells, scaffolds and skin repair," *Journal of Tissue Engineering and Regenerative Medicine*, vol. 9, no. 6, pp. 649–668, 2015.

[2] C. K. Mueller, S.-Y. Lee, and S. Schultze-Mosgau, "Characterization of interfacial reactions between connective tissue and allogenous implants used for subdermal soft tissue augmentation," *International Journal of Oral and Maxillofacial Surgery*, vol. 38, no. 11, pp. 1194–1200, 2009.

[3] J. G. Rheinwald and H. Green, "Serial cultivation of strains of human epidermal keratinocytes: the formation of keratinizing colonies from single cells," *Cell*, vol. 6, no. 3, pp. 331–334, 1975.

[4] E. Catalano, A. Cochis, E. Varoni, L. Rimondini, and B. Azzimonti, "Tissue-engineered skin substitutes: an overview," *Journal of Artificial Organs*, vol. 16, no. 4, pp. 397–403, 2013.

[5] M. Varkey, J. Ding, and E. Tredget, "Advances in skin substitutes—potential of tissue engineered skin for facilitating anti-fibrotic healing," *Journal of Functional Biomaterials*, vol. 6, no. 3, pp. 547–563, 2015.

[6] O. Arda, N. Göksügür, and Y. Tüzün, "Basic histological structure and functions of facial skin," *Clinics in Dermatology*, vol. 32, no. 1, pp. 3–13, 2014.

[7] M. Litwiniuk and T. Grzela, "Amniotic membrane: new concepts for an old dressing," *Wound Repair and Regeneration*, vol. 22, no. 4, pp. 451–456, 2014.

[8] S. C. G. Tseng, "Amniotic membrane transplantation for ocular surface reconstruction," *Bioscience Reports*, vol. 21, no. 4, pp. 481–489, 2001.

[9] S.-P. Wilshaw, J. N. Kearney, J. Fisher, and E. Ingham, "Production of an acellular amniotic membrane matrix for use in tissue engineering," *Tissue Engineering*, vol. 12, no. 8, pp. 2117–2129, 2006.

[10] L. Karalashvili, A. Kakabadze, G. Vyshnevska et al., "Acellular human amniotic membrane as a three-dimensional scaffold for the treatment of mucogingival defects," *Georgian Medical News*, no. 244-245, pp. 84–89, 2015.

[11] C. M. Zelen, R. J. Snyder, T. E. Serena, and W. W. Li, "The use of human amnion/chorion membrane in the clinical setting for lower extremity repair: a review," *Clinics in Podiatric Medicine and Surgery*, vol. 32, no. 1, pp. 135–146, 2015.

[12] W. U. Hassan, U. Greiser, and W. Wang, "Role of adipose-derived stem cells in wound healing," *Wound Repair and Regeneration*, vol. 22, no. 3, pp. 313–325, 2014.

[13] G. Caruana, N. Bertozzi, E. Boschi et al., "Role of adipose-derived stem cells in chronic cutaneous wound healing," *Annali Italiani di Chirurgia*, vol. 86, no. 1, pp. 1–4, 2015.

[14] S. Gomathysankar, A. S. Halim, and N. S. Yaacob, "Proliferation of keratinocytes induced by adipose-derived stem cells on a chitosan scaffold and its role in wound healing, a review," *Archives of Plastic Surgery*, vol. 41, no. 5, pp. 452–457, 2014.

[15] P. A. Zuk, M. Zhu, P. Ashjian et al., "Human adipose tissue is a source of multipotent stem cells," *Molecular Biology of the Cell*, vol. 13, no. 12, pp. 4279–4295, 2002.

[16] P. H. Wu, H. Y. Chung, J. H. Wang et al., "Amniotic membrane and adipose-derived stem cell co-culture system enhances bone regeneration in a rat periodontal defect model," *Journal of the Formosan Medical Association*, vol. 115, no. 3, pp. 186–194, 2016.

[17] E. Montelatici, B. Baluce, E. Ragni et al., "Defining the identity of human adipose-derived mesenchymal stem cells," *Biochemistry and Cell Biology*, vol. 93, no. 1, pp. 74–82, 2016.

[18] M. F. Forni, M. Trombetta-Lima, and M. C. Sogayar, "Stem cells in embryonic skin development," *Biological Research*, vol. 45, no. 3, pp. 215–222, 2012.

[19] R. Sánchez-Sánchez, A. Brena-Molina, V. Martínez-Lónez et al., "Generation of two biological wound dressings as a potential delivery system of human adipose-derived mesenchymal stem cells," *ASAIO Journal*, vol. 61, no. 6, pp. 718–725, 2015.

[20] M. Mahmoudi Rad, F. Talebpour Amiri, M. Mirhoseini, M. Ghasemi, M. Mirzaei, and N. Mosaffa, "Application of allogeneic fibroblast cultured on acellular amniotic membrane for full-thickness wound healing in rats," *Wounds*, vol. 28, no. 1, pp. 14–19, 2016.

[21] U. Sivan, K. Jayakumar, and L. K. Krishnan, "Constitution of fibrin-based niche for in vitro differentiation of adipose-derived mesenchymal stem cells to keratinocytes," *BioResearch Open Access*, vol. 3, no. 6, pp. 339–347, 2014.